

Stellingen behorende bij het proefschrift van Leo Kouwenhoven.

1.

Afgestudeerden werkzaam bij het bedrijfsleven krijgen meer onderwijs dan AIO/OIOs bij universiteiten.

2.

Het is mogelijk om via een periodieke gatestructuur een aantrekkende wisselwerking te verkrijgen tussen elektronen in een twee-dimensionaal elektronengas.

3.

Sommige theoretische concepten, zoals chaos en Wigner-rooster in de mesoscopische fysica, zijn te vergelijken met het concept hemel in religies; onbegrepen experimenten kunnen er altijd door worden verklaard.

4.

Zolang er Chinese wetenschappers gevangen zitten als gevolg van hun meningsuiting, is het onmogelijk dat de doelstelling van een wetenschappelijke bijeenkomst in China wordt bereikt.

5.

Het is veel eenvoudiger om een Wigner-molecuul te realiseren in een quantum dot dan een Wigner-rooster in een twee-dimensionaal elektronengas.

6.

Het culturele hoogtepunt in deze Spaanse zomer zal niet plaatsvinden in de culturele Europese hoofdstad Madrid, evenmin in Sevilla tijdens de wereldtentoonstelling of in Barcelona tijdens de Olympische spelen, maar traditiegetrouw in Pamplona tijdens de feesten voor de stadsheilige San Fermin.

7.

In tegenstelling tot het Landauer-Büttiker formalisme is een tunnel-Hamiltoniaan-formalisme in termen van creatie- en annihilatie-operatoren om fundamentele redenen ongeschikt om coherent transport te beschrijven.

8.

(Voetbal-) Vandalisme is niet te begrijpen zolang men humor als beweegreden niet onderkent.

9.

Het is mogelijk om een optisch analogon van de elektronenturnstile te realiseren met behulp van enkele excitonen in een quantum dot (dit proefschrift).

10.

De technologische complicaties om co-tunnelen te onderdrukken in metallische turnstile- of pomp-varianten, maakt dit soort systemen ongeschikt voor gebruik als stroomstandaard.

11.

Single-spin effecten in quantum dots geven aanleiding tot magnetische hysteresis.

12.

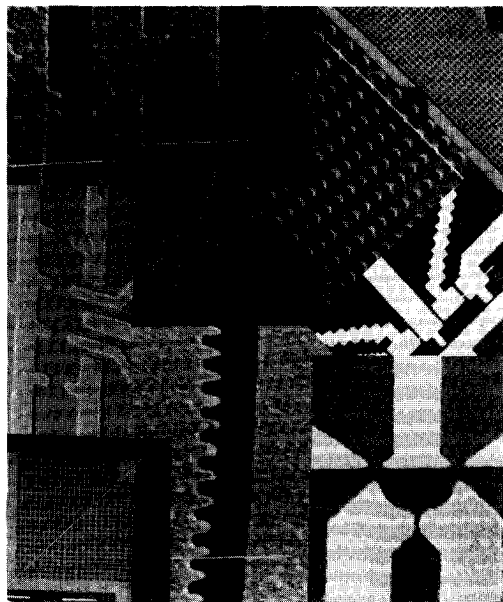
De aanvallen op het internationale rechtstelsel van bijvoorbeeld Saddam Hussein en Ghadaffi, zullen op lange termijn de Westerse arrogantie aan het licht brengen.

TR diss 2079

**TR diss
2079**

554663
3172701
TR diss 2079

**Transport of Electron-Waves and Single-Charges
in Semiconductor Nanostructures**



*Voor mijn moeder,
Gerry, Lenny, José,
Els, Astrid, en Carola.*

Transport of Electron-Waves and Single-Charges in Semiconductor Nanostructures

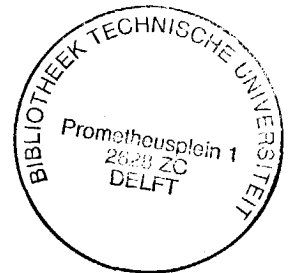
Proefschrift ter verkrijging van de graad van doctor
aan de Technische Universiteit Delft,
op gezag van de Rector Magnificus, prof. drs. P.A. Schenck,
in het openbaar te verdedigen ten overstaan van een commissie
aangewezen door het College van Dekanen, op

maandag 22 juni 1992 te 16.00 uur

door

Leonardus Petrus Kouwenhoven

geboren te Pijnacker
natuurkundig ingenieur



Dit proefschrift is goedgekeurd door de promotor prof. dr. ir. J.E. Mooij

Het onderzoek beschreven in dit proefschrift is financieel ondersteund door de
Stichting voor Fundamenteel Onderzoek der Materie (FOM).

Preface

This thesis describes a number of experiments in the young field of *mesoscopic physics*. To characterize mesoscopic systems we will compare them to much smaller atomic, microscopic systems and our much larger every day, macroscopic world.

Virtually all physical processes in our macroscopic world can be described by classical laws. Examples are Newton's equations of motion and his gravitation law describing the attraction between the Earth and other objects, and the Maxwell equations describing electromagnetism as in relations between currents and voltages or electric and magnetic fields. The typical length scales of the macroscopic world are set by the limitations of our eyes. The largest distance we can see is several hundred kilometers on earth and much larger if we look at the moon, and the sun. On the other hand, the smallest detail we can see is about a hundredth of a millimeter; i.e. the thickness of a hair.

The microscopic world is the world of nuclei, electrons, atoms, and molecules. The typical distance between atoms is a few tenths of a nanometer. A *nanometer* is a million times smaller than a millimeter. On this very small length scale, classical laws dramatically fail to describe the physical processes. To describe the behaviour of electrons, for instance, we have to use *quantum mechanics*. One consequence of quantum mechanics is the *particle-wave duality*, which implies that an electron can behave as a particle or as a wave. The wave-nature of an electron can lead to phenomena which are unthinkable in our macroscopic world. An example is that an electron can interfere with itself when there are different paths available for traveling between two points in space. In classical thinking this would imply something meaningless like a rolling ball that kicks itself and then turns around. Another example is that an electron can pass, i.e. tunnel, through a barrier while a ball thrown against a wall is classically not expected to go through the wall.

The size of mesoscopic systems is somewhere between those of microscopic and macroscopic systems. For instance, the systems studied in this thesis resembling wires and boxes have a typical size of 100 nanometers which corresponds to a millimeter divided by 10 thousand, or in microscopic units, to a row of about 500 atoms. The intriguing aspect of mesoscopic systems is that they sometimes behave as classical systems and at other times they show their quantum nature. We will discuss experiments in which we can tune the behaviour of a mesoscopic box from quantum mechanical to classical. The quantum mechanical aspects are sometimes particularly surprising. This is because in systems which are thousands of atoms large, the quantum mechanical wave-nature of single electrons can completely determine macroscopic currents and voltages.

The study of mesoscopic physics started about 10 years ago as a result of an advanced technology which enabled the fabrication of small systems in solids. There is an important concept which makes solids suitable to study quantum mechanical behaviour on distances much larger than the atomic distance. In clean, crystalline solids, meaning that the atoms form a regular lattice, a certain number of electrons can move as in free space. When the number of free electrons is zero, the material is insulating for electrical current as in quartz. In metals such as copper, each atom contributes one or two free electrons. So, a small metal cube of 100 nanometers still contains about a 1000 million free electrons. This very large number is the reason that the electron motion in a metal can often be described in a classical way, i.e. as if electrons move and bounce like billiard balls. In contrast to this, semiconductor materials, such as silicon have a number of free electrons which can be tuned by means of material parameters from zero to typically a thousand electrons in a cube of 100 nanometers. This small number of electrons makes it much easier to observe quantum mechanical behaviour which is the reason that the experiments of this thesis are performed on *semiconductor nanostructures*.

One consequence of the wave-nature of electrons is that they can be confined to a lower dimension. To explain lower-dimensionality we have schematically shown in the Figure a wave with a wavelength λ and three types of solids: one solid has the shape of a slice, the second of a pillar or wire, and the third of a box. The free electrons in these solids behave as waves with a wavelength depending on the density of free electrons in the solid. A smaller density of electrons yields a longer wavelength, which in semiconductors can greatly exceed the inter-atomic distance. The electron wave-nature becomes important when its wavelength is comparable to the size of the host solid. Similar to standing waves in a string which is bounded at its two ends (see the Figure), only electrons whose wavelength λ matches with the size of the solid are allowed in the system. In the solid slice, therefore, electrons have $\lambda/2$, λ , $3\lambda/2$, etc, equal to the thickness of the slice. As with any standing wave, the electron motion in this confined direction is completely frozen. The electrons have freedom of motion only in the other two directions. So, essentially, the electrons live in a two dimensional (2D) world where they have to obey "flatland" rules. These flatland rules can lead to phenomena which have no analog in our 3D world. In the pillar, or wire, electrons can only move in one direction, and there is no motion in the two confined directions. So, the pillar forms a 1D system for the electrons. Complete confinement is reached in the box, where the electron wave matches the length, width and height of this 0D-box. The physical rules belonging to the dimensionality of a system yield distinct electron behaviour, and even distinct predictions for macroscopic quantities like resistance. The experi-

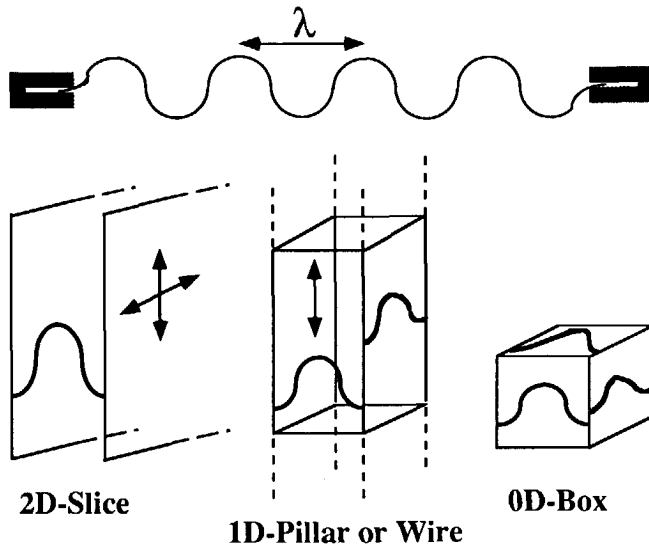


Figure. Upper part: Representation of a standing wave with a wavelength λ in a string bounded at both ends. Lower part: Three confined solids. In the 2D-slice the electron motion is free in only two directions; in the 1D-pillar, or wire only in one direction; and in the 0D-box the electron motion is frozen in all three directions. In the confined directions only the lowest mode of $\lambda/2$ equal to the size of the solid is shown.

mental observations resulting from reduced dimensionality have been one of the major subjects of mesoscopic physics.

In this thesis we use a special semiconductor material, which has the 2D slice built in. We obtain these materials from the Philips Research Laboratories, where they are made with very clean material growing techniques. At the Delft Institute for MicroElectronics and Submicron technology (DIMES) we use the lithography facilities to transform the slice into wires, boxes, and more complicated structures. The techniques to do this are much the same as used for the fabrication of computer chips, but are developed to be able to make structures which are ten to hundred times smaller than used in computer chips today. To probe the properties of the electrons in these small structures we perform current and voltage measurements in the Solid State group of Hans Mooij at the Faculty of Applied Physics in Delft. For observing quantum mechanical behaviour, it is important that the structures are cooled to extremely low temperature. Special refrigerators allow us to reach temperatures of 0.01 degree above absolute zero-tempera-

ture, which is about 273 degrees below 0 degrees Celsius.

This thesis is roughly divided into two parts. The first part, chapters 1 to 6, describes experiments probing the *wave-nature* of electrons. It includes the electron transport through a 1D-wire, a 0D-box, and a series of coupled 0D-boxes. The results on these systems demonstrate fundamental quantum behaviour, such as a conductance changing in quantized steps when the width of the 1D-wire is varied (classically the conductance is expected to rise linearly with increasing wire width); a total resistance smaller than two series resistances which enclose a 0D-box (the classical Ohm's law predicts the opposite result that the total resistance is the sum of the two resistances in series); and the formation of a 1D-solid in a series of periodically positioned coupled 0D-boxes. The second part mainly relies on the discreteness of the electronic charge in nature. In a neutral box the number of positive charges equals the number of negative charges. If we put an extra electron in the box, it becomes negatively charged, which costs a certain energy. In chapter 7 through 10, we use boxes having an entrance and an exit, which we can arbitrarily open or close. Employing the energy associated with a *single-charge*, we can manipulate single electrons in these boxes. One experiment is that we open the entrance and simultaneously close the exit. We supply just enough energy to charge the box by one single electron, which is therefore pulled into the box. The entrance is then closed and the exit opens, allowing one electron to leave in order to discharge the box. So, in every cycle of opening and closing the doors, one electron is transferred through the box. Repeating this process with a high frequency (typically ten million times per second) yields a current being equal to the electron charge times this frequency. Although, this experiment does not yield new physics, we thought that it would be fascinating to manipulate current at the most fundamental level of a single electron.

It takes many people to be able to transfer a single electron through a box, who I would like to thank for their vital contributions to the experiments described in this thesis. First of all, I wish to thank all researchers in the field for the open communication. Their work has continuously been stimulating and guided us in our own efforts. In Delft this research started several years ago in collaboration with the Philips Research Laboratories in Eindhoven. My own contributions started in 1986 as an undergraduate student. Bart van Wees was my adviser during these first few years. His original way of thinking taught me a lot and strongly motivated me to continue studying, which is something I gratefully acknowledge. During these first years we worked together closely with Carlo Beenakker, Henk van Houten, and John Williamson from Philips. I benefited very much from the intense and lively discussions and from the extensive experimental collaboration.

During the last few years new people joined this research. In the semiconductor section of Hans Mooij's group, I have been working close with Kees Harmans (giving me daily support on any imaginable subject), Bram van der Enden (who did most of the sample fabrication), Charlie Johnson (with whom I had some very good turnstile nights), and Nijs van der Vaart (talk to you later). The work done by the undergraduate students has been of prime importance. I would like to thank Rick Kraayeveld, Walter Kool, Diederik Maas, Wim de Jong, and Luuk Mur for all their hard work. The stay of Juanjo Palacios in our group has been a nice motivation to learn about difficult electron correlations. The connection with the theory group of Gerd Schön with all its famous visitors has been very stimulating. Especially, I would like to thank Frank Hekking for his 1D-crystal-work and for numerous discussions. From Philips I gratefully acknowledge Gerrit Bauer, Marcel Broekaart, Rob Eppenga, Tom Foxon, Laurens Molenkamp, Toine Staring, and Eugene Timmering for discussions and collaboration.

During my graduate study, I have had the opportunity to work a few months in the group of prof. Sakaki at Tokyo University. The work and life in Tokyo have been very exciting. I am hoping that our collaboration will last a long time. Chapter 10 describes the first promising results of this collaboration. I would very much like to thank Nagamune-san, Motohisa-san, and Sakaki-sensei for this joined work, Matsuya-san for her essential care to get me around in Tokyo, and all the other group members for introducing me into Japanese research and society.

Beside the research subject itself, I found that a group environment is sometimes very encouraging. I have great respect for the way Hans Mooij organizes his large group. The variety of subjects and the mixture of different people in the group stimulate many new activities. The complete freedom, coffee table, group excursions, and the very regular scientific meetings, make leaving a scary thought. A result from the group mixture can be found in the latter chapters of this thesis, which were motivated by discussions with Bart Geerligs on charging effects. I would also like to thank my office mate Herre van der Zant; our computer expert Huub Appelboom; Dick van der Marel for discussing fundamentals; Chris Gorter, Leo Lander, Gerard van der Gaag, Wim Schot, and Willem de Braver for their technical expertises, Ria van Heeren for her all-around help; and all other group members for their scientific and social contributions. Special thanks go to the people from DIMES for their essential help and advice on sample fabrication.

Finally, I wish to thank my family and friends. Although it is a strange comparison, you are much more important to me than this whole thesis.

TABLE OF CONTENTS

Preface

Table of contents

Chapter 1	Quantum Adiabatic Electron Transport in Ballistic conductors	1
1.1	Introduction	2
1.2	Fabrication and working principles of a split-gate device	3
1.3	Quantized conductance of a point contact	6
1.4	Depopulation of 1D magneto-electric subbands	12
1.5	Electron motion in a magnetic field	14
1.5.1	Electron focusing	14
1.5.2	Edge channels	17
1.5.3	Quantized longitudinal conductance	18
1.6	Anomalous Integer quantum Hall effect	20
1.7	Transition from Ohmic to adiabatic transport	23
1.7.1	Transport through two QPCs in series	23
1.7.2	Electron-beam collimation and electron focusing in a dot	29
1.8	Summary and conclusions	33
	References	34
 Chapter 2	 Non-Linear Conductance of Quantum Point Contacts	 39
 Chapter 3	 Selective Population and Detection of Edge Channels in the Fractional Quantum Hall Regime	 49
 Chapter 4	 Transport through Zero-Dimensional States in a Quantum Dot	 59
4.1	Introduction	60
4.2	Device description	61
4.3	Edge channels and selective transmission of QPCs	62
4.4	Adiabatic transport in series QPCs	64

4.5	Transport through 0D-states	66
4.5.1	Theory	66
4.5.2	Experiment	68
4.5.3	Discussion	73
4.6	Concluding remarks	75
	References	76
Chapter 5	Transport through a Finite One Dimensional Crystal	79
5.1	Introduction	80
5.2	Formation of a band structure in a finite 1D crystal	81
5.3	The 1D crystal device	85
5.4	Transport measurements	86
5.5	Discussion and conclusions	89
	References	92
Chapter 6	Quantized Photocurrent by creating Single Excitons	95
Chapter 7	Single Electron Charging Effects in Semiconductor Quantum Dots	103
7.1	Introduction	104
7.2	The split-gate quantum dot	104
7.3	Charging theory for semiconductor quantum dots	106
7.4	Experiments	111
7.4.1	Coulomb oscillations	111
7.4.2	Coulomb staircase	116
7.5	Discussions and conclusions	118
	References	120
Chapter 8	Quantized Current in a Quantum Dot Turnstile	123
8.1	Introduction	124
8.2	The split-gate quantum dot	125
8.2.1	Sample layout	125

8.2.2. Charging effects without applying RF signals	126
8.2.3 Electron pump using one oscillating barrier	128
8.3 Quantum dot turnstile	130
8.3.1 Operation principles	130
8.3.2 Experiment	132
8.4 Discussion and conclusions	139
References	141
 Chapter 9 Zero Dimensional States and Single Electron Charging in Semiconductor Quantum Dots	 143
 Chapter 10 Coulomb Oscillations with a Multiple Peak Structure	 153
10.1 Introduction	154
10.2 Gated-etched quantum dot device	155
10.3 Quantum dot turnstile	156
10.4 Coulomb oscillations with a multiple peak structure	157
10.5 Discussion and conclusions	162
References	164
 Summary	 165
 Samenvatting	 167
 Curriculum Vitae	 169

CHAPTER 1

Quantum Adiabatic Electron Transport in Ballistic Conductors

Leo P. Kouwenhoven

Faculty of Applied Physics, Delft University of Technology

P.O.Box 5046, 2600 GA Delft, The Netherlands

ABSTRACT

We review experiments in the quantum ballistic transport regime occurring in submicron conductors. The conductors are defined in a two dimensional electron gas (2DEG) by means of a split-gate technique, providing the possibility to tune the size of the conductor. The conductance of a short and narrow constriction, a quantum point contact (QPC), is quantized in multiples of $2e^2/h$ at zero and non-zero magnetic field. QPCs are further used to study electron focusing in a 2DEG; the quantized longitudinal conductance in a high magnetic field; the anomalous quantum Hall effect due to selective population and detection of edge channels; the transition from Ohmic to adiabatic transport in two QPCs in series; and electron-beam collimation.

1.1 INTRODUCTION

The properties of electron transport in small conductors are related to the relevant length scales. In the *diffusive* transport regime, in which the elastic mean free path l_e is much smaller than the dimensions of the conductor (see Fig. 1.1a), quantum interference effects can produce deviations from the predictions of classical transport theory. These interference effects result from phase differences acquired by an electron wave in travelling between two points in the sample along different possible trajectories. Many different trajectories can arise from scattering at impurities, resulting in phenomena like one-dimensional (1D) weak localization¹ and universal conductance fluctuations.² In a ring, where there are only two sets of possible trajectories from the entrance to the exit, the interference gives rise to periodic conductance oscillations known as the Aharonov-Bohm effect and Al'tshuler-Aronov-Spivak oscillations.³ To observe these quantum interference effects, the distance electrons can travel with conservation of phase coherence l_ϕ , must be larger or at least of order the sample dimensions.

Modern technology permits the fabrication of structures in which l_e is smaller than the length L but larger than the width W of the sample (see Fig. 1.1b). In this *quasi-ballistic* regime, scattering at the boundary of the conductor is important.^{4,5} If the irregularities in the boundary are much smaller than the Fermi wavelength λ_F , the scattering at the boundary is believed to be specular. For larger irregularities the scattering at the boundary becomes diffusive.

Recently, conductors in the fully *ballistic* regime ($l_e \gg L, W$) have been studied. Elastic scattering of electrons, which can give rise to resistance,⁶ occurs only at the boundary of the conductor (see Fig. 1.1c). In metals, the classical ballistic regime has been investigated using Sharvin point contacts.⁷ To study quantum confinement effects, however, λ_F must be of order the width of the conductor. Currently it is not possible to satisfy this condition for metals, where $\lambda_F \approx 0.1$ nm. Due to the much lower electron density in semiconductors, λ_F is typically ≈ 50 nm, which is a feasible dimension for fabricating small conductors. *Quantum transport* in such *ballistic conductors* is the subject of this review.

In this review we mainly present work done by the collaboration between Philips Research Laboratories in Eindhoven and Delft University of Technology (The Netherlands). For a broader perspective on the field of low dimensional quantum transport, we refer to recent larger review articles.⁸⁻¹⁴ In section 1.2, we outline the fabrication process and working principles of a split-gate sample. We discuss experiments on a short, narrow ballistic constriction, a quantum point contact (QPC), in section 1.3 for zero magnetic field and in section 1.4 when a magnetic field is

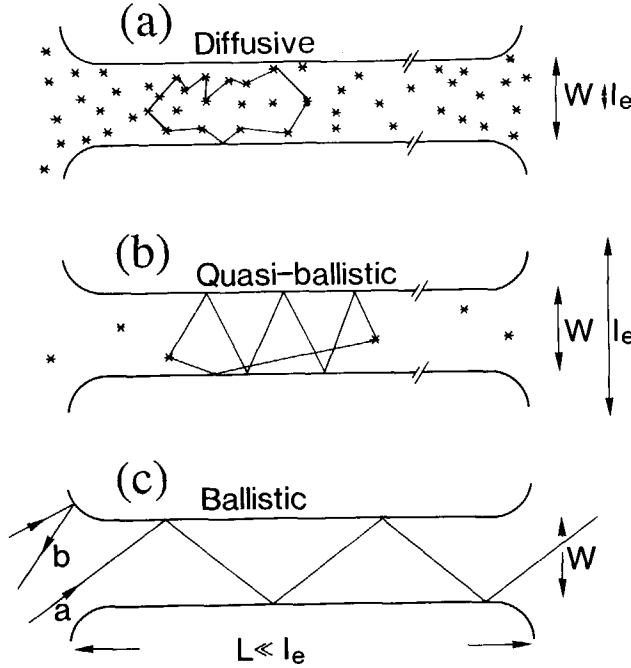


FIG 1.1. Typical electron trajectories in the diffusive ($l_e \ll L, W$), quasi-ballistic ($W < l_e < L$), and ballistic ($W, L \ll l_e$) transport regime with specular scattering at the boundary of the conductor. In the ballistic regime, the resistance is entirely due to backscattering at the geometrical narrowing from the wide region to the small conductor. (from van Houten et al. in Ref. 8)

applied. We show experimentally that a gradual transition exists from the quantized conductance of a point contact at zero magnetic field to the quantum Hall effect at high magnetic field. We interpret this in terms of the Landauer-Büttiker formalism. In section 1.5, we discuss electron motion in a magnetic field, including the concept of edge channels. We study adiabatic transport (i.e. with conservation of quantum number) in edge channels in sections 1.6 and 1.7, using two adjacent QPCs and two QPCs in series, respectively.

1.2 FABRICATION AND WORKING PRINCIPLES OF A SPLIT-GATE DEVICE

The starting point for studying quantum ballistic transport is a two-dimensional electron gas (2DEG) being present in various semiconductor devices. So far, the highest electron mobilities

have been obtained in the 2DEG of GaAs/AlGaAs hetero structures,¹⁵ making this the most suitable semiconductor system for studying ballistic transport. Fig. 1.2a shows a cross-section of this hetero structure. The 2DEG is at the GaAs-AlGaAs interface. The electron density n_s in the 2DEG depends on the amount of negative-doping in the AlGaAs layer. Typical values are $n_s \approx (1 - 5) \cdot 10^{15} \text{ m}^{-2}$ so $\lambda_F = (2\pi/n_s)^{1/2} \approx (80 - 30) \text{ nm}$. Due to the separation of the ionized donors from the 2DEG by the undoped AlGaAs spacer layer, the electron mobility in the 2DEG can be larger than $100 \text{ m}^2\text{V}^{-1}\text{s}^{-1}$, corresponding to a transport elastic mean free path larger than $10 \text{ }\mu\text{m}$.¹⁵ (Note that the transport mean free path includes the effectiveness of the scattering, and is larger than our definition of l_e which gives a measure of the mean distance between impurities.¹⁶)

To confine the electrons laterally in the 2DEG a pattern must be defined on top of the hetero structure, which is done by standard lithography. Depending on the desired pattern, one can choose between many variations in the lithography process steps (see for a review Ref. 17). One procedure is shown schematically in Fig. 1.3. An organic resist film (typically 100 nm thick) is spun on the substrate. For submicron structures one chooses an electron sensitive resist. Exposing the resist with an electron beam (using a modified electron microscope) results in a molecular-mass difference between the exposed and unexposed parts (see Fig. 1.3a). An appropriate developer removes only the exposed resist, resulting in the pattern shown in Fig. 1.3b. Due to this mask pattern, an evaporated material only sticks at the substrate where the resist has been removed (see Fig. 1.3c). The mask itself can be removed by dissolving the remaining resist (so-called lift-off), leaving a small pattern on top of the substrate (see Fig. 1.3d). The minimal resolution of such a pattern with present day electron-beam lithography facilities is about 10 nm.

From this point there are basically two ways to transfer the pattern to the 2DEG. The "hard" way is to use the pattern as an etch mask.¹⁷ Etching removes the portion of the 2DEG not protected by the pattern. The boundaries of the etched pattern cause a depletion region, so the conducting width in the 2DEG is unknown and often much smaller than the defined width.¹⁸ A "soft" way to transfer the pattern to the 2DEG is to use it as a gate for which reason the pattern must be made from a metal.^{19,20} Applying a negative voltage to the gate depletes the electron gas beneath it, thereby confining electron motion to the ungated region. For a split-gate geometry, as in Fig. 1.2a, this results in a small conducting channel. The advantage of the split-gate technique is that the conducting width in the 2DEG can be tuned from the defined lithographic width of the pattern to zero, by making the gate voltage more negative.

FIG 1.2. (a) Cross-section of a GaAs/AlGaAs hetero structure with typical layer thicknesses. A negative voltage V_g applied to the metal split-gate confines the electrons laterally in the 2DEG. (b) Top-view of a QPC. The dotted line indicates the depletion region in the 2DEG, which is tuned by V_g . The two wide 2DEG regions act as reservoirs, emitting electrons through the QPC with energies up to their electro chemical potentials μ_1 and μ_2 . A voltage difference $V = (\mu_1 - \mu_2)/e$ results in a net current I through the QPC.

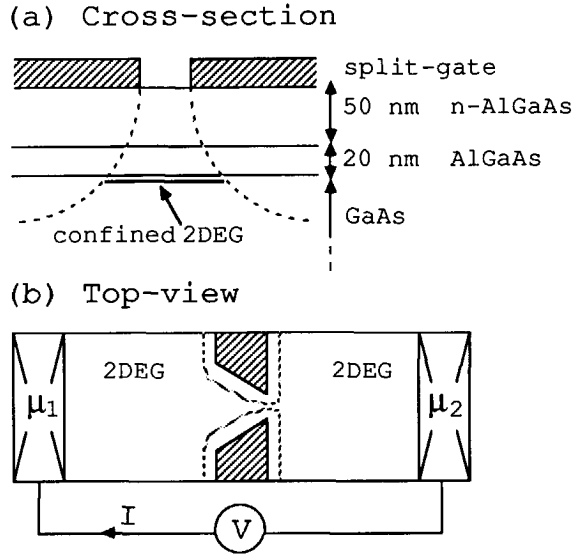
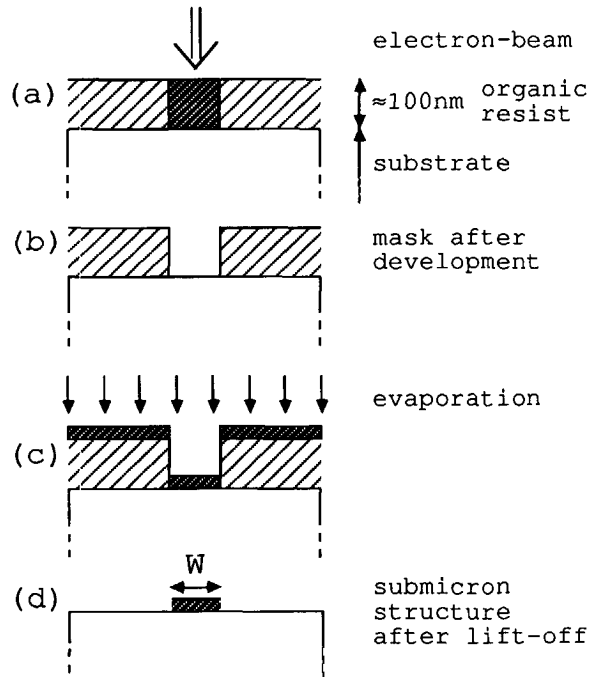


FIG. 1.3. Outline of the electron-beam lithography procedure for fabricating submicron structures.



A simple split-gate geometry with which one can define a short and narrow constriction in the 2DEG is shown in Fig. 1.2b. Transport between the two wide 2DEG regions occurs only through the point contact and can be studied as a function of the width by changing the gate voltage. The width of the constriction can be made comparable to the Fermi wavelength, so this device is called a quantum point contact (QPC). The actual induced potential in the 2DEG is unknown, but self-consistent calculations²¹ indicate that it has a saddle-shape (see Fig. 1.4a). In the constriction, electrons are confined in the lateral x -direction and slowed down by the presence of a potential barrier in the y -direction. Making the gate voltage more negative simultaneously reduces the width and increases the barrier height. For zero-width or a barrier which is higher than the Fermi energy E_F of the 2DEG, the QPC is pinched-off and electron transport between the wide 2DEG regions is impossible. Fig. 1.4b shows a scanning electron micrograph of a double point contact device.

1.3 QUANTIZED CONDUCTANCE OF A POINT CONTACT

The resistance of a point contact in the classical ballistic regime is known as the Sharvin resistance.⁶ The Sharvin resistance is entirely due to elastic backscattering at the geometrical narrowing of the ballistic point contact. Dissipative processes, which bring the electron system into thermodynamic equilibrium, take place far away from the point contact (a few times the inelastic mean free path). Therefore, the cause of the resistance in this system is spatially separated from its corresponding Joule heating. The conductance of a Sharvin point contact in a 2DEG is:²²

$$G_s = \frac{2e^2}{h} \frac{k_F W}{\pi} = \frac{2e^2}{h} \frac{2W}{\lambda_F}, \quad (1.3.1)$$

which is, as one expects, proportional to the width W of the point contact. $2e^2/h$ is the fundamental conductance unit²³ (the factor 2 accounts for the spin-degeneracy) and the Fermi wavevector k_F or wavelength λ_F are connected to the 2D electron density n_s by: $k_F = 2\pi/\lambda_F = (2\pi n_s)^{1/2}$. Deviations from Eq. 1.3.1 due to the wave nature of electrons occur when $\lambda_F \sim W$ (i.e. $k_F W/\pi \sim 1$). A derivation of the quantum version of the Sharvin conductance appears below. First we discuss the experimental results.

The conductance of a point contact is measured with an ac lock-in technique by passing a current I through the sample and measuring the voltage V between the current source and sink

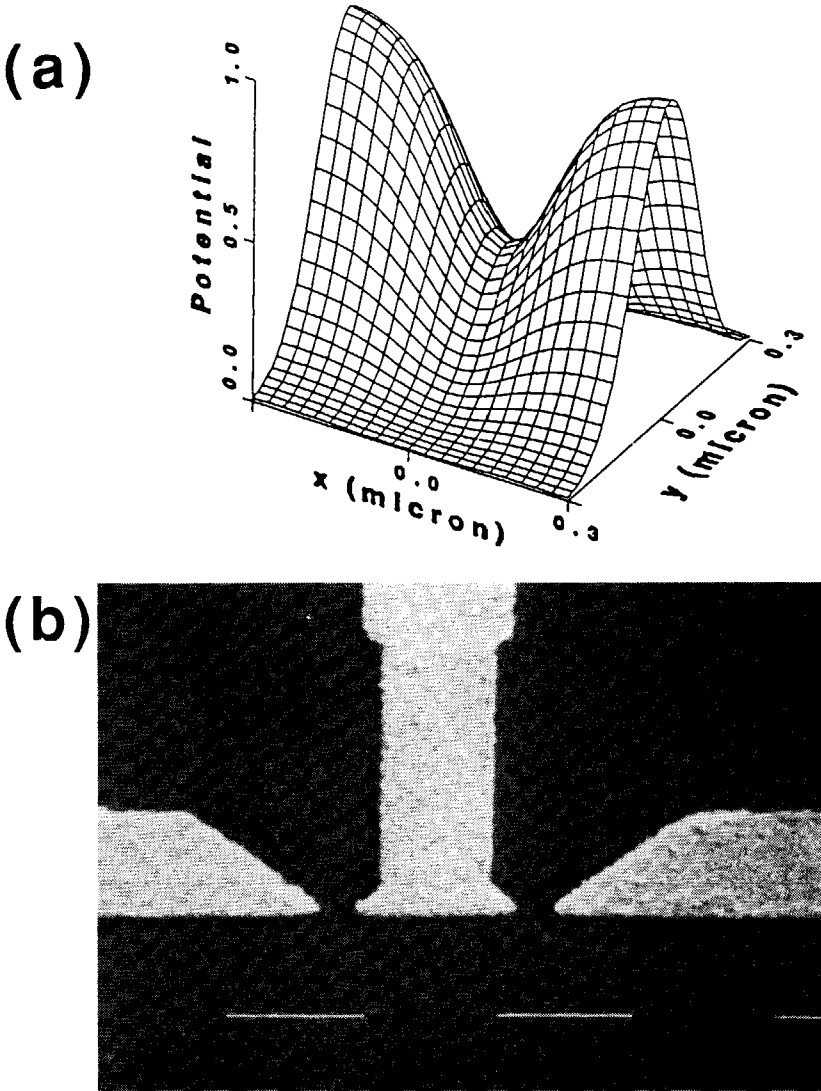


FIG. 1.4. (a) Saddle-shaped potential induced in the 2DEG upon application of a negative gate voltage, resulting in lateral confinement in the x -direction and a potential barrier in the longitudinal y -direction (from Beenakker, and van Houten in Ref. 14). (b) Scanning electron micrograph of a double-QPC device. The white areas are the Au gates, and the marker is $1\ \mu\text{m}$ long. The QPCs are $250\ \text{nm}$ wide and are separated by $1.5\ \mu\text{m}$.

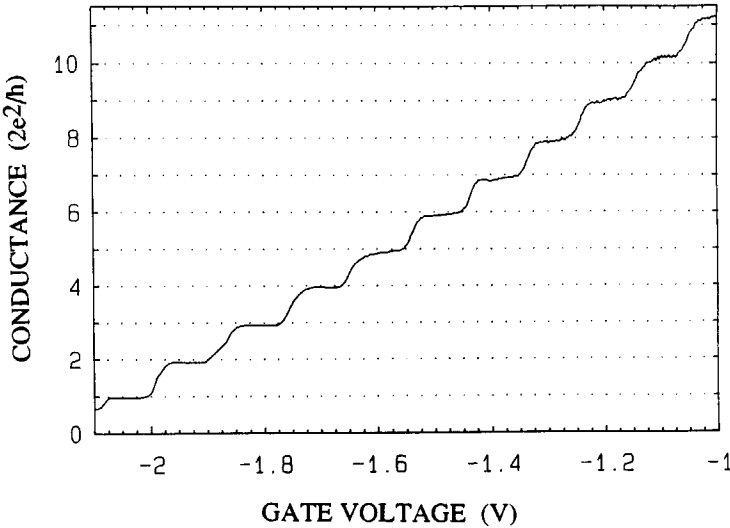


FIG. 1.5. Conductance versus gate voltage of a QPC at 0.6 K and $B = 0$, demonstrating the conductance quantization in units of $2e^2/h$ (from Ref. 22).

(see Fig. 1.2b). To prevent electron heating, eV is kept small compared to the thermal energy $k_B T$. Fig. 1.5 shows the conductance G in units of $2e^2/h = (12906 \Omega)^{-1}$ versus gate voltage V_g measured at 0.6 K and $B = 0$. Strikingly, G decreases in steps of $2e^2/h$ as V_g is made more negative. At $V_g = -2.2$ V, the conductance becomes zero, corresponding to a pinched-off point contact. The plateaus occur at integer multiples of the conductance-unit $2e^2/h$. In total 16 steps are observed between the formation of the QPC in the 2DEG at $V_g = -0.3$ V and pinch-off. This conductance quantization was discovered independently by Wharam et al.,²⁴ who also used a split-gate technique.

Fig. 1.6 shows the conductance versus gate voltage for different temperatures.²⁵ The conductance quantization gradually disappears as T is raised. $G(V_g)$ is roughly linear at 4.2 K, in accordance with the classical dependence of Eq. 1.3.1. Although the classical result cannot explain the quantization, we note that the plateau values are obtained in Eq. 1.3.1 whenever $\lambda_F/2$ is an integer times the width W . Eq. 1.3.1 predicts that an increase in W of $\lambda_F/2$ (which is 21 nm in this sample) increases G by $2e^2/h$. The observation of 16 steps then gives an estimate of the width W of the QPC at $V_g = -0.3$ V of about 340 nm, somewhat larger than the lithographic

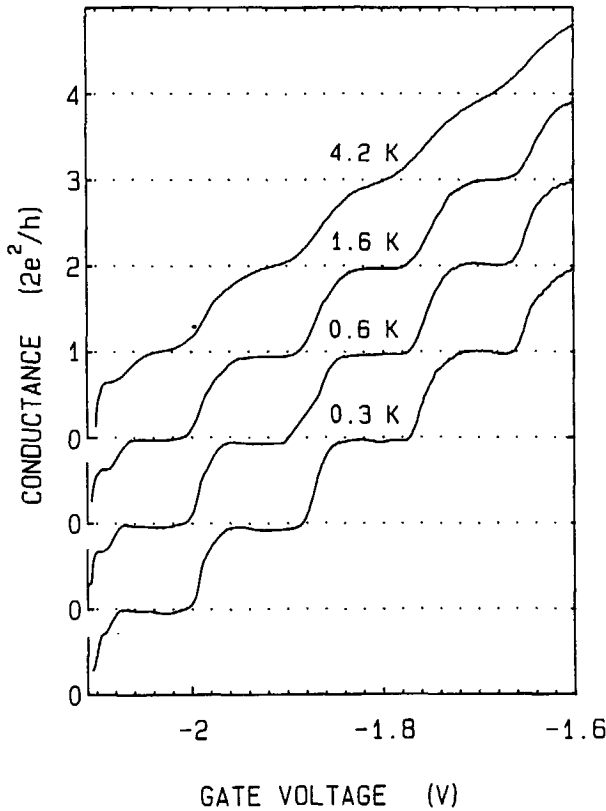


FIG. 1.6. Conductance versus gate voltage at $B = 0$ and different temperatures. Increasing the temperature thermally averages the higher plateaus first (from Ref. 25).

width of 250 nm. These considerations are reminiscent of the states of a particle-in-a-1D-box, which, as we show below, is the basic idea behind the conductance quantization.

We note that the conductance quantization is not exact. First, a series resistance ($\approx 400 \Omega$) originating from the wide 2DEG regions has been subtracted to line up the plateaus at their quantized values.²² Furthermore, the plateaus are not completely flat. This may be due to scattering at impurities in the vicinity of the QPC or, as we discuss below, the abruptness of the constriction.

We now show that the conductance quantization results from transport through 1D subbands. To calculate transport through a QPC we start with the Hamiltonian:

$$H = \frac{p_x^2}{2m^*} + eV(x) + \frac{p_y^2}{2m^*} \quad (1.3.2)$$

$m^* = 0.067 m_0$ is the effective mass in GaAs. This Hamiltonian does not contain the potential $V(y)$ in the longitudinal y -direction (see Fig. 1.4a), which describes the transition from the wide 2DEG regions to the narrowest point in the QPC. Glazman et al.²⁶ have shown that if $V(y)$ varies sufficiently smoothly (i.e. adiabatically), the potential variation in the x - and y -directions may be decoupled. The narrowest point then forms the bottleneck of the QPC in the sense that it completely determines the transport properties. We assume this to be the case and take the Hamiltonian of Eq. 1.3.2 to describe the transport at the bottleneck. For the confinement in the lateral x -direction, we follow Berggren et al.²⁷ and choose a parabolic confining potential $V(x) = 1/2 m^* \omega_0^2 x^2$. Self-consistent calculations of Laux et al.²¹ have shown that small split-gate samples have a confinement close to such a parabola. The advantage of using a parabolic potential is that the resulting Schrödinger equation can be written in the form of a harmonic oscillator having energy eigenvalues:

$$E_n = (n - \frac{1}{2}) \hbar \omega_0 + \frac{\hbar^2 k_y^2}{2m^*} \quad (n = 1, 2, \dots) \quad (1.3.3)$$

which contains a free-electron kinetic energy dispersion in the longitudinal y -direction. In the lateral x -direction the energy states, indexed by $n = 1, 2, \dots$, are quantized and separated in energy by $\hbar \omega_0$. Eq. 1.3.3 describes 1D subbands, because the electron motion is free in one direction only. Fig. 1.7 shows the 1D subband dispersion versus longitudinal wavevector k_y . The right-going electrons, with a velocity $v_n = 1/\hbar \cdot (dE_n/dk_y)$, originate from the left 2DEG reservoir, which populates at zero temperature all the states up to its electro chemical potential μ_1 . Similarly, the left-going electron states are occupied up to μ_2 , the electro chemical potential of the right 2DEG reservoir (see Fig. 1.2b). A voltage difference $V = (\mu_1 - \mu_2)/e$ between the two reservoirs results in a net current I , which is carried by the (uncompensated) electron states in the energy interval between μ_1 and μ_2 . Note that we define the Fermi energy E_F as $E_F = \mu_1 = \mu_2$ when $V = 0$. The net current I at zero temperature is:

$$I = e \sum_{n=1}^N \int_{\mu_2}^{\mu_1} dE \frac{1}{2} \frac{dN_n}{dE} v_n(E) T_n(E) \quad (1.3.4)$$

which includes the transmission probability of the n -th subband $T_n(E)$ to describe possible scattering events. N denotes the number of occupied subbands, the largest number for which

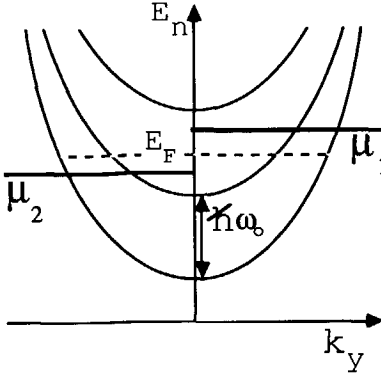


FIG. 1.7. Energy E_n versus longitudinal wavevector k_y from Eq. 1.3.3 at the bottleneck of a QPC assuming a parabolic confinement potential. The 1D subbands are separated by $\hbar\omega_0$. A net current results from the uncompensated occupied electron states in the interval between μ_1 and μ_2 , the electro chemical potentials of the two wide 2DEG reservoirs.

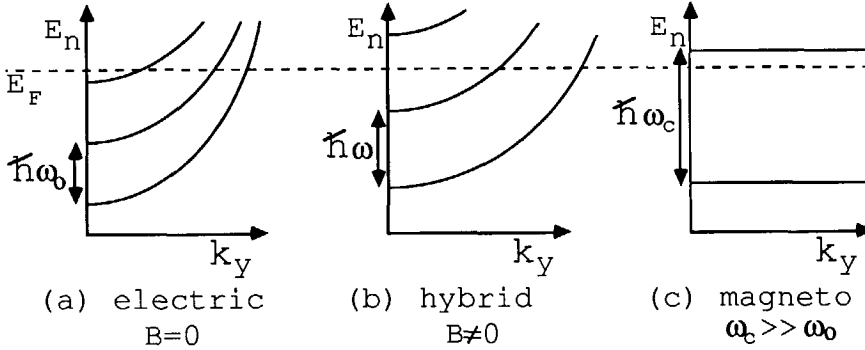


FIG. 1.8. 1D subband dispersion for three values of the magnetic field, illustrating magnetic depopulation. The energy splitting is electric ($\hbar\omega_0$) in (a), and hybrid ($\hbar\omega$, with $\omega^2 = \omega_0^2 + \omega_c^2$) in (b). For large magnetic fields (c) the 1D subbands are Landau levels with an energy splitting of $\hbar\omega_c$.

$E_N(k_y = 0) < E_F$. The 1D spin-degenerate density of states is: $dN_N/dE = 2/\pi \cdot (dE_N/dk_y)^{-1}$. The important aspect of 1D transport is the cancellation of the energy dependence in the product of velocity and density of states: $(dN_N/dE) \cdot v_n = 4/h$. For small voltages ($eV \ll E_F$), one can take $T_n(E) = T_n(E_F)$. Substituting in Eq. 1.3.4, one finds for the conductance $G = I/V = eI/(\mu_1 - \mu_2)$:

$$G = \frac{2e^2}{h} \sum_{n=1}^N T_n(E_F) \quad (1.3.5)$$

Eq. 1.3.5 is known as the 2-terminal Landauer formula.²⁸ If no backscattering takes place, so $\sum_{n=1}^N T_n(E_F) = N$, Eq. 1.3.5 reduces to:

$$G = \frac{2e^2}{h} N \quad (1.3.6)$$

demonstrating that each occupied subband contributes $2e^2/h$ to the conductance. The subbands are sometimes called 1D current channels to emphasize that each channel carries the same amount of current.

In the experiment, a decreasing V_g increases the barrier in the QPC, and simultaneously increases the lateral confinement and consequently the energy splitting $\hbar\omega_0$. Both effects increase the subband energies. As long as E_F is between two subband bottoms, N is constant and G is quantized. If a subband bottom moves through E_F , N changes by 1 and G by $2e^2/h$.

Several numerical calculations²⁹ have shown that Eq. 1.3.6 gives an accurate description of a QPC with the assumptions that impurity scattering is absent and that the potential variations are smooth. Sharp potential variations, possibly present at the entrance and exit of the QPC³⁰ or originating from donor impurities,^{31,32} can give rise to backscattering and destroy the quantization. The assumption of an adiabatic constriction in Eq. 1.3.2 is then no longer valid. At $T > 0$ the reservoirs inject electrons with a Fermi-Dirac distribution, which averages the conductance: $G(T) = \int (-\partial f / \partial E) \cdot G(T=0) \cdot dE$. Comparing this with the temperature dependence of the curves in Fig. 1.6, we found that the subband separation $\hbar\omega_0$ gradually increases from about 1 meV at $V_g = -1$ V to 3 meV at $V_g = -2.1$ V. This illustrates that thermal averaging has a stronger effect on the higher plateaus, as observed in Fig. 1.6.

1.4 DEPOPULATION OF 1D MAGNETO-ELECTRIC SUBBANDS

We now turn to the case of a finite 2DEG with an applied magnetic field in the z -direction. In the Hamiltonian of Eq. 1.3.2, the magnetic field B is incorporated by substituting $(\mathbf{p} - e\mathbf{A})$ for the momentum \mathbf{p} . In the Landau gauge for the vector potential $\mathbf{A} = A_y = Bx$, the Schrödinger equation is once again that of a harmonic oscillator, but now with energy eigenvalues:²⁷

$$E_n = (n - \frac{1}{2})\hbar\omega + \frac{\hbar^2 k_y^2}{2m_B} \quad (1.4.1)$$

describing *hybrid magneto-electric subbands*. With $\omega^2 = \omega_o^2 + \omega_c^2$ and the cyclotron frequency $\omega_c = eB/m^*$, the energy separation $\hbar\omega$ is now a combination of the electrical confinement and the magnetic field. $m_B = m^*\omega^2/\omega_o^2$ is a magnetic field dependent effective mass yielding a smaller dispersion for larger magnetic fields. The influence of the magnetic field on the subband dispersion is shown schematically in Fig. 1.8. For $B = 0$ the subbands are determined by the electrical confinement only. A small magnetic field increases the subband splitting and reduces the dispersion. For large magnetic fields, the subbands have the magnetic energy separation $\hbar\omega_c$ and a vanishing dispersion. In this case, the subbands are the well-known Landau levels. It can be seen from Fig. 1.8 that on increasing the magnetic field, the number of occupied subbands decreases. This process is known as the *depopulation of magneto-electric subbands*.

One can show that the velocity and density of states also cancel in a magnetic field and that Eqs. 1.3.5 and 1.3.6 are still valid.^{33,34} *The conductance quantization is therefore independent of the nature of the subbands.* From the above analysis it follows that a gradual transition exists between the quantized conductance $G = N \cdot 2e^2/h$ at zero magnetic field (with N the number of

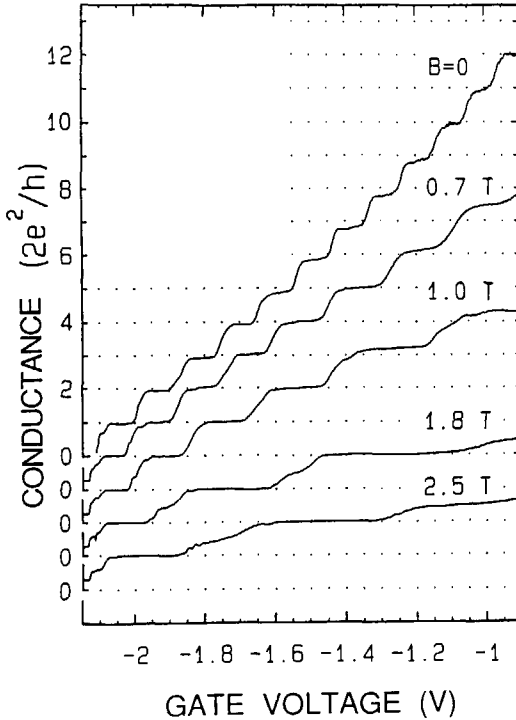


FIG. 1.9. QPC conductance versus gate voltage at 0.6 K for several values of magnetic field. The broadening of the plateaus demonstrate the increasing energy splitting in a magnetic field. The curves have been offset for clarity (from Ref. 34).

occupied electric subbands in Fig. 1.8a) to $G_H = N_L \cdot 2e^2/h$ at a high magnetic field (with N_L the number of occupied Landau levels in Fig. 1.8c), which is known as the quantum Hall conductance.

So far we have adopted a parabolic confining potential. We note however, that this choice does not affect the general conclusions, such as the cancellation of velocity with the density of states, and the conductance quantization at zero and non-zero magnetic field.

Fig. 1.9 shows the conductance of a QPC versus gate voltage for several values of the magnetic field.³⁴ As can be seen, the quantization is preserved in a magnetic field. Above $B = 1$ T, spin-resolved plateaus develop at odd multiples of e^2/h . The depopulation can be seen from the fact that at a fixed gate voltage, the number of plateaus (or, equivalently, the number of occupied subbands), decreases with increasing magnetic field. Several papers have reported a quantitative fitting of the depopulation of subbands and reasonable agreement was found for different models for the confining potential.^{27,35} From the measurements of Fig. 1.9, we deduced subband splittings $\hbar\omega_0$ of about 1 meV at $V_g = -1$ V and 3 meV at $V_g = -2$ V, in agreement with the values obtained from the temperature dependence of the plateaus mentioned earlier.²⁵ A third independent way to determine the subband splittings is by measuring the non-linear transport properties of a QPC, from which we have found similar values.³⁶

The transport properties of different kinds of single QPCs have been studied extensively experimentally as well as theoretically, and are quite well understood (see the review by van Houten, Beenakker, and van Wees in Ref. 13). In the remaining part of this review, QPCs will be used to study electron transport in a 2DEG. By using one QPC as an injector of electrons in the 2DEG and a second as a collector, one is able to study the electron motion between the injector and detector, especially related to scattering processes.

1.5 ELECTRON MOTION IN A MAGNETIC FIELD

In the previous section, we discussed the influence of a magnetic field on the subband dispersion in momentum space. We consider now the electron motion in real space, which yields a simple physical picture of the QHE and associated effects. To elucidate the quantized electron motion in a high magnetic field, we first discuss the classical motion in a small magnetic field.

1.5.1 Electron Focusing

In the absence of an electric field E , the balance of the Lorentz force $F_L = e\mathbf{v} \times \mathbf{B}$ and the

centripetal force $F = m^* v^2 / r$ leads to a *cyclotron motion* of the electrons, with (at the Fermi energy) a cyclotron radius $r_c = m^* v_F / eB$ and angular frequency $\omega_c = eB / m^*$ (see Fig. 1.10a). When the electric field $E = -\nabla V(x, y) \neq 0$, the electrons have a net drift velocity $v_D = E / B$. At the boundary of the sample, where E is large, the collisions at the boundary result in *skipping orbits*. The skipping electrons have a net velocity along the boundary of the sample, and the velocity direction is opposite for the two opposite edges (see Fig. 1.10a).

The skipping orbit motion of electrons along a 2DEG boundary in a small magnetic field has been observed in an electron focusing experiment by van Houten et al.³⁷ The geometry of Fig. 1.4b with two adjacent QPCs with a separation of $L = 3 \mu\text{m}$ was used, where one QPC injects electrons into the 2DEG and the second QPC is used as a collector. The injected electrons are focused by the magnetic field on the boundary at distances $p \cdot 2r_c$ ($p = 1, 2, \dots$) from the injector. Focusing into the collector occurs when $p \cdot 2r_c = L$. In the experiment the collector voltage is measured as a function of magnetic field B . From the condition $p \cdot 2r_c = L$ it follows that the largest number of electrons reaches the collector when $B_{foc} = p \cdot 2m^* v_F / eL$ which leads to periodic oscillations in the collector signal. This is shown in Fig. 1.11 for 4 different temperatures. The arrows indicate the expected focusing fields, which are in agreement with the measurements up to about the eighth focusing peak. The focusing experiment demonstrates that the collisions at the boundary are highly specular, since diffusive boundary scattering would

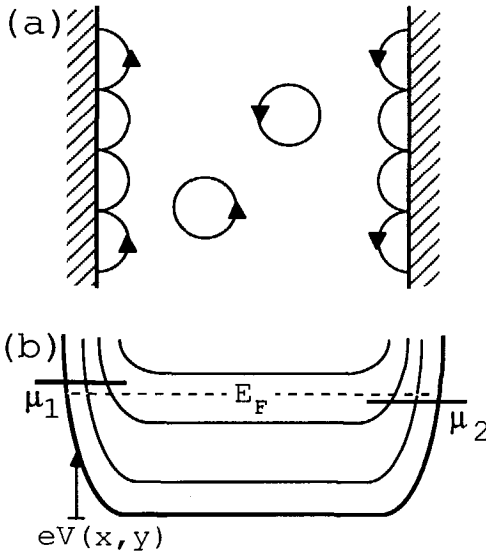


FIG. 1.10. (a) Schematic representation of the classical electron motion in a magnetic field.

(b) Corresponding quantum picture of the energy states of Eq. 1.5.1 along a cross-section of the 2DEG, illustrating the formation of edge channels at the boundary of the 2DEG [formed by the electrostatic potential energy $eV(x, y)$] where the Landau levels intersect the Fermi energy E_F .

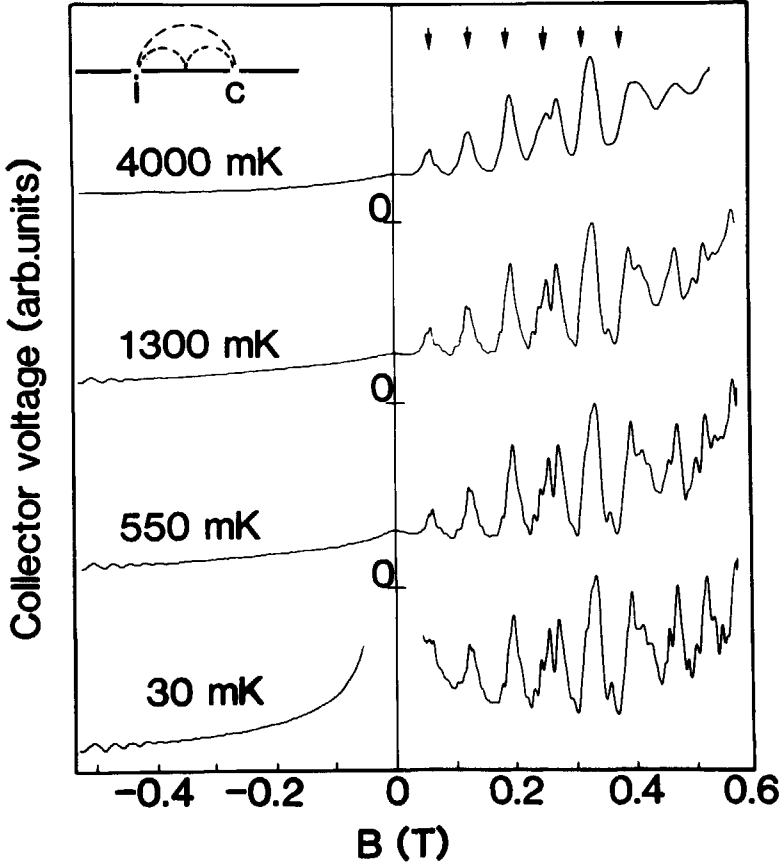


FIG. 1.11. Collector voltage versus magnetic field B , demonstrating the focusing of skipping electron orbits from injector to collector, as illustrated in the inset. The arrows indicate the expected focusing fields (from Ref. 37).

average the oscillations.³⁸ For negative magnetic fields, no focusing oscillations are observed, because the electrons are deflected away from the collector. The small oscillations seen for $B < 0$ at lower temperatures are Shubnikov-de Haas oscillations. At lower temperatures additional finestructure appears, which is explained by taking into account quantum interference effects between trajectories being injected at different angles.³⁷

1.5.2 Edge Channels

In a high magnetic field the electron motion is quantized. The flux ϕ enclosed by an electron in a cyclotron orbit equals an integer times the flux quantum $\phi_0 = h/e$, and the quantized electron energies are:

$$E_n = (n - \frac{1}{2})\hbar\omega_c + eV(x,y) \quad (1.5.1)$$

where $n = 1, 2, \dots$ is the spin-degenerate Landau level index, and we have ignored the Zeeman energy splitting $\pm \frac{1}{2} g\mu_B B$. We assume that the electro static potential $V(x,y)$ is flat in the interior of the sample and rises at the boundary. Electro static variations due to impurities are ignored, because we are dealing with ballistic samples. Fig. 1.10b shows schematically the Landau energy levels of Eq. 1.5.1. The electron states at the left boundary are occupied up to μ_1 , the electro chemical potential of the current source, and at the right boundary up to μ_2 , the electro chemical potential of the current sink (see Fig. 1.2b). The velocity v_n is proportional to the slope $\partial E_n / \partial x$, so that at the two sample boundaries, the electron states have opposite velocity directions, similar to the classical case of Fig. 1.10a.

The relevant electron states for linear transport are only those at the Fermi energy. As can be seen, these are located at the sample boundaries, where the Landau levels intersect the Fermi energy ($E_n = E_F$), and they extend in the direction perpendicular to the cross-section of Fig. 1.10b. The intersections are the current-carrying states, which are known as *edge channels*.^{33,39,40} The net current I only results from the uncompensated states in the interval between μ_1 and μ_2 . (The total current due to the states below μ_2 is zero.) The transport through edge channels is 1D.³³ Edge channels can therefore also be viewed as 1D current channels, each carrying a current $I_n = 2e/h \cdot (\mu_1 - \mu_2)$. With the Hall voltage $V_H = (\mu_1 - \mu_2)/e$ measured between the two sample boundaries, this directly gives the quantized Hall conductance $G_H = N_L \cdot I_n / V_H = N_L \cdot 2e^2/h$.

So far we have ignored all scattering processes. Büttiker⁴¹ pointed out that due to the spatial separation of the electron states with opposite velocity, *backscattering* requires scattering from one sample boundary to the other. Backscattering is therefore suppressed when the edge states between μ_1 and μ_2 are not connected by extended electron states. This is the case in Fig. 1.10b, where the Fermi energy is between two bulk Landau levels. (In the classical picture of Fig. 1.10a, backscattering is suppressed when $r_c \ll l_e$.⁴¹) In the next section we discuss the suppression of *forward scattering* which involves transitions between edge channels at the same

boundary.

The location of edge channels follows from the condition $E_F = E_n$ yielding:

$$E_G = eV(x,y) = E_F - (n - \frac{1}{2})\hbar\omega_c \quad (1.5.2)$$

E_G is referred to as the *guiding center energy*. Eq. 1.5.2 implies that edge channels at the same boundary but with a different Landau level index n are separated in the transverse direction and follow different equipotentials along the boundary. Edge channels with larger n follow a lower equipotential (see for instance that the $n = 2$ edge channel in Fig. 1.10b is located at a lower potential $eV(x,y)$ compared to the $n = 1$ edge channel).

1.5.3 Quantized Longitudinal Conductance

QPCs can be used as selective edge channel transmitters by means of their controllable barrier height E_B . The barrier reflects the n -th edge channel if $E_B > E_G(n)$. This is equivalent to saying that at the barrier the Landau level energy E_n is above the Fermi energy E_F , so this level is unoccupied. From $E_B = E_B(V_g)$ and $E_G = E_G(B)$ it follows that the number N of transmitted channels can be changed by varying the gate voltage V_g or the magnetic field B . If T is the partial transmission of the uppermost edge channel, the 2-terminal conductance G of a QPC is given by:

$$G = \frac{2e^2}{h} (N + T) \quad (1.5.3)$$

Quantization of the 2-terminal conductance therefore occurs in those intervals of B and V_g where $T = 0$. One can also define a 4-terminal conductance of a QPC. Fig. 1.12 shows schematically a QPC defined in a 2DEG to which 6 Ohmic contacts are attached. A magnetic field is applied such that M (spin-degenerate) edge channels are occupied in the bulk 2DEG regions of which N are transmitted through the QPC. The Fermi energy is assumed to be between two Landau levels so that no backscattering occurs in the bulk 2DEG regions. We define the 4-terminal conductance by $G_{12,34}$ denoting that the net current $I = N \cdot 2e/h \cdot (\mu_1 - \mu_2)$ flows from contact-1 to 2 and the voltage is measured between contacts-3 and 4: $G_{12,34} = eI/(\mu_3 - \mu_4)$. To calculate $G_{12,34}$ we note that the voltage contacts-3 to 6 do not draw a net current and, as can be seen in Fig. 1.12, contact-5 is in equilibrium with current contact-1 ($\mu_5 = \mu_1$), and similarly contact-4 with 2 ($\mu_4 = \mu_2$). (Note that $G_{12,12} = G_{12,54}$ implying that a 2-terminal conductance can be measured by using actually 4 contacts.) The incoming current I_{in} in contact-3 is the sum of the contributions

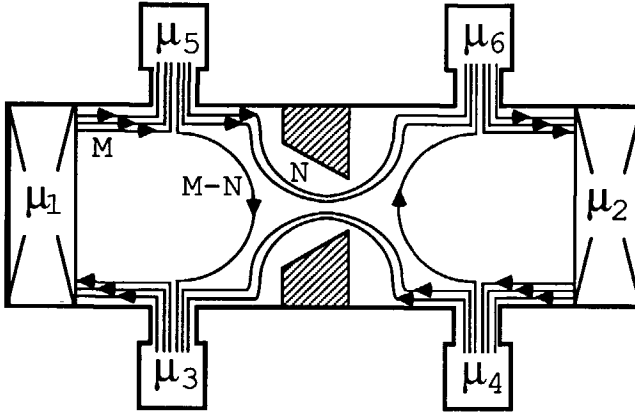


FIG. 1.12. Sample geometry with contiguously quantized regions. In the bulk 2DEG M edge channels are occupied, of which N are transmitted through the QPC and $(M - N)$ are reflected.

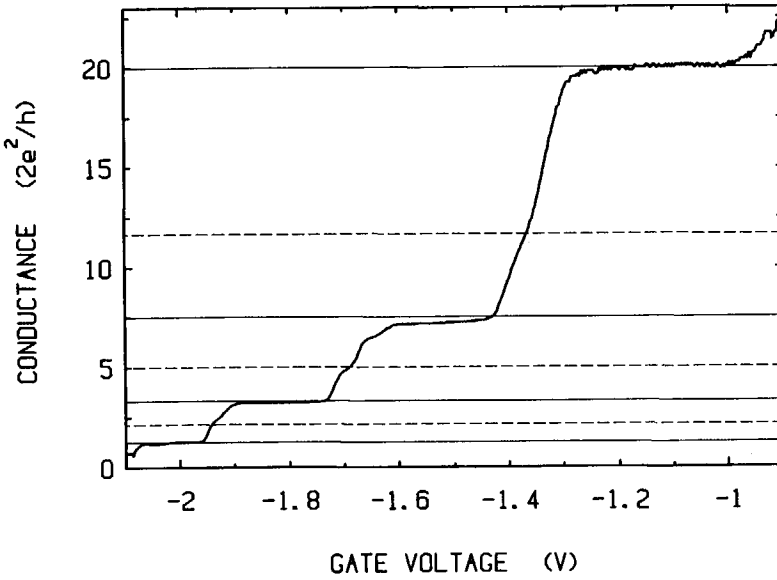


FIG. 1.13. Quantized longitudinal conductance versus gate voltage at 0.6 K defined as $G_{12,34}$ in the geometry of Fig. 1.12. In the bulk $M = 5$ edge channels are occupied ($B = 1.43$ T). On decreasing the gate voltage, the number N of transmitted channels decreases from 4 to 1, resulting in quantized plateaus in accordance with Eq. 1.5.4 at values 20 , $7\frac{1}{2}$, $3\frac{1}{3}$, and $1\frac{1}{4}$ times $2e^2/h$, indicated by the solid lines. The dashed lines indicate the expected values for spin-resolved plateaus.

of all incoming edge channels: $I_{in} = 2e/h \cdot \{N \cdot \mu_2 + (M - N) \cdot \mu_1\}$. Contact-3 will adjust its electrochemical potential μ_3 such that the outgoing current $I_{out} = M \cdot 2e/h \cdot \mu_3$ equalizes I_{in} . From $I_{in} = I_{out}$ it follows $\mu_3 = \{(M - N) \cdot \mu_1 + N \cdot \mu_2\}/M$. With $\mu_3 - \mu_4 = \frac{M - N}{M} \cdot (\mu_1 - \mu_2)$ one finds for the 4-terminal conductance:

$$G_{12,34} = \frac{2e^2}{h} \frac{MN}{M - N} \quad (1.5.4)$$

It is interesting to note that if a transmission probability is defined as $T = N/M$, Eq. 1.5.4 can be written as $G_{12,34} = M \cdot 2e^2/h \cdot T/(1 - T)$, which is reminiscent of the original Landauer formula.²⁸ It is easy to show that the Hall conductance $G_{12,35}$ still corresponds to the number of occupied Landau levels in the bulk: $G_{12,35} = M \cdot 2e^2/h$, despite the backscattering of $(M - N)$ edge channels. In standard QHE measurements $G_{12,34}$ is denoted as the longitudinal conductance containing the Shubnikov-de Haas oscillations. However, Eq. 1.5.4 implies that a longitudinal conductance quantization can occur at non-integer multiples of $2e^2/h$, simultaneously with a quantized Hall conductance.

Experiments on the quantized longitudinal conductance were reported first by Haug et al.⁴² and Washburn et al.⁴³. In Fig. 1.13, we show a measurement of $G_{12,34}(V_g)$ for $B = 1.43$ T where $M = 5$ (spin-degenerate). The longitudinal conductance displays plateaus at non-integer values of $2e^2/h$, in accordance with Eq. 1.5.4.

The above description of transport in the quantum Hall effect (QHE) regime in terms of edge channels, known as the Landauer-Büttiker formalism, is reviewed in Ref. 13. A more general derivation than given above can be obtained from Büttiker's multi-probe formula, which also gives reciprocity relations for reversal of the magnetic field.⁴⁴

1.6 ANOMALOUS INTEGER QUANTUM HALL EFFECT

The edge channel description gives an appealing physical picture of the QHE. However, the experiments described in this paper so far do not give direct evidence for the existence of edge channels. For instance, the quantized longitudinal conductance can also be explained by considering contiguous regions of different electron densities and Kirchoff's law for adding voltages⁴⁵ (note that $1/G_{12,34} = 1/G_{12,12} - 1/G_{12,35}$). Moreover, the previous experiments do not give any information about scattering between edge channels. In this section, we discuss an experiment involving two adjacent QPCs which directly probes the transport through a particular edge channel.

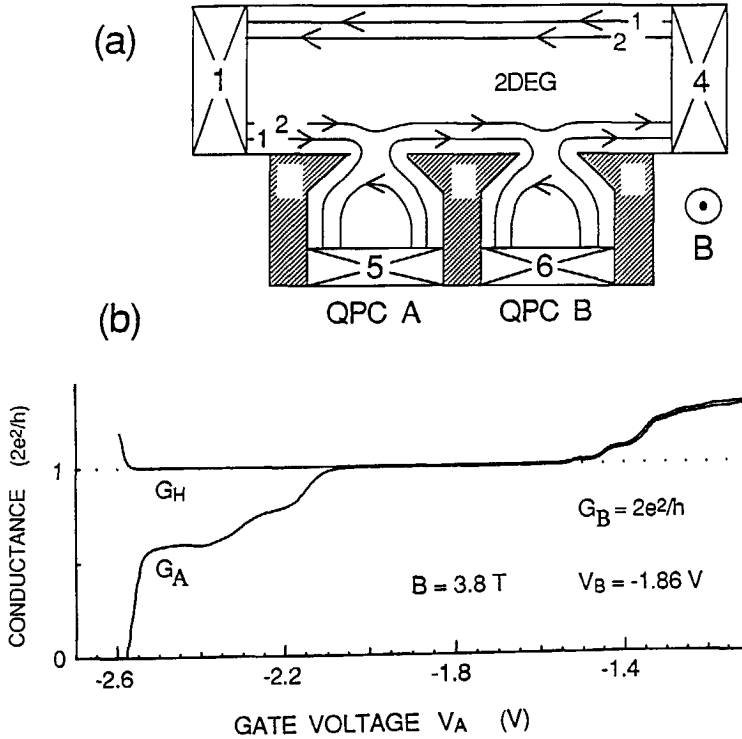


FIG. 1.14. (a) Geometry used to observe an anomalous quantization of the Hall conductance, for which QPC A is used as current probe and QPC B as voltage probe. (b) Comparison between the Hall conductance G_H and the 2-terminal conductance of the current probe G_A . The voltage probe conductance is kept fixed at $G_B = 2e^2/h$. Although the number of occupied Landau levels in the 2DEG is unchanged, G_H follows the largest probe conductance (from Ref. 46).

In section 1.5 we discussed the electron focusing from one QPC to an adjacent second QPC by small magnetic fields ($B < \sim 1$ T). These fields are too small to quantize the electron motion, and the focusing can be explained in terms of classical cyclotron motion. We consider now the same geometry in the high field regime ($B > \sim 1$ T). Fig. 1.14a shows schematically two adjacent QPCs A and B defined in a 2DEG with an applied magnetic field such that two edge channels are occupied. The 2-terminal conductances G_A and G_B of the individual QPCs measure the number

of transmitted channels and are given by Eq. 1.5.3. The Hall conductance G_H is normally thought to be independent of the characteristics of the current and voltage probes and to correspond directly to the number of occupied (spin-degenerate) Landau levels N_L in the 2DEG: $G_H = N_L \cdot 2e^2/h$. However, if QPC A in Fig. 1.14a is used as a current probe and QPC B as a voltage probe, one can obtain an anomalous quantization of the Hall conductance.⁴⁶

The edge channels shown in Fig. 1.14a are assumed to be independent, i.e. no scattering events occur among different channels or, equivalently, electrons travel with conservation of quantum-subband-number. In this case the transport is *adiabatic*. The edge channels are occupied up to the electro chemical potential of the last Ohmic contact they have left. (We assume ideal Ohmic contacts, meaning that all incoming electrons are absorbed and all outgoing states are occupied up to the same electro chemical potential.) Consequently, in the region between the two QPCs, the two edge channels have an unequal population. Channel-2 is occupied up to μ_1 , while current probe 5 populates channel-1 up to μ_5 . This process is called *selective population of edge channels*. If the voltage probe B detects all edge channels like an ideal Ohmic contact, the regular quantum Hall conductance is measured. However, this is not the case in Fig. 1.14a where the voltage probe *selectively detects* only the first channel. The second channel is neither populated by the current probe nor detected by the voltage probe and, therefore, does not contribute to the Hall conductance. The Hall conductance $G_{54,61}$ equals $2e^2/h$ instead of $4e^2/h$ which a regular Hall measurement would give. In general one can show that in the *absence of inter-edge channel scattering* the Hall conductance is given by:⁴⁶

$$G_H = \max (G_A, G_B) \quad (1.6.1)$$

implying that G_H is completely determined by the characteristics of the probes and is independent of the number of occupied Landau levels in the 2DEG.

Fig. 1.14b compares the measured probe conductances G_A and G_B with the Hall conductance G_H . The magnetic field is kept fixed at 3.8 T, corresponding to $N_L = 2$. The voltage on QPC B, defining the voltage probe, is also fixed such that only the first edge channel is transmitted, and therefore $G_B = 2e^2/h$. The voltage V_{gA} on QPC A, defining the current probe, is varied, resulting in a decreasing G_A in accordance with Eq. 1.5.3. Again we note that a normal Hall measurement would give a constant conductance $G_H = 4e^2/h$. However, Fig. 1.14b shows a Hall conductance which virtually follows the largest probe conductance in agreement with Eq. 1.6.1 (for $V_{gA} > -1.5$ V, $G_H = G_A > 2e^2/h$; for -2.1 V $< V_{gA} < -1.5$ V, $G_H = G_A = G_B = 2e^2/h$

corresponding to the edge channel flow of Fig. 1.14a; and for $V_{gA} < -2.1$ V, $G_H = G_B = 2e^2/h$). *The experiment demonstrates that QPCs can be used to selectively populate or detect edge channels and that on short distances of order μm the transport through edge channels is adiabatic.* Subsequent experiments have shown that a non-equilibrium population can persist up to larger distances (several tens of μm 's).⁴⁷ In particular, it is found that the topmost channel is virtually decoupled from the lower edge channels even over macroscopic distances of several times $100\ \mu\text{m}$.⁴⁷⁻⁵¹ These experiments have clarified the important role of measurement probes in the QHE regime. Moreover, it has become clear that *a local description in terms of a conductivity tensor is not appropriate to describe transport in the QHE regime.* The fact that a non-equilibrium population can persist even over macroscopic distances shows that a non-local description should be used, which includes the properties of the entire sample, conductor and measurement probes. This is naturally incorporated in the Landauer-Büttiker formalism. A combined local/non-local description has been proposed by McEuen et al.⁵¹ which agrees well with non-equilibrium experiments in macroscopic samples.

Recent theoretical⁵²⁻⁵⁴ and experimental^{55,56} work has suggested that a transport description in terms of edge channels may also be valid in the fractional QHE regime. With a geometry similar to that of Fig. 1.14a, one can measure a fractional QHE, while the 2DEG has an integer filling factor.⁵⁶ The value of the fractional quantization corresponds directly to the probe characteristics, which can be explained if one assumes the existence of *fractional edge channels*. However, the origin of these fractional edge channels is still controversial, partially due to the rather complicated many-body origin of the fractional QHE.

1.7 TRANSITION FROM OHMIC TO ADIABATIC TRANSPORT

In section 1.5 and 1.6 we discussed the transport between two adjacent QPCs. In a small magnetic field electron focusing is observed, and in a high field an anomalous QHE due to selective population and detection of edge channels. Similar effects occur in a configuration of two QPCs in series, however, reflected differently in the conductance. We show in this section that the series configuration may be used to investigate how and when adiabatic transport is established.⁵⁷

1.7.1 Transport through two QPCs in series

Fig. 1.15 shows a SEM photograph and a schematic layout of a sample with two QPCs in

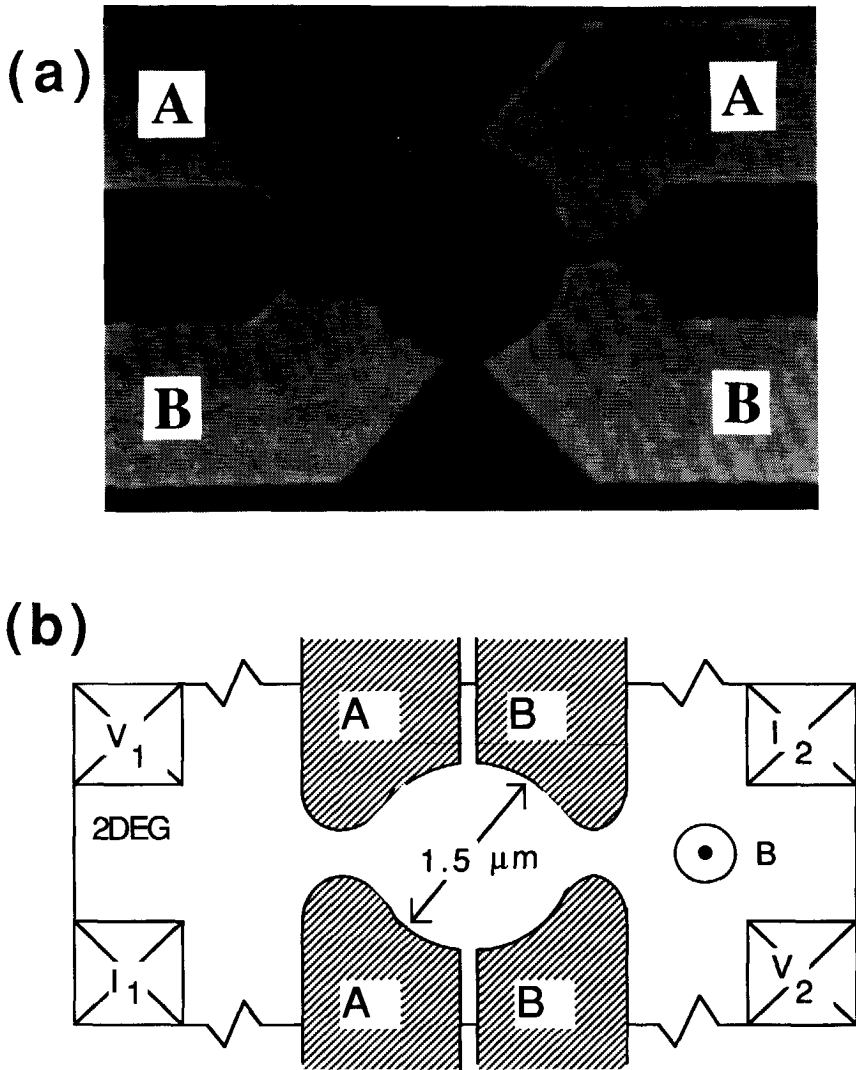


FIG. 1.15. SEM photograph (a) and schematic layout (b) of two gate pairs A and B, which define in the 2DEG two 300 nm wide QPCs, connected by a dot-shaped cavity with a diameter of $1.5 \mu\text{m}$.

series connected by a dot-shaped cavity with a diameter of 1.5 μm . The electron density of the ungated 2DEG is $2.3 \cdot 10^{15} \text{ m}^{-2}$ in this sample. The dot is built up from two pairs of gates A and B. Application of a negative voltage to only one pair of gates and zero-voltage to the other pair defines a single QPC. This allows the measurements of the conductances G_A and G_B of the individual QPCs as well as the conductance G_{ser} of the two QPCs in series. The narrow side channels, which separate the two gate pairs, are immediately pinched-off when the dot is formed in the 2DEG.

To describe the transport through the QPCs in series, we distinguish three regimes. If the occupation of the electron states equilibrates in the dot, G_{ser} is just the Ohmic addition of G_A and G_B :

$$\frac{1}{G_{ser}} = \frac{1}{G_A} + \frac{1}{G_B} \quad (1.7.1)$$

We call this the *Ohmic transport regime*. For the equilibration it is sufficient that the right- and left-going states in the dot are equally occupied, but not necessarily in the lowest available energy states. This equilibrium can be established by elastic scattering only. We expect Ohmic transport to occur in our structure when the magnetic field is zero. To illustrate this, a typical electron trajectory is shown in Fig. 1.16a for $B = 0$. The electron feels a completely different boundary between two collisions. The boundary is therefore not smoothly varying compared to the electron motion at $B = 0$. After a few collisions the electron has lost its direction memory and the probability to escape through QPC A is just: $G_A/(G_A + G_B)$ and equivalently through QPC B: $G_B/(G_A + G_B)$, resulting in the Ohmic addition for G_{ser} . An enhanced series conductance at $B = 0$ can occur due to beam collimation which we discuss below.

The second, intermediate regime is characterized by the absence of backward scattering and perfect equilibration in the forward direction. This means that the right-going states in the dot are in mutual equilibrium as are the left-going states. However, the right-going states do not equilibrate with the left-going states. In this case, the series conductance is given by:⁵⁸

$$\frac{1}{G_{ser}} = \frac{1}{G_A} + \frac{1}{G_B} - \frac{1}{M \cdot 2e^2/h} \quad (1.7.2)$$

where M is the number of subbands in the dot. Eq. 1.7.2 implies that with a finite number M of subbands in the dot, the series conductance is enhanced above the Ohmic value of Eq. 1.7.1. As mentioned before, suppression of backscattering occurs for $B \neq 0$ when the right- and left-going

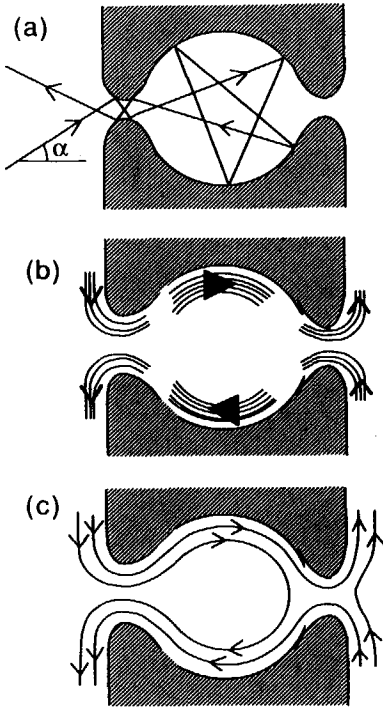


FIG. 1.16. Electron transport through the dot at different values of magnetic field B . (a) At $B = 0$ scattering in the dot equilibrates the electron states resulting in Ohmic transport. (b) At small B , backscattering is suppressed but forward scattering is not. (c) At high B , the edge channels are decoupled and scattering is absent, resulting in adiabatic transport.

states are separated at opposite sample boundaries, roughly taking place when twice the cyclotron radius r_c becomes smaller than the diameter of the dot. In our structure this occurs when $B > \sim 0.1$ T. The motion along one boundary can still be non-adiabatic, when the shape of the boundary changes strongly over a distance r_c . In quantum mechanical terms, the edge channels at one boundary overlap strongly and even small irregularities bring them in mutual equilibrium (see Fig. 1.16b). Let N_A, N_B denote the number of occupied subbands in the two QPCs. Due to the separation of right- and left-going states, an electron injected by QPC A will have a probability N_B/M to escape immediately through QPC B. Thereafter it has a smaller probability to escape through QPC A, which is equal to $(1 - N_B/M) \cdot (N_A/M)$. The second probability to escape through QPC B is accordingly smaller, etc. This difference in escape probability is the origin of the correction term in Eq. 1.7.2 compared to Eq. 1.7.1.

The third regime is the adiabatic transport regime, where there is neither forward nor backward scattering. In this case, none of the states equilibrate, and the electrons travel through the entire device with conservation of quantum-subband-number. The transport is now

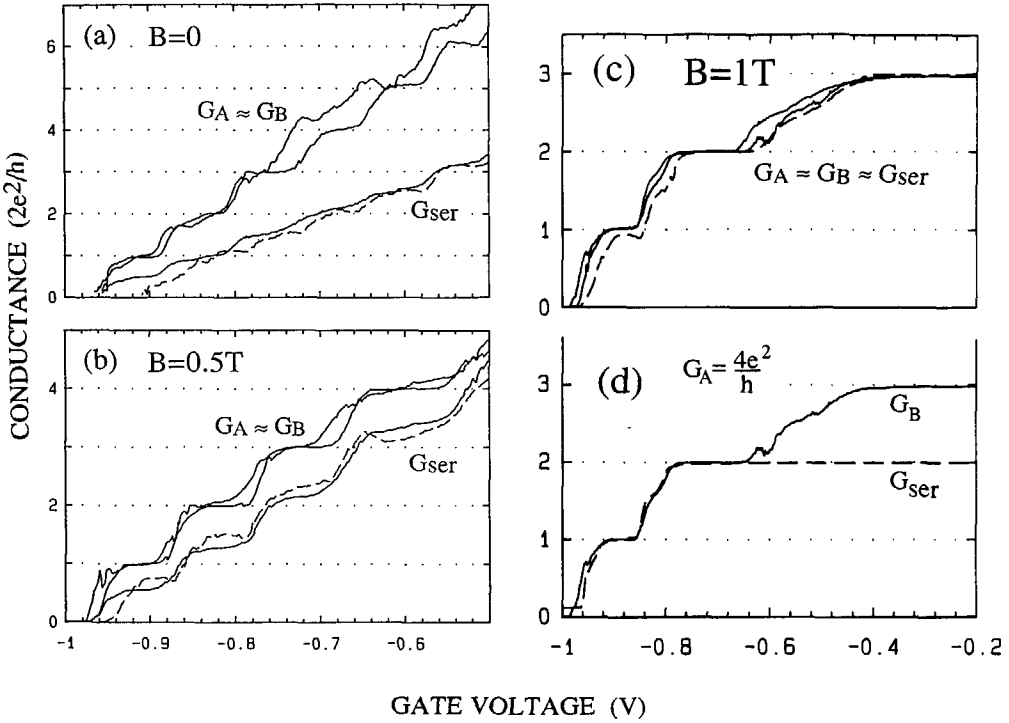


FIG. 1.17. Comparison of individual QPC conductances G_A and G_B with the series conductance G_{ser} (dashed lines) at 0.6 K for different values of magnetic field B . (a) G_{ser} is roughly half $G_A \approx G_B$ at $B = 0$ indicating Ohmic transport. The lower solid line is calculated from Eq. 1.7.1. (b) G_{ser} is larger than half $G_A \approx G_B$ at $B = 0.5 T$ indicating suppression of backscattering in the dot. The lower solid line is calculated from Eq. 1.7.2 (see text). (c) $G_{ser} \approx G_A \approx G_B$ at $B = 1 T$ demonstrating adiabatic transport. (d) In this case, $G_A = 4e^2/h$ is fixed, and G_B is changed. G_{ser} equals the smallest QPC conductance in accordance with Eq. 1.7.3.

determined by the bottleneck of the system in the sense that those electrons which can pass the highest barrier in the circuit can also pass the other barriers. G_{ser} is therefore determined only by the smallest conductance of the individual QPCs:

$$G_{ser} = \min (G_A, G_B) \quad (1.7.3)$$

Comparing Eqs. 1.7.1, 1.7.2 and 1.7.3 illustrates that if the amount of scattering is reduced, the series conductance increases accordingly. Obviously, the adiabatic regime is obtained when a high magnetic field is applied, so that the edge channels do not overlap, as illustrated in Fig. 1.16c. Besides the absence of backscattering, forward scattering is also completely suppressed, and Fig. 1.16c shows that the smallest QPC conductance determines the series conductance.

We show now experimentally that the different transport regimes correspond to different values of the magnetic field. Fig. 1.17 displays the conductances of the individual QPCs and the series conductance (dashed line) as a function of their corresponding gate voltages for three values of the magnetic field. At $B = 0$ (see Fig. 1.17a), G_{ser} is about half of the nearly equal QPC conductances $G_A \approx G_B$ indicating that we have Ohmic transport. A quantitative comparison is made by calculating G_{ser} from the measured G_A and G_B substituted in Eq. 1.7.1 and is shown by the lower solid line. Fig. 1.17b shows that at a small magnetic field of 0.5 T the series conductance is enhanced above the Ohmic value (G_{ser} is larger than half the QPC conductances.) The lower solid line is now calculated using Eq. 1.7.2 where we have taken $M = 5$, the expected number of occupied Landau levels in the dot. The agreement indicates that at $B = 0.5$ T backscattering is suppressed, but forward scattering is not. At $B = 1$ T, the transport is adiabatic. Fig. 1.17c shows that the series conductance is equal to the single QPC conductances. For a more striking demonstration of adiabatic transport, G_{ser} is measured with fixed $G_A = 4e^2/h$ and changing G_B . As can be seen in Fig. 1.17d, G_{ser} almost exactly follows the smallest QPC conductance, in accordance with Eq. 1.7.3 (for $V_{gB} > -0.65$ V, $G_{ser} = G_A = 4e^2/h$; for -0.75 V $< V_{gB} < 0.65$ V, $G_{ser} = G_A = G_B = 4e^2/h$; for $V_{gB} < -0.75$ V, $G_{ser} = G_B < 4e^2/h$).

The observation of a series conductance equal to the smallest conductance in the circuit is a striking consequence of quantum adiabatic transport. The fact that adiabatic transport occurs for $B > 1$ T is related to the geometry of our structure. Glazman and Jonson⁵⁹ have derived general conditions for the magnetic field above which adiabatic transport occurs in relation to the shape of the sample boundary.

We have not treated the situation here where both QPCs only partially transmit a certain edge channel. In this case, a 1D edge channel loop is formed in the dot in which 0D-states arise. These 0D-states have been observed at very low temperatures of about 10 mK and are described in detail in Ref. 60.

1.7.2 Electron-Beam Collimation and Electron Focusing in a Dot

In the first experiment on two QPCs in series, Wharam et al.⁶¹ found that in their structure at $B = 0$, the series conductance was enhanced about 40 % above the Ohmic value. Beenakker and van Houten⁵⁸ attributed this enhancement to collimation of the electrons in a beam. Strikingly, their classical model, which treats electrons as billiard balls, can describe a range of transport effects occurring in small conductors in which quantum effects were expected to be important.⁶² To illustrate the collimation of an electron-beam, Fig. 1.18 shows some typical trajectories for a constriction with sharp corners and one with smooth corners. The sharp-cornered constriction transmits the electrons from all incoming angles. The angular distribution function $P(\alpha)$ of the outgoing electrons is isotropic. The smooth-cornered constriction, in contrast, reflects electrons coming in with a large angle. The corresponding distribution function $P(\alpha)$ shows an enhanced number of electrons emitted in the forward direction. This collimation becomes stronger if a potential barrier is present in the constriction.⁵⁸ To observe the electron-beam collimation, a magneto-conductance experiment was performed by Molenkamp et al.⁶³ with one QPC forming the electron-beam and a second oppositely-placed QPC detecting the electrons transmitted directly through both QPCs. This set-up is illustrated in Fig. 1.19a for the dot device. Due to the collimation (with beam angle Δ) a fraction T_d of the electrons is transmitted directly through both QPCs, resulting in an enhanced series conductance above the Ohmic value. A small magnetic field B deflects the beam along the detecting QPC, thereby decreasing the number of directly

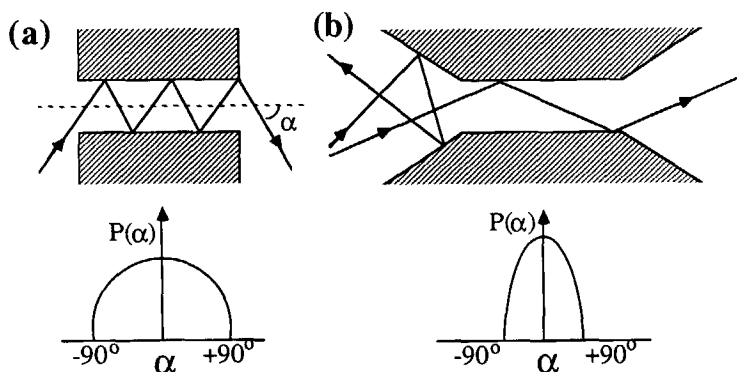


FIG. 1.18. Illustration of electron-beam collimation by a smooth constriction. The angle distribution function $P(\alpha)$ shows an enhanced number of electrons emitted in the forward direction.

transmitted electrons, and accordingly the series conductance. The electron-beam is deflected just beside the detecting QPC when $B = B_{min}$ following from:⁶³

$$\sin\left(\frac{\Delta}{2}\right) = \frac{L}{2r_c} = \frac{\pi L e B_{min}}{\hbar k_F} \quad (1.7.4)$$

where L is the distance between the two QPCs, in our case the diameter of the dot, $1.5 \mu\text{m}$.

Anticipating the measurements, we already note that similar to the case of two adjacent QPCs, electron focusing oscillations can be expected in the dot, as illustrated in Fig. 1.19b. For closed geometries like the dot, the focusing is sometimes referred to as geometrical resonances, leading to an increased transmission when the two involved length scales (r_c and L in our case) are commensurate.⁶² If a perfect circular dot is assumed, we find that (non-periodic) oscillations are expected at magnetic field values B_{foc}^{dot} :

$$B_{foc}^{dot} = \frac{\hbar k_F}{eR} \tan^{-1}\left(\frac{\pi/2}{p+1}\right) \quad (1.7.5)$$

with p the number of collisions in the dot. It is interesting to note that the ideas of electron-beam collimation and the geometrical resonances explain⁶² the quenching of the Hall effect⁶⁴⁻⁶⁶ and the negative bend resistance,⁶⁷ which have been observed in crossed-wires.

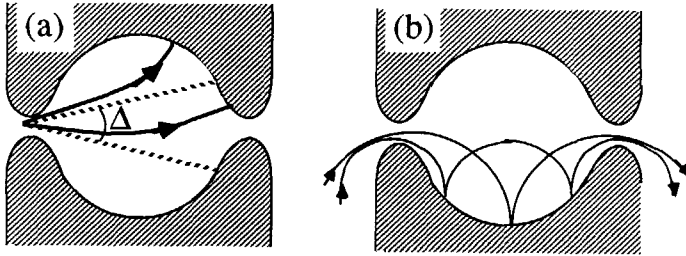


FIG. 1.19. (a) The collimation of the electron-beam, with angle Δ , results in an enlarged number of electrons directly transmitted from the injecting QPC through the collecting QPC. The deflection of the beam by a magnetic field decreases the direct transmission. (b) Illustration of electron focusing in the dot for $p = 1$ and $p = 2$ collisions.

The measured 2-terminal magneto-conductance of the dot shown in Fig. 1.20 contains a variety of effects, but they are easily identified. First we note that G_{ser} is symmetric around $B = 0$, a general property of a 2-terminal conductance. Increasing B from zero, G_{ser} decreases until a minimum is reached at $B_{min} \approx 0.07$ T. This decrease is due to the deflection of the electron-beam, and from Eq. 1.7.4 we estimate that the beam angle $\Delta = 70^\circ$; a similar value was observed by Molenkamp et al.⁶³

The arrows in Fig. 1.20 indicate the magnetic field values B_{foc}^{dot} where according to Eq. 1.7.5 focusing maxima are expected. The observed agreement suggests that the assumption of a circular-shape of the dot is valid for our structure.

The overall shape of the magneto-conductance is known as a camel-back shape which was predicted by Beenakker and van Houten⁵⁸ and observed also by Staring et al.⁶⁸ and Main et al.⁶⁹ in different geometries of two QPCs in series. The camel-back is described by Eq. 1.7.2. On increasing B , first the subbands in the dot start to depopulate. The decreasing number M of occupied subbands in the dot, results according Eq. 1.7.2 in an increasing series conductance. When the number of subbands in the QPCs also start to depopulate (roughly when $2r_c \approx W$) G_A and G_B decreases, which results according Eq. 1.7.2 in a decreasing series conductance. The camel-back shape is another demonstration of the intermediate transport regime discussed before, where backscattering is absent but forward scattering not.

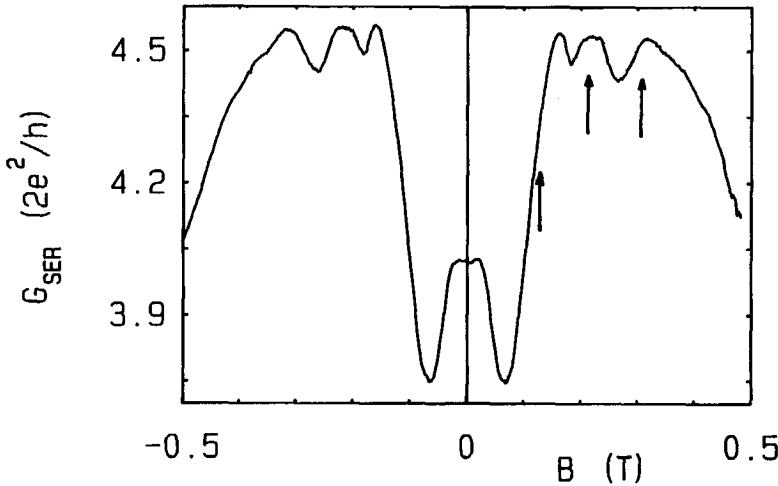


FIG. 1.20. Magneto series conductance G_{ser} for $V_g = -0.5$ V at 0.6 K. The arrows indicate the expected focusing maxima.

In Fig. 1.21 the series conductance normalized to its minimal value at B_{min} is shown versus a small range of magnetic field for several gate voltages between -0.2 V (lowest curve) to -0.75 V (uppermost curve), illustrating the influence of the shape of the QPC on the beam collimation. The conductance minima changes from $B_{min} = 0.07$ T for $V_g = -0.2$ V to $B_{min} = 0.05$ T for $V_g = -0.75$ V corresponding to beam angles of 70° to 50° , respectively. The increasing collimation indicates that a more-negative gate voltage smoothens the potential of the QPC (and increases the potential barrier). This is also evidenced by the increasing maxima which show that the percentage of directly transmitted electrons increases from about 3 % to 10 %. The additional structure, as for instance the minima at $B = 0$, are not well identified. To exclude possible diffraction effects, we have measured the traces at a relatively high temperature of 4.2 K. A possible explanation might be a beating effect between the depopulation of subbands in the dot (which increases G_{ser}) and the deflection of the electron-beam (which decreases G_{ser}). Similar fine structure was also observed by Main et al.⁶⁹

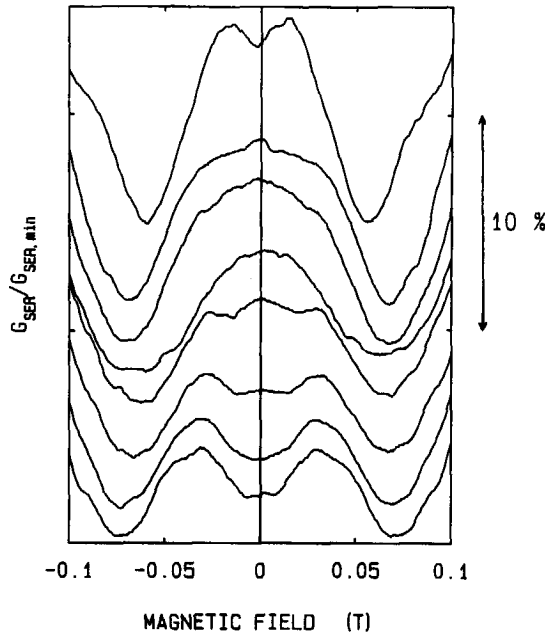


FIG. 1.21. Magneto series conductance G_{ser} normalized on its minimal value $G_{ser,min}$ for gate voltages between -0.2 V (lowest curve) and -0.75 V (uppermost curve) at 4.2 K. The scale indicates the percentage of directly transmitted electrons. The curves have been offset for clarity.

1.8 SUMMARY AND CONCLUSIONS

The state-of-the-art of submicron technology has reached the level which enables one to study quantum adiabatic electron transport occurring in ballistic conductors. An important development has been the use of split-gate devices which have the advantage that the properties of the conductor can be changed locally, i.e. without affecting the characteristics of the reservoirs. This has led to the observation of the quantized conductance, resulting from the (de-) population of 1D subbands in a QPC. Another example is the changing Hall conductance, while the characteristics of the 2DEG are unchanged and only the properties of the measurement probes are varied.

Many experiments have been performed in the quantum ballistic regime, of which we have discussed a few in this review. In nearly all cases, the Landauer-Büttiker formalism has been used successfully to describe the transport experiments, and moreover, has usually given an appealing physical picture. For the description, it has been sufficient to treat the electrons as independent particles. Further miniaturization of the devices can lead to structures which contain only a few electrons. Then the interesting possibility arises to study electron-electron interactions in a controlled-way.

ACKNOWLEDGEMENT

This work was performed by the collaboration between the Delft University of Technology and the Philips Research Laboratories, and I would like to thank A. van der Enden, C.J.P.M. Harmans, W. Kool, D. van der Marel, J.E. Mooij, and B.J. van Wees from Delft and C.W.J. Beenakker, R. Eppenga, H. van Houten, L.W. Molenkamp, A.A.M. Staring, C.E. Timmering, and J.G. Williamson from Philips for their contributions. We gratefully acknowledge C.T. Foxon and J.J. Harris for the supply of the high quality GaAs/AlGaAs hetero structures. The Delft Centre of Submicron Technology is acknowledged for the use of the lithography facilities, and the Stichting F.O.M. for financial support.

REFERENCES

This chapter will be published in *Physics of Low-Dimensional Semiconductor Structures*, edited by Butcher, March, and Tosi (Plenum, New York, 1992).

1. See for a review: S. Chakravarty, and A. Schmid, *Physics Reports* **140**, 193 (1986).
2. P.A. Lee, D.A. Stone, and H. Fukuyama, *Phys. Rev. B* **35**, 1039 (1987).
3. See for a review: S. Washburn, and R.A. Webb, *Advances in Physics* **35**, 375 (1986).
4. C.W.J. Beenakker, and H. van Houten, *Phys. Rev. B* **38**, 3232 (1988).
5. T.J. Thornton, M.L. Roukes, A. Scherer, and B.P. van de Gaag, *Phys. Rev. Lett.* **63**, 2128 (1989).
6. Yu. V. Sharvin, *Zh. Eksp. Teor. Fiz.* **48**, 984 (1965) [*Sov. Phys. JETP* **21**, 655 (1965)].
7. Metallic point contacts have been used extensively for the study of Fermi surfaces, electron-phonon interaction, etc. For a review see: A.G.M. Jansen, A.P. van Gelder, and P. Wyder, *J. Phys. C* **13**, 6073 (1980).
8. H. Heinrich, G. Bauer, and F. Kuchar, eds., *Physics and Technology of Submicron Structures* (Springer, Berlin, 1988).
9. M. Reed and W.P. Kirk, eds., *Nanostructure Physics and Fabrication* (Academic Press, New York, 1989).
10. S.P. Beaumont and C.M. Sotomayor-Torres, eds., *Science and Engineering of 1- and 0-Dimensional Semiconductors* (Plenum, London, 1990).
11. J.M. Chamberlain, L. Eaves, and J.C. Portal, eds., *Electronic Properties of Multilayers and Low-Dimensional Semiconductor Structures* (Plenum, London, 1990).
12. F. Kuchar, H. Heinrich, G. Bauer, eds., *Localization and Confinement of Electrons in Semiconductors* (Springer Verlag, Berlin, 1990).
13. M. Reed, volume ed., *Semiconductors and Semimetals* (Academic Press, New York, 1990).
14. H. Ehrenreich, and D. Turnbull, eds., *Solid State Physics* (Academic Press, New York, 1991).
15. C.T. Foxon, in: *Interfaces, Quantum Wells and Superlattices*, edited by C. Richard Leavens and Roger Taylor (Plenum Publishing Corporation, 1988);
C.T. Foxon, J.J. Harris, D. Hilton, J. Hewett, and C. Roberts, to be published.
16. N.W. Ashcroft, and N.D. Mermin, *Solid State Physics* (Holt-Saunders International Editions, 1976).
17. M.J. Kelly, and C. Weisbuch, eds., *The Physics and Fabrication of Microstructures and Microdevices* (Springer-Verlag, Berlin, 1986).
18. H. van Houten, B.J. van Wees, M.G.J. Heijman, and J.P. Andre, *Appl. Phys. Lett.* **49**, 1781 (1986).
19. T.J. Thornton, M. Pepper, H. Ahmed, D. Andrews, and G.J. Davies, *Phys. Rev. Lett.* **56**, 1198 (1986).

20. H.Z. Zheng, H.P. Wei, D.C. Tsui, and G. Weimann, *Phys. Rev. B* **34**, 5635 (1986).
21. S.E. Laux, D.J. Frank, and F. Stern, *Surf. Sci.* **196**, 101 (1988).
22. B.J. van Wees, H. van Houten, C.W.J. Beenakker, J.G. Williamson, L.P. Kouwenhoven, D. van der Marel, and C.T. Foxon, *Phys. Rev. Lett.* **60**, 848 (1988).
23. From 1992 the "von Klitzing" $R_K = h/e^2 = 25812.807 \, \Omega$ will be an official resistance constant.
24. D.A. Wharam, T.J. Thornton, R. Newbury, M. Pepper, H. Ahmed, J.E.F. Frost, D.G. Hasko, D.C. Peacock, D.A. Ritchie, and G.A.C. Jones, *J. Phys. C* **21**, L209 (1988).
25. B.J. van Wees, L.P. Kouwenhoven, E.M.M. Willems, C.J.P.M. Harmans, J.E. Mooij, H. van Houten, J.G. Williamson, and C.T. Foxon, *Phys. Rev. B* **43**, 12431 (1991).
26. L.I. Glazman, G.B. Lesovik, D.E. Khmel'nitskii, and R.I. Shekter, *JETP Lett* **48**, 238 (1988).
L.I. Glazman, and A.V. Khaetskii, *J. Phys.: Condens. Matter* **1**, 5005 (1989).
27. K.F. Berggren, T.J. Thornton, D.J. Newson, and M. Pepper, *Phys. Rev. Lett.* **57**, 1769 (1986).
28. R. Landauer, *IBM J. Res. Dev.* **1**, 223 (1957); *Phys. Lett.* **85A**, 91 (1981); *J. Phys.: Condens. Matter* **1**, 8099 (1989).
29. A. Szafer and A.D. Stone, *Phys. Rev. Lett.* **62**, 300 (1989);
E.G. Haanappel and D. van der Marel, *Phys. Rev. B* **39**, 5484 (1989);
G. Kirczenow, *Solid State Comm.* **68**, 715 (1988); *Phys. Rev. B* **39**, 10452 (1989);
An extending list of numerical calculations can be found in Ref. 13, 14, and 25.
30. Several authors have obtained transmission resonances in the calculated conductance of narrow constrictions, see Ref. 29.
31. J. Nixon, and J. Davies, *Phys. Rev. B* **41**, 7929 (1990).
32. J.G. Williamson, C.E. Timmering, C.J.P.M. Harmans, J.J. Harris, and C.T. Foxon, *Phys. Rev. B* **42**, 7675 (1990).
33. B.I. Halperin, *Phys. Rev. B* **25**, 2185 (1982).
34. B.J. van Wees, L.P. Kouwenhoven, H. van Houten, C.W.J. Beenakker, J.E. Mooij, C.T. Foxon, and J.J. Harris, *Phys. Rev. B* **38**, 3625 (1988).
35. D.A. Wharam, U. Ekenberg, M. Pepper, D.G. Hasko, H. Ahmed, J.E.F. Frost, D.A. Ritchie, D.C. Peacock, and G.A.C. Jones, *Phys. Rev. B* **39**, 6283 (1989).
36. L.P. Kouwenhoven, B.J. van Wees, C.J.P.M. Harmans, J.G. Williamson, H. van Houten, C.W.J. Beenakker, C.T. Foxon, and J.J. Harris, *Phys. Rev. B* **39**, 8040 (1989);
See also chapter 2 in this thesis.
37. H. van Houten, B.J. van Wees, J.E. Mooij, C.W.J. Beenakker, J.G. Williamson, and C.T. Foxon, *Europhys. Lett.* **5**, 721 (1988);
C.W.J. Beenakker, H. van Houten, and B.J. van Wees, *Europhys. Lett.* **7**, 359 (1988);
H. van Houten, C.W.J. Beenakker, J.G. Williamson, M.E.I. Broekaar, P.H.M. van Loosdrecht, B.J. van Wees, J.E. Mooij, C.T. Foxon, J.J. Harris, *Phys. Rev. B* **39**, 8556 (1989).
38. A study of focusing over large distances is reported by: J. Spector, H.L. Stormer, K.W.

- Baldwin, L.N. Pfeiffer, and K.W. West, *Surf. Sci.* **228**, 283 (1990).
39. P. Streda, J. Kucera, and A.H. MacDonald, *Phys. Rev. Lett.* **59**, 1973 (1987).
40. J.K. Jain and S.A. Kivelson, *Phys. Rev. Lett.* **60**, 1542 (1988).
41. M. Büttiker, *Phys. Rev. B* **38**, 9375 (1988).
42. R.J. Haug, A.H. MacDonald, P. Streda, and K. von Klitzing, *Phys. Rev. Lett.* **61**, 2797 (1988).
43. S. Washburn, A.B. Fowler, H. Schmid, and D. Kern, *Phys. Rev. Lett.* **61**, 2801 (1988).
44. M. Büttiker, *IBM J. Res. Dev.* **32**, 317 (1988).
45. F.F. Fang, and P.J. Stiles, *Phys. Rev. B* **27**, 6487 (1983); *Phys. Rev. B* **29**, 3749 (1984).
46. B.J. van Wees, E.M.M. Willems, C.J.P.M. Harmans, C.W.J. Beenakker, H. van Houten, J.G. Williamson, C.T. Foxon, and J.J. Harris, *Phys. Rev. Lett.* **62**, 1181 (1989).
47. G. Müller, D. Weiss, S. Koch, K. von Klitzing, H. Nickel, W. Schlapp, and R. Lösch, *Phys. Rev. B* **42**, 7633 (1990).
48. S. Komiyama, H. Hirai, S. Sasa, and S. Hiyamizu, *Phys. Rev. B* **40**, 12566 (1989).
49. B.J. van Wees, E.M.M. Willems, L.P. Kouwenhoven, C.J.P.M. Harmans, J.G. Williamson, C.T. Foxon, and J.J. Harris, *Phys. Rev. B* **39**, 8066 (1989).
50. B.W. Alphenaar, P.L. McEuen, R.G. Wheeler, and R.N. Sacks, *Phys. Rev. Lett.* **64**, 677 (1990).
51. P.L. McEuen, A. Szafer, C.A. Richter, B.W. Alphenaar, J.K. Jain, A.D. Stone, R.G. Wheeler, and R.N. Sacks, *Phys. Rev. Lett.* **64**, 2062 (1990).
52. C.W.J. Beenakker, *Phys. Rev. Lett.* **64**, 216 (1990).
53. A.H. MacDonald, *Phys. Rev. Lett.* **64**, 220 (1990).
54. A.M. Chang, *Solid State Commun.* **74**, 871 (1990).
55. A.M. Chang and J.E. Cunningham, *Solid State Commun.* **72**, 651 (1989).
56. L.P. Kouwenhoven, B.J. van Wees, N.C. van der Vaart, C.J.P.M. Harmans, C.E. Timmering, and C.T. Foxon, *Phys. Rev. Lett.* **64**, 685 (1990);
See also chapter 3 in this thesis.
57. L.P. Kouwenhoven, B.J. van Wees, W. Kool, C.J.P.M. Harmans, A.A.M. Staring and C.T. Foxon, *Phys. Rev. B* **40**, 8083 (1989).
58. C.W.J. Beenakker and H. van Houten, *Phys. Rev. B* **39**, 10445 (1989).
59. L.J. Glazman and M. Johnson, *J. Phys. Condens. Matter* **1**, 5547 (1989).
60. B.J. van Wees, L.P. Kouwenhoven, C.J.P.M. Harmans, J.G. Williamson, C.E. Timmering, M.E.I. Broekaart, C.T. Foxon, and J.J. Harris, *Phys. Rev. Lett.* **62**, 2523 (1989);
L.P. Kouwenhoven, B.J. van Wees, C.J.P.M. Harmans and J.G. Williamson, in Ref. 10.
L.P. Kouwenhoven, B.J. van Wees, C.J.P.M. Harmans and J.G. Williamson, *Surf. Science* **229**, 290 (1990);
See also chapter 4 in this thesis.
61. D.A. Wharam, M. Pepper, H. Ahmed, J.E.F. Frost, D.G. Hasko, D.C. Peacock, D.A. Ritchy, and G.A. Jones, *J. Phys. C: Solid State Phys.* **21**, L887 (1988).

62. C.W.J. Beenakker, and H. van Houten, *Phys. Rev. Lett.* **63**, 1857 (1989); and in Ref. 11.
63. L.W. Molenkamp, A.A.M. Staring, C.W.J. Beenakker, R. Eppenga, C.E. Timmering, J.G. Williamson, C.J.P.M. Harmans, and C.T. Foxon, *Phys. Rev. B* **41**, 1274 (1990).
64. M.L. Roukes, A. Scherer, S.J. Allen, H.G. Craighead, R.M. Ruthen, E.D. Beebe, and J.P. Harbison, *Phys. Rev. Lett.* **59**, 3011 (1987).
65. C.J.B. Ford, S. Washburn, M. Büttiker, C.M. Knoedler, and J.M. Hong, *Phys. Rev. Lett.* **62**, 2724 (1989).
66. A.M. Chang, T.Y. Chang, and H.U. Baranger, *Phys. Rev. Lett.* **63**, 996 (1989).
67. G. Timp, H.U. Baranger, P. de Vegvar, J.E. Cunningham, R.E. Howard, R. Behringer, and P.M. Mankiewich, *Phys. Rev. Lett.* **60**, 2081 (1988).
68. A.M.M. Staring, L.W. Molenkamp, C.W.J. Beenakker, L.P. Kouwenhoven, and C.T. Foxon, *Phys. Rev. B* **41**, 8461 (1990).
69. P.C. Main, B.R. Davidson, P.H. Beton, L. Eaves, J.R. Owers-Bradley, A.J.M. Neves, S.P. Beaumont, and C.D.W. Wilkinson, *J. Phys.: Condens. Matter* **2**, 6541 (1990);
P.C. Main, P.H. Beton, B.R. Snell, A.J.M. Neves, J.R. Owers-Bradley, L. Eaves, S.P. Beaumont, and C.D.W. Wilkinson, *Phys. Rev. B* **40**, 10033 (1989);
P.H. Beton, B.R. Snell, P.C. Main, A. Neves, J.R. Owers-Bradley, L. Eaves, M. Henini, O.H. Hughes, S.P. Beaumont, and C.D.W. Wilkinson, *J. Phys.: Condens. Matter* **1**, 7505 (1989).

CHAPTER 2

Non-Linear Conductance of Quantum Point Contacts

L.P. Kouwenhoven, B.J. van Wees and C.J.P.M. Harmans

*Department of Applied Physics, Delft University of Technology, P.O. Box 5046,
2600 GA Delft, The Netherlands*

J.G. Williamson, H. van Houten and C.W.J. Beenakker

Philips Research Laboratories, 5600 JA Eindhoven, The Netherlands

C.T. Foxon and J.J. Harris

Philips Research Laboratories, Redhill, Surrey RH15HA, United Kingdom

ABSTRACT

The conductance of ballistic quantum constrictions in a two dimensional electron gas has been studied experimentally as a function of the applied voltage. Large non-linearities are found in the current-voltage characteristics. We give a simple model, which explains the main features of the non-linear conductance. Breakdown of the conductance quantization occurs when the number of occupied one dimensional subbands becomes unequal for the two velocity-directions. A critical voltage is found for the breakdown, which is equal to the subband separation at the Fermi level.

The quantization of the conductance of a constriction in a two dimensional electron gas (2DEG) was recently discovered in the experiments of van Wees et. al.¹ and Wharam et. al.² They defined a ballistic constriction in the 2DEG of a high mobility GaAs-Al_xGa_{1-x}As hetero structure by means of a metallic split gate. Application of a negative voltage V_g on the gate forms the constriction in the 2DEG by electro static depletion. The two-terminal conductance G , measured at zero magnetic field between the two wide regions of 2DEG on each side of the constriction, was shown to change stepwise in units of $2e^2/h$ on varying V_g . The quantization of G can be explained from the formation of one dimensional (1D) subbands in the constriction due to the lateral confinement. Then G is given by the Landauer type formula³ $G = N_c 2e^2/h$, with N_c the number of occupied 1D subbands. A detailed analysis has shown that a variation of V_g changes the width as well as the electron density of the constriction.⁴ Both mechanisms move the Fermi energy E_F in the channel through the 1D subbands and whenever it passes a subband bottom G changes by the quantized amount of $2e^2/h$.

So far this new conductance quantization has been studied in the linear ballistic transport regime. Here we report on the non-linear conductance of *quantum point contacts*. Deviations from quantization are expected to occur when eV becomes comparable to the subband separation (with V the applied voltage over the constriction). We have studied the non-linear transport by measuring a set of current-voltage (I - V) characteristics using V_g as a parameter. The main features of the I - V characteristics can be accounted for by a simple qualitative model, which is based on ballistic electron transport over a potential barrier in the constriction. Related models have been used in the field of hot electron transport in layered semiconductor structures,⁵ and to explain the breakdown of the Quantum Hall effect.⁶⁻¹⁰

The measurements have been performed on a device which is similar to that in Ref. 1 (see inset Fig. 2.1). The 2DEG of the GaAs-Al_xGa_{1-x}As hetero structure has a transport mean free path of 8.5 μm and an electron density of $3.6 \cdot 10^{15} \text{ m}^{-2}$ resulting in a Fermi wavelength of 42 nm. At a gate voltage $V_g = -0.6 \text{ V}$ the constriction is just formed in the 2DEG and has its maximum width, which is approximately equal to the lithographic width of the opening in the gate (250 nm). Lowering V_g reduces the width and at $V_g = -2.2 \text{ V}$ the constriction is fully pinched-off. The experiments were done at 0.6 K with dc current biasing. The voltage V across the constriction is defined as the voltage of the upper contact in the inset of Fig. 2.1 minus the voltage of the lower contact. The measured voltage is corrected for a background resistance originating from the two wide 2DEG regions and from the resistance of the Ohmic contacts.¹¹

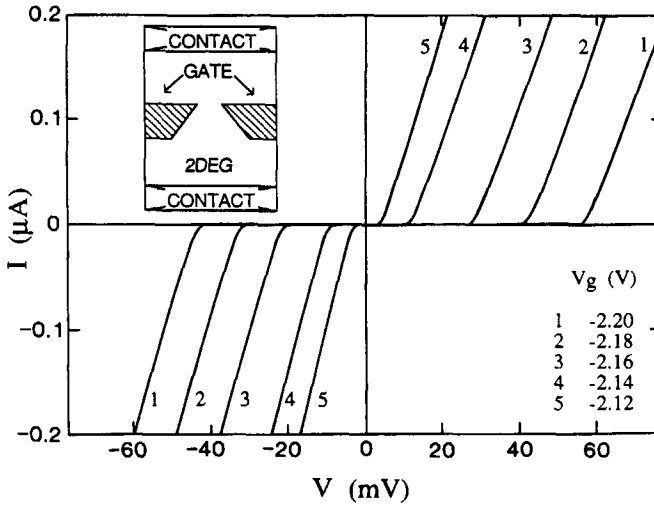


FIG. 2.1. *I-V characteristics at different values of gate voltage V_g for which the constriction is pinched-off for small voltage V . The inset shows the sample lay-out.*

In Fig. 2.1 the *I-V* characteristics are shown for several values of the gate voltage V_g , for which the constriction is pinched-off in equilibrium. For low V the current through the constriction is zero. At a certain critical voltage V_c there is a stepwise increase of the differential conductance $g = dI/dV$ from zero to a constant value [$\approx (80 \text{ k}\Omega)^{-1}$], which is found to be nearly independent of V_g . The critical voltage V_c however increases strongly with decreasing V_g . Note that the *I-V* characteristics are not anti-symmetric. The asymmetry is considerably influenced by the choice of zero reference of V_g , which in the experiment has been the lower contact in the sample lay-out of Fig. 2.1. Changing the zero reference to the upper contact results in a different gate voltage $V_g + V$, which gives for $V < 0$ a lower gate voltage. However, this change in zero reference does not account for the asymmetry in the curves of Fig. 2.1. This might be due to an intrinsic asymmetry in the electro static potential defining the constriction. In a second device of identical design the change of zero reference completely accounted for the asymmetry.

In Fig. 2.2 the *I-V* characteristics are shown for a range of V_g , for which the constriction is already conducting at a small applied voltage V . For comparison we display G at small V as a function of V_g for the lowest two quantized plateaus in the inset of Fig. 2.2a. As can be seen in the inset, V_g ranges from near pinch-off ($V_g = -2.10 \text{ V}$) to the onset of the second plateau ($V_g = -2.00 \text{ V}$). In Fig. 2.2a the curves are displayed for gate voltages corresponding to the lower part

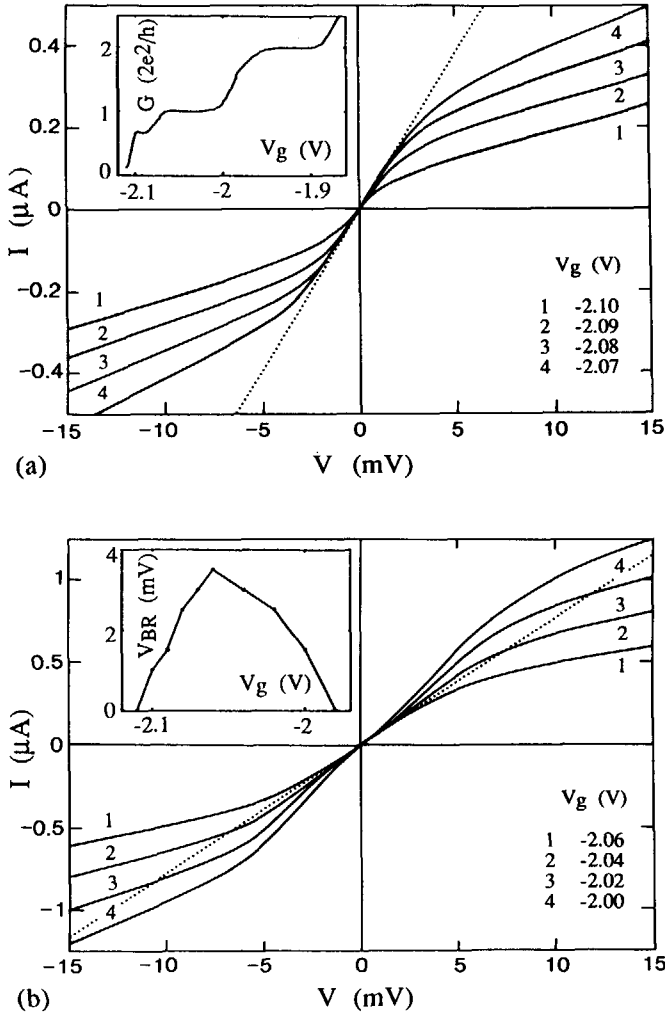


Fig. 2.2. I - V characteristics at different values of V_g for which the conductance G is quantized at $2e^2/h$ for small V , indicated by the dotted line. The inset of (a) shows G as function of V_g in equilibrium and of (b) the breakdown voltage V_{BR} as a function of V_g .

of the first plateau. For small V they follow the dotted line, which indicates the quantized value $2e^2/h$ of the first plateau. At a certain voltage V_{BR} , the quantization breaks down and g decreases from $2e^2/h$ [$\approx (13 \text{ k}\Omega)^{-1}$] to a lower value [$\approx (60 \text{ k}\Omega)^{-1}$]. In Fig. 2.2b the I - V characteristics are shown for gate voltages corresponding to the upper part of the first plateau. Again the curves follow the dotted line of quantization for small V and deviate from it above a breakdown voltage. However in contrast to Fig. 2.2a the deviation from quantization is now to a larger value for g [$\approx (8.7 \text{ k}\Omega)^{-1}$]. A further increase of V reduces g to a value much lower than $2e^2/h$. (Note that the relative effect of V on the gate voltage and hereby the asymmetry is much less in Fig. 2.2 as compared to Fig. 2.1.) We thus see that increasing V results in the breakdown of the conductance quantization, as manifested by either an increase or a decrease in g . As can be seen from Fig. 2.2, the breakdown voltage V_{BR} (the voltage where g deviates more than 10% from the quantized value) increases as V_g approaches the center of the first plateau. To illustrate this we have plotted V_{BR} as a function of V_g in the inset of Fig. 2.2b, which shows a triangular shape with a maximum value of 3.5 meV at $V_g = -2.06 \text{ V}$.

To understand the main features in the I - V characteristics we propose a simple model. Apart from the lateral confinement, the gate voltage V_g also gives rise to an electro static potential in the constriction,^{4,12} which results in a reduced electron density. For simplicity we neglect the voltage V dependence of V_g . Due to the lateral confinement 1D subbands are formed. On entering the constriction the bottom of the n th subband rises relative to the bulk 2DEG, as a combined result of the increased lateral confinement and the electro static barrier. The number of occupied states is lowest at the maximum of the potential barrier, where the n th subband bottom has an energy E_n constituting a "bottleneck" for the current. Extrapolating an approach valid in the linear transport regime,^{3,12} we calculate the net current I_n through the constriction carried by the n th subband by considering the occupation of the right- and left-moving states at the bottleneck E_n . The right-moving states are filled from E_n up to μ_1 , the electro chemical potential at the left of the constriction (provided that $\mu_1 > E_n$). Analogously, provided that $\mu_2 > E_n$, the left-moving states are filled from E_n up to μ_2 , the electro chemical potential at the right. We assume that the electrons with energy $\mu > E_n$ are fully transmitted through the constriction. A difference in occupation between the right- and left-moving states is determined by the applied voltage V , with $eV = \mu_1 - \mu_2$ (assuming a vanishing electric field outside the constriction), resulting in a net current. For $\mu_1 > \mu_2$ the n th subband carries a net current, which according to the well-known cancellation of group velocity with density of states in one dimension is given by

$$I_n = \frac{2e}{h} \cdot [\mu_l - \max(\mu_2, E_n)] \quad (2.1)$$

provided $\mu_l > \max(\mu_2, E_n)$, and $I_n = 0$ otherwise. On increasing V the population of the right-moving states increases to $\mu_l = E_F + meV$ and of the left-moving states decreases to $\mu_2 = E_F - (1 - m)eV$. Here m is a phenomenological parameter between 0 and 1, describing the fraction of V , which drops on the left of the bottleneck. Concurrently the fraction $(1 - m)$ of V drops on the right. At a certain voltage μ_l or μ_2 crosses the subband bottom E_n , in this way changing the contribution $\partial I_n / \partial V$ from the n th subband to the differential conductance g . We find for $E_F < E_n$,

$$\frac{\partial I_n}{\partial V} = \begin{cases} 0 & \text{if } |V| < V_c = -(E_F - E_n)/me \\ m \cdot \frac{2e^2}{h} & \text{if } |V| > V_c \end{cases} \quad (2.2)$$

while if $E_F > E_n$

$$\frac{\partial I_n}{\partial V} = \begin{cases} \frac{2e^2}{h} & \text{if } |V| < V_c' = (E_F - E_n)/(1 - m)e \\ m \cdot \frac{2e^2}{h} & \text{if } |V| > V_c' \end{cases} \quad (2.3)$$

Eq. 2.2 applies to a subband which in equilibrium is not occupied at the bottleneck of the constriction ($E_F < E_n$). The differential conductance from this subband *increases* beyond a critical voltage V_c to a value which is smaller than the quantized value. Eq. 2.3 applies to a subband which is occupied in equilibrium ($E_F > E_n$). Beyond a critical voltage V_c' the differential conductance due to this subband *decreases* from its normal quantized value of $2e^2/h$. Although the expressions for the critical voltages depend on the parameter m , these conclusions are general and model independent.

To illustrate the consequences of Eq. 2.2 and 2.3 on increasing the voltage we have schematically shown in Fig. 2.3 the energy of the two lowest subbands at the bottleneck as a function of longitudinal wavevector k_y . Note that positive k_y corresponds to a positive velocity. In equilibrium ($V = 0$) the subbands are occupied up to the Fermi energy E_F . A voltage V across the constriction gives a difference $\mu_l - \mu_2 = eV$ in occupation between the two velocity-directions (Fig. 2.3a), resulting in a net current. As long as the number of occupied subbands is the same for both velocity-directions the conductance is quantized. However at larger applied voltages, μ_2 can fall below the bottom of a subband. Here g reduces from $2e^2/h$ to a fraction $m \cdot 2e^2/h$, as shown in Fig. 2.3b (where E_F is near the bottom of the lowest subband) and as

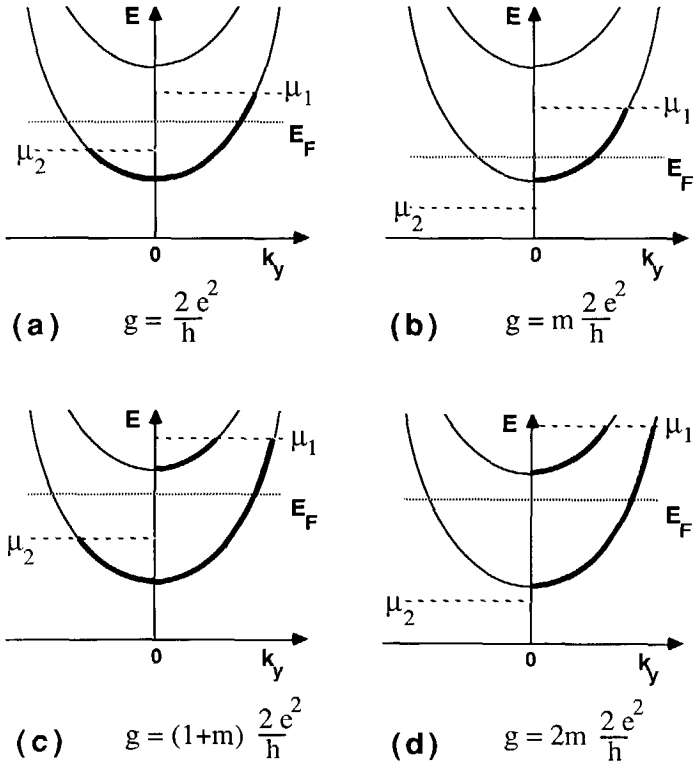


FIG. 2.3. Subband occupation at the bottleneck, where the conductance is determined. Four situations are illustrated for different V across the constriction (with $eV = \mu_1 - \mu_2$), and for different positions of E_F .

observed experimentally in Fig. 2.2a. The subband occupation of Fig. 2.3b can also be reached from the situation $E_F < E_I$, where there are no occupied states in equilibrium. For low voltages $g = 0$ as in Fig. 2.1, but at a critical voltage μ_1 crosses E_I and g increases to $m \cdot 2e^2/h$ according to Eq. 2.2. We emphasize that this explanation for the onset of conductance holds that μ_1 is lifted above the barrier in the constriction. The constant g above the critical voltage excludes tunneling through the barrier, which would lead to an exponential dependence of g on V .¹³ Fig. 2.3c and 2.3d correspond to the situation where E_F is close to the bottom of the second subband, as in the experimental figure 2.2b. On increasing V first the second subband starts to be populated (Fig. 2.3c) leading to an increase of g to $(1+m) \cdot 2e^2/h$. A further increase of V causes μ_2 to fall below

the bottom of the first subband (Fig. 2.3d), which then reduces g to a fraction $2m \cdot 2e^2/h$. This explains qualitatively the increasing and then decreasing slope in Fig. 2.2b. We note that the situation of Fig. 2.3d can also be reached directly from Fig. 2.3a, which is actually happening at $V_g = -2.06$ V in Fig. 2.2b.

The model presented here in terms of a single phenomenological parameter m does give qualitative insight, but it is not a realistic description of the complex interdependence of the electro static potential on V , and V_g . This is demonstrated by the fact that no universal value for m is found. If both velocity-directions are occupied the experiment yields $m \approx 0.5$. The maximum of the breakdown voltage V_{BR} at $V_g = -2.06$ V (for which E_F is approximately in the middle of the first and second subband bottom as can be seen from the insets of Fig. 2.2), also indicates $m \approx 0.5$. However if one velocity-direction is fully depopulated, m has an experimental value of ≈ 0.2 . It would be of interest to develop a more quantitative theory for our observations.

It follows from Eq. 2.2 and 2.3 that the maximum value of the breakdown voltage V_{BR} is equal to the subband separation at the Fermi level. This is independent of the parameter m and provides a fundamental limit for the conductance quantization. From the inset of Fig. 2.2b we thus find a subband separation of 3.5 meV, which is consistent with the value obtained from an analysis of magnetic depopulation.^{4,14} As we have discussed, the breakdown of the conductance quantization occurs whenever the number of occupied subbands differs for the two velocity-directions. We emphasize that this mechanism does not involve any inelastic process or inter-subband scattering. The triangular dependence of the breakdown voltage (see inset Fig. 2.2b) on the gate voltage is reminiscent of experiments on the breakdown of the quantum Hall effect, where a similar dependence of the breakdown Hall voltage on the magnetic field was found.⁶⁻⁹ A mechanism for breakdown of the quantum Hall effect also including only elastic processes has been proposed in Ref. 10.

In this paper we have presented I - V characteristics at fixed V_g . Glazman and Khaetskii¹⁵ have recently predicted that the differential conductance as a function of gate voltage at a fixed finite V should exhibit additional plateaus in between the plateaus at multiples of $2e^2/h$. We have found some evidence for these additional plateaus (which follow also from Eq. 2.2), but these are not well resolved in our device.

In conclusion we have reported the first experimental study on the non-linear behaviour of quantum ballistic point contacts. We have given a simple model explaining the main features in the non-linear conductance. The measured I - V characteristics reveal the occupation of the 1D subbands formed in the constriction, for the individual velocity-directions. Breakdown of the

quantization occurs when the number of occupied subbands becomes different for the two directions. A critical voltage equal to the subband separation at the Fermi level is derived for the complete breakdown of the two-terminal conductance quantization.

ACKNOWLEDGEMENT

We thank M.E.I. Broekaart, C.E. Timmering and L.W. Lander for technical support and L.J. Geerligs and E.M.M. Willems for assistance with the experiments. We thank J. Romijn of the Delft Centre for Submicron Technology (CST) for the facilities offered and the "Stichting voor Fundamenteel Onderzoek der Materie" (FOM) for financial support. L.P.K. gratefully acknowledges the financial support of the CST.

REFERENCES

This chapter was published in Phys. Rev. B **39**, 8040 (1989).

1. B.J. van Wees, H. van Houten, C.W.J. Beenakker, J.G. Williamson, L.P. Kouwenhoven, D. van der Marel and C.T. Foxon, Phys. Rev. Lett. **60**, 848 (1988).
2. D.A. Wharam, T.J. Thornton, R. Newbury, M. Pepper, H. Ahmed, J.E.F. Frost, D.G. Hasko, D.C. Peacock, D.A. Ritchie and G.A.C. Jones, J. Phys. C **21**, L209 (1988).
3. R. Landauer, Z. Phys. B **68**, 217 (1987).
4. B.J. van Wees, L.P. Kouwenhoven, H. van Houten, C.W.J. Beenakker, J.E. Mooij, C.T. Foxon and J.J. Harris, Phys. Rev. B **38**, 3625 (1988).
5. J.R. Hayes, A.F.J. Levi, and W. Wiegman, Phys. Rev. Lett. **54**, 1570 (1985); M. Heiblum, M.I. Nathan, D.C. Thomas and C.M. Knoedler, Phys. Rev. Lett. **55**, 2200 (1985).
6. G. Ebert, K. von Klitzing, K. Ploog, G. Weimann, J. Phys. C **16**, 15441 (1983).
7. J.R. Kirtley, Z. Schlesinger, T.N. Theis, F.P. Milliken, S.L. Wright and L.F. Palmateer, Phys. Rev. B **34**, 5414 (1986).
8. L. Blik, E. Braun, G. Hein, V. Kose, J. Niemeyer, G. Weiman and W. Schlapp, Semicond. Sci. Technol. **1**, 110 (1986).
9. P.G.N. de Vegvar, A.M. Chang, G. Timp, P.M. Mankiewich, J.E. Cunningham, R. Behringer and R.E. Howard; Phys. Rev. B **36**, 9366 (1987).
10. J.K. Jain and S.A. Kivelson, Phys. Rev. B **37**, 4276 (1988).
11. The resistance of the Ohmic contacts showed to be slightly non-linear. It is measured independently at $V_g = 0$ V, where it varied within (2.9 ± 0.4) k Ω over the current range and is subtracted from the measured data. The formation of the constriction at $V_g = -0.6$ V gives rise to a series resistance R_{2DEG} from the two wide 2DEG regions, due to the change

in geometry. R_{2DEG} ($= 980 \Omega$) has been obtained from the difference of the measured and quantized value of the first plateau and is taken constant for all I - V curves.

12. B.J. van Wees, H. van Houten, C.W.J. Beenakker, L.P. Kouwenhoven, J.G. Williamson, J.E. Mooij, C.T. Foxon and J.J. Harris, in *Proceedings of the 19th International Conference on the Physics of Semiconductors, Warsaw, Poland 1988*, edited by W. Zawadzki (Institute of Physics, Polish Academy of Sciences, 1988).
13. A. Palevski, M. Heiblum, C.P. Umbach, C.M. Knoedler, A.N. Broers and R.H. Koch, *Phys. Rev. Lett.* **62**, 1776 (1989).
14. B.J. van Wees, L.P. Kouwenhoven, E.M.M. Willems, C.J.P.M. Harmans, J.E. Mooij, H. van Houten, C.W.J. Beenakker, J.G. Williamson, and C.T. Foxon, *Phys. Rev. B* **43**, 12431 (1991).
15. L.I. Glazman and A.V. Khaetskii, *JETP Lett.* **48**, 591 (1988); and in *Europhys. Lett.* **9**, 263 (1989).

CHAPTER 3

Selective Population and Detection of Edge Channels in the Fractional Quantum Hall Regime.

L.P. Kouwenhoven, B.J. van Wees, N.C. van der Vaart, and C.J.P.M. Harmans
Faculty of Applied Physics, Delft University of Technology
P.O.Box 5046, 2600 GA Delft, The Netherlands

C.E. Timmering
Philips Research Laboratories, 5600 JA Eindhoven, The Netherlands

C.T. Foxon
Philips Research Laboratories, Redhill, Surrey RH1 5HA, United Kingdom

ABSTRACT

Transport in the fractional quantum Hall effect (FQHE) regime is studied in a two dimensional electron gas (2DEG) employing adjustable barriers as current and voltage probes. We find a fractionally quantized Hall conductance for integer filling factor in the bulk of the 2DEG, as a consequence of the fractional filling factor in the probes. We argue that this effect is the first manifestation of adiabatic transport in the FQHE. The results are in agreement with a proposed Landauer-Büttiker formula in which each fractional edge channel contributes a conductance $1/3 \cdot e^2/h$.

The similarity in experimental appearance between the integer quantum Hall effect (IQHE) and the fractional quantum Hall effect (FQHE) is striking in view of their theoretically different origins. While a single-particle description can be used for the IQHE, the FQHE originates from a many-body interaction.¹

A clear picture of the IQHE in terms of edge channels² has recently gained much attention, both theoretically and experimentally. The transport in the IQHE regime can then be described within the Landauer-Büttiker formalism.³⁻⁵ Recent experiments have demonstrated that edge channels can be selectively populated and detected by current and voltage contacts.^{6,7} The experiment of Ref. 7 shows that scattering between edge channels can be very weak on length scales of the order of a micrometer. On these length scales the IQHE can be described in terms of adiabatic transport in edge channels, which can be viewed as independent current channels.

In the IQHE edge channels are located at the boundary of the two-dimensional electron gas (2DEG), where the Landau levels intersect the Fermi energy. It is not obvious how to generalize this definition of edge channels to the FQHE, where a single-particle description no longer applies. The existing many-body theory^{1,8} based on Laughlin's trial wave function essentially considers a homogeneous system. The partially depleted region at the 2DEG boundary, where in the IQHE regime the edge channels are located, was not considered in these theories for the FQHE.

In this letter we study the transport along the boundary of a 2DEG having an integer filling factor, using adjacent current and voltage probes whose filling factors can be varied. From the observation of a fractional quantum Hall conductance which is completely determined by the filling factor in the probes, we conclude that adiabatic transport can occur in the FQHE regime. To describe our results we propose that *fractional edge channels* exist at the 2DEG boundary, which can be selectively populated and detected by current and voltage probes, similar to the edge channels in the IQHE regime.⁷ A Landauer-Büttiker formula generalized to the FQHE provides quantitative agreement with the measurements. This generalization as well as the concept of fractional edge channels is supported by a recent theoretical paper by Beenakker.⁹

Chang and Cunningham¹⁰ recently studied the transmission probabilities between regions with filling factor $\nu = 1$ and $\nu = 2/3$, and between regions with $\nu = 2/3$ and $\nu = 1/3$. They showed that their results could be described by the Landauer-Büttiker formalism if the electron charge e was replaced by e^* , the fractional charge of the quasi-particles in the FQHE. The results of these barrier resistance measurements are consistent with an interpretation in terms of transmission and reflection of edge channels, but do not demonstrate adiabatic transport in the FQHE, i.e. the

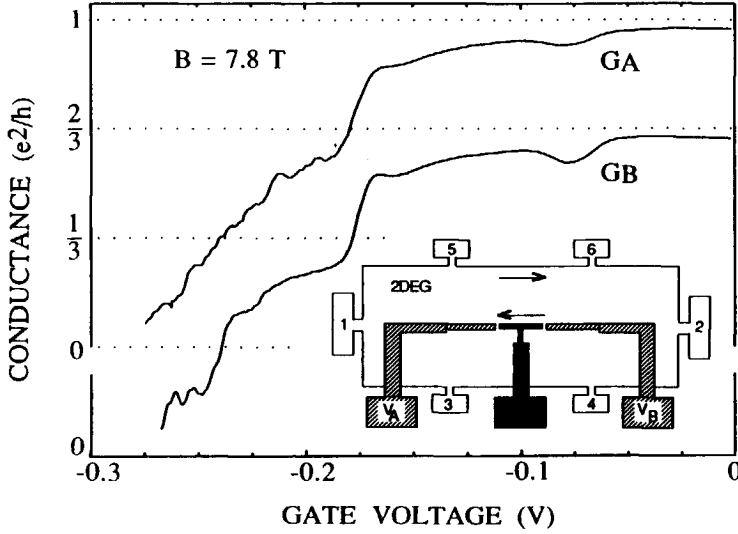


FIG. 3.1. Barrier conductances G_A and G_B as a function of gate voltage at a field of 7.8 T. The curve G_B has an offset for clarity. The double barrier geometry defined by three different gates is shown in the inset. The arrows indicate the direction of electron flow along the sample edges.

crucial issue whether or not the fractional edge channels can be treated as independent current channels on appropriate length scales. To demonstrate adiabatic transport two spatially separated barriers are required, which can act as injector and detector of edge channels- as in the experiment presented in this Letter.

The inset of Fig. 3.1 schematically shows the geometry of the double barrier device. A Hall-bar is etched in a high mobility GaAs/AlGaAs heterostructure to which Ohmic contacts, labelled from 1 to 6, are attached. The electron density of the 2DEG is $1.8 \cdot 10^{15} / \text{m}^2$ and the mean free path is $9 \mu\text{m}$. On top of the heterostructure three gates are fabricated. The voltage on the black center gate is kept fixed at a negative value of -3 V , in this way creating a sufficiently extended depletion region in the 2DEG to prevent conduction through the two narrow openings (width = 300 nm) separating the different gates (see also Fig. 3.3). A negative voltage V_A or V_B on the hatched gates (width = $0.5 \mu\text{m}$ and length = $40 \mu\text{m}$ of the smaller width section) creates a potential barrier underneath them, which locally reduces the electron density n_s and consequently the filling factor $\nu = h n_s / e B$.

Fig. 3.1 shows the two-terminal conductances¹¹ of the barriers as a function of gate voltage measured at 20 mK and at a fixed magnetic field of 7.8 T. At this field the filling factor of the bulk 2DEG is slightly less than one, which can be seen in Fig. 3.1 at zero gate voltage. The decreasing gate voltage gradually reduces the conductance of each barrier until pinch-off occurs at -0.27 V. Although the observed fractional plateaus are not fully developed, the change in slope at a gate voltage of -0.175 V can be attributed to the $2/3$ fractional state, as we will discuss below.

Fig. 3.2 shows the Hall conductances measured at $B = 7.8$ T, employing barrier *A* as the voltage probe and barrier *B* as the current probe. The Hall conductance is defined as $G_{H;14,23}$ indicating that the current flows from contact 1 to 4 and the voltage is measured between contacts 2 and 3. Fig. 3.2a shows the Hall conductance as a function of equal voltage on both gates *A* and *B*. Although the filling factor in the bulk 2DEG is unchanged in the fixed magnetic field, the Hall conductance drops from e^2/h to $2/3 \cdot e^2/h$ at -0.175 V. A similar behaviour is seen if one gate voltage is kept fixed and the other is varied. In Fig. 3.2b and 3.2c one voltage is fixed at -0.2 V and in Fig. 3.2d the voltage on gate *A* is fixed at -0.15 V. The dashed lines in Fig. 3.2a and 3.2d are calculated from the barrier conductances G_A and G_B (see Fig. 3.1), which will be discussed below.

The Hall-conductance $G_{H;23,14}$ measured by interchanging the current and voltage probe, did not show the anomalous drop to the $2/3$ plateau. Instead $G_{H;23,14}$ showed to be independent of the gate voltage and corresponded with the filling factor in the bulk 2DEG.

To describe our results we propose the existence of fractional edge channels, which follow different equipotential lines along the boundary of the sample. The adjustable barriers used as current and voltage probes in the experiment provide a selective coupling to these fractional edge channels. Coupling to a certain edge channel occurs if this channel follows an equipotential line which is higher than the probe potential barrier. Fractional edge channels following equipotential lines which are lower than the barrier potential of the probe are not transmitted over the barrier and thus will not be populated by a current probe nor detected by a voltage probe. Each populated or detected fractional edge channel is assumed to contribute $1/3 \cdot e^2/h$ to the Hall conductance (for simplicity only the $p/3$ fractional channels are considered, with $p = 1, 2, 3$). However, if no coupling of the current probe nor the voltage probe exists to a particular fractional edge channel and inter-edge channel scattering between the probes is absent, this channel will be irrelevant for transport measurements. In this way deviations in the measured Hall conductance from the expected bulk value are a direct demonstration of adiabatic transport in

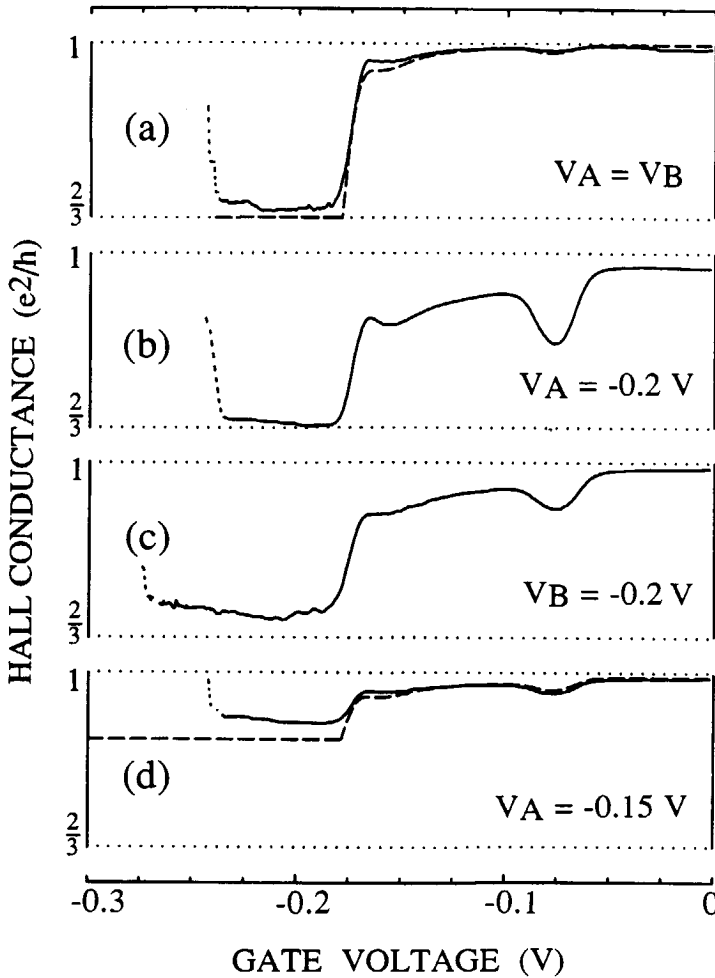


FIG. 3.2. Hall conductances as a function of gate voltage at a field of 7.8 T. In (a) both gate voltages V_A and V_B are varied simultaneously and in (b)–(d) one gate voltage is kept fixed. The rapidly rising parts (dotted) are measurement artefacts due to barrier pinch-off. The dashed lines are calculated from Eqs. 3.1, see text.

fractional edge channels over the distance between the current and the voltage probe.

Selective population and detection of edge channels has been investigated in the integer quantum Hall regime ^{6,7}. Ref. 7 gives a derivation of the Hall conductance depending on the transmission properties of the current and voltage probes. It follows from this derivation, which included only integer edge channels, that this Hall conductance cannot be smaller than e^2/h , even when the filling factors of the probes are less than one. The observation of a Hall conductance below e^2/h therefore indicates the failure of the integer formalism. For describing our present results we include the fractional edge channels proposed above in the derivation of Ref. 7. Considering only the $p/3$ -fractions we obtain

$$G_H = \frac{e^2}{3h} \max(N_I + T_I, N_V + T_V) \quad \text{if } N_I \neq N_V \quad (3.1a)$$

$$G_H = \frac{e^2}{3h} \frac{(N + T_I)(N + T_V)}{N + T_I T_V} \quad \text{if } N_I = N_V = N \quad (3.1b)$$

N_I and N_V denote the number of fully transmitted fractional channels through the current and voltage probe respectively. T_I and T_V are the transmission probabilities ($0 \leq T_I, T_V \leq 1$) through the current and voltage probe respectively of the partially transmitted upper channel. Note that Eqs. 3.1 are independent of the filling factor of the bulk 2DEG, but are completely determined by the transmission properties of the current and voltage probes. Consequently, the fractional quantization of the Hall conductance is determined by the filling factors in the probe barriers. A prerequisite for the validity of Eqs. 3.1 is the occurrence of adiabatic transport requiring the absence of scattering between adjacent channels over the distance between the current and voltage probe ($> 2 \mu\text{m}$ in our device).

In Fig. 3.3 we have illustrated the electron flow for the case of three fractional edge channels in the bulk 2DEG. The current probe populates only two of them ($N_I = 2, T_I = 0$) and the voltage probe detects two fractional edge channels ($N_V = 2, T_V = 0$). According to Eqs. 3.1 the Hall conductance for this case is equal to $2/3 \cdot e^2/h$, which corresponds to the experimental situation of $V_A \approx V_B \approx -0.2 \text{ V}$.

To compare the proposed description quantitatively with the measurements we have calculated the Hall conductance with the measured barrier conductances G_A as voltage probe conductance and G_B as current probe conductance (see Fig. 3.1), substituted in Eqs. 3.1. The results are shown in Fig. 3.2a and 3.2d (dashed lines) demonstrating a good agreement with the measured

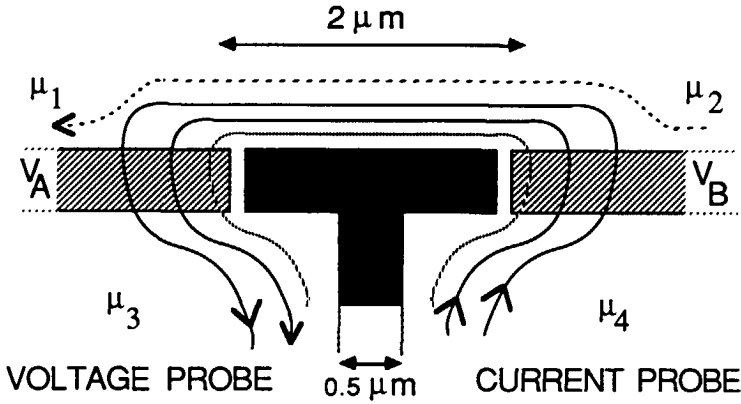


FIG. 3.3. Illustration of the selective population and detection of the first and second fractional edge channels. In this case the third channel does not contribute to the Hall conductance. The dotted line along the black center gate indicates the depletion area induced by the center gate voltage, which prevents conduction through the narrow openings separating the different gates.

Hall conductances. Note again that an integer calculation would give a constant Hall conductance at e^2/h . The Hall conductance in Fig. 3.2a is calculated from Eq. 3.1b with a fixed equal number of fully transmitted channels ($N_I = N_V = 2$) and the measured transmission of the third fractional channel of each barrier between 0 and 1, i.e. $2/3 \cdot e^2/h < G_A, G_B < e^2/h$ (Fig. 3.1). Fig. 3.2d shows that the Hall conductance can also be fixed at a value in between the plateaus, whenever the largest barrier conductance is fixed and not quantized (in this case $N_I < N_V = 2$, $T_V = 0.62$ when $V_B < -0.175$ V). In the region -0.175 V $< V_B < 0$ V the Hall conductance is determined by both barrier transmissions ($N_I = N_V = 2$ and $T_I, T_V \neq 0$). The curves in Fig. 3.2b and 3.2c can be compared directly with Fig. 3.1, because in these cases one probe is kept fixed at the $2/3$ quantized value. According to Eq. 3.1a, curve (b) in Fig. 3.2 should follow the current probe conductance G_B for $V_B > -0.175$ V ($N_I = N_V = 2$, $T_V = 0$ and $T_I \neq 0$) and be equal to $2/3 \cdot e^2/h$ for lower V_B ($N_V = 2 > N_I$). In Fig. 3.2c the Hall conductance should follow the voltage probe conductance G_A for $V_A > -0.175$ V ($N_V = N_I = 2$, $T_I = 0$ and $T_V \neq 0$) and be equal to $2/3 \cdot e^2/h$ for lower V_A ($N_I = 2 > N_V$). Comparing both curves 3.2b and 3.2c with Fig. 3.1, it can be seen that there is good agreement between the proposed description and experiment. Similar measurements as in Fig. 3.2b and 3.2c for a number of fixed voltages on one single gate between -0.19 V and -0.22 V, did not show any dependence of the measured Hall conductance

on this gate voltage. This indicates that in this range of gate voltage the barrier conductances G_A and G_B are indeed quantized at the $2/3$ fraction. The fact that the measured barrier conductances G_A and G_B do not show well defined fractional plateaus may be related to scattering in the not fully quantized bulk 2DEG, which is measured in series.

The observation that $G_{H;23,14}$ (i.e. with current and voltage probes being interchanged) is independent of V_A and V_B and equal to the bulk 2DEG value, can also be understood within the proposed description. In this case the Ohmic contact 1 (see inset Fig. 3.1) is the relevant voltage probe,⁷ which will equally couple to all edge channels in the 2DEG. The Hall conductance should now correspond to the bulk filling factor, as is found experimentally. Note that complete equilibration over the long distance from probe A to Ohmic contact 1 yields the same result.

The agreement between the proposed description in terms of fractional edge channels and the experiment demonstrates that adiabatic transport occurs over the distance between the current and voltage probe. Apparently, the boundary defined by the center gate (black gate in Fig. 3.3) is sufficiently smooth, such that scattering between the second and third fractional edge channel is suppressed. The fact that we did not observe a Hall conductance quantized at $1/3$ may indicate that the boundary is not sufficiently smooth to suppress scattering between the first and second fractional channel. Although the energy separation between the first and second and between the second and third fractional channels are expected to be equal, the separation in space may differ when the boundary potential changes nonlinearly. We have studied the influence of the smoothness of the boundary in more detail in a second sample of identical design, but with a higher electron density of $2.3 \cdot 10^{15} / \text{m}^2$. With -3.0 V applied to the center gate this sample did not show a deviation of the Hall conductance from the bulk 2DEG value, indicating that all channels are completely mixed. However, at lower voltages applied to the center gate, the Hall conductance showed quantization at anomalous values. With -4.5 V on the center gate the $2/3$ -fractional value was almost reached. Hall conductance measurements performed on this sample at a center gate voltage of -4.5 V confirmed the results presented in Fig. 3.2. Apparently a lower center gate voltage increases the depletion region until a sufficiently smooth boundary potential is formed at -4.5 V. Here the mixing between the second and third fractional channels is almost absent. It is difficult to determine quantitatively, including screening, the spatial locations of the fractional edge channels. However, the strong influence of the boundary potential evident from this experiment, clearly shows that the properties of the boundary are of prime importance for the anomalous fractional quantization of the Hall conductance, in accordance with the proposed description in terms of fractional edge channels.¹²

In a recent paper Beenakker⁹ extends the Landauer-Büttiker formalism to include the FQHE regime. He also theoretically demonstrates the formation of edge channels in the FQHE regime in a slowly varying boundary potential. The i th edge channel corresponding to the fractional filling factor ν_i contributes $(\nu_i - \nu_{i-1})e^2/h$ to the conductance, where ν_{i-1} is the lower filling factor corresponding to the next separated edge channel. If only the $p/3$ -states are considered, Eqs. 3.1 can be derived from the multi-terminal generalization given in Ref. 9.

In summary, transport in edge channels in the fractional quantum Hall regime has been studied experimentally by using two closely spaced adjustable barriers as current and voltage probes. By selectively populating and detecting these fractional edge channels, adiabatic transport over a distance exceeding $2\text{ }\mu\text{m}$ has been demonstrated. These results are in quantitative agreement with the generalized Landauer-Büttiker formalism for the fractional quantum Hall regime derived in Ref. 9.

ACKNOWLEDGEMENT

We thank C.W.J. Beenakker for communicating his results to us prior to publication. We also thank R. Eppenga, R.B. Laughlin, D. van der Marel, L.W. Molenkamp, J.E. Mooij, A.A.M. Staring and J.G. Williamson for valuable discussions, M.E.I. Broekaart and S. Phelps at the Philips Mask Centre, J.J. Harris at Philips (Redhill), and A. van der Enden at the Delft Centre for Submicron Technology for their contributions to the fabrication of the devices, and the Stichting F.O.M. for financial support.

REFERENCES

This chapter was published in Phys. Rev. Lett. **64**, 685 (1990).

1. See for two reviews: *The Quantum Hall Effect*, edited by R.E. Prange and S.M. Girvin (Springer-Verlag, New York, 1987); T. Chakraborty and P. Pietiläinen, *The Fractional Quantum Hall Effect*, (Springer-Verlag, New York, 1988).
2. B.I. Halperin, Phys. Rev. B **25**, 2185 (1982).
3. P. Streda, J. Kucera, and A.H. MacDonald, Phys. Rev. Lett. **59**, 1973 (1987).
4. J.K. Jain and S.A. Kivelson, Phys. Rev. Lett. **60**, 1542 (1988).
5. M. Büttiker, Phys. Rev. B **38**, 9375 (1988).
6. S. Komiyama, H. Hirai, S. Sasa, and S. Hiyamizu, Phys. Rev. B **40**, 12566 (1989).

- B.W. Alphenaar, P.L. McEuen, R.G. Wheeler, and R.N. Sacks, *Phys. Rev. Lett.* **64**, 677 (1990).
7. B.J. van Wees, E.M.M. Willems, C.J.P.M. Harmans, C.W.J. Beenakker, H. van Houten, J.G. Williamson, C.T. Foxon, and J.J. Harris, *Phys.Rev.Lett.* **62**, 1181 (1989).
 8. R.B. Laughlin, *Phys. Rev. Lett.* **50**, 1395 (1983).
 9. C.W.J. Beenakker, *Phys. Rev. Lett.* **64**, 216 (1990).
 10. A.M. Chang and J.E. Cunningham, *Solid State Commun.* **72**, 651 (1989).
 11. The experiments are performed with two adjacent Ohmic contacts on either side of the barrier. The configuration of voltage and current contacts was such that effectively the two-terminal conductance is measured.
 12. The strong influence of the boundary potential explains why we did not observe an anomalous fractional quantized Hall effect in a device with two adjacent point contacts, as being used in Ref. 7.

CHAPTER 4

Transport through Zero-Dimensional States in a Quantum Dot

Leo P. Kouwenhoven, Bart J. van Wees, and Kees J.P.M. Harmans

Faculty of Applied Physics, Delft University of Technology

P.O.Box 5046, 2600 GA Delft, The Netherlands

John G. Williamson

Philips Research Laboratories, 5600 JA Eindhoven, The Netherlands

ABSTRACT

We have studied the electron transport through zero-dimensional (0D) states. 0D-states are formed when one dimensional edge channels are confined in a quantum dot. The quantum dot is defined in a two dimensional electron gas with a split gate technique. To allow electronic transport, connection to the dot is arranged via two quantum point contacts, which have adjustable selective transmission properties for edge channels. The 0D-states show up as pronounced oscillations in the conductance (up to 40% of e^2/h), when the flux enclosed by the confined edge channel is varied, either by changing the magnetic field or the size of the dot. A prerequisite for the appearance of 0D-states is that the transport through the entire device is adiabatic (i.e. with conservation of quantum numbers), which will be shown to occur at high magnetic field. The experimental results are in good agreement with theory and show that in the ballistic quantum Hall regime the net current is carried entirely by edge channels.

4.1 INTRODUCTION

Advancing technology has made it possible to study the transport properties of a two-dimensional electron gas (2DEG) in the *ballistic regime*, for which the device dimensions must be much smaller than the elastic mean free path. One of the results is the observation of the quantum Hall effect (QHE) in ballistic submicron structures.¹ This observation shows that localized states can not be a prerequisite for the appearance of quantized Hall plateaus. An alternative approach to explain the QHE is based on the formation of *edge channels* when a high magnetic field is applied perpendicular to the 2DEG.² The description of the QHE can then be given within the Landauer-Büttiker formalism for electron transport.³ Besides their importance for explaining the QHE, edge channels have some fundamental properties which are interesting for further study. The electron transport in edge channels is one dimensional² and scattering between different channels can be extremely small.^{4,5}

Another result of studying ballistic transport is the discovery of the quantized conductance of short narrow wires or *quantum point contacts* (QPCs) at zero magnetic field. The conductance of QPCs is quantized at multiple values of $2e^2/h$, due to the formation of one dimensional (1D) subbands in the constriction.^{6,7} It was shown that in high magnetic fields QPCs can be used as selective transmitters of edge channels.⁸ Edge channels with different Landau level index can either be transmitted or reflected by a QPC. This enables one to study transport occurring in a selected edge channel, by selective current population or voltage detection of a particular edge channel.⁸

We have employed the properties of edge channels and QPCs for the construction of a *1D electron interferometer*, in which discrete zero-dimensional (0D) states are observed.⁹ The reduction to zero-dimensions is obtained by confining a 1D edge channel in a quantum dot between two partially transparent barriers. The transparency of the barriers allows a coupling to the 0D-states for electronic transport measurements. The 0D-states show up as pronounced oscillations in the conductance with maxima occurring whenever the energy of a 0D-state coincides with the Fermi energy. Electron transfer then takes place through resonant transmission. The experimental results are in good agreement with theory and confirm the Landauer-Büttiker description of confined electron transport in a quantizing magnetic field.

4.2 DEVICE DESCRIPTION

Fig. 4.1 shows the schematic layout of our device. A Hall-bar is defined in the 2DEG of a high mobility GaAs/AlGaAs hetero structure. The 2DEG has a transport mean free path of $9\text{ }\mu\text{m}$ and an electron density of $2.3 \cdot 10^{15}\text{ m}^{-2}$. On top of the hetero structure two pairs A and B of metallic gates are fabricated by standard optical and electron-beam lithographic techniques. A negative voltage of -0.2 V on both gate pairs depletes the electron gas underneath the gates and creates a quantum dot with a diameter of $1.5\text{ }\mu\text{m}$ in the 2DEG. The narrow channel separating the gate pairs is already pinched-off at this gate voltage. To allow electronic transport, connection from the wide 2DEG regions to the dot is arranged by two 300 nm wide QPCs. The transport properties of each individual QPC can be studied by applying the gate voltage to only one gate pair and zero voltage to the other. The electro static potential landscape at the QPC resembles a saddle shaped barrier. The height of the barrier E_B can be increased by reducing (making more negative!) the gate voltage until the QPC is pinched-off at -1 V .

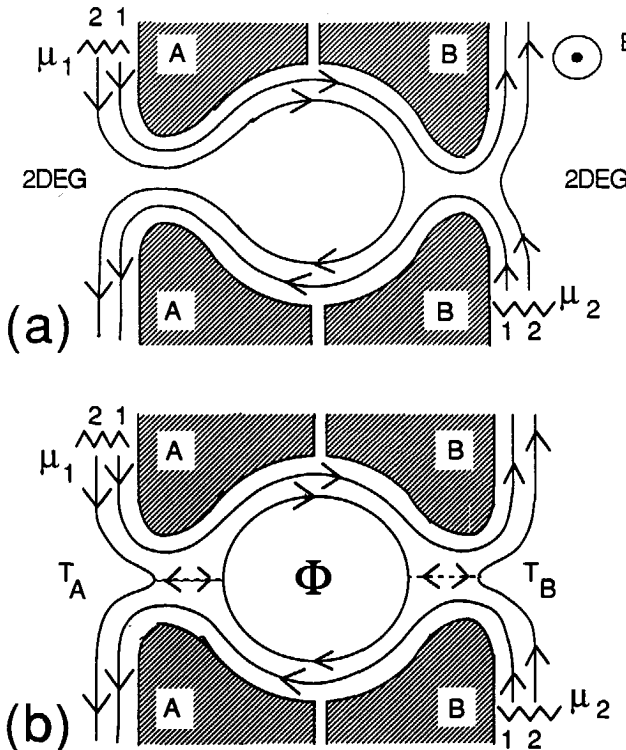


FIG. 4.1. Schematic layout of the quantum dot with diameter of $1.5\text{ }\mu\text{m}$ and two 300 nm wide quantum point contacts. The electron flow in edge channels is shown when a high magnetic field B is applied. (a) illustrates adiabatic transport for unequal QPCs A and B. (b) A 1D loop is formed when an edge channel is only partially transmitted by both QPCs.

4.3 EDGE CHANNELS AND SELECTIVE TRANSMISSION OF QPCs

In this section we describe the main properties of edge channels and the selective transmission of them by QPCs. In a high magnetic field the energy of the electrons is given by:

$$E_n = (n - \frac{1}{2})\hbar\omega_c \pm \frac{1}{2}g\mu_B B + eV(x,y) \quad (4.1)$$

with $n = 1, 2, 3, \dots$ the Landau level index, $g\mu_B B$ the spin splitting, and $V(x,y)$ is the electro static potential, which will be nominally flat in the interior of the sample and rising at the boundary (see Fig. 4.2). Electro static variations due to impurities are ignored because we are dealing with ballistic samples. The electron states at the left-hand side of the sample are occupied up to μ_1 , the electro chemical potential of the current source, and their velocity direction is perpendicular to the cross-section of Fig. 4.2. At the right-hand side the electron states are filled up to μ_2 , the electro chemical potential of the current drain and their velocity is in opposite direction. The difference in occupation $eV = \mu_1 - \mu_2$ (determined by the voltage V between current source and drain) between the two edges results in a net current flowing along the boundary of the sample. It can be shown ² that the transport in edge channels is one dimensional. From the well-known cancellation of density of states with velocity in one dimension it follows that the net current in each (spin split) Landau level is given by $I = e/h(\mu_1 - \mu_2)$. The location of the current-carrying electron states elucidates the name of edge channels. The ratio current/voltage yields the quantized conductance e^2/h contributed by each occupied Landau level.

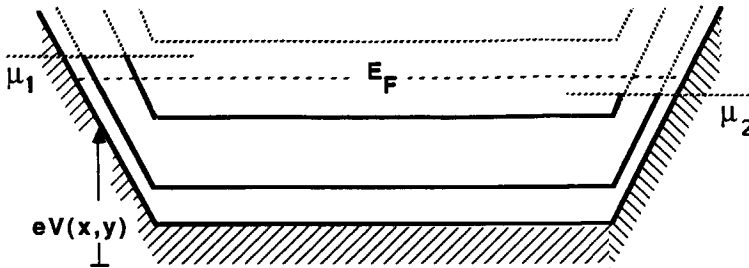


FIG. 4.2. Occupied electron states (bold) in Landau levels in the presence of a current flow, illustrating the formation of edge channels at the 2DEG boundary potential $V(x,y)$ where the Landau levels intersect the Fermi energy E_F .

Although the above model is obviously highly simplified, it leads to some important features of transport in a high magnetic field. Büttiker¹⁰ has pointed out that backscattering involves scattering between the opposite sample edges, which is suppressed when the current-carrying electrons with energies between μ_1 and μ_2 are not connected to the other boundary through available electron states. This is the case when the Fermi energy is between two bulk Landau levels (see Fig. 4.2). Experimentally it was also shown that forward scattering between different edge channels at the same sample boundary is surprisingly low, even over macroscopic distances much larger than the zero field mean free path.^{4,5} This means that the transport in edge channels is primarily *adiabatic*, i.e. with conservation of quantum index n . The fact that the transport in edge channels is adiabatic justifies they are being viewed as *independent 1D current-channels*.

The relevant electron states for transport are only those at the Fermi energy E_F . The spatial location of the current-carrying electrons results from the condition $E_F = E_n$, yielding:

$$eV(x,y) = E_G = E_F - (n - \frac{1}{2})\hbar\omega_c \pm \frac{1}{2}g\mu_B B \quad (4.2)$$

E_G is known as the guiding energy.¹¹ Eq. 4.2 implies that edge channels with different Landau level index n or opposite spin direction, while all located at the sample boundary, follow different equipotential lines.

Using their controllable barrier height E_B , QPCs can be used as selective edge channel transmitters. Those edge channels for which $E_G < E_B$ will be reflected by a QPC and those with $E_G > E_B$ can pass through the QPC. Because only the transmitted edge channels contribute, the two-terminal conductance G of a single QPC is given by:

$$G = \frac{e^2}{h} (N + T) \quad (4.3)$$

Here N denotes the number of fully transmitted channels and T the partial transmission of the upper edge channel. From $E_B = E_B(V_g)$ and $E_G = E_G(B)$, it follows that the number of transmitted channels can be changed by varying the magnetic field or the gate voltage. Conductance quantization occurs in those intervals for B and V_g where $T = 0$. From experiments^{5,8} we know that Eq. 4.3 holds very well, meaning that QPCs fully transmit the lower indexed edge channels (which follow higher equipotential lines, see Eq. 4.2) and partially transmit the upper channel without inducing scattering between the available edge channels.

4.4 ADIABATIC TRANSPORT IN SERIES QPCs

When two QPCs are placed in series the question arises whether the series resistance in the ballistic transport regime is just the Ohmic addition of the individual QPC resistances.¹² We have studied this for the geometry of Fig. 4.1, where the two QPCs are connected by a cavity. At zero magnetic field the incoming electrons will scatter randomly in the cavity and establish a more or less isotropic velocity distribution. In this way the cavity acts as a reservoir and the series resistance is just the Ohmic addition of the individual QPC resistances. This situation changes at a high magnetic field when the electron motion is confined to edge channels. If no scattering occurs between different channels the transport is adiabatic. The QPC with the highest barrier and consequently with the lowest number of transmitted channels will form the "bottleneck" for the total system. Those channels which can pass the highest barrier in the circuit can also pass the other barriers (see Fig. 4.1a). The series conductance G_D then is completely determined by the smallest of the two conductances of the individual QPCs: $G_D = \min(G_A, G_B)$, where G_A and G_B are given by Eq. 4.3.

If both QPCs transmit the same number of channels N and the upper edge channel is only partially transmitted (see Fig. 4.1b), the dot conductance G_D is given by:

$$G_D = \frac{e^2}{h} (N + T_2) \quad (4.4)$$

The partial transmission T_2 of the upper edge channel through the 2 barriers in series can easily be calculated from the transmissions T_A and T_B of the individual QPCs. Ignoring interference effects which will be considered in the next section, an incoming electron will be directly transmitted through both QPCs with probability $T_A T_B$. After making one loop around the dot, the next probability to be transmitted is $T_A R_B R_A T_B$ (with $R = 1 - T$). A second loop gives $T_A (R_B R_A)^2 T_B$, etc. Summing all contributions yields for the total transmission probability:

$$T_2 = T_A T_B [1 + R_A R_B + (R_A R_B)^2 + \dots] = \frac{T_A T_B}{1 - R_A R_B} \quad (4.5)$$

Eq. 4.5 is the classical result for the transmission of a single channel through two barriers.

In Ref. 13 a detailed study is described on the transition from Ohmic transport (at $B = 0$ T) to adiabatic transport (at $B = 1$ T) in series QPCs. The measurements at $B = 1$ T and at a temperature of 0.6 K (so interference effects are averaged out) are shown in Fig. 4.3. The

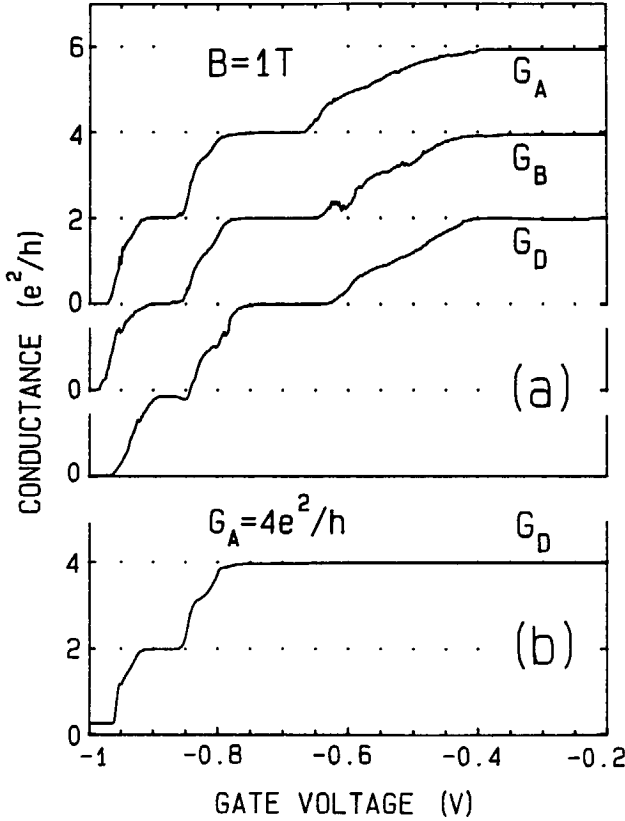


FIG. 4.3. Conductances G_A and G_B of the individual QPCs and G_D of the two QPCs in series demonstrating adiabatic transport at $B = 1$ T. (a) for equal voltage on both gate pairs A and B. (b) for fixed -0.7 V on gate pair A and varying the gate voltage on pair B.

conductances G_A and G_B measured with zero voltage applied to the other gate pair, show (spin degenerate) plateaus at integer multiples of $2e^2/h$. The series conductance G_D plotted in Fig. 4.3a is measured with equal voltage applied to both gate pairs. G_D also shows quantized plateaus whenever both conductances G_A and G_B are quantized. The step height of $2e^2/h$ demonstrates adiabatic transport through the series QPC device. Scattering between different edge channels would yield smaller steps (which is observed for $B < 1$ T, see Ref. 13). The transition regions between the plateaus are in good agreement with a calculation from Eq. 4.5 (not shown here). A

further test if adiabatic transport takes place is shown in Fig. 4.3b. In this experiment the gate voltage V_g on pair A is fixed at -0.7 V and the voltage on gate pair B is varied. The series conductance should now be equal to $G_A = 4e^2/h$ for $V_g > -0.7$ V and equal to G_B for $V_g < -0.7$ V. Comparing Fig. 4.3b with 4.3a it can be seen that the series conductance is indeed in good agreement with $G_D = \min(G_A, G_B)$. *We conclude that the transport through the series QPC device is adiabatic, whenever transport through edge channels takes place at a sufficiently high magnetic field.*

4.5 TRANSPORT THROUGH 0D-STATES

4.5.1 Theory

In the previous section we derived the classical transmission probability T_2 for a 1D double barrier structure. Here we give a simple quantum mechanical derivation.¹⁴ Consider an incoming electron with a wavefunction Ψ_{in} from the left in the partial transmitted edge channel of Fig. 4.1b. The right- and left-moving waves Ψ_R and Ψ_L in the dot are mutually connected through: $\Psi_R = \sqrt{T_A} \Psi_{in} + \sqrt{R_A} \Psi_L$ and $\Psi_L = \sqrt{R_B} \Psi_R \exp(i\theta)$, when both are evaluated at QPC A . θ denotes the acquired phase after making one revolution around the dot (we neglect the constant phase-shift due to reflection or transmission by the barrier). With $\Psi_{out} = \sqrt{T_B} \Psi_R$ for the outgoing wave at the right, the transmission probability $T_2 = |\Psi_{out}|^2 / |\Psi_{in}|^2$ is given by:

$$T_2 = \frac{T_A T_B}{1 - 2 \sqrt{R_A R_B} \cos \theta + R_A R_B} \quad (4.6)$$

To illustrate Eq. 4.6, the transmission T_2 is shown versus the phase θ for 3 combinations of the barrier transmissions T_A and T_B in Fig. 4.4, where it is seen that T_2 is periodic in phase with a period of 2π . The amplitude and shape of the oscillations are determined by the values of the barrier transmissions. For small barrier transmissions the oscillations appear as sharp (Lorentzian-shaped) peaks with minima approaching 0. The effect of increasing the barrier transmissions is that the oscillations round off and the minima are lifted. The striking quantum mechanical aspect of Fig. 4.6 is that the transmission probability of 2 barriers in series can be larger than the probabilities of the individual barriers. This is known as *resonant transmission* and is most apparent for equal barrier transmissions $T_A = T_B$ for which the maxima in T_2 are equal to 1. The maxima are smaller than 1 for asymmetric barrier transmissions $T_A \neq T_B$. The above considerations are general for transport through 0D-states in non-interacting systems. The

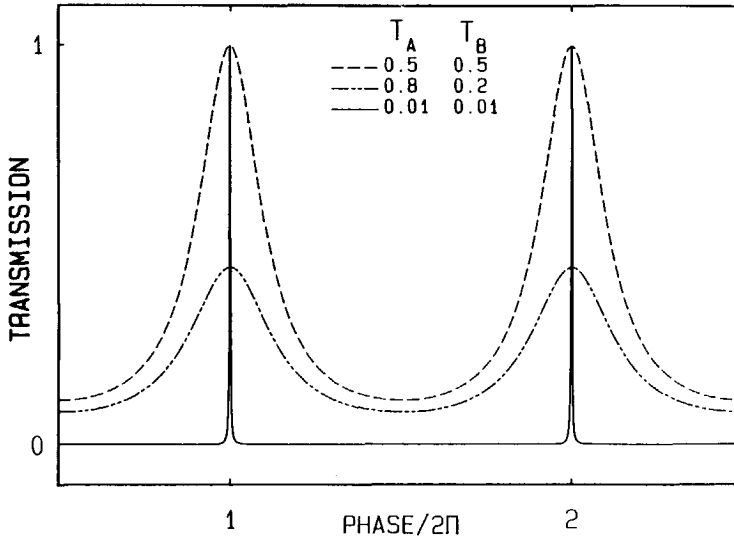


FIG. 4.4. Transmission probability T_2 versus phase for different barrier transmissions T_A and T_B . Note that at resonance T_2 can be larger than T_A and T_B .

same properties were deduced from numerical calculations on the transmission of small quantum boxes in which 0D-states are formed at zero magnetic field.¹⁵

In our quantum dot the phase θ is determined by the enclosed flux: $\theta = 2\pi BA/\phi_0$, where A denotes the area enclosed by the edge channel loop and $\phi_0 = h/e$ is the flux quantum. Whenever the enclosed flux $\Phi = BA$ equals an integer number of flux quanta the transmission T_2 is resonant. In terms of energies, the resonance results from the formation of 0D-states in the confined edge channel due to the finite circumference of this 1D loop. Resonant transmission occurs whenever the Fermi energy E_F of the reservoirs coincides with a 0D-state. This is most clear for very weak coupling ($T_A = T_B = 0$) to the quantum dot. Then the eigenstates of the dot are nearly undisturbed so that resonant transmission through the discrete 0D-states will give rise to sharp peaks in the conductance with a maximal amplitude of e^2/h .

Note that Eq. 4.6 is exactly the formula for a 1D interferometer. While in our case the phase is determined by the enclosed flux, Eq. 4.6 also holds for a 1D cavity in between two barriers, where the product of cavity length and longitudinal wave vector determines the phase θ . This configuration has been investigated recently by Smith et al.¹⁶ in an experiment where they were

able to vary the distance between the two barriers. Also other related transport experiments have shown the formation of 0D-states due to electro static confinement in all three spatial dimensions.¹⁷

4.5.2 Experiment

The two-terminal conductance measurements presented in this section are all performed at 6 mK. In Fig. 4.5, the two-terminal magneto-conductance G_D of the dot is plotted. G_D shows quantized (spin-split) plateaus above 1 T at integer multiples of e^2/h . Note that despite the two-terminal measurement no Shubnikov-de Haas resistance oscillations originating from the wide regions of 2DEG are seen, superposed on the quantized plateaus. This is because the non-equilibrium population between the transmitted and reflected edge channels by the QPCs is maintained over macroscopic distances, which was studied in detail in Ref. 4 and 5. At the plateaus in Fig. 4.5, edge channels are either fully transmitted or completely reflected by the QPCs (so $T_2 = 0$), which corresponds to 1D transport through the dot. The transitions between the plateaus (where $T_2 \neq 0$) correspond to the situation of Fig. 4.1b, where an edge channel is confined into a loop and where transport through 0D-states is expected.

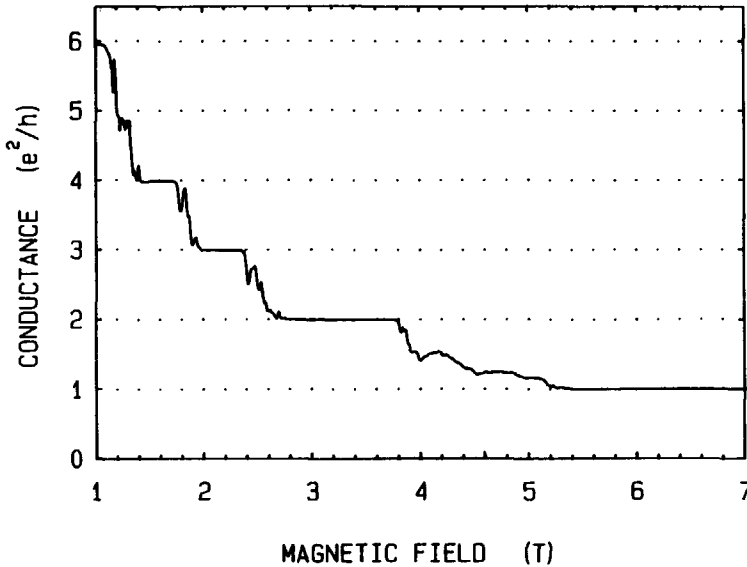


FIG. 4.5. Conductance G_D of the quantum dot as a function of magnetic field with $V_g = -0.35$ V applied to both gate pairs. The quantized (spin-split) plateaus indicate 1D-transport, while at the transitions 0D-transport is expected.

To show this we have measured, on an expanded scale, the transition from the second to the third plateau, where the lowest two channels are fully transmitted ($N = 2$) and the third channel is partially transmitted ($T_2 \neq 0$). First we have plotted in Fig. 4.6a and 4.6b the conductances G_A and G_B of the individual QPCs to enable a comparison with the conductance G_D of the complete device. The conductance G_A and G_B are obtained with -0.35 V on the corresponding gate pair, and zero voltage applied to the other pair. The increasing magnetic field gradually reduces the transmissions T_A and T_B of the third edge channel from 1 to 0. The irregular structure can be attributed to random interferences in the QPCs.¹⁸ The conductance G_D of the dot is shown in Fig. 4.6c, which is measured with $V_g = -0.35$ V on both gate pairs. Large oscillations are seen in between the plateau regions. The amplitude modulation of the oscillations is up to 40% of e^2/h . The fact that the oscillations do not exceed $3e^2/h$ nor drop below $2e^2/h$ indicates that the oscillations originate from the third edge channel only. The curve plotted in Fig. 4.6d is calculated from Eq. 4.6 with the measured conductances G_A and G_B substituted for T_A and T_B . We will discuss this comparison between theory and experiment in more detail below.

Fig. 4.7a shows the *0D-oscillations* on an expanded scale, and illustrates their regularity. The period B_o of the oscillations smoothly varies from $B_o = 2.5$ mT at $B = 2.5$ T to $B_o = 2.8$ mT at $B = 2.7$ T. Fig. 4.7b shows the region of low transmission where due to the weak coupling the oscillations appear as sharp peaks. The contribution to the conductance of the third edge channel is nearly zero except when the Fermi energy coincides with the energy of a 0D-state. *The discrete narrow peaks clearly demonstrate the resonant transmission through the quantum dot.*

0D-states belonging to other partially transmitted edge channels are also observed. In Fig. 4.7c the oscillations are shown which originate from the second channel. A striking feature is that the period ($B_o = 5.3$ mT at $B = 5.1$ T) differs from the period of the oscillations belonging to the third edge channel. Also the observed oscillations from the fourth ($B_o = 2.1$ mT at $B = 1.85$ T) and fifth ($B_o = 1.4$ mT at $B = 1.25$ T) edge channels differ in their period. The origin of the difference in period for different edge channels will be discussed below. *However, the observation of a distinct period for each transition again indicates that the oscillations originate from a single edge channel only.*

To estimate the energy separation between consecutive 0D-states, we have measured the oscillations for different temperatures and voltages across the sample. The oscillations disappear above 200 mK and 40 μ V, which both lead to an energy separation of about 40 μ eV.

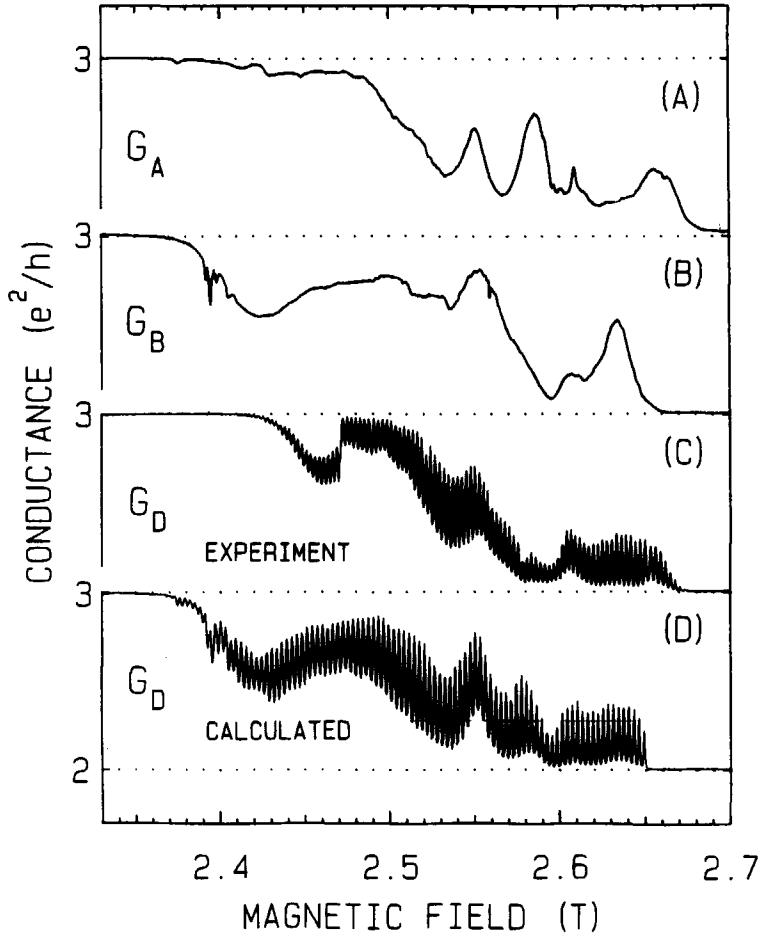


FIG. 4.6. Transition from the second to the third plateau of the QPC conductances G_A (a) and G_B (b) and of the dot G_D (c). Large oscillations are seen in G_D whenever both G_A and G_B are not quantized. A calculation of G_D from Eq. 4.6 is shown in (d); see text.

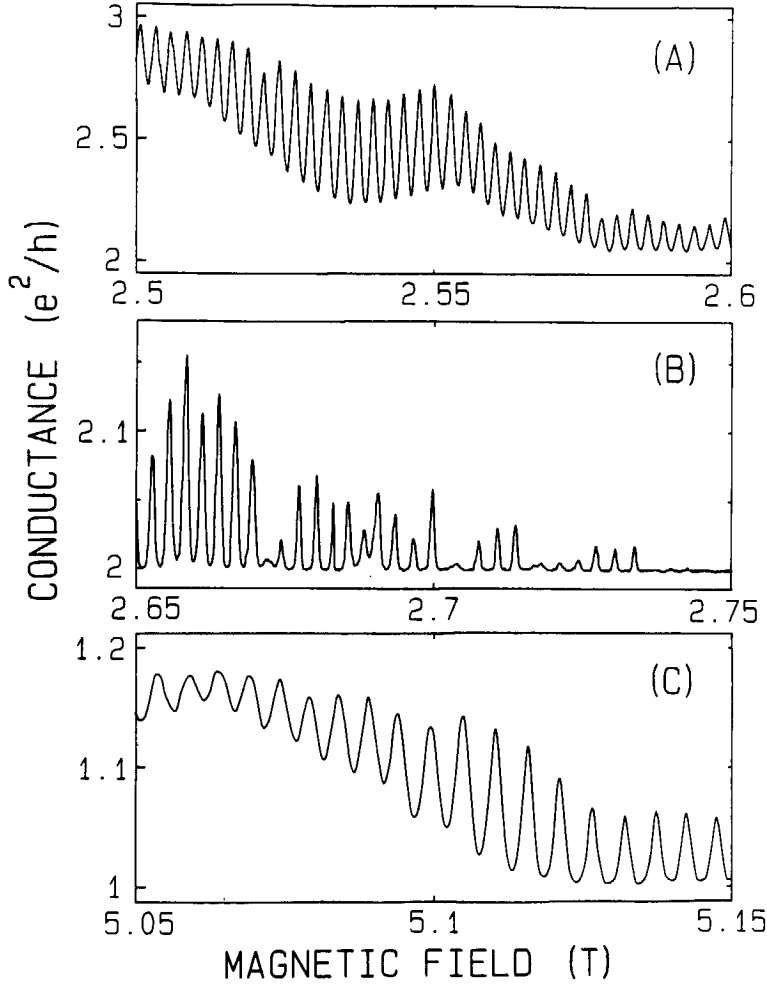


FIG. 4.7. (a) Enlarged oscillations from Fig. 4.6c showing their regularity (period $B_0 = 2.5$ mT). (b) Region of low transmissions of the third edge channel ($G_A, G_B \approx 2$). The discrete conductance peaks demonstrate resonant transmission through 0D-states. (c) 0D-oscillations belonging to the second edge channel (period $B_0 = 5.3$ mT).

In Fig. 4.6 the QPCs are in the transition between $2e^2/h$ and $3e^2/h$ over the same magnetic field range, which gives rise to 0D-oscillations in the conductance of the dot over the entire range between the two plateaus. The oscillations of Fig. 4.6c are plotted again in Fig. 4.8 (lower curve). The upper curve is measured with different voltages on the gate pairs, such that the transition from the second to the third plateau of QPC *B* is shifted to a lower magnetic field. It follows from Eq. 4.6 that if $T_A = 1$ then $T_2 = T_B$, and if $T_B = 0$ then $T_2 = 0$; so no 0D-oscillations are expected when one of the QPC conductances is quantized. The 0D-oscillations are expected only when both QPCs are in the transition between two plateaus (i.e. when $0 < T_A, T_B < 1$). This is observed in the upper curve of Fig. 4.8 where the 0D-oscillations do appear in the region near the second plateau, but are suppressed near the third plateau.

An alternative way to change the flux is by changing the area enclosed by the confined edge channel. This is accomplished by varying the gate voltage at a fixed magnetic field. Fig. 4.9a shows the 0D-states for $B = 2.5$ T and a changing gate voltage on both gate pairs. The oscillation period is 1 mV. For a fixed voltage (-0.35 V) on one gate pair and a changing voltage on the

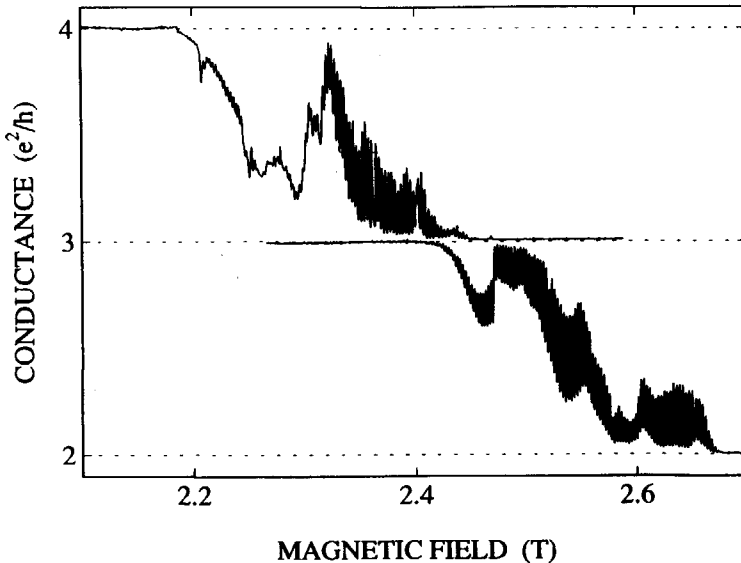


FIG. 4.8. Comparison of the 0D-oscillations for roughly equal barrier transmissions (lower curve where the voltage on both gate pairs is -0.35 V) with those with differing transmissions (upper curve where the voltage on pair A is -0.35 V and on pair B is -0.47 V). The upper curve has an offset for clarity.

other pair the observed period is 2 mV, as can be seen in Fig. 4.9b. Assuming that in the latter case only half of the area in the dot is effected, we conclude that a variation in gate voltage changes the area enclosed by the edge channels. *Thus our device also provides an electro static control of the resonant transmission through 0D-states.*

4.5.3 Discussion

Eq. 4.6 shows that the envelope of the 0D-oscillations is determined by the coupling to the quantum dot through the barrier transmissions T_A and T_B . Only for very weak and equal coupling ($T_A = T_B \approx 0$) the amplitude modulation can approach 100% of e^2/h . To illustrate this we have calculated the envelope function from the measured conductances G_A and G_B (see Fig. 4.6a and 4.6b) of the individual QPCs. The outer curves in Fig. 4.10 are calculated for $\cos\theta = 1$ (upper curve) and $\cos\theta = -1$ (lower curve) substituted in Eq. 4.6. This envelope function would be the amplitude modulation of the 0D-oscillations at zero temperature. The conductance G_D calculated from the measured G_A and G_B and taken temperature averaging into account, is also

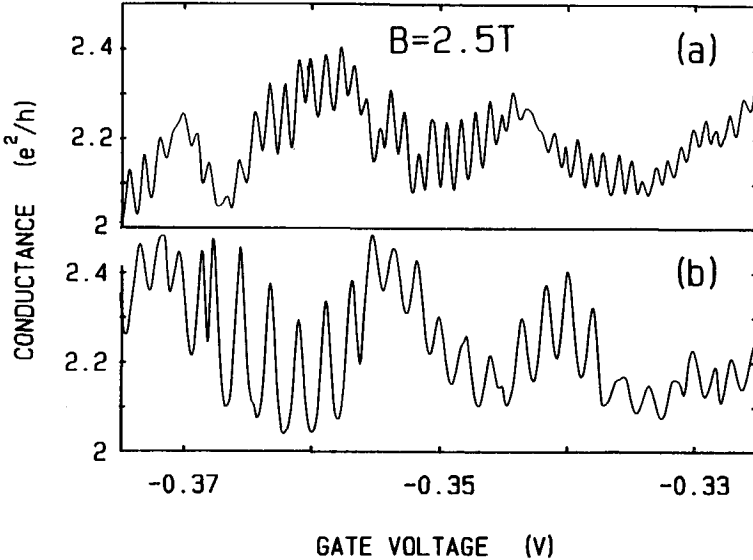


FIG. 4.9. Conductance oscillations as a function of gate voltage for a fixed magnetic field $B = 2.5$ T. In (a) the voltage on both gate pairs is varied (period = 1 mV) and in (b) the gate voltage on one pair is kept fixed at -0.35 V and varied on the other gate pair (period = 2 mV).

plotted in Fig. 4.10. We have included temperature averaging in the calculation with the expression $G_D(T) = \int G_D(E) \cdot [\partial f / \partial E] \cdot dE$ in which $f(E, T)$ is the Fermi distribution function and $G_D(E)$ the energy dependent conductance at zero temperature. The latter can be obtained from Eq. 4.4 and 4.6 by noting that a change in phase of 2π corresponds to a change in energy of $40 \mu\text{eV}$. Note that averaging of Eq. 4.6 over a large energy range (larger than the energy range corresponding to a change in phase of 2π) gives the classical result of Eq. 4.5. We have chosen a fixed period of 3 mT in the calculation and an effective temperature of 20 mK, which is the sample temperature (6 mK) plus a contribution from the voltage ($\approx 6 \mu\text{V}$) across the sample. The difference between the outer curves and the oscillating curve illustrates how the finite temperature of 20 mK affects the 0D-oscillations. The temperature averaging is strongest around 2.6 T where due to the weak coupling ($T_A, T_B \approx 0$) the oscillations have a peak shape. Temperature averaging is less effective on the rounded oscillations between 2.4 and 2.5 T (where $T_A, T_B \approx 0.5$). The calculated conductance G_D of Fig. 4.10 is also plotted in Fig. 4.5d where it can be seen to be in good agreement with the measured conductance. The exact modulation is not reproduced in the calculation, which is probably due to a slight mutual influence when voltages are applied to both gate pairs.

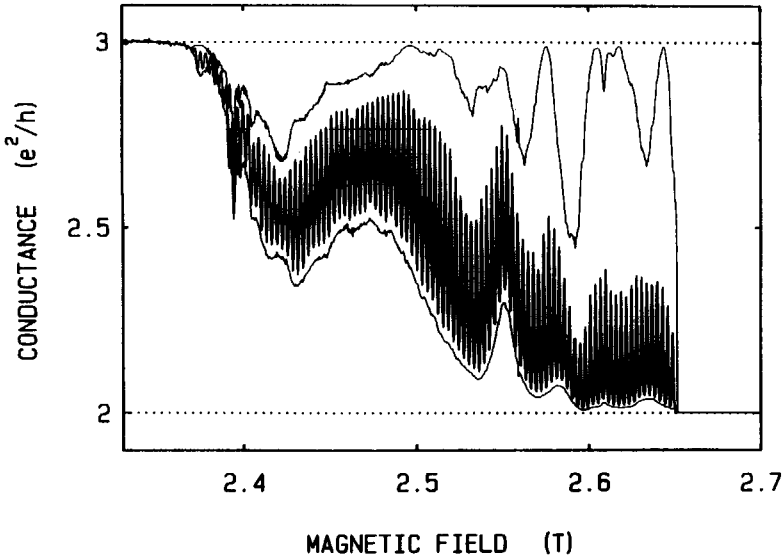


FIG. 4.10. Calculation from Eq. 4.6 of the amplitude modulation of the 0D-oscillations at 0 K (outer curves) from the measured conductances G_A and G_B (taken from Fig. 4.5a and 4.5b) and of the conductance G_D for which an energy averaging is taken into account corresponding to 20 mK.

The conductance oscillations described in this paper are reminiscent of the Aharonov-Bohm effect observed in small metal¹⁹ and semiconductor rings.²⁰ However, in these systems the electrons are already confined in a ring in the absence of a magnetic field. The conductance of such rings oscillates as a function of B with a period ϕ_0/A (A is the fixed area enclosed by the ring) even if the wires are not 1D. In semiconductor rings this Aharonov-Bohm effect quenches for high magnetic fields when edge channels are formed in the wires.²⁰ In contrast to this, edge channels are the starting point for the occurrence of oscillations in the quantum dot. The period of our oscillations is also not simply determined by the dot area because of the change in location of the edge channels when the magnetic field is varied. The change in radius Δr of the edge channel loop follows from Eq. 4.2 as: $\Delta r = \Delta V(x,y)/E = \Delta E_G/(eE)$ which varies with the magnetic field, differs for different indices n or spin direction, and depends on the "hardness" of the boundary potential given by the radial electric field E . Assuming circular symmetry for the edge channel loop we can write the change in enclosed flux $\Delta\Phi$ resulting from a change in field ΔB as:

$$\Delta\phi = \Delta(B\pi r^2) = \pi r^2 \Delta B + B 2\pi r \Delta r = (\pi r^2 + \frac{B 2\pi r}{eE} \frac{\partial E_G}{\partial B}) \Delta B \quad (4.7)$$

Evaluation of Eq. 4.7 with $r = 750$ nm, $B = 2.5$ T and a rough estimate $E \approx 10^4 - 10^5$ V/m shows that the second term (which is negative!) can be of the same order of magnitude as the first term.²¹ The observed period $B_0 = \phi_0 \Delta B / \Delta\Phi$ is therefore not simply determined by the enclosed area. The observation of distinct periods at different transitions, well separated by quantized regions, shows that the oscillations originate from single 1D edge channels. This conclusion provides strong evidence that *in the ballistic quantum Hall regime the net current is completely carried by edge channels*.

4.6 CONCLUDING REMARKS

Edge channels in combination with QPCs provide a simple and elegant system for studying electron transport of reduced dimensionality. Using the adjustable barriers of QPCs we have realized a 1D electron interferometer. The rigidity of edge channels is illustrated by the occurrence of adiabatic transport through the series QPC device. Single electron 0D-states are formed when a 1D edge channel is confined between two barriers. The Fermi energy can be tuned through the 0D-states by varying the magnetic field and/or the gate voltage. The resonant

transmission through 0D-states is clearly observed as regular oscillations in the conductance. Each oscillation corresponds to the (de)population of an edge channel by a single electron. The experiment confirms the edge channel description of transport in the ballistic quantum Hall regime.

ACKNOWLEDGEMENT

We thank L.W. Molenkamp and A.A.M. Staring for valuable discussions, W. Kool for assistance with the experiments, M.E.I. Broekaart, S. Phelps and C.E. Timmering at the Philips Mask Centre, C.T. Foxon, J.J. Harris and the Delft Centre for Submicron Technology for their contribution in the fabrication of the devices, and the Stichting F.O.M. for financial support.

REFERENCES

The main part of this chapter was published in *Phys. Rev. Lett.* **62**, 2523 (1989) and in *Surface Science* **229**, 290 (1990).

1. G. Timp, A.M. Chang, P. Mankiewich, R. Behringer, J.E. Cunningham, T.Y. Chang, and R.E. Howard, *Phys. Rev. Lett.* **59**, 732 (1987);
M.L. Roukes, A. Scherer, S.J. Allen, H.G. Craighead, R.M. Ruthen, E.D. Beebe, and J.P. Harbison, *Phys. Rev. Lett.* **59**, 3011 (1987);
B.E. Kane, D.C. Tsui, and G. Weimann, *Phys. Rev. Lett.* **59**, 1353 (1987).
2. B.I. Halperin, *Phys. Rev. B* **25**, 2185 (1982).
3. P. Streda, J. Kucera, and A.H. MacDonald, *Phys. Rev. Lett.* **59**, 1973 (1987);
J.K. Jain and S.A. Kivelson, *Phys. Rev. Lett.* **60**, 1542 (1988).
4. S. Komiyama, H. Hirai, S. Sasa, and S. Hiyamizu, *Phys. Rev. B* **40**, 12566 (1989).
5. B.J. van Wees, E.M.M. Willems, L.P. Kouwenhoven, C.J.P.M. Harmans, J.G. Williamson, C.T. Foxon, and J.J. Harris, *Phys. Rev. B* **39**, 8066 (1989).
6. D.A. Wharam, T.J. Thornton, R. Newbury, M. Pepper, H. Ahmed, J.E.F. Frost, D.G. Hasko, D.C. Peacock, D.A. Ritchie, and G.A.C. Jones, *J. Phys. C* **21**, L209 (1988).
7. B.J. van Wees, H. van Houten, C.W.J. Beenakker, J.G. Williamson, L.P. Kouwenhoven, D. van der Marel, and C.T. Foxon, *Phys. Rev. Lett.* **60**, 848 (1988);
See also chapter 1 in this thesis.
8. B.J. van Wees, E.M.M. Willems, C.J.P.M. Harmans, C.W.J. Beenakker, H. van Houten, J.G. Williamson, C.T. Foxon, and J.J. Harris, *Phys. Rev. Lett.* **62**, 1181 (1989);
See also chapter 1 in this thesis.

9. The main results of this paper are also described in: B.J. van Wees, L.P. Kouwenhoven, C.J.P.M. Harmans, J.G. Williamson, C.E. Timmering, M.E.I. Broekaart, C.T. Foxon, and J.J. Harris, *Phys. Rev. Lett.* **62**, 2523 (1989);
L.P. Kouwenhoven, B.J. van Wees, C.J.P.M. Harmans and J.G. Williamson, in *Proceedings of the Workshop on Science and Engineering of 1- and 0-dimensional Semiconductors*, edited by C.M. Sotomayor-Torres and S.P. Beaumont (Plenum Press, New York, 1990).
10. M. Büttiker, *Phys. Rev. B* **38**, 9375 (1988).
11. *The Quantum Hall Effect*, edited by R.E. Prange and S.M. Girvin (Springer-Verlag, New York, 1987).
12. This has been studied first by: D.A. Wharam, M. Pepper, H. Ahmed, J.E.F. Frost, D.G. Hasko, D.C. Peacock, D.A. Ritchie, and G.A.C. Jones, *J.Phys.C* **21**, L887 (1988);
A theoretical study is described in: C.W.J. Beenakker and H. van Houten, *Phys. Rev. B* **39**, 10445 (1989).
13. L.P. Kouwenhoven, B.J. van Wees, W. Kool, C.J.P.M. Harmans, A.A.M. Staring, and C.T. Foxon, *Phys. Rev. B* **40**, 8083 (1989);
See also chapter 1 in this thesis;
General conditions for the occurrence of adiabatic transport is described by: L.I. Glazman and M. Jonson, *J. Phys. Condens. Matter* **1**, 5547 (1989).
14. A theoretical study of a 2D dot to which narrow leads are attached is given by U. Sivan, Y. Imry, and C. Hartzstein, *Phys. Rev. B* **39**, 1242 (1989);
U. Sivan, and Y. Imry, *Phys. Rev. Lett.* **61**, 1001 (1988).
15. D. van der Marel, in *Proceedings of the International Symposium on Nano-Structure Physics and Fabrication*, edited by M.A. Reed and W.P. Kirk (Academic Press, New York, 1989).
16. C.G. Smith, M. Pepper, H. Ahmed, J.E. Frost, D.G. Hasko, D.C. Peacock, D.A. Ritchie and G.A.C. Jones, *J. Phys. C* **21**, L893 (1988).
17. M.A. Reed, J.N. Randall, R.J. Aggarwal, R.J. Matyi, T.M. Moore, and A.E. Wetsel, *Phys. Rev. Lett.* **60**, 535 (1988);
T.P. Smith III, K.Y. Lee, C.M. Knoedler, J.M. Hong, and D.P. Kern, *Phys. Rev. B* **38**, 2172 (1988);
18. Regular Aharonov-Bohm oscillations in a single QPC has been reported by P.H.M. van Loosdrecht, C.W.J. Beenakker, H. van Houten, J.G. Williamson, B.J. van Wees, J.E. Mooij, C.T. Foxon, and J.J. Harris, *Phys. Rev. B* **38**, 10162 (1988).
19. R.A. Webb, S. Washburn, C.P. Umbach, R.B. Laibowitz, *Phys. Rev. Lett.* **54**, 2696 (1985).
20. G. Timp, A.M. Chang, J.E. Cunningham, T.Y. Chang, P. Mankiewich, R. Behringer, and R.E. Howard, *Phys. Rev. Lett.* **58**, 2814 (1987);
C.J.B. Ford, T.J. Thornton, R. Newbury, M. Pepper, H. Ahmed, C.T. Foxon, J.J. Harris, and C. Roberts, *J. Phys. C Solid State Phys.* **21**, L325 (1988);
G. Timp, P.M. Mankiewich, P. de Vegvar, R. Behringer, J.E. Cunningham, R.E.

Howard, H.U. Baranger, and J.K. Jain, Phys. Rev. B **39**, 6227 (1989).

21. At the 2DEG boundary the electro static potential changes by an amount E_F/e (≈ 9 mV) in a depletion region which is about 300 nm wide. This gives a typical field strength $E \approx 3 \cdot 10^4$ V/m. A derivation of the period is also given by L.I. Glazman and M. Jonson in Ref. 13.

CHAPTER 5

Transport through a Finite One Dimensional Crystal

L.P. Kouwenhoven, F.W.J. Hekking, B.J. van Wees, and C.J.P.M. Harmans

Faculty of Applied Physics, Delft University of Technology

P.O.Box 5046, 2600 GA Delft, The Netherlands

C.E. Timmering

Philips Research Laboratories, 5600 JA Eindhoven, The Netherlands

C.T. Foxon

Philips Research Laboratories, Redhill, Surrey RH1 5HA, United Kingdom

ABSTRACT

We have studied the magneto-transport properties of an artificial one dimensional crystal. The crystal consists of a sequence of 15 quantum dots, defined in the two dimensional electron gas of a GaAs/AlGaAs hetero structure by means of a split-gate technique. At a fixed magnetic field of 2 T, two types of oscillations with different amplitude and period are observed in the conductance as a function of gate voltage. A simple model demonstrates that the oscillations arise from the formation of a mini-band structure in the periodic crystal, including energy gaps and mini-bands which contain 15 discrete states.

5.1 INTRODUCTION

One of the basic principles of solid state theory is the formation of an energy band structure in a regular crystal. The coupling between atomic states in a perfect crystal results in a collective state which is characterized by energy bands separated by energy gaps. The conductivity properties of a solid strongly depend on the location of the Fermi energy in the band structure. The solid is an electrical insulator (at 0 K) if the Fermi energy lays within an energy gap or an electrical conductor if the Fermi energy is within an energy band.

Early in the seventies, Esaki and Tsu¹ proposed that the periodic potential in a structure of alternating layers of different semiconductor alloys can form a *superlattice* with a period much larger than the period of the host atomic lattice. Besides the band structure of the atomic crystal, it was shown that the superlattice can give rise to a second band structure in the same material. Due to the smaller Brillouin zones, bandwidths and gaps, the latter was called a *mini-band structure*. A few years later Esaki and Chang² found experimentally a negative differential conductance in the non-linear transport properties of a vertically grown superlattice, which was argued to be a direct consequence of the mini-band structure. Since these early works, much effort has been put in transport and optical studies on grown superlattices.

A disadvantage of grown superlattices is that the mini-band structure and the Fermi energy are fixed after the growing process. This leaves only non-linear methods to probe the electron states in the mini-band structure, for instance by measuring non-linear transport properties² or by optical excitation of electrons into higher mini-bands and measuring the resulting luminescence spectra.³ We have used a different technique to induce the periodic potential, which allows us to tune the Fermi energy through the mini-band structure. We have fabricated a lateral one dimensional (1D) crystal in a two dimensional electron gas (2DEG) by means of electro static depletion induced by metallic gates on top of a GaAs/AlGaAs hetero structure. The *1D crystal* consists of a sequence of 15 coupled quantum dots, in which the spatial quantization is realized in all three directions. This in contrast to the so-called 1D superlattices,¹⁻³ where the periodic potential is in one direction and the electron motion is still free in the two other directions.

In a single quantum dot, discrete electron states can arise either due to the lateral electro static confinement⁴⁻⁶ or by a combination of this with a magnetic field.⁷ In a series of coupled quantum dots, these zero dimensional (0D) states are expected to develop into mini-bands separated by energy gaps. As we will discuss in this paper, the linear conductance reflects the formation of a mini-band structure in such an artificial 1D crystal, when the Fermi energy is

tuned through the bands by varying the voltage on the gates.⁸ The outline of this paper is as follows. In section 5.2, we will illustrate theoretically the formation of a band structure from a transport point of view. The device with 15 coupled quantum dots will be discussed in section 5.3 and the experiments follow in section 5.4. Some conclusions are summarized in section 5.5.

5.2 FORMATION OF A BAND STRUCTURE IN A FINITE 1D CRYSTAL

To calculate the band structure of an infinite crystal one can incorporate the translational invariance of the lattice in the electron wave function by means of Bloch's theorem. In a finite crystal, consisting of a small number of unit cells, the translational invariance is broken and the proper boundary conditions have to be included in a calculation of the electron states. Different methods have been used to calculate the band structure of a finite periodic structure.⁹⁻¹² We will illustrate the formation of a band structure in a finite 1D crystal with on both sides infinite 1D leads, by calculating the transmission probability T_N of an electron wave through a 1D chain of N barriers at periodic positions.^{8,13} To illustrate the procedure, an explicit derivation for the two barrier system (or single quantum dot) shown in Fig. 5.1a will be described in detail, while for the N barrier system of Fig. 5.1b we refer to Ref. 13 for a full derivation. The starting point is the scattering matrix $S = \begin{pmatrix} t_r & t'_r \end{pmatrix}$ which relates the outgoing waves from a single barrier to the

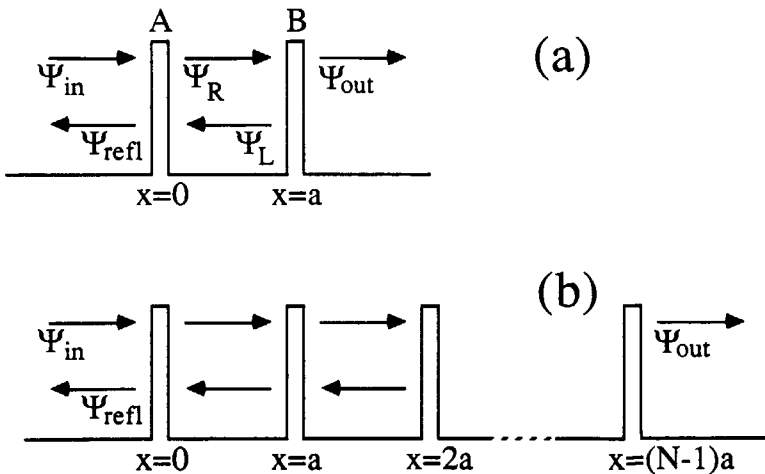


FIG 5.1. Schematic representation of an electron wave in a 1D 2-barrier (a) and N -barrier (b) system.

incoming waves. For an asymmetric barrier in a magnetic field (which breaks time reversal symmetry) the complex transmission and reflection amplitudes t and r for an incoming wave in one direction differ from the amplitudes t' and r' for an incoming wave from the opposite direction. For simplicity we will assume symmetric barriers which gives $t = t'$ and $r = r'$. Conservation of current yields the condition that S is unitary, which leads to the relations: $t t^* + r r^* = 1$ and $t/t^* = -r/r^*$. To allow unequal barriers we label them by A and B . The right- and left-moving waves in the cavity between the two barriers at $x = 0$ in Fig. 5.1a are given by: $\Psi_R = t_A \Psi_{in} + r_A \Psi_L$ and $\Psi_L = r_B \Psi_R \exp(i\theta)$, in which θ is the phase acquired by an electron wave after travelling back and forth once within the cavity. With the outgoing wave $\Psi_{out} = t_B \Psi_R$ one finds for the transmission amplitude $t_2 = \Psi_{out}/\Psi_{in}$ through the two barriers:

$$t_2 = \frac{t_A t_B}{1 - r_A r_B \exp(i\theta)} \quad (5.1a)$$

and with the definitions $T_A = t_A t_A^*$, $R_A = r_A r_A^*$, $T_B = t_B t_B^*$, and $R_B = r_B r_B^*$ for the transmission probability $T_2 = t_2 t_2^*$:

$$T_2 = \frac{T_A T_B}{1 - 2\sqrt{R_A R_B} \cos(\theta + \theta_r) + R_A R_B} \quad (5.1b)$$

θ_r is the total phase shift after reflection at the barriers A and B , and follows from the imaginary parts of r_A and r_B . The striking aspect of Eq. 5.1b is that even with the single barrier transmissions $T_A = T_B < 1$, the two barriers in series have a transmission $T_2 = 1$ whenever the total phase $\theta + \theta_r$ is an integer times 2π . This aspect is well-known as *coherent resonant tunneling*. In terms of energies, the cavity forms a confined 1D system in which discrete 0D-energy-states arise (when $T_A = T_B \approx 0$), similar to particle-in-a-box states. When the energy of an incoming electron coincides with a 0D-state, the electron is transmitted with probability equal to 1.

For N barriers in series (see Fig. 5.1b), we calculate the transmission $T_N = t_N t_N^*$ from a numerical solution of the recursive formula for the transmission amplitude t_N :^{8,13}

$$t_N = \frac{t t_{N-1}}{1 - r r_{N-1} \exp(i\theta)} \quad (5.2)$$

in which t denotes the transmission amplitude of a single barrier. The current conservation relations also hold for t_N and r_N .

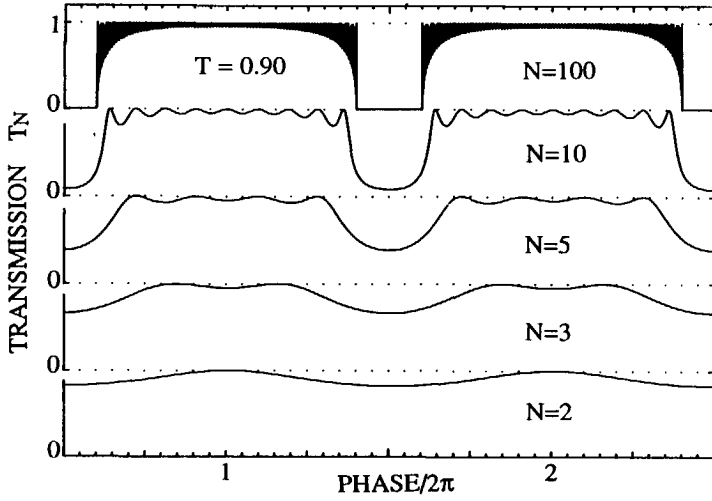


FIG. 5.2. Transmission T_N versus phase $\theta/2\pi$ of a periodic 1D chain of N barriers, calculated from Eq. 5.2 with single barrier transmissions $T = 0.90$.

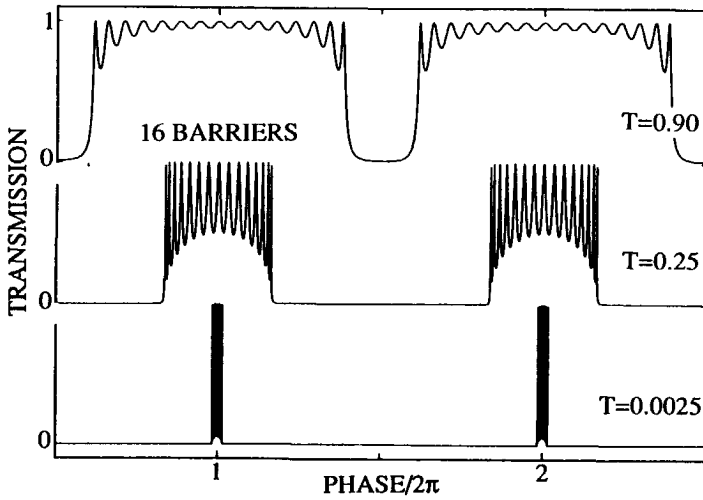


FIG. 5.3. Transmission T_N versus phase $\theta/2\pi$ of a periodic 1D chain of 16 barriers, for different single barrier transmissions T .

In Fig. 5.2 the transmission T_N versus phase θ is plotted for a different number N of equal barriers with transmissions $T = 0.90$ (the constant phase shift θ_r is ignored). The lowest curve with $N = 2$ oscillates with a period 2π . The two maxima correspond with consecutive OD-states. The oscillations in T_2 are broadened due to the large coupling (T is nearly 1) to the OD-states. For small barrier transmission ($T \approx 0$) these oscillations appear as sharp Lorentzian-shaped peaks. Fig. 5.2 shows that if the OD-states of two adjacent cavities ($N = 3$) are coupled, an extra oscillation comes in. The two maxima which correspond to the OD-states of the two coupled cavities, are seen to group together. In band structure theory this is referred to as the symmetric and anti-symmetric superposition of the independent OD-states in two uncoupled cavities. The anti-symmetric superposition shifts a little up in energy (or in phase in our calculations), while the symmetric superposition goes down in energy relative to the energy of the independent OD-states. A further increase of the number of barriers N shows that the number of oscillations increases accordingly. As can be seen in Fig. 5.2, a change in phase of 2π contains a number of oscillations equal to the number of cavities $N - 1$. The oscillations form *bands* of high transmission T_N . These bands are separated by regions of low transmission T_N , which are associated with the *gaps*.

In Fig. 5.3 the transmission T_N is shown for $N = 16$ barriers, but now for three different values of the transmission T through the single barriers, illustrating the effect of the coupling between the adjacent cavities. Weak coupling (i.e. small T) results in a band structure with narrow bands and large gaps ("tight-binding regime"), while strong coupling (i.e. T nearly 1) yields wide bands and small gaps ("nearly-free-electron regime"). In an energy picture, the bands of high transmission correspond to a situation where the Fermi energy is located in an energy band, while in the regions of low transmission the Fermi energy is in a gap. So, when the Fermi energy of the system is varied, the transmission through a finite crystal reflects the energy gap as well as the discrete states forming the so-called mini-bands. Note that in a normal crystal, the discrete states in the energy bands are usually unnoticeable due to the large number of participating atoms.

The transmission T_N is directly related to the conductance G by the Landauer formula: $G = T_N e^2/h$, which therefore also reflects the band structure if one is able to vary experimentally the phase θ . In zero magnetic field, the phase is given by: $\theta = 2\pi(2a/\lambda_F)$, i.e. it is determined by the number of half Fermi wavelength's $\lambda_F/2$ matching the distance a between adjacent barriers. Smith et al.⁵ have reported the observation of OD-states for $B = 0$ in a single quantum dot device in which they were able to vary the distance a . However, in a device with more than two barriers

this is experimentally very difficult to realize. An alternative for varying the phase θ is by changing the Fermi energy and thereby λ_F . This has been done recently by means of a gate covering a single quantum dot.⁶

We have chosen a different approach to vary the phase θ . We have used the fact that in a high magnetic field the current carrying electron states of a 2DEG are confined to *1D edge channels*, which are located at the sample boundary.¹⁴ It has been shown that on short distances of order μm , the scattering between edge channels is absent in a sufficiently high magnetic field.¹⁵ Edge channels can therefore be treated as *independent* 1D current channels, which make them an ideal model system for confinement to zero dimensions.⁷ Moreover, they form the physical analog of our 1D model. By confining an edge channel in a quantum dot it forms a 1D loop (see Fig. 4.1). Due to the Aharonov-Bohm effect, an electron which makes one revolution around the dot acquires a change in phase of $2\pi(\phi/\phi_0)$, where $\phi = BA$ is the magnetic flux, A denotes the area enclosed by the edge channel loop and $\phi_0 = h/e$ is the flux quantum.¹⁶ In this case of a high magnetic field, the phase θ can be varied either by changing the magnetic field B or the enclosed area A . For a single quantum dot this corresponds to moving the Fermi energy through the 0D-states while for coupled dots the Fermi energy is tuned through the band structure. The correspondence between the phase $\theta = 2\pi(2a/\lambda_F)$ at $B = 0$ and $\theta = 2\pi\phi/\phi_0$ at $B \neq 0$ has been pointed out by Büttiker et al.¹⁷ for a 1D ring structure, which encloses an Aharonov-Bohm flux $\phi = BA$.

5.3 THE 1D CRYSTAL DEVICE

Our device consists of an array of 15 quantum dots, which are electro statically defined in a two dimensional electron gas (2DEG) by means of two metallic gates on top of a GaAs/AlGaAs hetero structure. Fig. 5.4 shows a scanning electron micrograph of the gate geometry of which the dimensions are given in the inset of Fig. 5.6. The ungated 2DEG has an electron density of $2.7 \cdot 10^{15} \text{ m}^{-2}$ and a transport mean free path of $10 \mu\text{m}$. A negative voltage of -0.44 V on the gates, depletes the electron gas underneath the gates and forms a corrugated ballistic channel in the 2DEG of $3 \mu\text{m}$ length and a width alternating between 250 and 400 nm. The voltage V_{g1} on the first gate defines the depletion region around the "fingers" (in total 16 fingers or correspondingly 15 quantum dots) at a period of 200 nm. The effect of lowering (making more negative) the voltage V_{g2} on the second gate is threefold. The increasing depletion area around the second gate reduces the coupling between adjacent dots, reduces the area of each dot, and

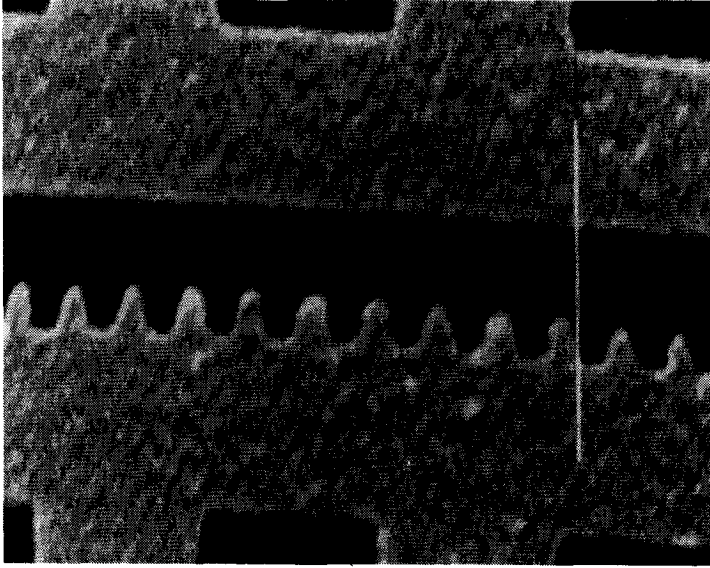


FIG. 5.4. *Scanning Electron Microscope photograph of the 1D crystal device. The corrugated gate contains 16 fingers in total. The white marker indicates 1 μm .*

lowers the Fermi energy in the conducting regions. The detailed shape of the depletion region in the 2DEG is unknown, but presumably resembles a periodic (asymmetric) saddle-shaped electrostatic potential with the maxima in the narrow regions.

5.4 TRANSPORT MEASUREMENTS

We have performed conductance measurements as a function of gate voltage V_{g2} on the second gate, for several fixed values V_{g1} on the first, finger gate, and for several fixed magnetic fields. The measurements are performed at a temperature of 10 mK with a standard lock-in technique using ac current biasing of 0.2 nA rms. At zero magnetic field no evidence has been found for the formation of a band structure. Nor did we find quantized plateaus in the conductance resulting from the transverse confinement in the corrugated channel. The quantization, which would indicate *adiabatic* transport, is destroyed due to inter-subband scattering either by the fingers or by potential fluctuations in the 3 μm long channel.¹⁸ At a constant magnetic field of 2 T we find quantum Hall plateaus at multiples of e^2/h in the

conductance G as a function of gate voltage V_{g2} . The effect of a magnetic field is to establish adiabatic transport through the corrugated channel, as is known from theoretical¹⁹ and experimental²⁰ work on two quantum point contacts in series. In the case of adiabatic transport, the subbands can be treated as independent 1D edge channels. The scattering now only takes place in a controlled way within a single edge channel at the potential maxima defined by the fingers. This periodic scattering corresponds to Bragg reflection and was modelled by the barrier transmissions T in section 5.2.

In Fig. 5.5 the first (spin-resolved) conductance plateau is shown for several fixed voltages V_{g1} on the finger gate. Below the first plateau (i.e. $G < e^2/h$) large oscillations are seen, while in the plateau region deep downward peaks enclose smaller oscillations. Above the plateau only downward peaks are seen, which are clearly separated. Some of the deeper peaks in Fig. 5.5 are marked to indicate their shift when the voltage V_{g1} is varied.

The plateau region of the curve with $V_{g1} = -0.45$ V is measured and shown enlarged in Fig. 5.6. As can be seen, the two deeper peaks enclose 15 oscillations, which exactly corresponds with the number of quantum dots in the 1D crystal. This simple counting comparison between the number of oscillations and the number of quantum dots, shows that the observed oscillations can be associated with the formation of a mini-band structure in the periodic 1D crystal device. The deeper peaks correspond to the energy gaps and the smaller oscillations with the discrete states, which form the mini-bands. This interpretation is supported by the calculations shown in Fig. 5.2 and 5.3. The formation of energy gaps is also indicated by the downward peaks above the plateau region in Fig. 5.5. The spacing between these downward peaks differs from those in the plateau region, which may be related to additional peaks originating from the second subband.

In the plateau region the average conductance is nearly constant (here the transmission probability of the lowest subband through a single barrier is nearly equal to one) indicating that the coupling is approximately constant, which roughly yields constant energy gaps. The effect of lowering the gate voltage V_{g2} here is mainly the decrease in Fermi energy and the reduction in dot area. Note that the reduction in area results in larger energy separations which increases the bandwidth. Both effects move the Fermi energy through the mini-band structure. From going vertically through Fig. 5.3 one can see that when the transmissions T are varied relatively fast compared to the phase θ , the Fermi energy also moves through the mini-band structure. This leads to the large oscillations below the first plateau, where T changes from 0 (at pinch-off) to 1.

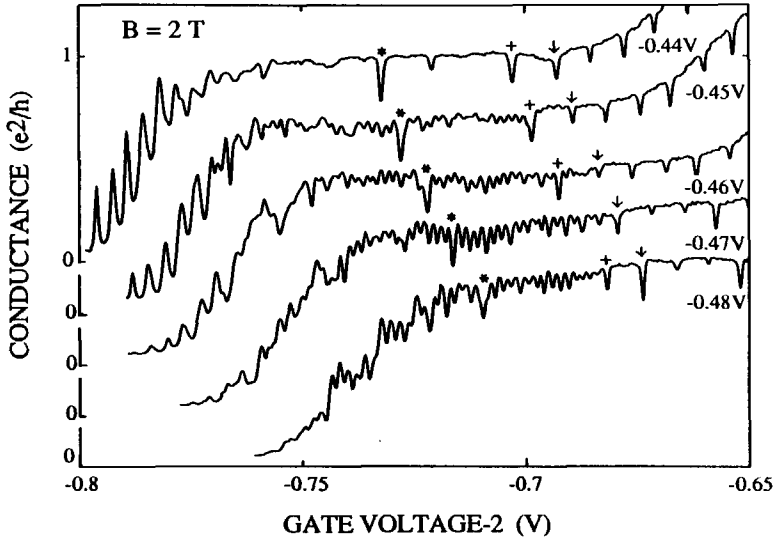


FIG. 5.5. Conductance as a function of gate voltage-2 V_{g2} on the second gate at a fixed magnetic field of 2 T and for different values of gate voltage-1 V_{g1} on the first gate. Corresponding peaks are marked. The curves have been offset for clarity.

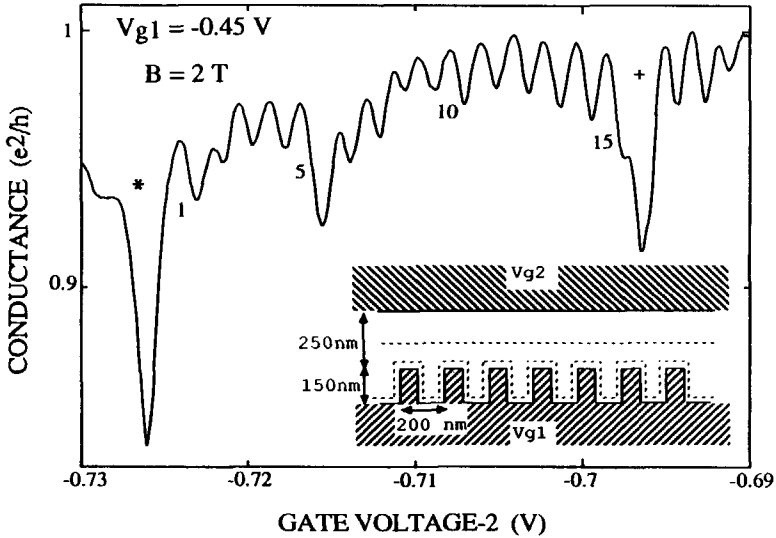


FIG. 5.6. Conductance as a function of gate voltage-2 V_{g2} on the second gate at 2 T and $V_{g1} = -0.45$ V on the first gate. The inset shows schematically the gate geometry; the dashed lines indicate the depletion regions in the 2DEG. The upper depletion region is moved towards the fingers when V_{g2} is made more negative.

The effect of irregularities on the mini-band structure can also be seen in Fig. 5.5. For the curves of $V_{g1} = -0.45$ V and -0.48 V the number of oscillations is 15 in accordance with the number of dots. However, the curve of $V_{g1} = -0.46$ V shows 16 (reproducible) oscillations and in the curve of $V_{g1} = -0.47$ V the gap marked by "+" is not seen. The disappearance of the gap is presumably caused by irregularities, which introduces mixing between mini-bands. The 16 oscillations in $V_{g1} = -0.46$ V cannot be understood from the number of quantum dots, not even when the dots are considered to be unequal. Additional scattering at an impurity or at the exit or entrance of the channel may be the cause for this extra oscillation. The smaller oscillations on the left of the mark "*" in Fig. 5.1, indicate another discrete mini-band, although less regular. The influence of irregularities on the mini-band structure will be discussed further below. The oscillations reproduce very well if the sample is kept cold (< 4 K), but not after warming up to room temperature. So far the oscillations have only been studied in one 16-finger sample. In a 1-finger sample of identical design, we found that the conductance versus V_{g2} shows quantized plateaus at zero magnetic field, which shows that a single finger acts as a quantum point contact.¹⁸ In a 2-finger sample we have observed structure at 2 T with a period of $\Delta V_{g2} \approx 25$ mV. This period corresponds to the energy difference between consecutive 0D-states in the single quantum dot and is approximately the same, as one would expect, as the gate voltage difference between the two downward peaks in Fig. 5.6. From these different finger samples we can conclude that the additional smaller oscillations in Fig. 5.5 and 5.6 indeed originate from the coupling between the quantum dots.

5.5 DISCUSSION AND CONCLUSIONS

To simulate our conductance measurements, using Eq. 5.2 and $G = T_N \cdot e^2/h$, we varied the phase θ and the transmission amplitude t simultaneously. In this way the effect of the gate voltage on the confining potential and on the coupling between adjacent dots is simulated. The transmission T_N for $N = 16$ is plotted as a function of phase in Fig. 5.7, where the lowest curve is the simultaneously varying transmission probability $t \cdot t^*$ of a single barrier. The two calculated transmissions illustrate the effect of deviating barriers. In the upper curve the first and last barrier have a smaller transmission amplitude by a factor of 0.999. We found that this kind of irregularity has a strong effect on the depth of the gaps. While for equal barriers the minima of the gaps approach zero, this small irregularity lifts the minima to values similar as found experimentally. Additionally, in the curve in the middle of Fig. 5.7, the barrier in the middle of

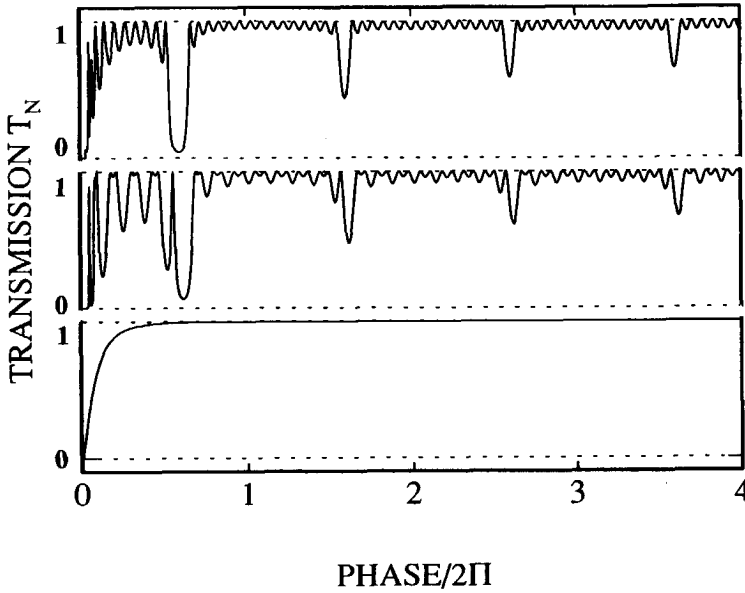


FIG. 5.7. Calculations from Eq. 5.2 of the transmission T_N as a function of phase θ of a 1D chain of $N = 16$ barriers. The lowest curve shows the simultaneously varying transmission probability $T = t \cdot t^*$ through a single barrier. In the middle curve all barriers have equal transmissions T except the first and last barrier have $T_{\text{first}} = T_{\text{last}} = 0.999 \cdot T$. In the upper curve the barrier in the middle has in addition a smaller transmission $T_{\text{middle}} = 0.97 \cdot T$.

the crystal is reduced by a factor 0.97. The effect is that the crystal slightly breaks into two parts. This is reflected in the smaller oscillations which group together in pairs of two, very similar to the pattern seen in the experimental curves of $V_{g1} = -0.46$ V and -0.47 V in Fig. 5.5. We note that for an asymmetric barrier in a magnetic field, both amplitudes t and r are unequal to the amplitudes t' and r' for a wave in the opposite direction. Incorporating this in the calculation we found that this also affects the depth of the gaps. We conclude that our 1D model can account for all features observed in the experimental curves. Further calculations show that if the amount of disorder is increased (accomplished by variations in the individual t 's and θ 's), the oscillations become more irregular and eventually the gaps disappear.¹³

More recently, several authors have calculated the transmission probability of a finite corrugated channel at zero^{21,22} and non-zero magnetic field.^{23,24} A special feature of our

magnetically induced band structure is that the energy dispersion is asymmetric yielding *skew mini-bands*. This is a direct consequence of the fact that the time reversal symmetry is broken in a magnetic field.^{23,24}

These calculations and our 1D model are all within the independent electron approximation, ignoring interaction effects as for instance screening. Because of the absence of states in the gaps, it may be possible that the Fermi energy does not change continuously with the gate voltage, but jumps from the top of a mini-band to the bottom of the next one. This may result in observing smaller gaps. It is, however, difficult to estimate screening effects in small low-electron-density samples. Another electron-electron interaction effect ignored here is the occurrence of charging effects. Experimentally, we have checked that the two periods in the mini-bands in the plateau region scale with magnetic field. This confirms the band structure interpretation and rules out an explanation in terms of single electron charging. However, when the conductance is made smaller than the plateau value, this scaling gradually disappears. For a conductance much smaller than e^2/h , we have found clear evidence for charging effects by observing a Coulomb staircase in our 1D crystal.²⁵ This shows that a gradual transition exists at lower conductances to a regime where charging effects dominate transport. Charging effects will be discussed in detail in chapter 7.

In summary, the transport properties of the 1D crystal reflect the formation of a mini-band structure of which the discreteness is clearly observable. In contrast with the vertically grown superlattices, the electrostatic definition of the 1D crystal by means of a split-gate allowed us to tune the Fermi energy through the mini-band structure. The fact that the mini-band structure originates from a modulation of the lowest 1D magnetic subband makes this device a true 1D crystal. The mini-band structure is reflected in the conductance, in a way that the 1D crystal is electrically insulating or conducting whether the Fermi energy is in a gap or a mini-band respectively. A simple 1D model can account for the observed features in the conductance and illustrates the formation of a band structure in the solid state in terms of resonant transmission.

ACKNOWLEDGEMENT

We thank C.W.J. Beenakker, J.E. Mooij, T.P. Orlando, G. Schön, and J.G. Williamson for valuable discussions, M. van Eijck for performing the calculations, J.R. Kraayeveld for assistance with the experiment, A. van der Enden for his contributions to the fabrication of the devices, and the Stichting F.O.M. for financial support.

REFERENCES

The main results of this chapter were published in Phys. Rev. Lett. **65**, 361 (1990).

1. L. Esaki and R. Tsu, IBM J. Res. Dev. **14**, 61 (1970).
2. L. Esaki and L.L. Chang, Phys. Rev. Lett. **33**, 495 (1974).
3. For a review on grown superlattices in a magnetic field, see J.C. Maan, Festkörperprobleme **27**, 137 (1987).
4. M.A. Reed, J.N. Randall, R.J. Aggarwal, R.J. Matyi, T.M. Moore, and A.E. Wetsel, Phys. Rev. Lett. **60**, 535 (1988).
5. C.G. Smith, M. Pepper, H. Ahmed, J.E. Frost, D.G. Hasko, D.C. Peacock, D.A. Ritchie and G.A.C. Jones, J. Phys. C. **21**, L893 (1988).
6. Y. Hirayama and T. Saku, Solid State Commun. **73**, 113 (1990).
7. B.J. van Wees, L.P. Kouwenhoven, C.J.P.M. Harmans, J.G. Williamson, C.E. Timmering, M.E.I. Broekaart, C.T. Foxon, and J.J. Harris, Phys. Rev. Lett. **62**, 2523 (1989);
L.P. Kouwenhoven, B.J. van Wees, C.J.P.M. Harmans and J.G. Williamson, in *Proceedings of the Workshop on Science and Engineering of 1- and 0-dimensional Semiconductors*, edited by C.M. Sotomayor-Torres and S.P. Beaumont (Plenum Press, New York, 1990);
L.P. Kouwenhoven, B.J. van Wees, C.J.P.M. Harmans, and J.G. Williamson, Surface Science **229**, 290 (1990);
See also chapter 4 in this thesis.
8. See also: L.P. Kouwenhoven, F.W.J. Hekking, B.J. van Wees, C.J.P.M. Harmans, C.E. Timmering, and C.T. Foxon, Phys. Rev. Lett. **65**, 361 (1990).
9. R. Tsu and L. Esaki, Appl. Phys. Lett. **22**, 562 (1973).
10. D.J. Vezzetti and M.M. Cahay, J. Phys. D. **19**, L53 (1986).
11. H.W. Lee, A. Zysnarski, and P. Kerr, Am. J. Phys. **57**, 729 (1989).
12. S.E. Ulloa, E. Castano and G. Kirczenow, Phys. Rev. B **41**, 12350 (1990).
13. M. van Eijck, F.W.J. Hekking, L.P. Kouwenhoven, and G. Schön, Physica B **165&166**, 849 (1990).
14. B.I. Halperin, Phys. Rev. B **25**, 2185 (1982);
P. Streda, J. Kucera, and A.H. MacDonald, Phys. Rev. Lett. **59**, 1973 (1987);
J.K. Jain and S.A. Kivelson, Phys. Rev. Lett. **60**, 1542 (1988);
M. Büttiker, Phys. Rev. B **38**, 9375 (1988).
15. B.J. van Wees, E.M.M. Willems, C.J.P.M. Harmans, C.W.J. Beenakker, H. van Houten, J.G. Williamson, C.T. Foxon, and J.J. Harris, Phys. Rev. Lett. **62**, 1181 (1989);
See also chapter 1 in this thesis.
16. A theoretical study of a 2D dot to which narrow leads are attached is given by: U. Sivan, Y.

- Imry, and C. Hartzstein, Phys. Rev. B **39**, 1242 (1989);
U. Sivan, and Y. Imry, Phys. Rev. Lett. **61**, 1001 (1988);
Transmission through single quantum dots in the quantum Hall regime is treated also in a review by M. Büttiker, in *Nanostructured Systems*, edited by M.A. Reed (Academic, Orlando, FL, 1990).
17. M. Büttiker, Y. Imry, and R. Landauer, Physics Letters **96A**, 365 (1983).
 18. Conductance quantization at zero magnetic field has been observed in narrow wires or quantum point contacts having a typical length of 100-300 nm; See B.J. van Wees, H. van Houten, C.W.J. Beenakker, J.G. Williamson, L.P. Kouwenhoven, D. van der Marel, and C.T. Foxon, Phys. Rev. Lett. **60**, 848 (1988); See also chapter 1 in this thesis.
D.A. Wharam, T.J. Thornton, R. Newbury, M. Pepper, H. Ahmed, J.E.F. Frost, D.G. Hasko, D.C. Peacock, D.A. Ritchie, and G.A.C. Jones, J. Phys. C **21**, L209 (1988).
 19. L.J. Glazman and M. Johnson, J. Phys. Condens. Matter **1**, 5547 (1989).
 20. L.P. Kouwenhoven, B.J. van Wees, W. Kool, C.J.P.M. Harmans, A.A.M. Staring and C.T. Foxon, Phys. Rev. B **40**, 8083 (1989);
P.C. Main, P.H. Beton, B.R. Snell, A.J.M. Neves, J.R. Owers-Bradley, L. Eaves, S.P. Beaumont, and C.D.W. Wilkinson, Phys. Rev. B **40**, 10033 (1989).
 21. J.A. Brum, Phys. Rev. B **43**, 12082 (1991).
 22. F.M. de Aguiar, and D.A. Wharam, Phys. Rev. B **43**, (1991).
 23. C.W.J. Beenakker, and H. van Houten, in Solid State Physics **44**, edited by H. Ehrenreich, and E. Turnbull, (Academic, Boston, 1991), p.1
 24. C.S. Lent, and M. Leng, Appl. Phys. Lett. **58**, 1650 (1991); and J. Appl. Phys. **70**, 3157 (1991).
 25. L.P.Kouwenhoven, B.J.van Wees, A. van der Enden, and C.J.P.M. Harmans, in *Proceedings of the 20th International Conference on Physics of Semiconductors*, edited by J. Joannopoulos (World Scientific, London, 1990), p.2325.

CHAPTER 6

Quantized Photocurrent in a Single Exciton Pump

Leo P. Kouwenhoven

Faculty of Applied Physics, Delft University of Technology

P.O.Box 5046, 2600 GA Delft, The Netherlands

ABSTRACT

We propose that a vertical quantum dot under illumination of a pulsed laser can operate as a single exciton pump. The photocurrent resulting from the creation of a single exciton per laser pulse, is equal to the electron charge times the frequency of the laser pulses. The experimental conditions for realizing such a single exciton pump and its applications are discussed.

The ability to control the transport of single electrons is a fascinating new field of research, not only from a fundamental point of view, but also for obtaining an accurate current standard and for various device applications. So far, most of the effort has been put in the control of single electron transport through small metallic tunnel junctions. Due to the small junction capacitance C (of order 10^{-16} F), the tunneling of an electron alters the energy of the system by a charging energy $E_c = e^2/2C$ (of order meV) which exceeds the thermal energy at low temperature ($T < 1$ K). This can result in a Coulomb blockade for other electrons to tunnel.¹ Geerligs et al.² were able to modulate the Coulomb blockade with a radio frequent (RF) signal, resulting in the passage of one electron per cycle through their so-called *single-electron-turnstile* device. The current I was found to be given within the error of the experimental set up (~ 0.3 %) by $I = ef$, where f is the frequency of the RF signal. In a similar system, Pothier et al.³ have realized a *single-electron-pump*. Two phase shifted RF signals were used to generate a current $I = ef$, even for zero bias voltage across the junctions. In a pioneering experiment of Delsing et al.,⁴ single-electron-tunneling oscillations were phase-locked with a RF signal, also resulting in a current $I = ef$. A semiconductor variant of the single-electron-turnstile, which is based on oscillating tunnel barriers, has recently been discussed by Odintsov⁵ and realized by Kouwenhoven et al.⁶

Besides the above experimental realizations of passing electrons one-by-one, Niu⁷ has proposed a system in which the velocity of a Bloch-wave can be controlled. Guinea and Garcia⁸ proposed that with an oscillating tip of an STM near a metallic grain, one could realize the passage of one electron per cycle from the tip to the grain. The above experiments and proposals are all based on a frequency modulation of the conduction band. In this letter, we consider an alternative way to obtain a frequency determined current. We propose that due to the creation of a single exciton in a semiconductor quantum dot per cycle of a pulsed laser, the resulting photocurrent is determined by the frequency of the laser pulses. We will first point out the general operating principles of this *single-exciton-pump* and specify the details later.

The non-linear transport properties of a quantum dot have been studied by Reed et al.⁹ Their quantum dot was defined by etching techniques in a vertical layered heterostructure, consisting of n^+ GaAs (contact), AlGaAs (tunnel barrier), InGaAs (quantum dot), AlGaAs (tunnel barrier), and n^+ GaAs (contact). The structure observed in the I - V characteristics was identified to result from zero dimensional (0D) electron states with energy separations of about 25 meV. Fig. 6.1a shows schematically the bottom of the conduction band and the top of the valence band vertically through the quantum dot structure of Fig. 6.1b, whose optical properties we discuss in this letter. In the regions I, II, and III of Fig. 6.1a, the Fermi energy E_F is taken to lie in the gap. The

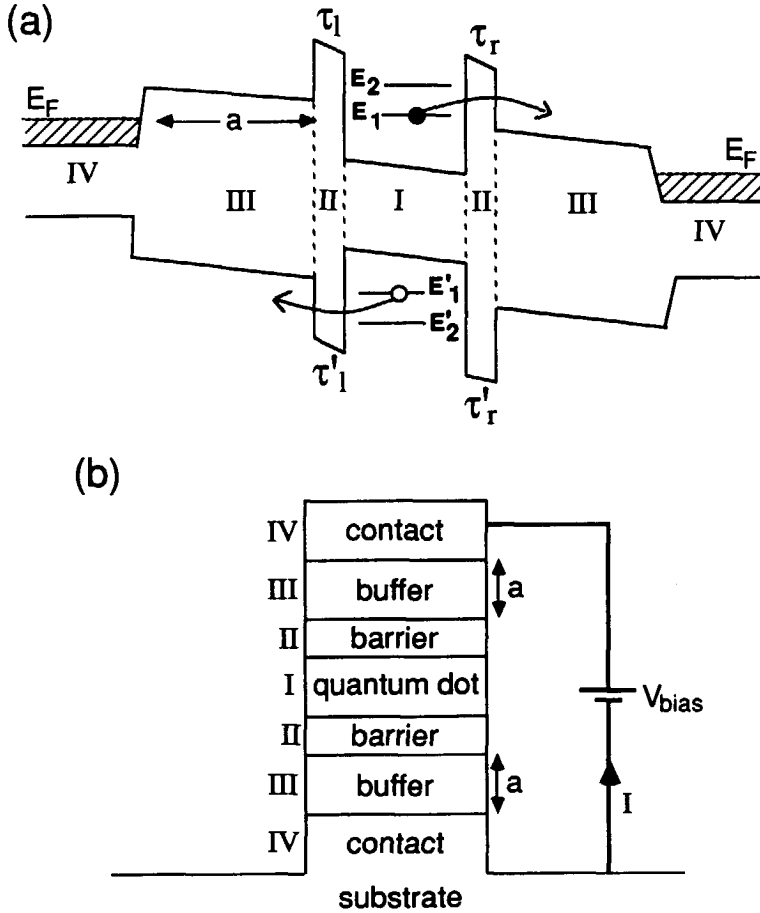


FIG. 6.1. (a) Bottom of the conduction and top of the valence band, which defines a quantum dot (region I) between two barriers (regions II) and separated by two buffers (regions III) from the two electron reservoirs (regions IV). The bands are slanted by a voltage between the reservoirs. (b) Pillar of different layers of semiconductor alloys, which has the band gap modulation of (a), see also Reed et al.⁹

energy states in the quantum dot (i.e. between the barriers) are quantized in all three spatial directions and are therefore 0D electron states. The 0D-states can be doubly occupied due to spin-degeneracy. We denote the energy of the n^{th} 0D-state by E_n . The 0D-states can be populated by applying a large electric field over the structure, which lifts the Fermi energy of one of the contacts above the conduction band in the buffer region, allowing electrons to tunnel through the barrier into the dot. This is the way Reed et al.⁹ observed the 0D-states, demonstrated by resonant transmission occurring when E_F was lined up with the discrete energy of a 0D-state.

An alternative way to populate the 0D-states is by creating excitons with a laser.¹⁰ Information about the confined exciton energy states can be obtained by measuring the luminescence spectrum.¹¹ We take the energy of the laser $h\nu_l = E_l + E'_l + E_{\text{gap}} - E_B$ such that at most two excitons can be created in the lowest energy state, while the higher states corresponding to $E_{n>1}$ stay empty. The binding energy E_B includes the Coulomb interaction between the electrons and holes, which gives a correction to the single-particle discrete states E_n and E'_n . Due to stimulated emission, which is of equal probability as the absorption of a photon, the mean occupation is only one exciton. The statistical deviation from this is small if many events are considered. For the moment we take the occupation to be exactly one and return to this point later.

We denote the time for an electron to tunnel to the left as τ_l and to the right as τ_r . Similar, τ'_l and τ'_r denote the tunnel times for the hole (we neglect the dependence of the times $\tau_{l,r}$ and $\tau'_{l,r}$ on the discrete energies E_n and E'_n). If the bands are slanted by a voltage across the structure, as indicated in Fig. 6.1a, the excited electron has a preference to tunnel to the right ($\tau_r \ll \tau_l$). Similarly, the hole will preferably tunnel to the left ($\tau'_l \ll \tau'_r$). The energy E_B to break up the exciton is delivered by the voltage source. With a continuous operation of the laser, the resulting photocurrent is of order $e/(\tau_{\text{exc}} + \tau_r + \tau'_l)$, where τ_{exc} is the time to create an exciton. It is important to note that this current from the left- to the right-reservoir results from the pumping action by the laser in the quantum dot only. The excitations in the reservoirs relax in the same reservoir, if the relaxation length is much shorter than the distance a of the buffer regions (the regions III in Fig. 6.1), which separate the quantum dot from the reservoirs. In the buffer regions no excitations can occur, because the energy gap there is larger than the laser energy. *So the pumping takes place in the quantum dot, and only the first state contributes to the photocurrent.*

We now consider the pumping if the laser is pulsed with a pulse time T_{pulse} and a waiting

time T_{wait} between pulses, so that the pulse frequency $f = 1/(T_{pulse} + T_{wait})$. If $T_{pulse} \gg \tau_{exc}$, the first state will be populated with one exciton. If $\tau_r \ll \tau_{rec}$, (τ_{rec} is the recombination time of the exciton, or equivalently, the radiative life time), and taking $T_{wait} \gg \tau_r$, the electron will tunnel out to the right-reservoir before recombining and before the next pulse. Taking also $T_{wait} \gg \tau_l$, i.e. the hole tunnels to the left, then one electron has been transported from the left- to the right-reservoir in the cycle time $T_{pulse} + T_{wait}$. Note that "multi-pumping" can occur when T_{pulse} is of order $\max(\tau_r, \tau_l)$. In this case, an exciton can tunnel out of the dot within the pulse time, which leaves the possibility that an extra exciton is created during the pulse. Multi-pumping is suppressed if $T_{pulse} \ll \max(\tau_r, \tau_l)$. If we combine all the above conditions for the different times we get

$$\tau_{exc} \ll T_{pulse} \ll \max(\tau_r, \tau_l) \ll \tau_{rec}, T_{wait} \quad (6.1)$$

If condition 6.1 is satisfied, one electron is transported from the left to the right reservoir within the cycle time $T_{pulse} + T_{wait}$. Repeating this process with a frequency f yields a quantized photocurrent $I = ef$. Returning to the statistical deviation in the occupation of the first state by one exciton due to stimulated emission, we note that currents are measured on a time scale of a second, which makes the relative deviation $\sqrt{f}/f \approx 10^{-4}$ for a frequency of 100 MHz. The practical implications of condition 6.1 will be discussed below. Furthermore, we note that in contrast to the electron turnstiles and pumps,^{2,3,6} the charging energy does not affect the operation of this exciton pump.

Spin-flip processes do not affect the photocurrent. In fact, a spin-flip of the excited electron suppresses stimulated emission, which enhances the probability of an occupation of one exciton. Spin-flip processes do affect the photocurrent if the laser light is circular polarized, such that only electrons with the proper spin direction are excited. This results in an occupation probability of 1/2, and consequently in a photocurrent $I_{pol} = ef/2$. In this case, spin-flip processes increase the photocurrent to a value between $ef/2$ and ef .

If the (non-polarized) laser energy $h\nu$ is increased to $h\nu_n = E_n + E'_n + E_{gap} - E_B$, excitons can be excited to the n^{th} state. All states up to E_n can be populated if the laser has a (quasi-continuous) energy band with minimum energy $h\nu_l$ and maximum $h\nu_n$. The pulsed mode now results in the transportation of n electrons per cycle, yielding a photocurrent $I = n \cdot ef$. The photocurrent increases in steps of ef when the maximum laser energy is increased. The plateau width is a direct measure of the energy difference between consecutive exciton states.

If the pulse frequency f is changed, the photocurrent will change proportionally with a slope ne depending on the laser energy $h\nu_n$. Deviations from this dependence can give information about the tunnel-, recombination- and excitation times. For instance, if $I > ef$ for $h\nu = h\nu_I$, multi-pumping may occur when $T_{pulse} \approx \max(\tau_r, \tau'_I)$. On decreasing T_{pulse} until $I = ef$, one can obtain information about the tunnel times τ_r and τ'_I . In a similar way, if $I < ef$ for $h\nu = h\nu_I$, one can compare T_{pulse} with τ_{exc} by changing the power of the laser.

The photocurrent can, in principle, be enhanced to $I = N \cdot ef$ by putting N equal quantum dots in parallel, which can considerably increase the quantized photocurrent. The condition is that the spread in energy levels should be much smaller than the energy separation between consecutive states.

A realization of a single exciton pump depends on the possibility of satisfying condition 6.1. Starting from the left, we note that the time τ_{exc} to create an exciton depends on the laser power and is typically of order 1 fs. The spread $\delta h\nu$ in the laser energy should be much smaller than the separation ΔE_{0D} between consecutive 0D-states. This gives a lower limit for the pulse time, because of Heisenberg's uncertainty principle: $\delta h\nu \approx \hbar/T_{pulse} \ll \Delta E_{0D}$. Taking $\Delta E_{0D} \approx 25$ meV,⁹ yields $T_{pulse} \gg 0.01$ ps. For the waiting time there is no fundamental restriction. Technically, T_{wait} is tunable in multiples of ~ 10 ns. The typical quantized photocurrent is then $e \cdot 100$ MHz = 16 pA, which is easily measurable. The times $\tau_{I,r}$ and $\tau'_{I,r}$ to tunnel out of the quantum dot include the single-particle dwell time (following from the confinement), and the effect of the binding energy on the non-radiative exciton life time, which both depend strongly on the voltage across the sample. With appropriate barriers, the tunnel times can, therefore, be tuned by the voltage across the sample. Tunnel times of order 10 ps would still satisfy condition 6.1. The most uncertain time is the recombination time τ_{rec} , which is unknown for quantum dots. In 3D GaAs a recombination time of 3.3 ns was found.¹² When the volume of the quantum dot becomes smaller than the exciton coherence volume, it is expected that the recombination time increases.¹³ For our purposes a recombination time of order 1 ns is required. Combining again the different times, we get

$$\tau_{exc} \approx 0.001 \text{ ps} \ll T_{pulse} \approx 0.1 \text{ ps} \ll \max(\tau_r, \tau'_I) \approx 10 \text{ ps} \ll \tau_{rec} \approx 1000 \text{ ps}$$

With these numbers the photocurrent is quantized in multiples of ef with an accuracy of about 1 %.

The main problem in realizing the single exciton pump is the fabrication of the quantum dots.

The etching usually induces a depletion region containing trapped surface states. This gives the possibility for the hole to hop out of the confined state to a surface state. This destroys luminescence, because the excited electron cannot recombine anymore with a hole in the confined state in the valence band. Consequently, such a process may be advantageous for the exciton pump, because it suppresses recombination. The exciton pump may therefore serve as a tool to study the time and energy properties of 0D-exciton-states.

I would like to thank Luis Viña for the discussion which initiated this work, and Gerrit Bauer and Dick van der Marel for detailed discussions on the manuscript.

REFERENCES

This chapter is published in *Europhys. Lett.* **18**, 607 (1992).

1. See for a review: D.V. Averin and K.K. Likharev, in *Quantum Effects in Small Disordered Systems*, edited by B. Al'tshuler, P. Lee, R. Webb (Elsevier, Amsterdam, 1991).
2. L.J. Geerligs, V.F. Anderegg, P.A.M. Holweg, J.E. Mooij, H. Pothier, D. Esteve, C. Urbina, and M.H. Devoret, *Phys. Rev. Lett.* **64**, 2691 (1990).
3. H. Pothier, P. Lafarge, P.F. Orfila, C. Urbina, D. Esteve, and M.H. Devoret, *Physica B* **169**, 573 (1991).
4. P. Delsing, K.K. Likharev, L.S. Kuzman, and T. Claeson, *Phys. Rev. Lett.* **63**, 1861 (1989).
5. A.A. Odintsov, *Appl. Phys. Lett.* **58**, 2695 (1991).
6. L.P. Kouwenhoven, A.T. Johnson, N.C. van der Vaart, C.J.P.M. Harmans, C.T. Foxon, *Phys. Rev. Lett.* **67**, 1626 (1991); See also chapter 8 of this thesis.
7. Q. Niu, *Phys. Rev. Lett.* **64**, 1812 (1990).
8. F. Guinea and N. Garcia, *Phys. Rev. Lett.* **65**, 281 (1990).
9. M.A. Reed, J.N. Randall, R.J. Aggerwal, R.J. Matyi, T.M. Moore, and A.E. Wetsel, *Phys. Rev. Lett.* **60**, 535 (1988).
10. See for a review: *Excitons in confined systems*, eds. R. del Sole, A. d'Andrea, and A. Lippicirella, (Springer-Verlag, 1988).
11. The 1D quantum-confined energy states of a narrow wire have been observed in photoluminescence measurements by: M. Kohl, D. Heitman, P. Grambow, and K. Ploog, *Phys. Rev. Lett.* **63**, 2124 (1989). To our knowledge no successful luminescence experiments have been performed, which probe the 0D-states in quantum dots.
12. G.W. 't Hooft, W.A.J.A. van der Poel, L.W. Molenkamp, and C.T. Foxon, *Phys. Rev. B* **35**, 8281 (1987).
13. J. Feldmann, G. Peter, E.O. Göbel, P. Dawson, K. Moore, C.T. Foxon, and R.J. Elliott, *Phys. Rev. Lett.* **59**, 2337 (1987).

CHAPTER 7

Single Electron Charging Effects in Semiconductor Quantum Dots

L.P. Kouwenhoven, N.C. van der Vaart, A.T. Johnson, W.Kool, and C.J.P.M. Harmans

Faculty of Applied Physics, Delft University of Technology

P.O.Box 5046, 2600GA Delft, The Netherlands

J.G. Williamson, and A.A.M. Staring

Philips Research Laboratories, 5600JA Eindhoven, The Netherlands

C.T. Foxon

Philips Research Laboratories, Redhill, Surrey RH15HA, United Kingdom

ABSTRACT

We have studied charging effects in a lateral split-gate quantum dot defined by metal gates in the two dimensional electron gas (2DEG) of a GaAs/AlGaAs hetero structure. The gate structure allows an independent control of the conductances of the two tunnel barriers separating the quantum dot from the two 2DEG leads, and enables to vary the number of electrons that are localized in the dot. We have measured Coulomb oscillations in the conductance and the Coulomb staircase in current-voltage characteristics and studied their dependence on the conductances of the tunnel barriers. We show experimentally that at zero magnetic field charging effects start to affect the transport properties when both barrier conductances are smaller than the first quantized conductance value of a point contact at $2e^2/h$. The experiments are described by a simple model in terms of electro chemical potentials, which includes both the discreteness of the electron charge and the quantum energy states due to confinement.

7.1 INTRODUCTION

Single-electron charging effects have mostly been studied in granular films, metal tunnel junctions, and STM-grain junctions.¹ More recently, it has become apparent that charging effects can strongly affect the transport properties of semiconductor submicron structures weakly coupled to the contact leads by tunnel barriers. The study of charging effects in semiconductor devices started with the observation of conductance oscillations in disordered wires,²⁻⁴ which were later explained to result from the confinement of electron charges between impurity potential barriers.^{5,6} This stimulated the work by Meirav et al.,⁷ in which a lateral quantum dot with controllable potential barriers was used. Their device could change the number of electrons in the dot one-by-one, which was seen in the conductance by the appearance of oscillations, and they confirmed the explanation in terms of charging effects. Later work by McEuen et al.⁸ on the same kind of device nicely showed the interplay between charging effects and magnetically-induced zero dimensional (0D) energy states,⁹ which we will discuss in more detail below. These various experiments are reviewed in Ref. 10.

In this paper, we report experiments on lateral quantum dots¹¹ defined by split-gates in a two dimensional electron gas (2DEG). The split-gate geometry allows a detailed study of the conditions for observing charging effects, because of the ability to control the coupling of the quantum dot to the environment. In particular, we will emphasize the special properties and possibilities in which semiconductor quantum dots differ from metal structures; for example, the quantized conductance of a point contact and resonant tunneling in relation to single-electron charging, and different experimental ways to determine the charging energy.

The outline of this paper is as follows: in section 7.2 we discuss our split-gate device; in section 7.3 we give a theoretical description of charging effects in quantum dots; the experimental results are presented in section 7.4; followed by a discussion and conclusions in section 7.5.

7.2 THE SPLIT-GATE QUANTUM DOT

Fig. 7.1 shows a SEM photograph of the gate geometry, which is fabricated on top of a GaAs/AlGaAs hetero structure containing a two dimensional electron gas (2DEG). The plane of the 2DEG is about 100 nm below the surface of the hetero structure. The ungated 2DEG has a mobility of $2.3 \cdot 10^6 \text{ cm}^2/\text{Vs}$ and an electron density of $1.9 \cdot 10^{15} \text{ m}^{-2}$ at 4.2 K. We denote gate F

as the finger gate, gates 1 to 4 as Quantum Point Contact (QPC) gates,^{12,13} and gate *C* as the center gate. A negative voltage of -0.4 V depletes the 2DEG underneath the gates. The narrow channels between gates 3-1, 1-*C*, *C*-2, and 2-4 are completely pinched-off at this gate voltage. In most of the experiments discussed in this paper, we do not use QPC gates 3 and 4; the gates are at zero potential and have no effect on the 2DEG. Applying a negative voltage to the gates *F*, 1, 2 and *C* forms a dot in the 2DEG. Accounting for the estimated depletion regions yields a dot radius $R \approx 300$ nm. QPC gates 1 and 2 are used to control the conductance of the tunnel barriers between the dot and the wide 2DEG regions, and with the center gate we can vary the number of electrons in the dot. A single QPC can be defined in the 2DEG by applying only a negative voltage to the finger gate and to one QPC gate, while keeping zero voltage at the other gates. In this way, we can measure the conductances of the individual QPCs, and compare them to the conductance of the dot.

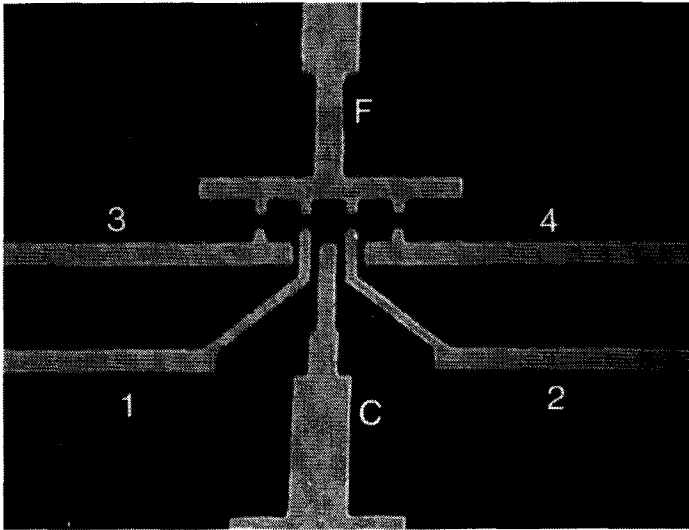


FIG. 7.1. Scanning Electron Micrograph of the gate geometry. The 6 gates are labelled by *F* for the finger gate, *C* for the center gate, and 1 to 4 for the QPC gates. The distance between gate *F* and *C* is $1\ \mu\text{m}$, and between two adjacent QPCs is $0.8\ \mu\text{m}$. The narrow channels between the gates 3-1, 1-*C*, *C*-2, and 2-4, immediately pinch-off when the device is formed in the 2DEG. Electron transport occurs from the 2DEG beneath the black upper left region (between 3 and *F*) to the 2DEG beneath the black upper right region (between *F* and 4).

As we discuss below, the charging effects are described in terms of the capacitance C between the dot and its environment. An estimate of C can be obtained from the self-capacitance $C_o = 8\epsilon_r\epsilon_o R$ between a 2D dot with a disc-shape and infinity. This estimate neglects the existence of the conductors in the vicinity of the dot (the gates and the wide 2DEG regions), but we usually find it to be correct within a factor of 3. For a dot with radius $R = 300$ nm and $\epsilon_r = 13$ in GaAs gives $C_o = 2.8 \cdot 10^{-16}$ F and a charging energy $e^2/C_o = 0.6$ meV, which exceeds the thermal energy $k_B T$ for temperatures below 4 K. From the electron density of the ungated 2DEG and the dot area, we estimate that the number N of electrons in the dot is about 500. The average energy separation between the discrete states is therefore about $2E_F/N \approx 0.03$ meV,⁹ where $E_F = 7$ meV is the 2DEG Fermi energy. This is less than one-tenth of the charging energy, so we expect the charging effects to be dominant in this structure.

7.3 CHARGING THEORY FOR SEMICONDUCTOR QUANTUM DOTS

To describe charging effects in quantum dots, we follow the recent literature¹⁴⁻¹⁶ in which the charging theory for metal systems¹ is generalized to include discrete energy states. Fig. 7.2a schematically shows the potential landscape of the quantum dot, which is induced by the gates. In Fig. 7.2b the equivalent circuit is shown. At sufficiently large negative voltage applied to the QPCs, the induced potential barriers will strongly localize the electrons in the dot. The number of electrons in the dot is therefore determined being an integer and can only be changed by an integer. We write the electro static energy E_{e-s} of the dot as:

$$E_{e-s} = \frac{(-en + Q_o)^2}{2C} \quad \text{with: } n = N - N_o \quad (7.1)$$

$$Q_o = C_l V_l + C_r V_r + \sum C_g V_g$$

$$C = C_l + C_r + \sum C_g$$

The integer part of the excess charge in the dot is $en = e(N - N_o)$, where N is the number of electrons in the dot, and the elementary charge e is taken positive. N_o is the number of electrons at zero gate voltage and zero bias voltage (so $N_o > N$), which compensates the positive background charge originating from the donors. Q_o represents the continuous part of the excess charge, which is induced by voltage differences V_l and V_r between the dot and the leads ($eV_l = \mu_l - \mu_d(N)$, $eV_r = \mu_d(N) - \mu_r$, where $\mu_d(N)$ is the electro chemical potential of the dot calculated below¹⁷), and by the gate voltages. C is the total capacitance of the dot to ground, which

consists of the capacitances C_l and C_r between the dot and the two leads, and the sum of the capacitances ΣC_g between the dot and the gates. Note that for $n = 1$ and $Q_o = 0$, Eq. 7.1 gives the charging energy $e^2/2C$ for a single electron. For our description, however, it is more convenient to take $E_C = e^2/C$ as the unit for charging energy. Moreover, at zero bias voltage and at fixed gate voltage, the induced charge Q_o can be compensated by tunneling of as many electrons into or out of the dot as required to reduce the total charge to a value smaller than the elementary charge e , so the electro static energy is minimized to a value below e^2/C .

In the experiment, we measure the conductance with a small bias voltage $V = (\mu_l - \mu_r)/e$ across the sample as one gate voltage is varied. We therefore simplify $Q_o = C_g V_g$ ($V_g < 0$), where V_g denotes the gate voltage which is varied, and C_g the capacitance between this gate and the dot. The ground state energy for N electrons in the dot at zero temperature is the sum over the single particle energies E_p relative to the bottom of the conduction band, and the electro static energy:

$$U(N) = \sum_{p=1}^N E_p + \frac{(-en + C_g V_g)^2}{2C} \quad (7.2)$$

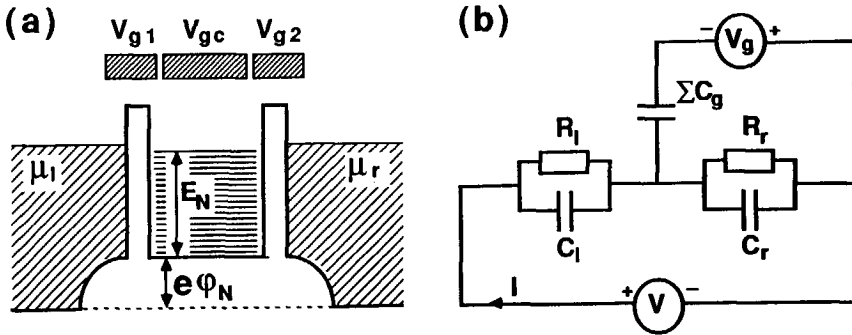


FIG. 7.2. (a) Potential landscape in the 2DEG induced by the gates F, C, 1, and 2. μ_l and μ_r are the potentials of the wide 2DEG reservoirs. ϕ_N is the electro static potential with N electrons in the dot. E_N is the energy level of the N^{th} electron in the dot, relative to the bottom of the conduction band. (b) Equivalent circuit of (a), with a simplification of the different gate voltages by a single voltage source.

From Eq. 7.2 we calculate the electro chemical potential which by definition is the minimum energy necessary to add the N^{th} electron to the dot: $\mu_d(N) = U(N) - U(N-1)$,

$$\mu_d(N) = E_N + \frac{(n-1/2)e^2}{C} - e \frac{C_g}{C} V_g \quad (7.3)$$

In a more familiar form $\mu_d(N) = \mu_{ch}(N) + e\varphi_N$, i.e. the electro chemical potential is the sum of the chemical potential $\mu_{ch}(N) = E_N$ and the electro static potential $e\varphi_N$. When the number of electrons is changed by one, the resulting change in electro chemical potential is (at fixed gate voltage):

$$\mu_d(N+1) - \mu_d(N) = E_{N+1} - E_N + \frac{e^2}{C} \quad (7.4)$$

Equation 7.4 implies that the electro chemical potential changes by a finite energy when an electron is added to the dot. $\mu_d(N+1) - \mu_d(N)$ is large for large energy splitting between consecutive 0D-states, and/or for a small capacitance. This energy gap can lead to a blockade for tunneling of electrons into and out of the dot, as shown schematically in Fig. 7.3a, where N electrons are localized in the dot. The $N+1$ electron can not tunnel into the dot, because the resulting electro chemical potential $\mu_d(N+1)$ is higher than the electro chemical potentials of the reservoirs. So for $\mu_d(N) < \mu_l, \mu_r < \mu_d(N+1)$ the electron transport is blocked, which is known as the *Coulomb blockade*. Transport is only possible by thermal activation or tunneling via virtual states.¹⁸ Note that the energy gap of Eq. 7.4 takes place at the Fermi energy, which determines the transport properties and the activation energy. Below $\mu_d(N)$, the energy states are separated by $E_N - E_{N-1}$, which in our case, are much smaller energy differences.

The Coulomb blockade can be eliminated by changing the gate voltage (or equivalently, the induced charge Q_0), so that $\mu_d(N+1)$ is lined up between μ_l and μ_r [$\mu_l > \mu_d(N+1) > \mu_r$], as illustrated in Fig. 7.3b. Now an electron can tunnel from the left 2DEG reservoir into the dot [$\mu_l > \mu_d(N+1)$]. The electro chemical potential in the dot increases by the amount given by Eq. 7.4, which in our structure is dominated by the increase in electro static potential $e\varphi_{N+1} - e\varphi_N = e^2/C$. Because $\mu_d(N+1) > \mu_r$, one electron can tunnel out the dot to the right 2DEG reservoir, causing the electro chemical potential to drop to $\mu_d(N)$. Now, a new electron can tunnel into the dot and repeat the cycle. This process, where current is carried by successive discrete charging and discharging of the dot, is known as *single charge tunneling*.¹⁰

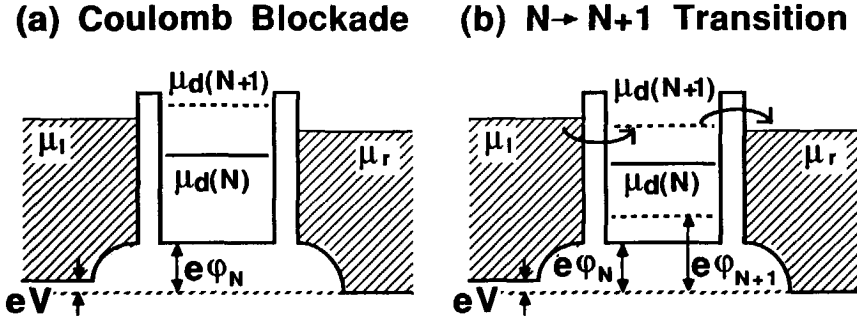


FIG. 7.3. Two situations for different gate voltages. (a) Coulomb blockade of electron tunneling [$\mu_d(N) < \mu_r < \mu_l < \mu_d(N+1)$]. (b) One-by-one electron tunneling at the $N \rightarrow N+1$ transition [$\mu_r < \mu_d(N+1) < \mu_l$]. V denotes the small voltage across the sample [$eV \ll \mu_d(N+1) - \mu_d(N)$].

As the gate voltage is changed, the conductance of the quantum dot oscillates between zero (Coulomb blockade), and non-zero (no Coulomb blockade). These so-called *Coulomb oscillations* are illustrated in Fig. 7.4a. In the case of the Coulomb blockade, at a conductance minimum, the number of electrons in the dot is fixed (see Fig. 7.4b). At a conductance maximum, this number oscillates by one electron, and the electro static potential $e\phi$ oscillates by e^2/C (see Fig. 7.4c). In between two conductance maxima, $e\phi$ changes by $E_{N+1} - E_N + e^2/C$. The average slope of $e\phi$ versus V_g reflects the (de)population of the dot without charging effects. From Eq. 7.3 and the condition $\mu_d(N, V_g) = \mu_d(N+1, V_g + \Delta V_g)$, we get for the period of the oscillations in gate voltage ΔV_g corresponding to a change of one electron:

$$\Delta V_g = \frac{C}{C_g} \left(\frac{E_{N+1} - E_N}{e} \right) + \frac{e}{C_g} \quad (7.5)$$

For vanishing energy splitting $E_{N+1} - E_N \approx 0$, the usual voltage-capacitance relation for a single electron charge is obtained: $\Delta V_g = e/C_g$.

A non-vanishing energy splitting would affect the period ΔV_g . For instance, in the case of spin-degenerate states two periods will be observable. One corresponds to electron N and $N+1$ having opposite spin and being in the same OD state and the other to electron $N+1$ and $N+2$ being in a different OD state.

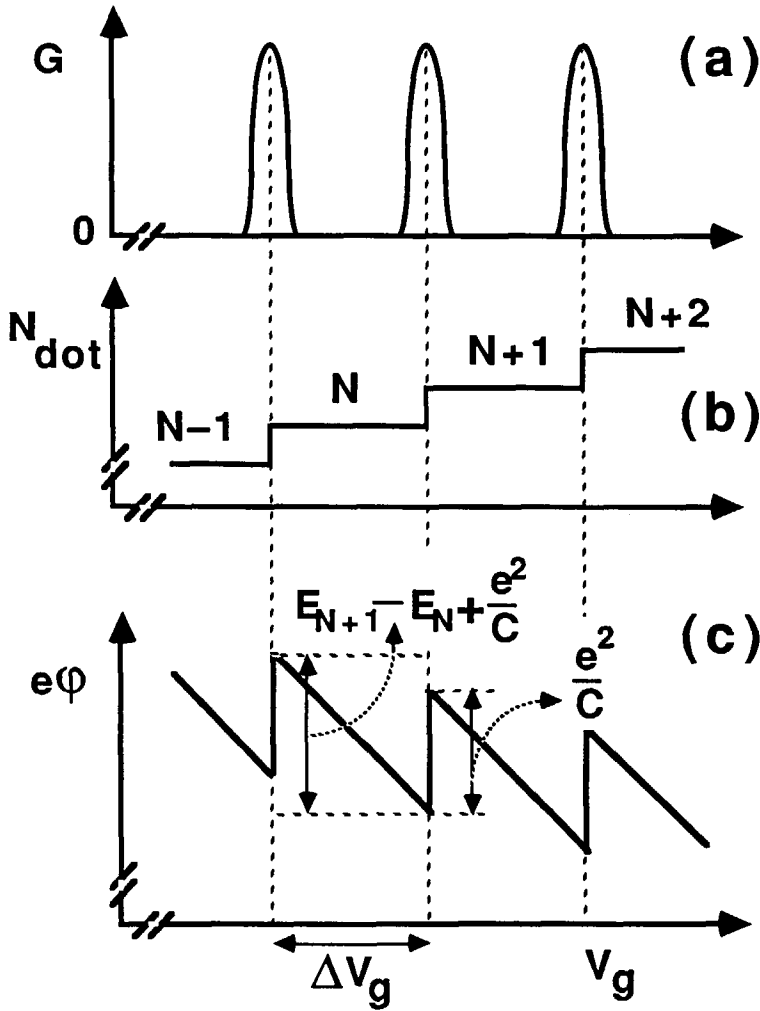


FIG. 7.4. Comparison of the conductance G (a), number of electrons N_{dot} (b), and electrostatic energy $e\phi$ (c), of the dot versus gate voltage V_g . Between the Coulomb oscillations, N_{dot} is fixed, which corresponds to the Coulomb blockade (see Fig. 7.3a). At the maximum of the oscillations, N_{dot} oscillates by one electron, and $e\phi$ oscillates by e^2/C . In this case, the Coulomb blockade is removed, resulting in transport (see Fig. 7.3b).

The Coulomb blockade, as illustrated in Fig. 7.3a, can be removed by increasing the bias voltage between the reservoirs. The resulting energy interval $eV = \mu_l - \mu_r$ determines the transport through the quantum dot. As long as the interval between μ_l and μ_r does not contain a charge state [when $\mu_d(N) < \mu_r < \mu_l < \mu_d(N+1)$ as in Fig. 7.3a] the current is zero. However, current flow will start when either $\mu_l > \mu_d(N+1) > \mu_r$ or $\mu_l > \mu_d(N) > \mu_r$, depending on how the voltage drops across the two barriers. In this case, one can speak of opening a *single charge channel*, corresponding to either the $N \rightarrow (N+1)$ or the $(N-1) \rightarrow N$ transition. On further increasing the bias voltage, a second channel will open up when two charge states are contained between μ_l and μ_r , giving rise to a second increase of the current.

For a highly asymmetric quantum dot, for instance when the barriers are unequal, the voltage will mainly drop across one of the barriers. This keeps the electro chemical potential of one of the reservoirs fixed relative to the charge states in the dot, while the electro chemical potential of the other reservoir moves in accordance with the bias voltage. In this asymmetric case, the current changes are expected to appear in the I - V characteristics as pronounced steps; this is the so-called *Coulomb staircase*. The current steps ΔI occur at voltage intervals $\Delta V = e/C$. For a symmetric quantum dot, both μ_l and μ_r move relatively to the dot (one going up, the other going down), such that both electro chemical potentials are crossing charge states. This smears the steps in the Coulomb staircase,¹ yielding a more gradual increase of the current when the voltage becomes larger than the threshold voltage to overcome the Coulomb blockade (i.e. to open the first channel).

In this section, we have given a rather qualitative description of the charging phenomena occurring in quantum dots. In Refs. 14-16, formal expressions are given for calculating the conductance and current-voltage characteristics.

7.4 EXPERIMENTS

7.4.1 Coulomb Oscillations

The measurements are performed in a dilution refrigerator at a temperature of 10 mK, at zero magnetic field, and using an ac lock-in technique. To characterize the sample, first the conductances G_1 of QPC₁ and G_2 of QPC₂ are measured individually. Fig. 7.5a shows G_1 and G_2 as a function of the voltage applied to, respectively, QPC₁ and QPC₂, with zero voltage on the other QPC. The voltage on the finger gate F is kept constant at -1.2 V. G_1 and G_2 both show a quantized plateau at $2e^2/h$, resulting from the formation of 1D subbands in the QPCs.^{12,13} At

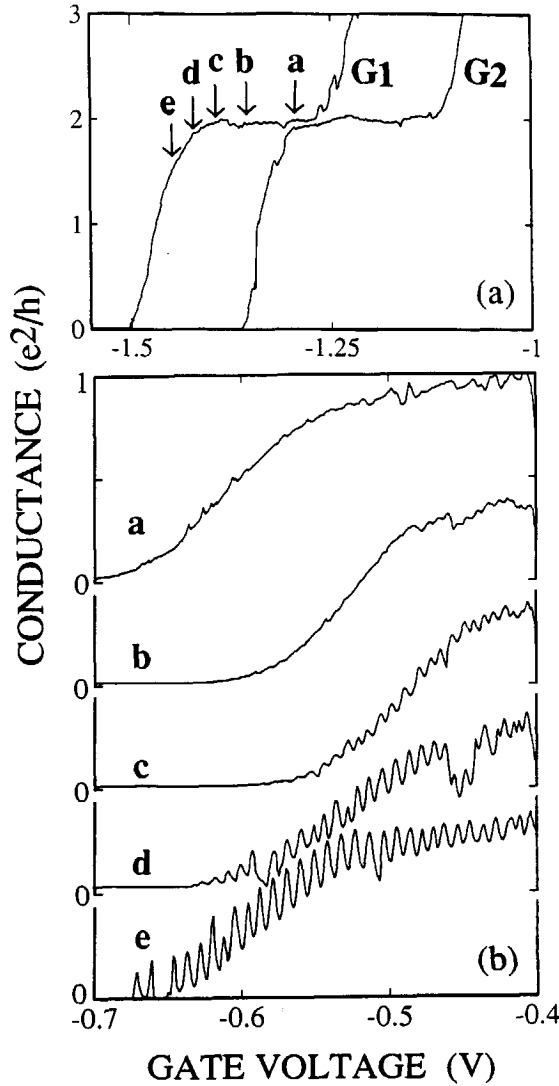


FIG. 7.5. Comparison of the QPC conductances and the appearance of Coulomb oscillations. (a) Conductances G_1 and G_2 of the individual QPCs versus gate voltage, both showing a quantized plateau at $2e^2/h$. (b) Conductance of the dot versus center gate voltage V_C for different voltages on QPC_1 . The labels 'a' to 'e' correspond with the same labels in the conductance curve of QPC_1 shown in (a). The conductance of QPC_2 is fixed below the plateau at about half $2e^2/h$. The curves have been offset for clarity.

the plateau the transmission probability $T_1 = 1$ for electrons in the first 1D subband and $T_{m>1} = 0$ for electrons in all higher subbands. Below the plateau, when $G_1, G_2 < 2e^2/h$, the transmission probability $T_1 < 1$, meaning that electrons in the first subband have a non-zero probability to be reflected in the QPC.

In Fig. 7.5b the conductance of the dot is shown as a function of the voltage V_C on the center gate C with fixed voltages on QPC gates 1 and 2, and zero voltage on gates 3 and 4. The conductance of QPC₂ is fixed below the plateau at a value of about e^2/h (i.e. QPC₂ has $T_1 \approx 0.5$). The different curves in Fig. 7.5b correspond to different conductances G_1 of QPC₁ ranging from the plateau value $2e^2/h$ (curve *a*) to well below the plateau value (curve *e*). In curve *a*, the conductance of the dot smoothly decreases as the voltage V_C on the center gate is reduced. This decrease is due to the influence of V_C on the conductance of the QPCs. The influence is probably largest on QPC₂, which has the smaller conductance. In curve *b*, where QPC₁ is in the middle of the plateau (see Fig. 7.5a), the conductance shows a behaviour similar to that of curve *a*. However, small oscillations appear in curve *c*, where the conductance of QPC₁ is just below the quantized value. The amplitude of the oscillations increases in curves *d* and *e*, which correspond to lower values of G_1 . The oscillations are seen to disappear when the average dot conductance becomes too small. We note that G_1 is somewhat smaller than expected from Fig. 7.5a due to the influence of QPC₂ on QPC₁ when voltages are applied to both QPC gates. Moreover, we note that the oscillations also disappear when $V_C > -0.4$ V, because the center gate no longer depletes the 2DEG beneath it. The sample then consists of two QPCs in series with a very large 2DEG region in between.

Fig. 7.6 shows the oscillations, when both QPCs are put well in pinch-off ($G_1, G_2 \ll 2e^2/h$). Now, the oscillations appear as sharp peaks with an amplitude up to e^2/h . Interestingly, the maximum of the oscillations is considerably larger than both G_1 and G_2 , indicating that the transmission through the dot is of a coherent resonant nature. Resonant transmission is a signature of tunneling through a particular 0D energy state. We will return to this point below. *The comparison between the individual QPC conductances and the dot conductance in Figs. 7.5 and 7.6 demonstrates that at zero magnetic field charging effects occur only when both QPC conductances are below the quantized plateau value $2e^2/h$, and that the amplitude of the Coulomb oscillations increase as the QPC conductances decrease.*

As illustrated in Fig. 7.4, each period corresponds to a change of one electron in the dot. If we neglect the discreteness of the energy states, we derive from the period $\Delta V_C = 8.3$ mV a capacitance between the dot and the center gate $C_C = e/\Delta V_C = 0.19 \cdot 10^{-16}$ F. To determine the

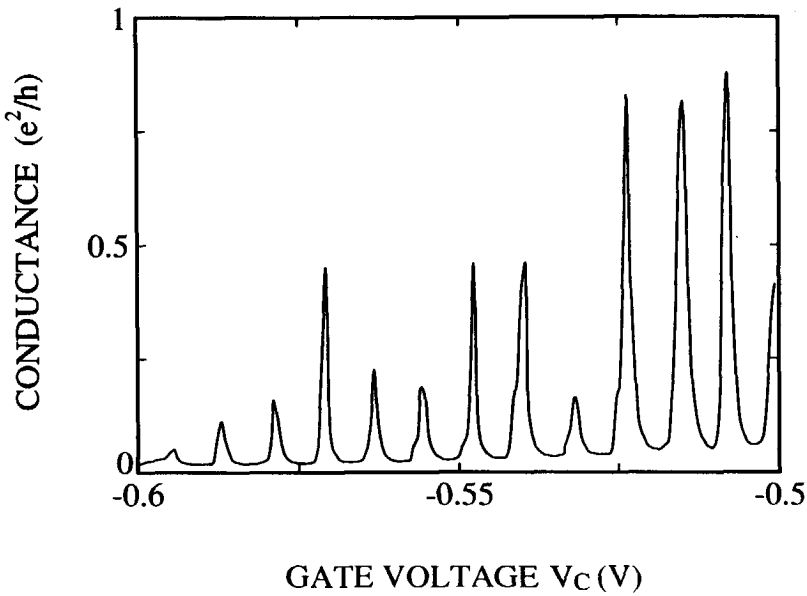


FIG. 7.6. Conductance of the dot versus center gate voltage V_C for $G_1, G_2 \ll 2e^2/h$. The Coulomb oscillations appear as sharp peaks with an amplitude of about e^2/h .

total capacitance ΣC_g between the dot and the six gates of the sample, we have measured the oscillations by varying the voltage on the different gates, while keeping the voltage on the remaining gates fixed. The results are:

ΔV_F	$= 2.1 \text{ mV}$	\rightarrow	C_F	$= 0.76 \cdot 10^{-16} \text{ F}$
ΔV_1	$= 7.5 \text{ mV}$	\rightarrow	C_1	$= 0.21 \cdot 10^{-16} \text{ F}$
ΔV_2	$= 5.8 \text{ mV}$	\rightarrow	C_2	$= 0.28 \cdot 10^{-16} \text{ F}$
ΔV_{3+4}	$= 6.0 \text{ mV}$	\rightarrow	C_{3+4}	$= 0.27 \cdot 10^{-16} \text{ F}$
ΔV_C	$= 8.3 \text{ mV}$	\rightarrow	C_C	$= 0.19 \cdot 10^{-16} \text{ F}$
				<hr/>
				$\Sigma C_g = 1.71 \cdot 10^{-16} \text{ F}$

The capacitance of gates 3 and 4 was measured by varying both gate voltages V_3 , and V_4 simultaneously, while keeping their values $V_3, V_4 > -0.3 \text{ V}$ such that the two outer dots were not

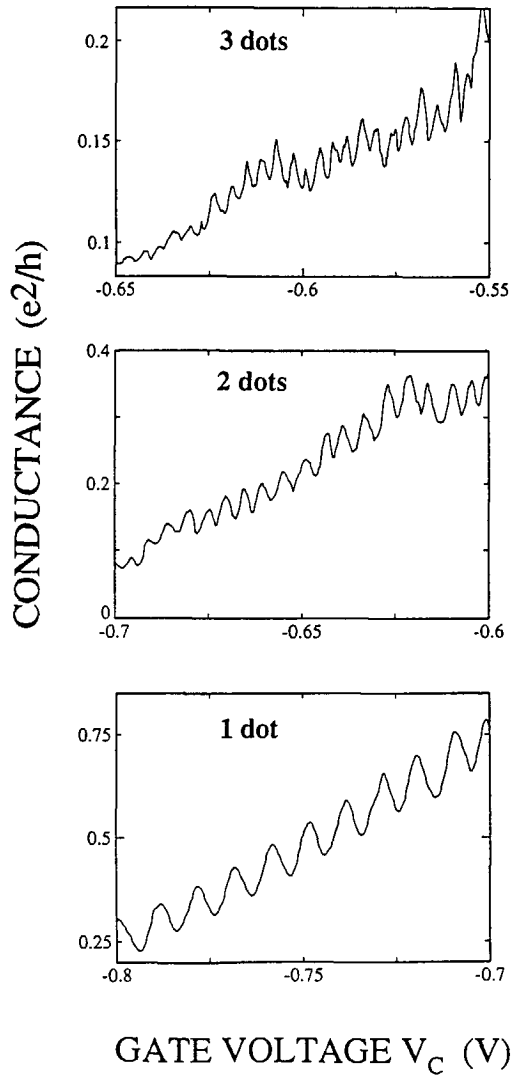


FIG. 7.7. Conductance of the dot versus center gate voltage V_C for different sizes of the dot. The period of the oscillations roughly scales with the size of the dot.

yet formed in the 2DEG. Note that the largest capacitance is associated with the large finger gate, all other values being of a comparable value, as expected from Fig. 7.1. If we neglect the capacitances between the dot and the 2DEG reservoirs ($C_l + C_r \ll \Sigma C_g$), we get for the total capacitance $C \approx \Sigma C_g = 1.7 \cdot 10^{-16} \text{ F}$. The corresponding charging energy is $E_C = e^2/C = 0.94 \text{ meV}$. These values agree reasonably well with the estimate of the self-capacitance $C_0 = 2.8 \cdot 10^{-16} \text{ F}$ from the geometry. An independent way to estimate E_C is by energy averaging of the Coulomb oscillations, by increasing either the temperature or the bias voltage across the sample. We find that the size of the oscillations decrease as the voltage across the sample is raised, from which we deduce $0.7 \text{ meV} < E_C < 1.4 \text{ meV}$. Non-linear transport measurements, such as I - V characteristics from which E_C and C can directly be determined, will be discussed in the next section.

Using QPC gates 3 and 4, we can increase the dot size to two strongly coupled dots (i.e. effectively one dot with a double size), and three strongly coupled dots (i.e. one dot with three times the size of the center dot). Fig. 7.7 shows the Coulomb oscillations versus center gate voltage. The periods in gate voltage are $\Delta V_{1dot} = 9.0 \text{ mV}$, $\Delta V_{2dots} = 5.3 \text{ mV}$, $\Delta V_{3dots} = 3.6 \text{ mV}$, yielding capacitances between the center gate and the dot: $C_{C,1dot} = 1.8 \cdot 10^{-17} \text{ F}$, $C_{C,2dots} = 3.0 \cdot 10^{-17} \text{ F}$, $C_{C,3dots} = 4.4 \cdot 10^{-17} \text{ F}$, which have the ratios 1.2:2:3. This result shows that *the gate capacitance scales with the size of the dot*.

7.4.2 Coulomb Staircase

We have measured I - V characteristics on a different sample with the same gate geometry, which showed Coulomb oscillations with a period of 4.6 mV in center gate voltage.^{19,20} The I - V characteristics are shown in Fig. 7.8, where the different curves have been given an offset for clarity ($I = 0$ occurs at $V = 0$). The curves are measured for different center gate voltages, where in Fig. 7.8a the lowest curve corresponds to a maximum in the Coulomb oscillations (i.e. $N \rightarrow N + 1$ transition), having a finite conductivity $\partial I / \partial V$ for small V . The curve in the middle corresponds to a conductance minimum, showing a gap around $V = 0$. The uppermost curve corresponds to the adjacent maximum, again showing a finite conductivity $\partial I / \partial V$ for small V . The periodicity of this Coulomb staircase is an important check to distinguish non-linear charging effects from other non-linearities (for instance due to lifting the Fermi energy over the top of one of the barriers). The difference between Fig. 7.8a and 7.8b illustrates the effect of the QPC conductances on the I - V curves. In Fig. 7.8a the QPC conductances are about equal, and only the first current step (from $V = 0$) appears as a rapid increase. The increase is more gradual

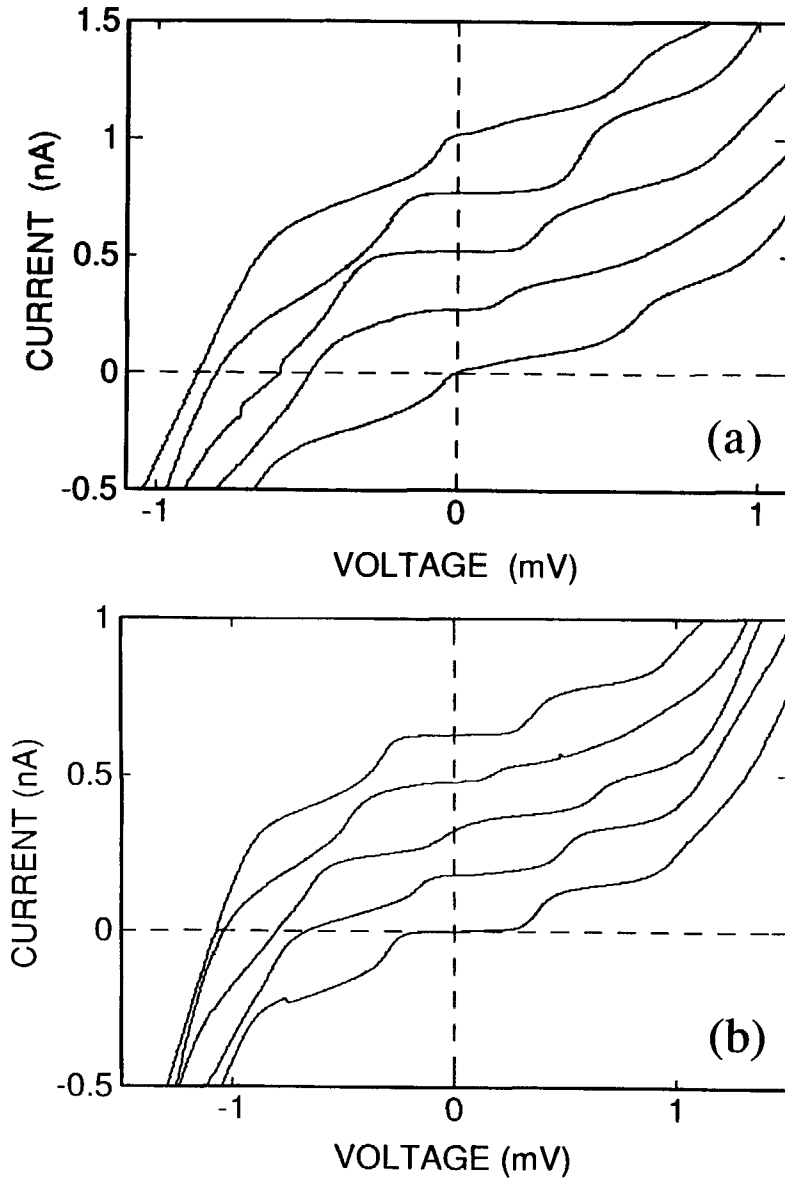


FIG. 7.8. *I-V characteristics for different center gate voltage, demonstrating the Coulomb staircase and its periodicity in gate voltage for roughly equal (a) and differing QPC conductances (b). In the latter case the staircase shows more pronounced steps due to the induced asymmetry in the dot. The curves are offset for clarity ($I = 0$ occurs at $V = 0$).*

at the other current changes. In Fig. 7.8b, the current changes appear as more pronounced steps, and form the Coulomb staircase. Here, the QPC conductances are made more unequal, thereby inducing an asymmetric quantum dot which is necessary for a well-developed staircase.¹

The current steps $\Delta I \approx 0.2$ nA occur at voltage intervals $\Delta V \approx 0.67$ mV. This voltage difference is a direct measure of the charging energy in this second sample: $\Delta V = e/C$, from which we get a total capacitance $C = 2.4 \cdot 10^{-16}$ F. The current step height ΔI gives an estimate for the total tunnel conductance $1/G = 1/G_1 + 1/G_2$. Due to the opening of an extra single charge channel, one extra elementary charge e is transported through the dot in a typical time C/G , yielding $\Delta I \approx eG/C$. This gives $G \approx (4 \text{ M}\Omega)^{-1}$ and a time $C/G \approx 10^{-10}$ s. In Ref. 19 and 20, we have shown that this total tunnel time can be locked with an external frequency f , by creating oscillating tunnel barriers. With this so-called turnstile operation,²¹ we found a quantized current at integer multiples of ef .

7.5 DISCUSSION AND CONCLUSIONS

In most aspects, the experiments performed on semiconductor devices, as reported in Refs. 2,3,4,7, and in this paper, can be described by the theory developed for metal systems.¹ The unique advantage of quantum dots defined by gates in a 2DEG, is that the conditions for the occurrence of charging effects can be studied by simply tuning the gate voltages. We showed that at zero magnetic field a sharp transition exists at QPC conductances $G_1, G_2 = 2e^2/h$ for charging effects to appear. This sharp transition is due to the conductance quantization of the QPCs, which couple the dot to the 2DEG leads. To understand this, we note that the transmission probability defined as $T = |\Psi_{out}|^2/|\Psi_{in}|^2$ (averaged over time), also defines the quantum leakage or fluctuations in time of the electron wave functions through the barrier. For the occurrence of charging effects, the fluctuations in the number N of electrons in the dot must be smaller than 1. This starts to occur just below the first quantized plateau, where $T_1 < 1$. In a high magnetic field the conductance of a QPC is quantized in units of e^2/h . Although not shown here, we found that charging effects now occur when the conductance of both QPCs is smaller than e^2/h , like expected from the above given argument.

To apply these arguments to the metal junctions, we note that in this case the barriers are thin but much higher than the Fermi energy. Although the subbands have a small transmission probability $T_m \ll 1$, many subbands ($m \approx 10^6 - 10^8$) contribute incoherently to the conductance. The total fluctuation becomes of order 1 when $\sum_m T_m$ is of order 1. Experimentally it is found that

for tunnel junctions the charging effects occur much more gradually when the tunnel conductances become $G \approx 2e^2/h$.²²

When both QPCs are well in pinch-off ($T_I \ll 1$), the fluctuations are suppressed, and the number of electrons becomes a well-defined classical integer variable. This suppression results in an increase of the amplitude of the Coulomb oscillations, and in an oscillation minimum that approaches zero when the Coulomb blockade becomes well-defined. The large amplitude of the oscillations in this regime with conductance maxima larger than the individual barrier conductances, indicates that coherent resonant transmission occurs through the dot. This means that no inelastic relaxation or complete phase-randomization takes place in the dot, which would result in conductance maxima being smaller than the barrier conductances. Resonant transmission demonstrates that electron transport through the dot takes place through a particular 0D-state. So with the dimensions of our structure, the energy scale of the oscillations is mostly determined by charging effects, but the exact shape and amplitude reflects the presence of 0D-states. Fine structure seen in the Coulomb oscillations at high magnetic field indicates the presence of magnetically altered 0D states in our device.²³

McEuen et al.⁸ have carried out a careful study of the amplitude and the position of the peaks as a function of magnetic field. Measuring small changes in the positions of the oscillations and large changes in the amplitude by varying the magnetic field, they could deduce the 0D-energy spectrum in their structure in the quantum Hall regime by subtracting a constant value for the charging energy from the oscillation period in gate voltage (see also Eq. 7.5).

The experiments performed on quantum dots containing more than 100 electrons, show that although the Coulomb interaction between the electrons is included in the charging theory only as a constant capacitance parameter, this simplification nevertheless gives a good description. Moreover, in the devices studied so far, the charging energy has been much larger than the energy separation between the 0D-states. A new regime would be reached with smaller quantum dots where charging energy and 0D-splitting are comparable, and where the number of electrons in the dot can be changed starting from zero. In this regime, the description of electron-electron interaction by a constant capacitance parameter, is expected to fail.²⁴

ACKNOWLEDGEMENT

We wish to thank L.J. Geerligs, H. van Houten, K.K. Likharev, J.E. Mooij, and B.J. van Wees for stimulating discussions, A. van der Enden, P.A.M. Holweg, and D.J. Maas for their contributions to the device fabrication, and the Delft Institute for MicroElectronics and Submicrontechnology for the use of their facilities. Financial support from FOM and ESPRIT (project 3133, NANSDEV) is gratefully acknowledged. L.P.K. acknowledges the Sakaki Quantum Wave Project in Tokyo for the hospitality during the preparation of the manuscript.

REFERENCES

This chapter was published in *Zeitschrift für Physik B-Condensed Matter* **85**, 367-373 (1991).

1. See for a review: D.V. Averin and K.K. Likharev, in *Quantum Effects in Small Disordered Systems*, edited by B.Al'tshuler, P. Lee, and R. Webb (Elsevier, Amsterdam, 1990).
2. J.H.F. Scott-Thomas, S.B. Field, M.A. Kastner, H.I. Smith, and D.A. Antonadis, *Phys. Rev. Lett.* **62**, 583 (1989).
3. S.B. Field, M.A. Kastner, U. Meirav, J.H.F. Scott-Thomas, D.A. Antonadis, H.I. Smith, and S.J. Wind, *Phys. Rev. B* **42**, 3523 (1990).
4. A.A.M. Staring, H. van Houten, C.W.J. Beenakker, and C.T. Foxon, *High magnetic fields in semiconductor physics III*, edited by G. Landwehr (Springer, Berlin, 1990).
5. H. van Houten and C.W.J. Beenakker, *Phys. Rev. Lett.* **63**, 1893 (1989).
6. L.I. Glazman, and R.I. Shekhter, *J. Phys.: Condens. Matter* **1**, 5811 (1989).
7. U. Meirav, M.A. Kastner, and S.J. Wind, *Phys. Lett.* **65**, 771 (1990).
8. P.L. McEuen, E.B. Foxman, U. Meirav, M.A. Kastner, Y. Meir, N.S. Wingreen, and S.J. Wind, *Phys. Rev. Lett.* **66**, 1926 (1991).
9. B.J. van Wees, L.P. Kouwenhoven, C.J.P.M. Harmans, J.G. Williamson, C.E. Timmering, M.E.I. Broekaart, C.T. Foxon, and J.J. Harris, *Phys. Rev. Lett.* **62**, 2523 (1989).
10. "Single Charge Tunneling", H. Grabert, J.M. Martinis, and M.H. Devoret, eds. (Plenum, New York, 1991).
11. See also: L.P. Kouwenhoven, N.C. van der Vaart, A.T. Johnson, C.J.P.M. Harmans, J.G. Williamson, A.A.M. Staring, and C.T. Foxon, *Festkörperprobleme/Advances in Solid State Physics*, U. Rössler (ed.) Vol. **31**, pp. 329-340.
12. B.J. van Wees, H. van Houten, C.W.J. Beenakker, J.G. Williamson, L.P. Kouwenhoven, D. van der Marel, and C.T. Foxon, *Phys. Rev. Lett.* **60**, 848 (1988).
13. D.A. Wharam, T.J. Thornton, R. Newbury, M. Pepper, H. Ahmed, J.E.F. Frost, D.G.

- Hasko, D.C. Peacock, D.A. Ritchie, and G.A.C. Jones, J. Phys. C **21**, L209 (1988).
14. A.N. Korotkov, D.V. Averin, and K.K. Likharev, Physica B **165&166**, 927 (1990);
D.V. Averin, A.N. Korotkov, and K.K. Likharev, Phys. Rev. B **44**, 6199 (1991).
 15. A. Groshev, T. Ivanov, and V. Valtchinov, Phys. Rev. Lett. **66**, 1082 (1991).
 16. C.W.J. Beenakker, H. van Houten, A.A.M. Staring, Phys. Rev. B **44**, 1657 (1991);
C.W.J. Beenakker, Phys. Rev. B **44**, 1646 (1991);
H. van Houten, C.W.J. Beenakker, A.A.M. Staring, in Ref. 10.
 17. Note that V_l and V_r as defined here differ from the results of ordinary circuit analysis, e.g. capacitor divider equations. This comes from our inclusion of the discrete electron charge, while circuit analysis implicitly assumes a continuous charge fluid.
 18. D.V. Averin, and Yu. V. Nazarov, Phys. Rev. Lett. **65**, 2446 (1990).
 19. L.P. Kouwenhoven, A.T. Johnson, N.C. van der Vaart, C.J.P.M. Harmans, and C.T. Foxon, Phys. Rev. Lett. **67**, 1626 (1991).
 20. L.P. Kouwenhoven, A.T. Johnson, N.C. van der Vaart, A. van der Enden, C.J.P.M. Harmans, and C.T. Foxon, Z. Phys. B - Condensed Matter **85**, 381 (1991);
See also chapter 8 of this thesis.
 21. L.J. Geerligs, V.F. Anderegg, P.A.M. Holweg, J.E. Mooij, H. Pothier, D. Esteve, C. Urbina, and M.H. Devoret, Phys. Rev. Lett. **64**, 2691 (1990).
 22. L.J. Geerligs, *Classical and quantum charge dynamics in small tunneljunctions*, thesis, Delft University of Technology (1990).
 23. A.T. Johnson et al., to be published.
See also chapter 9 of this thesis
 24. A. Kumar, S.E. Laux, and F. Stern, Phys. Rev. B **42**, 5166 (1990).

CHAPTER 8

Quantized Current in a Quantum Dot Turnstile

L.P. Kouwenhoven, A.T. Johnson, N.C. van der Vaart,

A. van der Enden, and C.J.P.M. Harmans

Faculty of Applied Physics, Delft University of Technology

P.O.Box 5046, 2600GA Delft, The Netherlands

C.T. Foxon

Philips Research Laboratories, Redhill, Surrey RH15HA, United Kingdom

ABSTRACT

We have performed RF experiments on a lateral quantum dot defined in the two dimensional electron gas (2DEG) of a GaAs/AlGaAs hetero structure. The small capacitance of the quantum dot gives rise to single-electron charging effects, which we employed to realize a quantum dot turnstile device. By modulating the tunnel barriers between the quantum dot and the 2DEG leads with two phase-shifted RF signals, we pass an integer number of electrons through the quantum dot per RF cycle. This is demonstrated by the observation of quantized current plateaus at multiples of ef in current-voltage characteristics, where f is the frequency of the RF signals. When an asymmetry is induced by applying unequal RF voltages, our quantum dot turnstile operates as a single-electron pump producing a quantized current at zero bias voltage.

8.1 INTRODUCTION

The ability to control current on a single-electron level has become feasible by employing the Coulomb blockade in submicron devices. This single-electron control is not only interesting from a fundamental point of view, but may find applications in an accurate current standard and other novel devices. Many proposals have been made for circuits producing a current determined by the frequency of an externally applied signal. Metal tunnel junction systems have already demonstrated the transport of one electron per cycle of a RF signal.^{1,2} In a 1D array of tunnel junctions, Delsing et al.³ were able to lock the time-correlated tunneling of charge solitons to a RF signal. Geerligs et al.⁴ used a gate capacitor to couple a RF signal to the central island of 4 junctions in series, modulating the Coulomb gap so that exactly one electron passed their *turnstile* device per RF cycle. Using two phase-shifted RF signals to modulate the Coulomb gap in two neighbouring islands, Pothier et al.⁵ realized a single-electron *pump*: a device transporting one electron per RF cycle at zero bias voltage. This control of single-electrons was demonstrated in the above experiments by observing a current plateau at $I = ef$ in I - V characteristics, where f is the frequency of the RF signals. The best accuracy of a few times 10^{-4} was obtained in Ref. 4. It has been argued^{2,4} that improved devices could reach an accuracy of 10^{-8} , and may serve as a current standard. Related experiments have demonstrated the control of Cooper pairs in Josephson junctions by the observation of time-correlated tunneling of Cooper pairs⁶ and the realization of a single-Cooper pair pump.⁷ New systems have been proposed for phase locking a Bloch wave with external signals⁸ and for passing single-electrons through a STM-grain junction.⁹

The realization of the metal turnstile stimulated this effort to produce a similar device in a semiconductor system.¹⁰ Although, a close analogy could have been studied in which the Coulomb gap in a semiconductor quantum dot is modulated, we have chosen a different approach that employs the electro static control inherent to gated hetero structures. Our *quantum dot turnstile* relies on applying two phase shifted RF signals to the gates forming the tunnel barriers between the quantum dot and the wide two dimensional electron gas (2DEG) leads.¹¹ The out-of-phase oscillating tunnel barriers open and close the entrance and exit of the quantum dot. If the entrance is open, and simultaneously, the exit is closed, an integer number n of electrons tunnels into the dot, determined by the Coulomb gap and the bias voltage. After closing the entrance and opening the exit, the same number of electrons tunnels out of the dot. This process of transporting n electrons per RF cycle through the quantum dot is demonstrated by our

observation of quantized current plateaus at the values $n \cdot e f$ in I - V characteristics.¹⁰ Moreover, we show that the flexibility of a gated quantum dot allows us to tune the various parameters which control the transport. The introduction of an asymmetry in the quantum dot turnstile allows it to pump a discrete number of electrons at zero bias voltage.

The outline of this paper is as follows; in section 8.2 we describe the gate geometry and how we characterize the quantum dot; in section 8.3 we describe the device operation principles and experiments; a discussion and conclusions follow in section 8.4.

8.2 THE SPLIT-GATE QUANTUM DOT

8.2.1 Sample Layout

Fig. 8.1 shows a SEM photograph of the gate geometry, which is fabricated on top of a GaAs/AlGaAs hetero structure with a 2DEG about 100 nm below the surface. The ungated 2DEG has a mobility of $2.3 \cdot 10^6$ cm²/Vs and an electron density of $1.9 \cdot 10^{15}$ m⁻². We denote gate F as the finger gate, gates 1 to 4 as Quantum Point Contact (QPC) gates, and gate C as the center

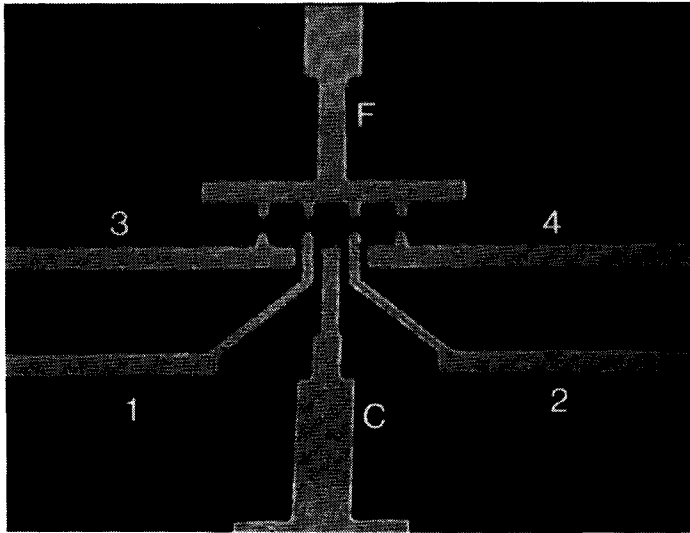


FIG. 8.1. Gate geometry; F denotes the finger gate, 1 and 2 the QPC gates, and C the center gate. Gates 3 and 4 are not used. The distance between gate F and C is 1 μ m and between two adjacent QPCs is 0.8 μ m.

gate. In the experiments discussed in this paper, we do not use QPCs 3 and 4; these gates are grounded and have no effect on the 2DEG. Applying a negative voltage to the gates $F, 1, 2$ and C forms a dot in the 2DEG. Subtracting the estimated depletion regions from the dimensions of the gate geometry yields a dot radius $R \approx 300$ nm. The narrow channels between gates 1- C , and C -2 immediately pinch-off when the dot is formed in the 2DEG. The QPCs are used to control the tunnel barriers between the dot and the wide 2DEG regions, and with the center gate we can vary the number of electrons in the dot. Current flows from the 2DEG beneath the black upper left region in Fig. 8.1 (between 1 and F) to the 2DEG beneath the black upper right region (between F and 2).

In addition to the dc gate voltages, RF signals can be applied to the QPCs by capacitively coupling RF coaxial cables to the dc gate wires in the vicinity of the sample. The RF signals are strongly attenuated at 1.4 K. All experiments were performed in a dilution refrigerator at a temperature of 10 mK and in zero magnetic field. We apply a dc bias voltage between the two wide 2DEG regions and measure the dc current in a two-terminal configuration with a resolution of less than 0.1 pA.

8.2.2 Charging effects without applying RF signals

The gate structure lets us independently tune the 4 different dc gate voltages, the 2 RF signals, and their phase difference. This flexibility may, on the other hand, make it difficult to tune all parameters to the regime appropriate for a turnstile operation. In this section, we describe a way to determine suitable values for the various experimental parameters.

In all measurements we keep the voltage on the finger gate constant at $V_F = -700$ mV. The QPC conductances G_1 and G_2 are characterized individually by varying the voltage on one QPC gate with zero voltage on the other, from which we obtain the pinch-off gate voltages $V_1 = -850$ mV for QPC₁, and $V_2 = -815$ mV for QPC₂.

To obtain the various dot-gate capacitances, voltages are applied to QPC₁, QPC₂ and C such that the barrier conductances $G_1, G_2 \ll 2e^2/h$. This is the regime where single-electron charging regulates tunneling through the dot, resulting in for instance the *Coulomb oscillations*.¹²⁻¹⁴ Fig. 8.2a shows the Coulomb oscillations obtained by varying respectively the voltage on QPC₁, QPC₂, and the center gate C , while keeping the other voltages fixed. Because each period ΔV_g in gate voltage corresponds to a change of one electron in the dot, we obtain the dot-gate capacitances from the relation $\Delta V_g = e/C_g$ yielding for the dot-QPC₁ capacitance $C_1 = 0.44 \cdot 10^{-16}$ F, the dot-QPC₂ capacitance $C_2 = 0.44 \cdot 10^{-16}$ F, and for the dot-center gate capacitance $C_C =$

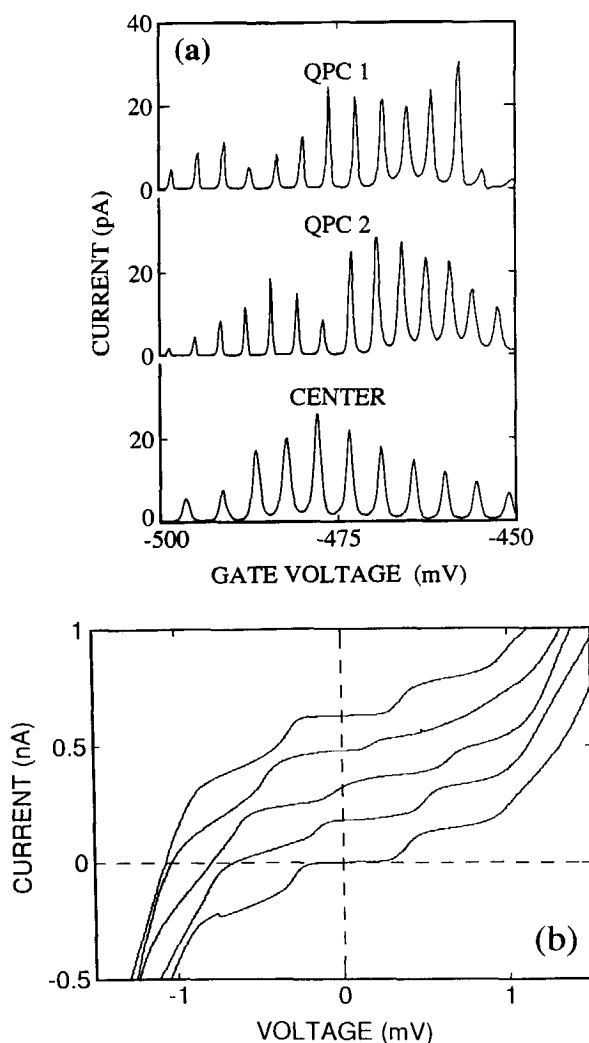


FIG. 8.2. (a) Coulomb current oscillations versus the gate voltages. The x-axis values refer to the bottom curve (center gate voltage). Top curve: the voltage on QPC₁ varies from -830 mV to -780 mV. The center gate voltage is -450 mV, while that on QPC₂ is -780 mV. The oscillation period is 3.6 mV. Middle curve: the voltage on QPC₂ varies from -800 mV to -750 mV. The center gate voltage is -450 mV, while that on QPC₁ is -820 mV. The oscillation period is 3.6 mV. Bottom curve: The voltages on QPC₁ and QPC₂ are -820 mV and -770 mV, respectively. The oscillation period is 4.6 mV. (b) Coulomb staircase I-V characteristics: the curves correspond to different values of V_C (steps of 1 mV) and are offset for clarity ($I = 0$ occurs at $V = 0$).

$0.35 \cdot 10^{-16}$ F. Since $C_1 = C_2$, the influence of the two QPC gate voltages on the dot are equal in this sample.¹⁵ The charging energy $E_C = e^2/C$ is determined by the total capacitance $C = \sum_i C_i$ between the dot and the 2DEG leads, and between the dot and the gates. We obtain this value from the plateau width $\Delta V = e/C = 0.67$ mV in the *Coulomb staircase* shown in Fig. 8.2b, which gives $C = 2.4 \cdot 10^{-16}$ F. The different I - V characteristics are measured for different center gate voltages V_C , illustrating the periodicity in V_C in accordance with the Coulomb oscillations in Fig. 8.2a. A gap with $I = 0$ around $V = 0$ corresponds to an oscillation minimum, while a maximal conductivity $\partial I / \partial V$ corresponds to an oscillation maximum.

8.2.3 Electron pump using one oscillating barrier

To determine how a RF signal is transferred from the gates into the 2DEG, we have performed measurements where we apply a RF signal in addition to a dc voltage to one QPC. Only a dc voltage is applied to the other QPC, and we keep the voltage on the center gate fixed. We sweep one of the dc QPC voltages and measure the current at zero bias voltage for different RF amplitudes and $f = 10$ MHz. The lower set of 5 curves in Fig. 8.3b are measured for sweeping QPC₁ and keeping QPC₂ fixed at its pinch-off voltage. Without RF the current is zero, as expected from the zero bias voltage. However, if RF is applied to QPC₁, the current shows a negative peak at the pinch-off voltage of QPC₁, which is the one being varied. When we change the RF signal to QPC₂, the current peak reverses sign, but is still located at the pinch-off voltage of the sweeping QPC. Similar curves are obtained when the voltage on QPC₂ is varied with QPC₁ fixed at its pinch-off voltage (see the upper part of Fig. 8.3b). Now, the current peaks are located at the pinch-off voltage of QPC₂. A positive current peak again occurs when RF is applied to QPC₂, while a negative current peak appears for applying RF to QPC₁. The amplitude and the width of the current peak is seen to increase on increasing the RF amplitude. The fact that the current peaks are about equal in size for applying RF to one or the other QPC, shows that the RF is equally transferred from the two QPCs to the 2DEG. We emphasize again that the non-zero current occurs for *zero bias voltage*, indicating that the electrons are pumped to a higher energy by the system's only energy source, which is the RF signal.

To explain this *electron pumping*, we show in Fig. 8.3a the potential landscape of the dot with one fixed barrier, and one oscillating barrier. The electro chemical potentials μ_l and μ_r of the 2DEG reservoirs are equal, corresponding to zero bias voltage. On increasing the left barrier, the conduction band bottom in the dot will be lifted by an amount determined by the capacitance between the QPC gate and the dot. The increase of the band bottom pumps the electrons in the

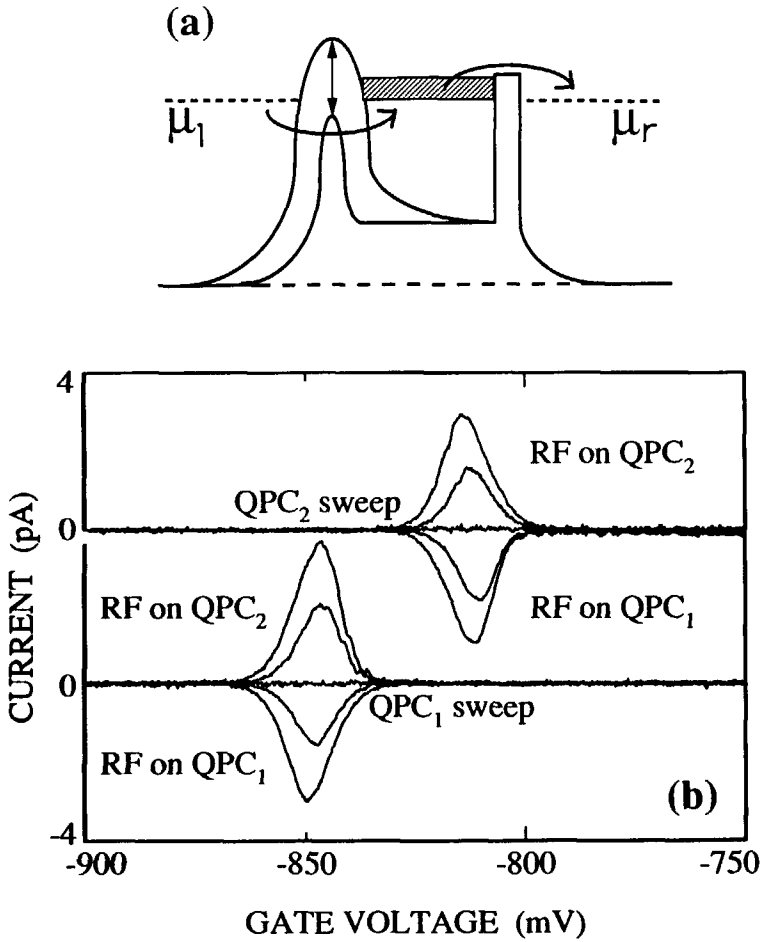


FIG. 8.3. (a) Schematic picture of the electron pump using one oscillating tunnel barrier. (b) Current versus dc gate voltage on QPC₁ with a fixed voltage $V_2 = -815$ mV on QPC₂ (lower set of curves) and versus dc gate voltage on QPC₂ with a fixed voltage $V_1 = -850$ mV on QPC₁ (upper set of curves) at zero bias voltage. The curves are measured without RF ($I = 0$ curves) and for a RF amplitude of 8 mV (smaller current peaks) and 11 mV (larger current peaks). When RF is applied to QPC₁ the current peak is negative, while a positive current peak appears for RF applied to QPC₂. The upper set curves have an offset of 4 pA.

dot to a higher energy, lifting the electro chemical potential μ_d in the dot above μ_l and μ_r (indicated by the hatched energy region). Electrons can now tunnel out of the dot, which preferentially occurs to the right reservoir at this point because the right barrier is smaller. When the left barrier is lowered, the dot will fill with electrons from the left reservoir, because now the left barrier is smaller. So, *the oscillating barrier is pumping electrons over the fixed barrier*; this picture predicts a sign of the pumped current which agrees with the measurements. Changing the RF to the right barrier reverses the current direction, which is also seen in the measurements of Fig. 8.3b. The pumping only occurs when the fixed barrier is just in pinch-off and the other barrier oscillates around pinch-off. At other gate voltages, one barrier always forms the bottle-neck for transport, while Fig. 8.3a shows that for pumping the bottle-neck alternates from one barrier to the other. This is the reason that zero current is observed away from the pinch-off voltages.

For the turnstile operation, two RF signals with a phase difference π are applied to the QPC gates. In this case, the influence of the RF signals on the band bottom is mostly compensated. This can already be seen from Fig. 8.3b by adding the positive and negative current peaks, but we discuss this point in more detail below. From Fig. 8.3b we also choose the dc QPC voltages for the turnstile operation. Taking $V_1 = -865$ mV and $V_2 = -825$ mV, the barriers oscillate between the zero-current region left from the peak into the current peak region.

8.3 QUANTUM DOT TURNSTILE

8.3.1 Operation principles

Fig. 8.4 schematically shows the potential landscape of the dot for 4 stages of a RF cycle. The two barriers oscillate with a phase difference π . In (a) the barriers are in their equilibrium position, which is the same as without applying RF. The electron states in the 2DEG reservoirs are occupied up to the electro chemical potentials μ_l and μ_r , which differ due to the bias voltage $V = (\mu_l - \mu_r)/e$. The level N in the dot denotes the electro chemical potential $\mu_d(N)$ when N electrons are localized in the dot (i.e. the minimum energy for the N^{th} electron). Addition of an extra electron to the dot into the lowest available energy state, would increase the electro chemical potential to $\mu_d(N + 1)$, indicated by the $(N + 1)$ level in Fig. 8.4. The difference $\mu_d(N + 1) - \mu_d(N) = e^2/C$ is an electro static energy increase,¹⁶ which we represent as an increase of the band bottom (compare the band bottom in (a) where there are N electrons in the dot with the band bottom in (c) where the number of electrons is $N + 1$). In principle, the $(N + 1)$ electron could

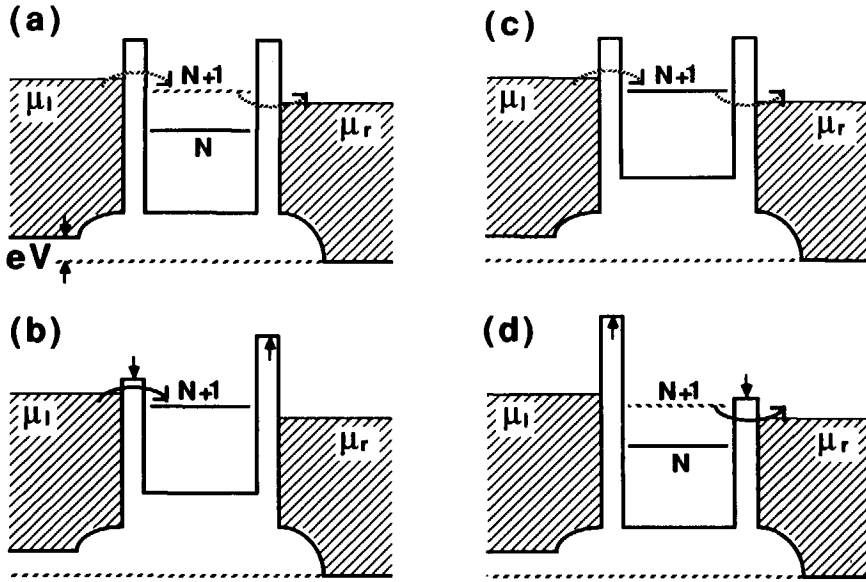


FIG. 8.4. Schematic potential landscape through the quantum dot, where μ_l and μ_r denote the electro chemical potentials of the left and right reservoirs; $V = (\mu_l - \mu_r)/e$ is the bias voltage; the level N indicates the electro chemical potential $\mu_d(N)$ when N electrons are confined in the quantum dot, while the level $(N + 1)$ indicates $\mu_d(N + 1)$. (a) to (d) represent 4 stages of a RF cycle where the probability for electron tunneling is large when the barrier is low (solid arrows), and small for high barriers (dashed arrows).

tunnel from the left reservoir into the dot, thereby increasing the electro chemical potential of the dot from $\mu_d(N)$ to $\mu_d(N + 1)$. Tunneling out of the dot to the right reservoir, returns the dot to the initial situation. This process where the number of electrons in the dot alternates between N and $N + 1$, can occur when a charge state is enclosed by the electro chemical potentials of the reservoirs [$\mu_l > \mu_d(N + 1) > \mu_r$], and corresponds to a maximum of a Coulomb oscillation. The typical time for tunneling of an electron through the dot is the RC time, where R is the total tunnel resistance of the two barriers in series. During turnstile operation, these tunnel events (indicated by the dashed arrows in Fig. 8.4), contribute an unwanted leakage current, which can be suppressed by increasing the resistance of the dc tunnel barriers. For the dc gate voltages used for the turnstile operation, this suppression of tunneling appears as a vanishing amplitude of the Coulomb oscillations.

We start the description of the turnstile operation in (a) with N electrons in the dot. The $(N + 1)$ electron has a large probability to tunnel into the dot in (b) at $1/4$ the RF cycle, when the left barrier is at its minimum. Simultaneously, the right barrier is strongly increased, suppressing the probability to tunnel out of the dot to the right reservoir to virtually zero. At half the cycle time in (c), the barriers are in their equilibrium position again, however, compared to (a) one extra electron is localized in the dot. The dashed arrows again indicate possible leakage. In (d), at $3/4$ the cycle time, the right barrier is lowered to its minimum value, so the $(N + 1)$ electron has a large probability for tunneling to the right reservoir, as indicated by the solid arrow. If the wanted tunnel events (solid arrows) have a probability of one, and the unwanted leakage events (dashed arrows) have zero probability, then exactly one electron is transported during the cycle from (a) - (d). Repeating this process with frequency f , gives a frequency-determined current $I = ef$. If the bias voltage is increased, so that the number of charge states in the interval between μ_l and μ_r is increased to n , then exactly n electrons will pass through the quantum dot per RF cycle, yielding a quantized current $I = n \cdot ef$. This quantized current corresponds to the current steps $\Delta I \approx e/RC$ in the Coulomb staircase, but in the case of the turnstile the stepheight $\Delta I = ef$ is determined by the externally applied frequency. The steps in the staircase come at voltage intervals e/C , so we predict an average conductance of the turnstile I - V characteristic proportional to frequency $\langle G \rangle = ef/(e/C) = fC$.

The accuracy of this quantized current can be estimated by comparing the tunnel times for leakage and for wanted tunnel events with the frequency f of the RF signal.¹¹ With the dc gate voltages chosen from the pump experiment of Fig. 8.3b, the tunnel resistance $R = 1/G$ is about $100 \text{ G}\Omega$, which yields a typical time for leakage $RC/_{leak} \approx 10^{-5}$. When a barrier is minimal, its tunnel resistance is of order $1 \text{ M}\Omega$, yielding a tunnel time for wanted events $RC/_{tunnel} \approx 10^{-10} \text{ s}$. If the frequency $f = 10 \text{ MHz}$, the time ratio $(1/f)/RC/_{leak} \approx 10^{-2}$ gives a probability for leakage per cycle of $1 - \exp(-0.01) \approx 0.01$, while $(1/f)/RC/_{tunnel} \approx 10^3$ gives a probability for wanted tunnel events of $1 - \exp(-1000) \approx 1$. The thermal energy $k_B T$ at 10 mK is two orders of magnitude less than e^2/C , so excess electron transport via thermal activation is exponentially suppressed. These considerations predict a turnstile accuracy of about 1 %, and show the feasibility of a quantum dot turnstile.

8.3.2 Experiment

For the turnstile experiments we apply gate voltages to QPC₁, and QPC₂, which are somewhat more negative than their pinch-off voltages, as we deduced from the pump experiment of Fig.

8.3. The I - V characteristic without RF is shown in Fig. 8.5, which shows a gap between $V = -4$ mV and $V = 6$ mV. From an expansion of the I - V curve around $V = 0$, we estimate the tunnel resistance $R = 100$ G Ω . Within the gap, a Coulomb staircase may be hidden with current steps $\Delta I \approx e/RC \approx 10$ fA, which is smaller than the measurement resolution. This shows that the large barriers will suppress unwanted tunnel events during turnstile operation. The rapid current increase at $V = -4$ mV and 6 mV is due to the non-linear QPC conductances,¹⁷ and occurs when one of the electro chemical potentials of the reservoirs is lifted over the top of the barriers.

The measured I - V curves for RF signals with a phase difference of π applied to QPC₁ and QPC₂ are shown in Fig. 8.6 for $f = 10$ MHz. The RF amplitudes $V^{RF} \approx 30$ mV are about 10 times the period of the Coulomb oscillations. The quantized current values $n \cdot ef$ are indicated by the dotted lines ($e \cdot 10$ MHz = 1.6 pA). The different curves correspond to different center gate voltages V_C , again illustrating the periodicity in V_C , and are offset from each other by ef . Fig. 8.6 shows that on applying RF, the I - V curves have current plateaus at multiple values of ef , demonstrating that a discrete number of electrons are transferred through the quantum dot for each RF cycle.¹⁸ For some values of n , the plateau is missing or weakly developed. Note that

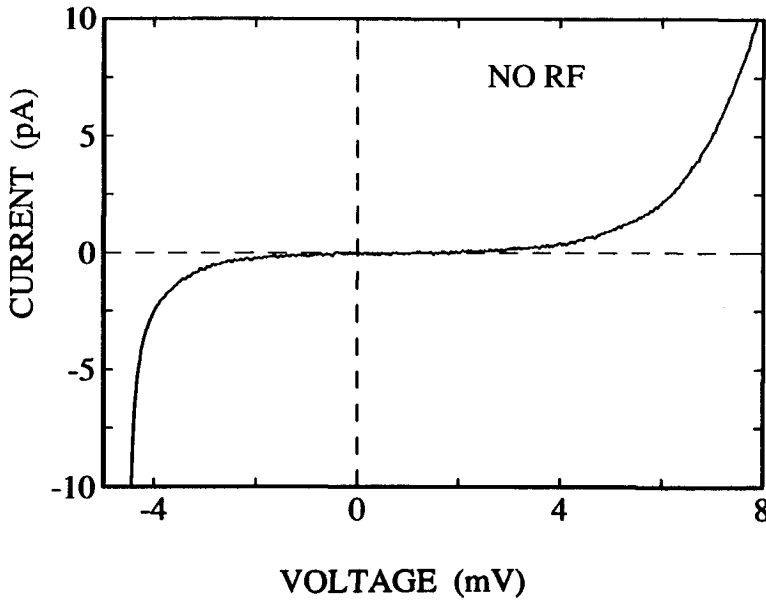


FIG. 8.5. I - V characteristic for the gate voltages used for the turnstile operation ($V_1 = -865$ mV and $V_2 = -825$ mV) without applying RF.

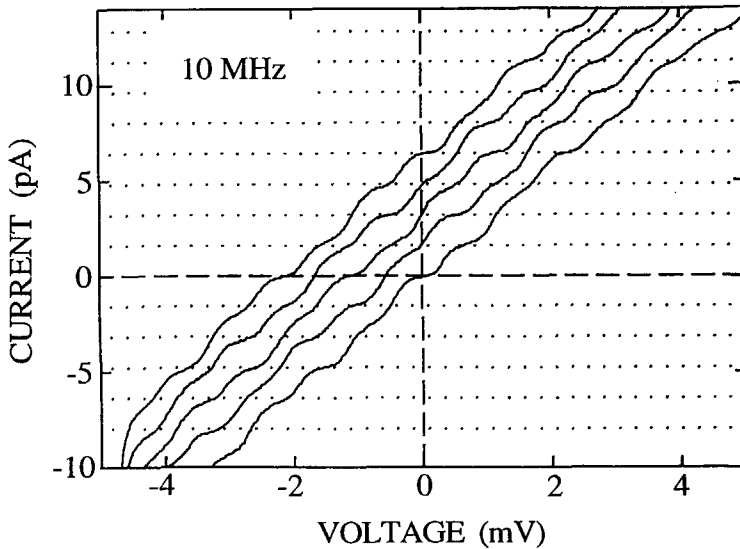


FIG. 8.6. *I-V characteristics when two phase shifted RF signals are applied with a frequency $f = 10$ MHz, showing current plateaus at integer values of ef (dotted lines). The curves correspond to different center gate voltages (in steps of 1 mV) and are offset for clarity by an integer times ef ($I = 0$ occurs at $V = 0$).*

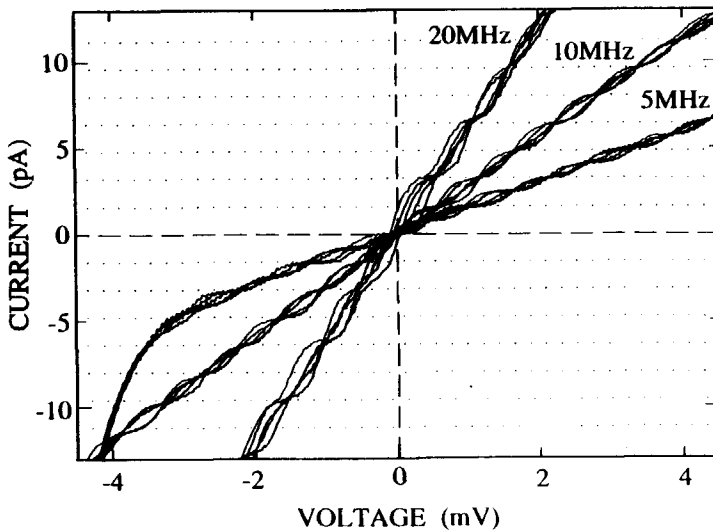


FIG. 8.7. *I-V curves for RF frequency $f = 5, 10$, and 20 MHz, demonstrating scaling with frequency by the observed scaling of the quantized current values and the average slope $\langle G \rangle = fC$. Dotted lines indicate multiples of ef for $f = 10$ MHz.*

this always occurs with two neighbouring plateaus. This plateau smearing occurs if the tunnel barriers are about equal, such that the voltage drops across both barriers instead dropping mainly over one barrier, which is required for a well-developed staircase.^{1,14}

The current plateaus are shown in a different way in Fig. 8.7, where for $f = 10$ MHz the same curves are shown as in Fig. 8.6, but now without offsets. The dotted lines indicate the quantized current values $n \cdot ef$ for $f = 10$ MHz. The different curves cross each other at multiple values of ef for n ranging from -7 to 7 , which, as expected, occur at multiple voltage values of $e/C \approx 0.6$ mV. To demonstrate scaling with frequency, also I - V curves are shown for $f = 5$ and 20 MHz, which have, respectively, twice and half as many crossings compared to the curves for 10 MHz. Moreover, the average slope of the I - V curves scales with frequency, as expected from the relation $\langle G \rangle = fC$, and is in agreement with the value for C obtained from the Coulomb staircase shown in Fig. 8.2b.

An alternative way of measuring the same curves is shown in Fig. 8.8a, where the current is shown versus center gate voltage for different bias voltages and $f = 10$ MHz. The current is independent of center gate voltage and equal to $n \cdot ef$, when the bias voltage corresponds to a crossing in the I - V curves. At other bias voltages, the current oscillates with a period equal to the period of the Coulomb oscillations shown in Fig. 8.2a. However, the oscillation amplitude is now determined by the RF frequency: current lies between $n \cdot ef$ and $(n + 1) \cdot ef$. Note that a current maximum below a constant current $I = n \cdot ef$ curve becomes a minimum beyond it, while a minimum turns into a maximum. An analogous measurement was obtained for the metal turnstile of Ref. 4. To explain these *frequency determined Coulomb oscillations*, we schematically show in Fig. 8.8b the electro chemical potentials of the reservoirs differing by eV , and the charge states differing by e^2/C , for two different center gate voltages and two bias voltages. In the left part, where $V < e/C$, either one or zero charge states contribute to the current, which therefore oscillates between 0 and ef on varying the gate voltage. In the right part, the bias voltage is increased to $V > e/C$. Now, either one or two charge states contribute to the current, so the oscillations are bounded by ef and $2ef$. When $V = e/C$ there is always one charge state between the electro chemical potentials of the 2DEG reservoirs: this corresponds to the first crossing in Fig. 8.7 and the constant current $I = ef$ curve in Fig. 8.8a. Fig. 8.8b also illustrates that at fixed gate voltage an oscillation minimum for $V < e/C$ turns into a maximum for $V > e/C$, while a maximum becomes a minimum.

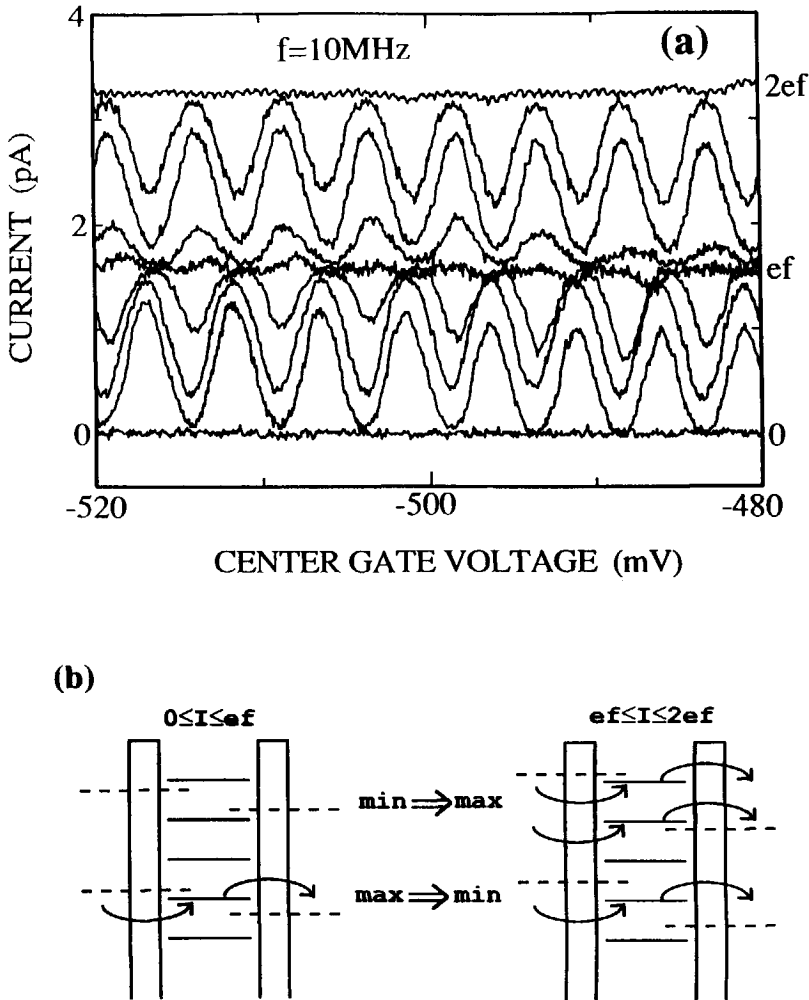


FIG. 8.8. (a) Current versus center gate voltage for $f = 10$ MHz and fixed different bias voltages. The current oscillates with a frequency determined amplitude in the interval between $n \cdot ef$ and $(n + 1) \cdot ef$. (b) Schematic representation of tunneling through the dot for two different bias voltages (left and right figures), and center gate voltage, indicated by the difference of the locations of the electro chemical potentials of the reservoirs (dashed lines) with respect to the charge states in the dot (solid lines).

To examine the dependence of the current plateaus on RF amplitude, we have measured I - V curves for $f = 10$ MHz and fixed RF amplitude on QPC₂. The RF amplitude on QPC₁ is increased in constant steps from the uppermost curve in Fig. 8.9 to the lowest curve. *Fig. 8.9 shows that for the same center gate voltage, all the plateaus from $n=-7$ to 7 are made visible by changing the RF amplitude on one QPC gate.* A striking feature is that around zero voltage, a non-zero current is observed, which can be either positive or negative. This is due to the non-compensated influence of the unequal RF signals on the bottom of the conduction band in the dot, as explained in relation to the pump experiment using one RF signal in section 8.2.3. The direction of the pumped current is in agreement with the model and the measurements in Fig. 8.3. For the upper curves in Fig. 8.9 where $V_2^{RF} > V_1^{RF}$, the pumped current is positive, while for the lower curves where $V_1^{RF} > V_2^{RF}$, the current around $V = 0$ is negative. We return to this point quantitatively in the next section.

A similar plot as Fig. 8.9 has been measured by taking constant and compensating RF amplitudes, but now inducing an asymmetry by changing the phase difference around π between

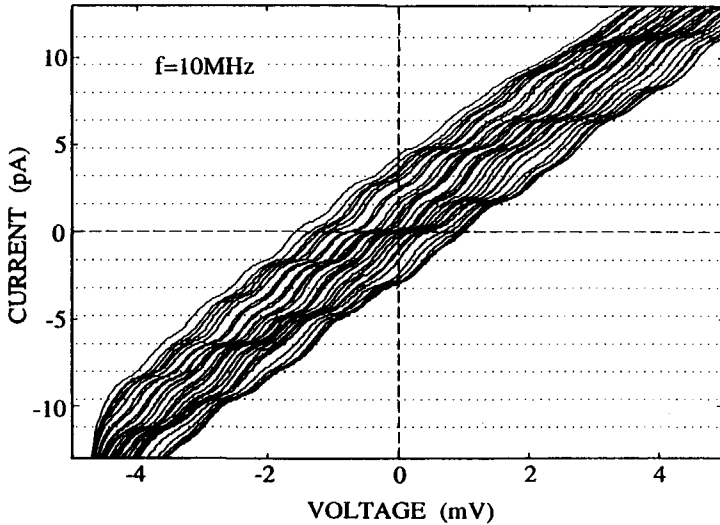


FIG. 8.9. I - V curves with fixed RF amplitude on QPC₂ ($V_2^{RF} = 33$ mV) and taking different RF amplitudes on QPC₁ (from $V_1^{RF} = 28$ mV for the uppermost curve to 42 mV for the lowest curve in steps of 0.53 mV), showing all the current plateaus from $-7ef$ to $7ef$. The I - V curves are not offset.

the two RF signals. A few curves are shown in Fig. 8.10 for $f = 20$ MHz and the phase difference $\phi = \phi_1 - \phi_2$ ranges from π (uppermost curve) to $\pi + \pi/10$ (lowest curve). It is seen that the average slope $\langle G \rangle = fC$ is not affected by the phase difference around π . Instead the curves shift to lower currents, where pumping takes place in the quadrant $V \geq 0, I < 0$. Note that around $V = 0$, current plateaus are seen at $-3 \cdot ef$ and $-5 \cdot ef$. From Figs. 8.3 and 8.4, one can deduce that for $V = 0$ and $V_1^{RF} = V_2^{RF}$, QPC₁ pumps electrons over the barrier induced by QPC₂ when $\phi > \pi$. In our case this yields a negative current in accordance with the measurements. The pumped current is positive when the asymmetry is reversed to $\phi < \pi$ (not shown).

From these measurements, we have been able to deduce the effect on the quantized current plateaus of the various parameters as the center gate voltage, the RF amplitudes, and the phase difference. To demonstrate the tunability of the quantum dot turnstile, we have measured the pumping in more detail, which is shown in Fig. 8.11. Tuning the different parameters, we produced quantized current plateaus from $n=-5$ to 5 around zero voltage, showing that a discrete number of electrons are pumped per RF cycle.

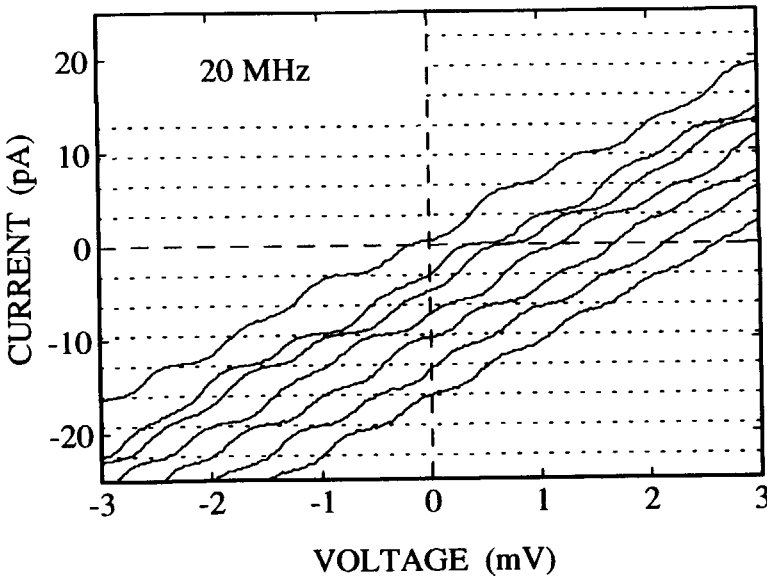


FIG. 8.10. *I-V characteristics where the phase difference between the two equal RF signals is changed from π (uppermost curve) to $\pi + \pi/10$ (lowest curve). The I-V curves are not offset.*

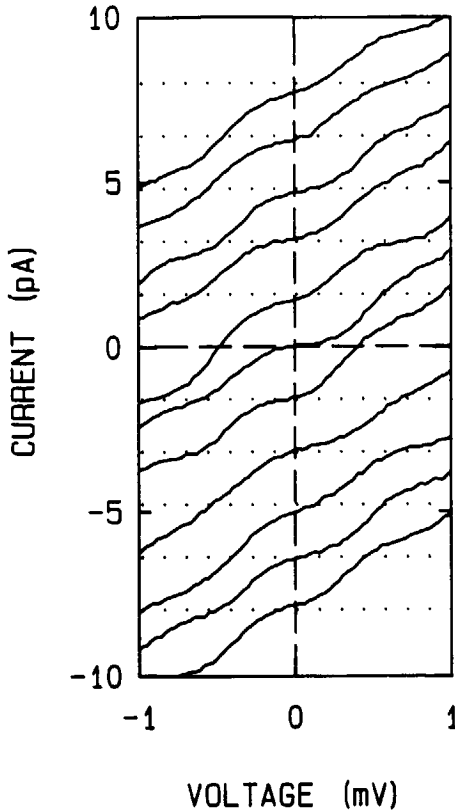


FIG. 8.11. *I-V characteristics with tuned center gate voltage, RF amplitudes, and phase difference such that quantized current plateaus are obtained from $-5ef$ to $5ef$ at zero bias voltage, demonstrating discrete electron pumping. The I-V curves are not offset.*

8.4 DISCUSSION AND CONCLUSIONS

Our simple model in terms of electro chemical potentials explains all the qualitative aspects of the data, e.g. the existence and location of the current plateaus, their sensitivity on the center gate voltage, and the dependence of the I - V curves on the RF amplitudes and phase difference, including the direction of the pumped current. We now use the model for a quantitative estimate of the turnstile measurements for the case when an asymmetry causes pumping of a discrete number of electrons. First we note that in a symmetric system, the net current is always zero. Usually the symmetry is broken by applying a bias voltage. In our quantum dot system, an asymmetry is also induced when the RF voltages differ in amplitude or when the phase difference ϕ is not equal to π or 0. Such an asymmetry can result in a pumping of electrons to higher energy and creates a preferred current direction. To estimate quantitatively the pumping

for non-compensating RF signals, we write the change in electro static potential in the dot as :

$$\Delta\phi = \frac{C_1 V_1^{RF}}{C} \sin(2\pi f t) + \frac{C_2 V_2^{RF}}{C} \sin(2\pi f t + \phi) \quad (8.1)$$

The influence on the band bottom does not give rise to pumping when $\Delta\phi \ll e/C$. To discuss Fig. 8.9, with Eq. 8.1 we take $\phi = \pi$, but different RF amplitudes $V_1^{RF} \neq V_2^{RF}$. The number of electrons which are pumped between the maximal amplitude $V_1^{RF}/_{max} = 42$ mV (i.e. the lowest curve in Fig. 8.9) and the minimal amplitude $V_1^{RF}/_{min} = 28$ mV is given by $(V_1^{RF}/_{max} - V_1^{RF}/_{min})/(e/C_1) \approx 4$ (Note that $e/C_1 = \Delta V_1 = 3.6$ mV is the period of the Coulomb oscillations in Fig. 8.2a.) This is in good agreement with the measured difference of just under 5 electrons per cycle.

The estimation of the accuracy of the quantized current plateaus of about 1 % is roughly what we observe in the experiments. The prospects for the quantum dot turnstile for serving as a highly accurate current device, can be deduced from the analysis in section 8.3.1. The probability of the wanted tunnel events (solid arrows in Fig. 8.4) differs from 1 by an exponentially small amount which can be made virtually zero. Deviations of the current plateaus from the quantized values caused by thermally activated transport can also be neglected at measurement temperatures below 0.1 K. The limiting factor of the current accuracy is the leakage probability P_{leak} of the barriers in their equilibrium position (dashed arrows in Fig. 8.4). $P_{leak} = 1 - \exp[-(I/f)/RC/_{leak}] \approx (I/f)/RC/_{leak}$ decreases only linear with the leakage resistance. For $f = 10$ MHz, and $C = 10^{-16}$ F, a leakage resistance of $10^{15} \Omega$ is required to obtain an accuracy $\delta I/ef \approx 10^{-8}$. Such a large resistance can be obtained by increasing the width of the tunnel barriers on which it depends exponentially. Note that the leakage current between the gates and the 2DEG should also be smaller than δI , which can be accomplished by an insulating layer between the semiconductor and the gates. Moreover, we note that tunneling via virtual states which limits the accuracy of the metal turnstile,¹⁹ is suppressed by the large barrier resistance, and does not play a limiting role in our quantum dot turnstile. However, for typical frequencies of 10 MHz, the resulting current $ef = 1.6$ pA is much too small for practical applications. A parallel-configuration could upgrade the quantized current level by several orders of magnitude. The unresolved problem of a parallel configuration is the distribution of offset charges among the dots, which would effectively average the current plateaus. For any application involving large scale integration of charging effect devices, methods must be developed to relax these offset charges.

In summary, we have described the realization of a turnstile operation in a semiconductor

quantum dot. For the first time, *oscillating tunnel barriers* are used to control current on a single-electron level. We have observed *quantized current* plateaus at multiples of ef , which demonstrates the passage of a discrete number of electrons through our *quantum dot turnstile*. The device can pump a discrete number of electrons at zero bias voltage when an asymmetry is induced by applying non-compensating RF voltages to the barrier gates. The prospects of the quantum dot turnstile to serve as an accurate current device depends on the technological realization of operating many of them in parallel.

ACKNOWLEDGEMENTS

We wish to thank L.J. Geerligs, P. Hadley, K.K. Likharev, J.E. Mooij, and B.J. van Wees for stimulating discussions, and D.J. Maas for his contributions to the device fabrication, and the Delft Institute for MicroElectronics and Submicrontechnology for the use of their facilities. Financial support from FOM and ESPRIT (project 3133, NANSDEV) is gratefully acknowledged. L.P.K. acknowledges the Sakaki Quantum Wave Project in Tokyo for the hospitality during the preparation of the manuscript.

REFERENCES

The results in this chapter have been published in Phys. Rev. Lett. **67**, 1626 (1991), and in Zeitschrift für Physik B-Condensed Matter **85**, 381- 388 (1991).

1. See for a review: D.V. Averin and K.K. Likharev, in *Quantum Effects in Small Disordered Systems*, edited by B.Al'tshuler, P. Lee, and R. Webb (Elsevier, Amsterdam, 1990).
2. See for a recent review, including various semiconductor systems: *Single Charge Tunneling*, H. Grabert, J.M. Martinis, and M.H. Devoret, eds. (Plenum, New York, 1991).
3. P. Delsing, K.K. Likharev, L.S. Kuzmin, and T. Claeson, Phys. Rev. Lett. **63**, 1861 (1989), and in Ref. 2.
4. L.J. Geerligs, V.F. Anderegg, P.A.M. Holweg, J.E. Mooij, H. Pothier, D. Esteve, C. Urbina, and M.H. Devoret, Phys. Rev. Lett. **64**, 2691 (1990).
5. H. Pothier, P. Lafarge, P.F. Orfila, C. Urbina, D. Esteve, and M.H. Devoret, Physica B **169**, 573 (1991).
6. L.S. Kuzmin, and D.B. Haviland, Phys. Rev. Lett. **67**, 2890 (1991).
7. L.J. Geerligs, S.M. Verbrugh, P. Hadley, J.E. Mooij, H. Porthier, P. Lafarge, C. Urbina, D. Esteve and M.H. Devoret, Z. Phys. B - Condensed Matter **85**, 349 (1991).

8. Q. Niu, Phys. Rev. Lett. **64**, 1812 (1990).
9. F. Guinea, and N. Garcia, Phys. Rev. Lett. **65**, 281 (1990).
10. See also: L.P. Kouwenhoven, A.T. Johnson, N.C. van der Vaart, C.J.P.M. Harmans, and C.T. Foxon, Phys. Rev. Lett. **67**, 1626 (1991).
11. A.A. Odintsov, Appl. Phys. Lett. **58**, 2695 (1991).
12. U. Meirav, M.A. Kastner, and S.J. Wind, Phys. Rev. Lett. **65**, 771 (1990).
13. The interplay between charging effects and discrete energy states are reported by: P.L. McEuen, E.B. Foxman, U. Meirav, M.A. Kastner, Y. Meir, N.S. Wingreen, and S.J. Wind, Phys. Rev. Lett. **66**, 1926 (1991).
14. Charging experiments on this structure without applying RF signals are reported by: L.P. Kouwenhoven, N.C. van der Vaart, A.T. Johnson, W.Kool, C.J.P.M. Harmans, J.G. Williamson, and A.A.M. Staring, Z. Phys. B - Condensed Matter **85**, 367 (1991); L.P. Kouwenhoven, N.C. van der Vaart, A.T. Johnson, C.J.P.M. Harmans, J.G. Williamson, and A.A.M. Staring, Festkörperprobleme/Advances in Solid State Physics, U. Rössler (ed.) Vol. **31** (1991).
15. The device described in this paper is different from the device in Ref. 14, but has the same gate geometry.
16. We neglect the energy separation between the dot's discrete levels, which in this sample is less than a tenth of the charging energy; see also Ref. 14.
17. L.P. Kouwenhoven, B.J. van Wees, C.J.P.M. Harmans, J.G. Williamson, H. van Houten, C.W.J. Beenakker, C.T. Foxon, and J.J. Harris, Phys. Rev. B **39**, 8040 (1989).
18. We also found a current plateau at ef in a previous sample, but due to intrinsic sample instabilities these results were less clear.
19. D.V. Averin, and Yu. V. Nazarov, Phys. Rev. Lett. **65**, 2446 (1990).

CHAPTER 9

Zero Dimensional States and Single Electron Charging in Semiconductor Quantum Dots

A.T. Johnson, L.P. Kouwenhoven, W. de Jong, N.C. van der Vaart,
and C.J.P.M. Harmans

*Faculty of Applied Physics, Delft University of Technology,
P.O. Box 5046, 2600GA Delft, The Netherlands*

C.T. Foxon

Philips Research Laboratories, Redhill, Surrey RH1 5HA, United Kingdom

ABSTRACT

We have observed new effects in transport through lateral quantum dots where zero-dimensional (0D) states and single electron charging coexist. In linear transport we see *coherent* resonant tunneling, described by a Landauer formula despite the many-body charging interaction. In the non-linear regime, Coulomb oscillations of a quantum dot with about 25 electrons develop 0D shoulders as the bias voltage increases, and the current-voltage characteristic has a double staircase shape.

Electron transport through semiconductor quantum dots shows striking effects due to the electron wave nature and its finite charge. The first leads to the formation of zero dimensional (0D) states with discrete energies in a system confined in all three directions,^{1,2} and the possibility of coherent resonant tunneling.² The latter induces Coulomb effects, which cause a strong shift in the dot energy upon addition of a single electron. This phenomenon has been investigated in many systems,³ and may soon be used in devices such as ultra-sensitive charge meters⁴ and frequency-based current standards.^{5,6}

Experiments are beginning to be done on quantum dots in which these effects coexist. McEuen et al.⁷ used transport measurements to determine the magnetic field dependence of *N*-electron *ground state* energies in such a system, and related it to the calculated energies of single-particle levels in the absence of charging. Similar issues have been addressed in the few electron limit using capacitive⁸ and optical⁹ techniques. In properly designed double barrier resonant tunneling structures, 0D-states or charging can be important, depending on the sign of the bias voltage.¹⁰ Here we report new results from dots where 0D-states and charging appear together. We observe *coherent* resonant tunneling in the linear regime (low bias voltage), well described by a Landauer formula despite the presence of the many-body charging interaction. In nonlinear transport, we see the signature of the coexistence of these phenomena, allowing a qualitative spectroscopy of the *excitations* of a quantum dot containing about 25 electrons.

The two quantum dots used for this work were defined by metal gates on top of a GaAs/AlGaAs hetero structure with a two dimensional electron gas (2DEG) 100 nm below the surface. The ungated 2DEG has mobility 230 m²/Vs, and electron density $1.9 \times 10^{15} \text{ m}^{-2}$ at 4.2 K. In each case, applying -300 mV to the gates depletes the 2DEG beneath them and forms a quantum dot coupled to large electron reservoirs via quantum point contacts (QPCs). The geometry of dot 1 was discussed in Ref. 6. It has lithographic dimension 800 nm x 1 μm ; with the effects of depletion, we expect this dot to be circular with a diameter of about 600 nm. The inset of Fig. 9.3 shows the layout for sample 2, with QPC gate pairs 1 and 2, and center gate pair C. The central region is 200 nm x 600 nm. By applying a more negative voltage to the center gate pair (typically -900 mV), we again make a dot that is roughly circular, but now with diameter 100 nm. Channels between gates are fully depleted and do not conduct. All measurements were done in a dilution refrigerator with a base temperature below 20 mK. Measurements on sample 1 were made at a magnetic field $B = 7 \text{ T}$. Transport through the dot occurs via the edge channel¹¹ of the lowest energy Landau level, and is essentially one-dimensional.²

If a quantum particle of appropriate energy propagates without loss of phase memory between

two barriers, *coherent* resonant tunneling can occur. Multiply reflected partial waves constructively interfere, as in an optical Fabry-Perot cavity, and the transmission chance can approach 1, even if each barrier alone is highly reflecting. At zero temperature, in one dimension, and in the *absence* of charging effects, the conductance of this interferometer is given by:

$$G_{1D} = \frac{e^2}{h} \frac{T_1 T_2}{1 + (1 - T_1)(1 - T_2) - 2[(1 - T_1)(1 - T_2)]^{1/2} \cos \varphi} \quad (9.1)$$

where T_1 and T_2 are the barrier transmissions, and φ is the phase acquired by a wave during one round trip between the barriers. Eq. 9.1 combines the two-barrier transmission formula of basic quantum mechanics with the Landauer relation between transmission and conductance. Finite temperature leads to energy averaging by the derivative of the Fermi function, reducing the peak transmission and increasing the resonance width.

Fig. 9.1a shows the measured conductance of QPC₁, proportional to its transmission T_1 , as a function of gate voltage V_1 in the region near pinch-off when QPC₂ is set to be fully transmitting. The irregular structure in $G(V_1)$ is typical of our QPCs at high field, and is probably due to potential fluctuations in or near the point contact. When we set QPC₂ in the tunnel regime ($T_2 \approx 0.02$), sweeping V_1 produces the periodic conductance peaks of Fig. 9.1b. These are the well-known Coulomb oscillations³ of the charging regime. The peak height of the oscillations shows a striking modulation that is correlated with the transmission T_1 of QPC₁ (Fig. 9.1a), but in a *non-classical* manner. Near $V_1 = -770$ mV and -850 mV, for example, *the peak conductance is strongly suppressed, even though T_1 is at a maximum of 0.6*. The classical, sequential tunneling prediction for the conductance maxima is shown by the dashed line in Fig. 9.1b: $G_{cl} = (e^2/h) T_1 T_2 / (T_1 + T_2 - T_1 T_2)$. The fit to the data is poor, with the measured conductance exceeding the prediction by as much as a factor of 15.

In contrast, the peak conductance ($\cos \varphi = 1$) from the quantum transmission formula of Eq. 9.1 agrees well with the data, when thermal averaging of 40 mK is taken into account (Fig. 9.1b, heavy line). This agrees well with the temperature and measuring voltage (5 μ V) of the experiment. In a coherent system, the barrier transmissions must match in order to have total transmission well above the sequential value. Since $T_2 \approx 0.02$ in the experiment of Fig. 9.1b, increasing the transmission QPC₁ above this value actually *decreases* the total transmission predicted by Eq. 9.1, precisely the effect seen in the data.

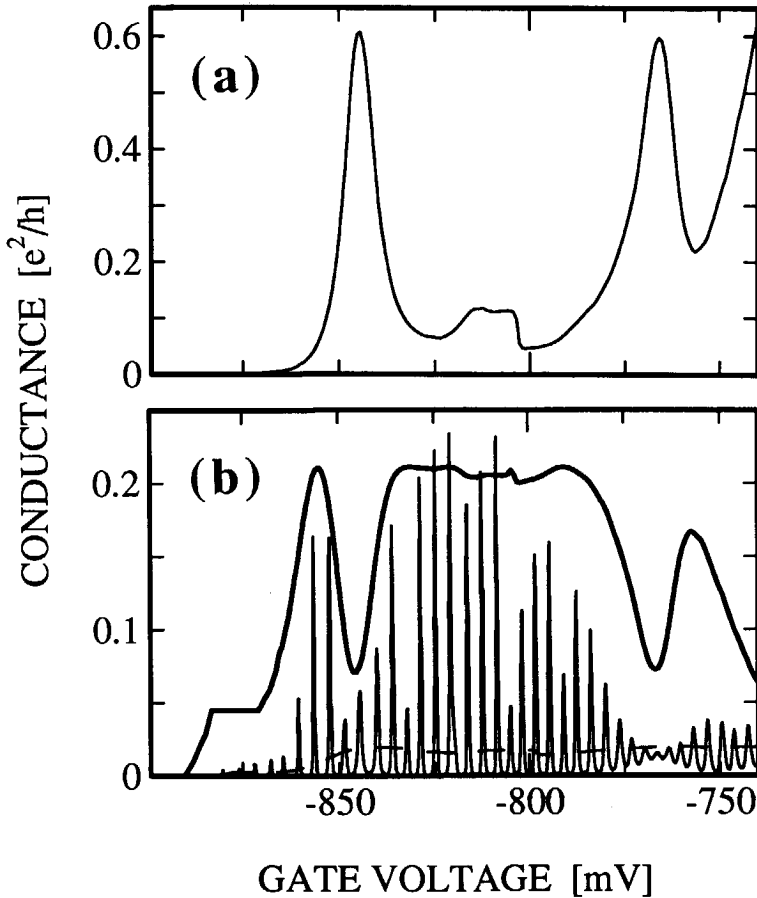


FIG. 9.1. (a) Conductance of QPC_1 versus gate voltage V_1 for the first sample. QPC_2 is set at full transmission. (b) Coulomb oscillations of dot 1 as V_1 is swept, changing T_1 . T_2 is about 0.02. The maximum peak height calculated with Eq. 9.1 and an effective temperature of 40 mK is shown with a heavy line. The dashed line is the classical prediction (see text). The magnetic field is 7 T.

This experiment demonstrates for the first time that coherent electron transport described by the independent electron Landauer formula is possible even in the presence of the strong Coulomb interaction. Although initially surprising, this result is in agreement with the idea that transport in the linear regime occurs only when the electro chemical potential of the dot is equal to that of the reservoirs.¹² Transport of the N th electron is an energy-conserving process, so its phase memory is maintained, even though the other $N - 1$ electrons undergo a Coulomb energy

change. Meir and Wingreen¹³ have recently developed a Landauer-type formula for an interacting system.

The second experiment on the smaller dot 2 demonstrates properties of *non-linear* transport in the presence of both charging and 0D-states. When a set of 0D-states with energy E_N and charging coexist, the electrochemical potential (ECP) of the dot changes discontinuously as the number of electrons increases: $\mu_d(N+1) - \mu_d(N) = E_C + \delta E$,¹² giving a "ladder" of ECP levels. Here $E_C = e^2/C$ is the electro static energy associated with charging the quantum dot by one electron (C is the total capacitance from the dot to ground), and $\delta E = E_{N+1} - E_N$ is the energy between 0D-states. This is also the minimum energy δE needed to excite the N -electron ground state at a fixed number of electrons. With diameter $d = 100$ nm, dot 2 contains about $N = 25$ electrons at the bulk density. We roughly estimate the charging energy $E_C = e^2/C \approx e^2/4\epsilon_r\epsilon_0d = 3.5$ meV, where $\epsilon_r = 13$ for GaAs, and excitation energy $\delta E = E_F/N = 300$ μ eV. Both these values far exceed $k_B T$ at 20 mK. Although we refer here to independent charging and 0D-state energies, the concepts can be generalized: even in a correlated system we can speak of a change in ECP associated with *adding* one electron to the dot and an excitation energy when the number is *fixed*. These are the analogs of $E_C + \delta E$ and δE , respectively.

Calculations for I - V characteristics exist,¹⁴ but the potential landscape of Fig. 9.2a gives a qualitative understanding. At zero temperature, the states of the left (right) reservoir are fully occupied up to the ECP level μ_L (μ_R) and empty at higher energies. The ECPs $\mu_d(N)$ and $\mu_d(N+1)$ characterizing the N - and $(N+1)$ -electron ground states are indicated by solid lines, while dashed lines represent the discrete 0D excited states of the dot.

Suppose the bias voltage is such that $\mu_L > \mu_R$. Electrons flow from left to right only if the transport condition $\mu_L > \mu_d(N) > \mu_R$ is satisfied. When this is true, all states in the dot between μ_L and μ_R are energetically allowed to contribute to the current. More allowed states give a larger transition rate and a larger current. Changing V_C shifts the conduction band bottom and the ECP ladder. If $\mu_L - \mu_R < E_C + \delta E$, the transport condition is alternately satisfied and not satisfied, giving well separated Coulomb oscillations in the current with minima going to zero. In the metallic limit, when the broadening of the 0D-states is much larger than the splitting δE , the dot excitation spectrum is continuous. As the bias voltage $eV = \mu_L - \mu_R$ increases from zero, the oscillations broaden and grow in amplitude, but remain featureless.

This is no longer true when discrete 0D-states exist. At small bias $eV \ll E_C, \delta E$, the number of states in the allowed energy window between μ_L and μ_R changes from 0 to 1 to 0 as V_C is scanned, giving a smooth oscillation (Fig. 9.2a). When eV is of order δE , however, this model

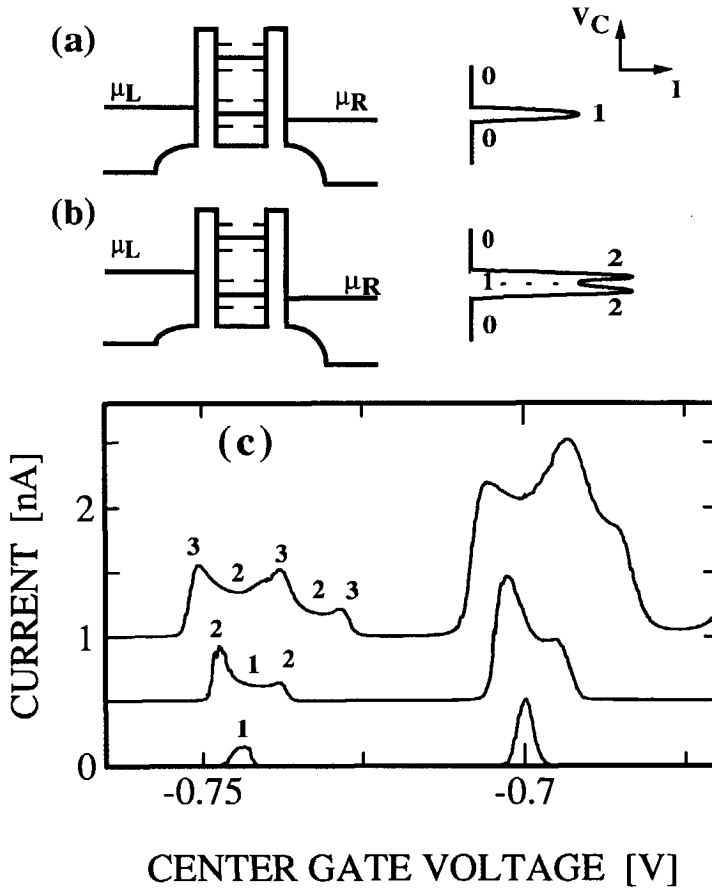


FIG. 9.2. (a) Potential energy landscape (left) and Coulomb oscillation (right) for a quantum dot with a voltage bias $V \ll \delta E/e$. Solid lines are ECP levels for N and $N + 1$ electrons, while dashed lines represent excitations. The number of states available for transport is shown as the gate voltage is scanned. (b) Same as (a), but with bias $V \approx \delta E/e$, showing the appearance of 0D shoulders. (c) Evolution of 0D shoulders with increasing bias voltage in dot 2. The curves are offset for clarity. From the bottom, the bias voltages are: 100 μV , 400 μV , and 700 μV . The magnetic field is 4 T.

predicts the appearance of "0D-shoulders" in the oscillations. While the transport condition is satisfied, the number of allowed states alternates between p and $p + 1$, where $p < eV/\delta E < p + 1$, and the current changes accordingly. When $p > 0$, the Coulomb oscillations are not simple peaks, but have a more complicated shape reflecting the discrete spectrum of 0D-excitations.

This is shown in Fig. 9.2b for the case when the number of states available for transport changes as 0-2-1-2-0.

The appearance of 0D shoulders in the Coulomb oscillations of dot 2 with increasing bias voltage is shown in Fig. 9.2c. The magnetic field is 4 T. Starting with the bottom curve, the bias voltages are 100 μV , 400 μV , and 700 μV ; the traces are offset for clarity. Above the shoulders we show the number of states contributing to transport. We can estimate the 0D splitting δE by noting that since 2 and 3 0D-states appear in intervals of 400 μV and 700 μV respectively, we have $270 \mu\text{V} < \delta E < 350 \mu\text{V}$, if we assume a constant δE , as is more or less true in the data. This measured typical excitation energy agrees with the estimate given above based on the inferred dot size, and confirms the fact that the dot contains about $E_F/\delta E \approx 25$ electrons.

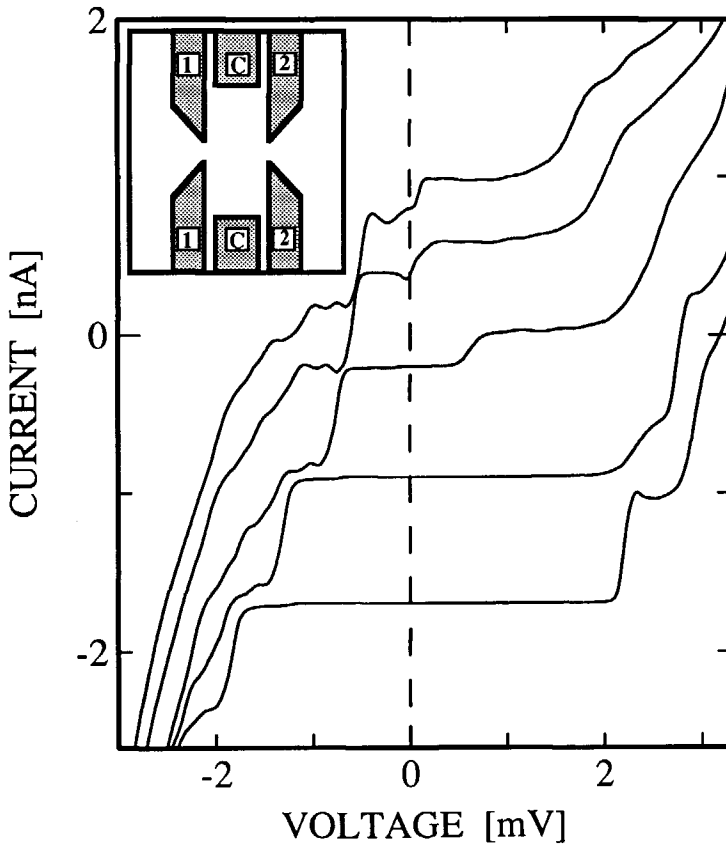


FIG. 9.3. *I-V characteristics for dot 2 at $B = 0$ and different center gate voltages, showing the double staircase structure. Inset: gate geometry of sample 2. Transport is from left to right through the QPC's 1 and 2.*

The dot's 0D excitation spectrum also causes structure in the I - V characteristic.¹⁴ Consider again the energy landscape of Fig. 9.2a, and imagine increasing μ_L from $\mu_L = \mu_R$, while μ_R is held fixed. At small bias, the Coulomb blockade suppresses current until $\mu_L > \mu_d(N) > \mu_R$. As μ_L increases from this point, the current grows in small steps as 0D-states enter the window between μ_L and μ_R one-by-one and contribute to transport. Eventually an extra charge level $\mu_d(N+1)$ is included between μ_L and μ_R . At this point a larger current jump will occur, since transport can occur two electrons at a time. The I - V characteristic has a double step structure with small 0D excitation steps and larger steps of the Coulomb staircase familiar from the metallic regime.¹²

This double step structure is clearly visible in the I - V characteristics of Fig. 9.3, taken at zero magnetic field. The different curves are taken for different center gate voltages. The uppermost curve corresponds to a minimized Coulomb gap, while in the lowest curve the Coulomb gap is maximal. The typical spacing between 0D-states is 300 μ V, in good agreement with the above estimates of δE .

The current increases in steps as additional 0D-states fall between μ_L and μ_R , so peaks occur in the differential conductance dI/dV at the dot excitation energies. A qualitative tunnel spectroscopy of the discrete levels is possible, although it is complicated by the voltage drop across the tunnel barriers, which shift the dot energy levels as the bias voltage is scanned.

In Fig. 9.4 we show a succession of traces of dI/dV versus bias voltage for magnetic fields from 0 (top curve) to 2.5 T (bottom curve). The center gate voltage V_C was tuned at $B = 0$ so that there was no Coulomb blockade. From the maximum Coulomb blockade observed in the I - V characteristics, we know that $E_C + \delta E \approx 3.5$ mV, in agreement with the estimated dot size. All peaks in dI/dV at $|V| < 3.5$ mV, then, correspond to excitations of the dot *at fixed electron number*. These measurements let us track the field dependence of the discrete *excitation* energies of a quantum dot in the charging regime.

In summary, our quantum dot samples show the combined effect of 0D-states and single electron charging in both linear and non-linear transport. Coherent resonant tunneling can occur, well described by the Landauer formula, despite the charging interaction. Coulomb oscillations and I - V characteristics show additional structure due to the dot's 0D-excitation spectrum.

We thank J.E. Mooij and J.J. Palacios for useful discussions; D.J. Maas, W. Kool, and A. van der Enden for sample fabrication; and the Delft Institute for Microelectronics and Submicron Technology for the use of their facilities. This research was supported by FOM and ESPRIT (NANSDEV, project 3133).

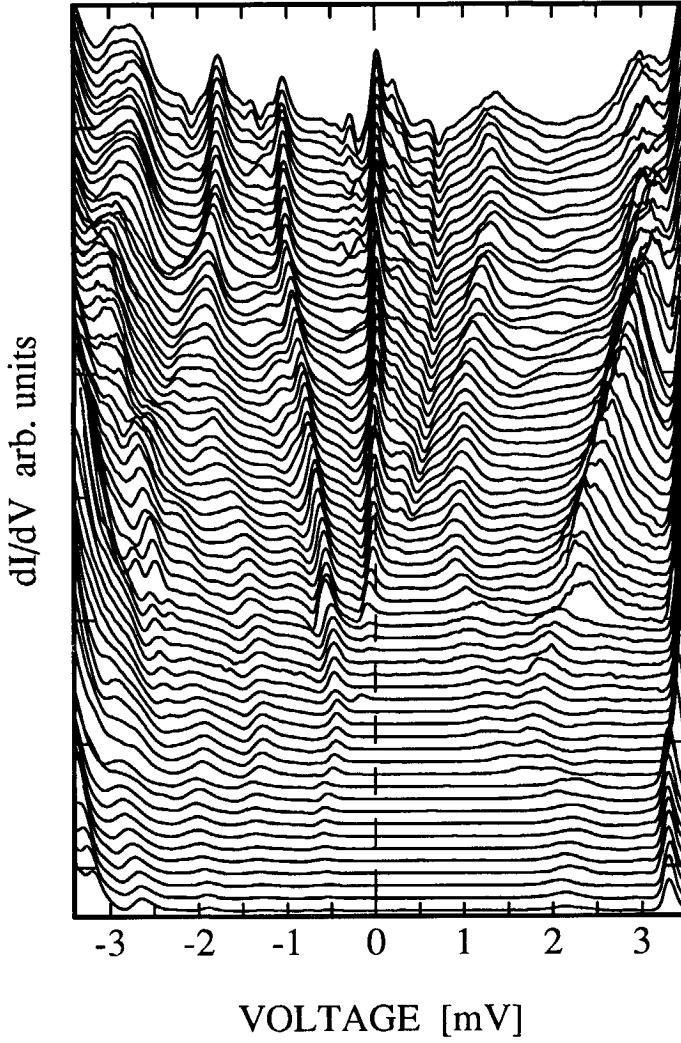


FIG. 9.4. Traces of dI/dV versus V for sample 2 for equally spaced magnetic fields from 0 (top) to 2.56 T (bottom). Peaks in dI/dV correspond to discrete excitations of the quantum dot.

REFERENCES

This chapter is submitted for publication in Phys. Rev. Lett.

1. M.A. Reed, J.N. Randall, R.J. Aggarwall, R.J. Matyi, T.M. Moore, and A.E. Wetsel, Phys. Rev. Lett. **60**, 535 (1988).
2. B.J. van Wees, L.P. Kouwenhoven, C.J.P.M. Harmans, J.G. Williamson, C.E. Timmering, M.E.I. Broekaart, C.T. Foxon, and J.J. Harris, Phys. Rev. Lett. **64**, 2691 (1990).
3. D.V. Averin, and K.K. Likharev, in *Quantum Effects in Small Disordered Systems*, edited by B. Al'tshuler, P.A. Lee, and R.A. Webb (Elsevier, Amsterdam, 1990).
4. T.A. Fulton and G.J. Dolan, Phys. Rev. Lett. **59**, 109 (1987).
5. L.J. Geerligs, V.G. Andereg, P. Holweg, J.E. Mooij, H. Pothier, D. Esteve, C. Uribna, and M.H. Devoret, Phys. Rev. Lett. **64**, 2691 (1990).
6. L.P. Kouwenhoven, A.T. Johnson, N.C. van der Vaart, C.J.P.M. Harmans, and C.T. Foxon, Phys. Rev. Lett. **67**, 1626 (1991).
7. P.L. McEuen, E.B. Foxman, U. Meirav, M.A. Kastner, Yigal Meir, Ned S. Wingreen, and S.J. Wind, Phys. Rev. Lett. **66**, 1926 (1991).
8. R.C. Ashoori, H.L. Störmer, J.S. Weiner, L.N. Pfeiffer, S.J. Pearton, K.W. Baldwin, and K.W. West, to be published.
9. B. Meurer, D. Heitmann, and K. Ploog, Phys. Rev. Lett. **68**, 1371 (1992).
10. Bo Su, V.J. Goldman, and J.E. Cunningham, Science **255**, 313 (1992).
11. B.I. Halperin, Phys. Rev. B **25**, 2185 (1981).
12. L. P. Kouwenhoven, N.C. van der Vaart, A.T. Johnson, W. Kool, C.J.P.M. Harmans, J.G. Williamson, A.A.M. Staring, and C.T. Foxon, Z. Phys. B **3**, 367 (1991).
13. Yigal Meir and Ned S. Wingreen, to be published.
14. D.V. Averin, A.N. Korotkov, and K.K. Likharev, Phys. Rev. B **44**, 6199 (1991).

CHAPTER 10

Coulomb Oscillations with a Multiple Peak Structure

Leo Kouwenhoven,^{1,2} Yasushi Nagamune,² Jun-ichi Motohisa,^{2,3} Hiroyuki Sakaki,^{2,3}

Luuk Mur,¹ and Kees Harmans.¹

*¹Faculty of Applied Physics, Delft University of Technology,
P.O.Box 5046, 2600GA Delft, The Netherlands.*

*²Research Center for Advanced Science and Technology, University of Tokyo,
4-6-1 Komaba, Meguro-ku, Tokyo 153, Japan.*

*³Quantum Wave Project, Erato, JRDC, 302 Keyaki-house,
4-3-24 Komaba, Meguro-ku, Tokyo 153, Japan.*

ABSTRACT

In a novel type of quantum dot fabricated by combined techniques of etching and gates, we have performed single electron charging experiments. In this new structure the number of electrons localized in the dot can be tuned down to of order 10. We found that a change of one electron in the dot does not result in a single Coulomb peak, but instead a multiple peak structure is observed in the linear response conductance. In addition, we show that the accuracy of the quantized current plateaus during turnstile operation can be largely improved.

10.1 INTRODUCTION

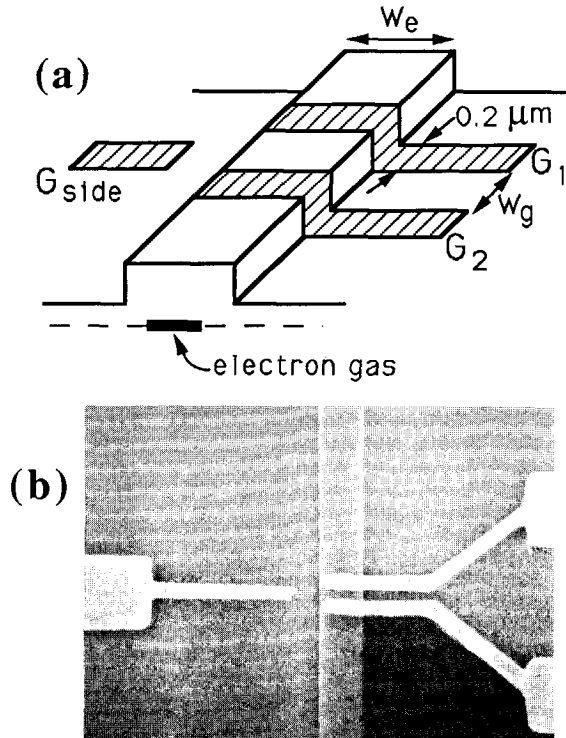
The number of electrons localized on an isolated Coulomb island is necessarily an integer. This is the basic ingredient for the numerous experiments on single electron charging of metallic and semiconductor islands.¹⁻³ In these experiments the Coulomb island is weakly coupled to conducting leads by tunnel barriers, in order to allow transport. The voltage on a third, gate, terminal is used to change the number of electrons on the island. The competition between the continuously changing electro static energy coming from the gate potential and the discrete electron charging energy, results in periodic transport behaviour. At the transition between N and $N + 1$ electrons on the island, the system is conducting. Transport is blocked between transitions by the charging energy. The periodic oscillations in the island conductance versus gate voltage are known as Coulomb oscillations and each period reflects a change of one electron on the island. In metallic systems where the density of states is continuous, the oscillations are perfectly periodic and have a constant amplitude.¹⁻³ In semiconductor quantum dots, however, the density of states may be discrete due to the quantum confinement. In the semiconductor islands investigated so far, which are a few hundred nm in size, this results in Coulomb oscillations which are slightly non-periodic. The deviation from perfect periodicity reflects the energy separation $E_{N+1} - E_N$ between adjacent zero dimensional (0D) states compared to the constant, usually much larger, charging energy e^2/C .⁴ The amplitude of the Coulomb peaks is often found to be modulated in an irregular way. This is due to the very sensitive nature of resonant tunneling through a particular 0D-state on the precise scattering at the tunnel barriers or at potential fluctuations on the island.⁵ However, the basic charging ingredient continues to be clearly observable; each period corresponds to a change of one electron.

In this chapter we discuss charging experiments on a novel quantum dot structure in which we can tune the number of electrons down to the regime of order 10. The preliminary data we have obtained on this new structure shows Coulomb oscillations in the linear response conductance where each Coulomb peak consists of a multiple peak structure. In this data, it is no longer possible to associate each conductance peak with the change of one electron. Employing the particular gate geometry we will also show that strong current quantization is obtained when we operate the device as a quantum dot turnstile.⁶

10.2 GATED - ETCHED QUANTUM DOT DEVICE

Fig. 10.1a schematically shows a cross-section of a new hybrid type of quantum dot, which is fabricated with a combined shallow-etch and gate technique. First, a narrow wire is defined in the two dimensional electron gas (2DEG) of a GaAs/AlGaAs hetero structure by wet shallow etching.⁷ Before processing, the mobility of the 2DEG is $80 \text{ m}^2\text{V}^{-1}\text{s}^{-1}$ and the electron density is $4 \cdot 10^{15} \text{ m}^{-2}$. The shallow etching removes only part of the doped AlGaAs layer. Due to surface depletion a shallow etch can be sufficient to confine the electrons into the unetched region. We found that the conducting width is roughly $0.4 \text{ }\mu\text{m}$ less than the geometrically etched width W_e of the channel. On top of the wire two gates are fabricated which are used to induce two tunnel barriers separated by a distance W_g . Negative voltages applied to the gates G_1 and G_2 induce two barriers in the etched channel which weakly couple the intermediate submicron sized island to the conducting leads. An extra side gate is fabricated for tuning the width and electron density of the wire in the region of the dot. About $5 \text{ }\mu\text{m}$ away from the quantum dot, the wire widens into current and voltage Ohmic contacts.

FIG. 10.1. (a) Cross-section of the quasi 1D wire fabricated with a combined shallow-etch and gate technique. (b) Scanning electron micrograph of a device with an etched wire width $W_e = 0.7 \text{ }\mu\text{m}$ and a distance between the barrier gates $W_g = 0.2 \text{ }\mu\text{m}$.



Several devices have been fabricated with different combinations of the etched wire width W_e and distance between the barrier gates W_g . Fig. 10.1b shows a scanning electron micrograph of a typical device with dimensions $W_e = 0.7 \mu\text{m}$ and $W_g = 0.2 \mu\text{m}$. The expected advantage of this type of device compared to quantum dots which are completely defined by metal gates, is that the amount of conductors in the vicinity of the dot is reduced, so the expected capacitance of the dot will be smaller. Another aspect we want to explore is that electrons will have to tunnel through the region underneath the gates, in contrast to tunneling through barriers induced by split-gates. In addition, the barrier gates have been made rather wide ($0.2 \mu\text{m}$). This will give a much stronger dependence of the barrier conductance on gate voltage, which in the next section we will use to obtain an improved accuracy of the quantized current plateaus in a quantum dot turnstile.⁶

10.3 QUANTUM DOT TURNSTILE

In a device with dimensions $W_e = 0.5 \mu\text{m}$ and $W_g = 0.5 \mu\text{m}$ we have repeated the turnstile experiment discussed in chapter 8. In Fig. 10.2 an I - V characteristic is shown measured for a RF frequency $f = 10 \text{ MHz}$ at 10 mK . The data is corrected by subtracting a constant parallel resistance of $150 \text{ M}\Omega$. We note that without applying RF we found that this parallel resistance was larger than $500 \text{ G}\Omega$. From other experiments we have learned that RF signals can lead to conduction through regions which are non-conducting when no RF is applied. The reason is that the RF signals can pump electrons to a higher energy such that they are lifted over a relatively low barrier.⁶ The parallel conducting path is most likely located between the barrier gates and the side gate underneath the shallow etched region. Apparently, the etching has not been deep enough to prevent conduction during turnstile operation through this nearly depleted 2DEG region. The necessary correction makes the data unreliable for precise conclusions on the accuracy of the observed quantized current plateaus. However, Fig. 10.2 shows that this new device geometry can lead to very strong current quantization. The strong dependence, presumably exponentially, of the barrier conductances on gate voltage, causes a large suppression of the leakage events, the main effect limiting the current quantization in the previous experiments.⁶ The result is that the plateaus are now rather wide (1.2 mV) compared to the stepwidth (0.5 mV). Moreover, in this device all plateaus are observed, while in the previous split-gate device some were only weakly developed or absent.

The period in voltage ΔV of the plateaus directly reflects the charging energy: $e\Delta V = e^2/C = 1.7 \text{ meV}$. This value is a factor 3 to 5 larger than obtained in dots which are completely defined by

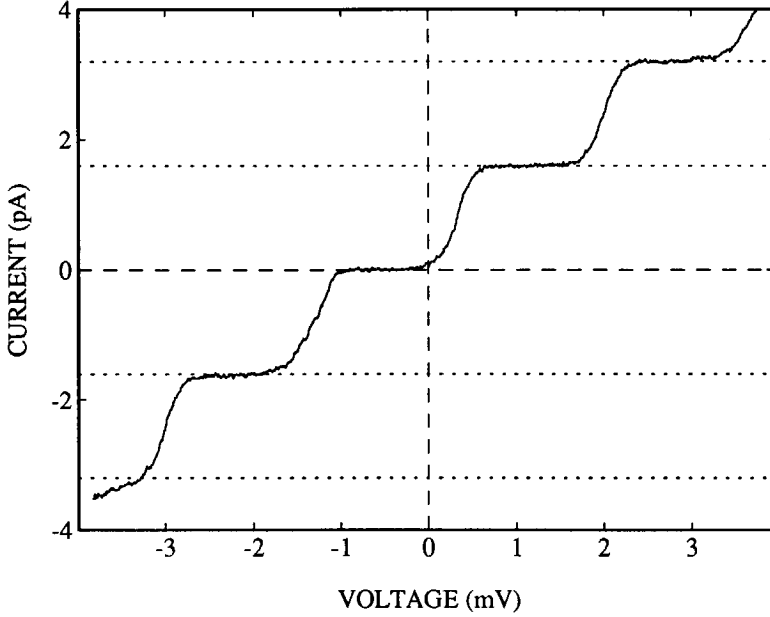


FIG. 10.2. *I-V characteristic on applying RF signals to the barrier gates with frequency $f = 10$ MHz and a phase difference of π . The dotted lines indicate multiples of $ef = 1.6$ pA. The data is corrected for a parallel resistance of 150 M Ω .*

split-gates, and is due to the reduced amount of conductors (i.e. gates) in the vicinity of the dot. The larger charging energy indicates that the current quantization may also be observed at higher temperatures.

10.4 COULOMB OSCILLATIONS WITH A MULTIPLE PEAK STRUCTURE

In this section we discuss Coulomb oscillations in the few electron regime. The conductance measurements are performed at 10 mK with a dc source-drain voltage bias V and measuring the dc current I . First, we discuss the results on a sample with an etched width $W_e = 0.7$ μm and a distance between the barrier gates $W_g = 0.2$ μm . Fig. 10.3 shows the conductance $G = I/V$ versus side gate voltage V_{side} at zero magnetic field. The different curves are measured for different bias

voltages V . The barrier conductances are made much smaller than the conductance quantum $2e^2/h$. The traces in Fig. 10.3 show two types of oscillations: regular oscillations with a period changing from 30 to 40 mV, and less regular finestructure with a typical period of a few mV. Note that in the traces with the smaller bias voltage the minima in the finestructure approach zero conductance. The finestructure is seen to disappear when the bias voltage is raised up to 0.4 mV. The larger oscillations are found to disappear at a bias voltage of about 2 mV (not shown).

The oscillations with the larger period are Coulomb oscillations where each period corresponds to a change of one electron in the dot. We deduce this from the fact that the periodicity in the Coulomb staircase in I - V characteristics and in turnstile measurements are the same. From the stepwidth in the (turnstile) staircase we found that the charging energy for adding a single electron depends quite strongly on the gate voltages and gradually increased from about 1.7 meV for gate voltages as in Fig. 10.3 to about 3 meV at larger negative gate voltages. These values are in

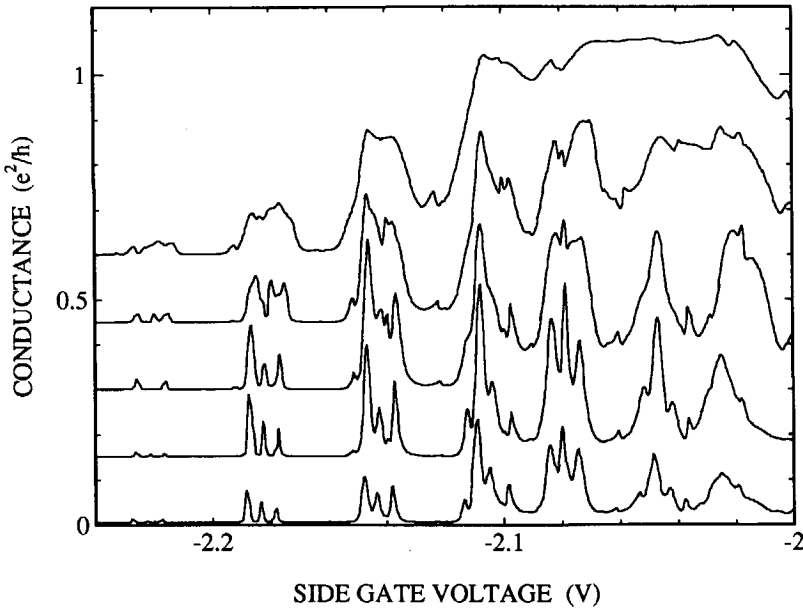


FIG. 10.3. Conductance versus side gate voltage at zero magnetic field. The different curves are measured for different bias voltage (from lowest to uppermost curve: 0.01, 0.03, 0.1, 0.2, 0.4 mV) and are offset for clarity.

accordance with the observed disappearance of the Coulomb oscillations when the bias voltage is raised to about 2 mV. So, while the Coulomb oscillations represent counting electrons, the multiple peak structure occurs within a Coulomb peak at the transition between N and $N+1$ electrons in the dot.

In Fig. 10.4 traces are shown for different magnetic fields which are measured at small bias voltage $V = 10 \mu\text{V}$. It can be seen that a magnetic field up to a few Tesla does not change the period of the Coulomb oscillations, but does affect the precise shape of the finestructure. However, a magnetic field of a few Tesla does not change the observation that the Coulomb oscillations contain finestructure. In another device with dimensions $W_e = W_g = 0.5 \mu\text{m}$, we found that all the finestructure disappeared at a field of 1.5 T and regular Coulomb oscillations remained.

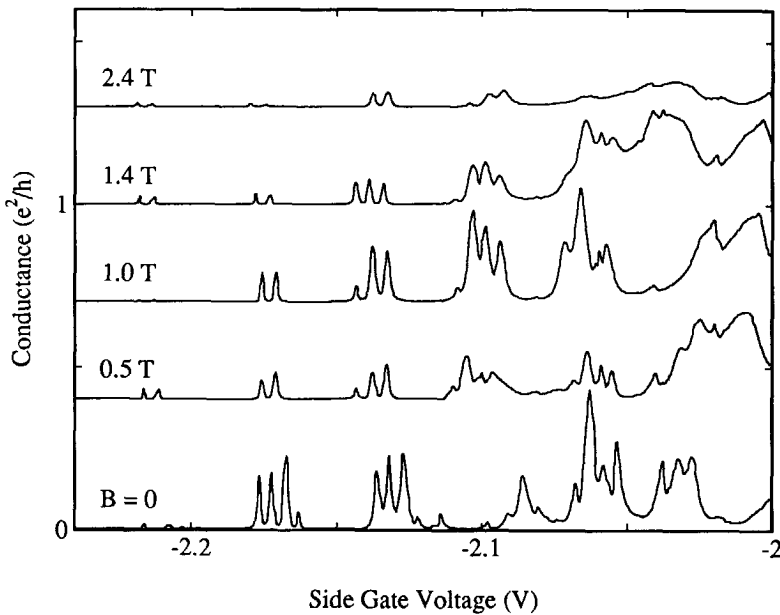


FIG. 10.4. Conductance versus side gate voltage for small bias voltage $V = 10 \mu\text{V}$ and for different magnetic fields.

To obtain an estimate of the energy separation $E_{N+1} - E_N$ between the 0D-states we have measured a single Coulomb oscillation for different bias voltages V in order to look for the "0D-shoulders" discussed in Ref. 8 and in chapter 9. Fig. 10.5 shows one Coulomb oscillation which at small bias voltage is split into two well-separated peaks. On increasing the bias voltage it is seen that the amplitude of the left peak decreases and gradually goes to zero. The right peak, however, seems to be of a different nature because on increasing the bias voltage it starts to show shoulders. In contrast to the vanishing conductance between the two peaks in the lowest trace, the minima between shoulders stay finite which is expected from the tunnel rate modulation due to an alternating number of 0D-states between the two electro chemical potentials of the reservoirs.⁸ This illustrates that the multiple peaks are from a different origin than the 0D-shoulders. In the topmost curve, 5 shoulders are seen which means that the number of 0D-states available for tunneling into the dot, alternates between 5 and 4. The energy separation between (spin-degenerate) adjacent 0D-states ΔE_{0D} can be estimated from $4 \cdot \Delta E_{0D} < eV \approx 1 \text{ mV} < 5 \cdot \Delta E_{0D}$ from which we get $\Delta E_{0D} \approx 0.2 \text{ meV}$.

The multiple peak structure is also seen when one of the voltages V_1 and V_2 on the barrier gates is varied, while keeping the voltages on the other gates fixed. From the Coulomb oscillation periods in these measurements we deduced the capacitances $C_1 = 0.27 \cdot 10^{-16} \text{ F}$ between the dot and barrier gate G_1 , and $C_2 = 0.40 \cdot 10^{-16} \text{ F}$ between the dot and barrier gate G_2 . The capacitance between the dot and the side gate is much smaller $C_{side} = 0.04 \cdot 10^{-16} \text{ F}$, in accordance from what we expect from the gate geometry. We note again that the different capacitances depend on the absolute values of the gate voltages. The sum of the capacitances between the gates and the dot leads to roughly the same charging energy $e^2/(C_1 + C_2 + C_{side}) = 2.25 \text{ meV}$ as obtained from the Coulomb staircase. The finestructure disappears when only one or no barrier is formed, implying that the formation of the dot is necessary in order to obtain the multiple peak structure. Other experimental facts are that the conductance of the channel without applying gate voltages is about 3 times $2e^2/h$. This relatively large conductance means that there are no impurities in the channel which can localize electrons strongly enough to give rise to charging. Moreover, the observation of the 0D-shoulders demonstrate that electro static potential fluctuations in the dot are too small for destroying the 0D-states.

Finestructure similar to what we have observed was recently reported by Ford et al.⁹ When they made their dot as small as possible by squeezing the gate voltages, they found that a few maxima in the Coulomb oscillations started to split up in double peaks.

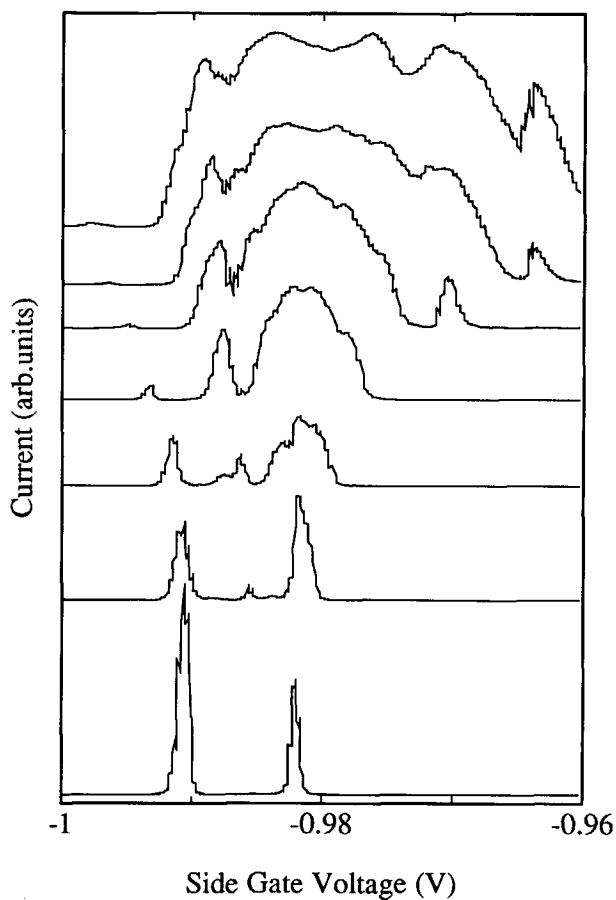


FIG. 10.5. A single Coulomb oscillation measured for different bias voltages (from lowest to uppermost curve: 0.01, 0.1, 0.2, 0.4, 0.6, 0.8, and 1.0 mV) showing OD-shoulders.

10.5 DISCUSSION AND CONCLUSIONS

Let us first make a crude estimate of the number of electrons in the dot from the area times the density. With $V_{side} = -2$ V, and $V_1 = V_2 = 0$ V, the channel conductance is about $2e^2/h$, which indicates that the conducting channel width is between 20 and 40 nm, i.e. of order the Fermi wave length. The distance between the gates is 0.2 μm , so we have about 15 to 30 electrons localized in an elliptical dot. This number is a rough estimate and is likely to be an upper limit because the electron density and the distance between the barriers will be smaller when voltages V_1 and V_2 are applied to the barrier gates.

We will first attempt to explain the multiple peak structure within the standard model for charging effects. The mixture of the observed two types of oscillations could result from the convolution of broadened oscillations with a large period and sharp peaks with a smaller period. The physical origin of such a convolution could be two Coulomb islands in series, one large island with high barriers (so the charge states are close together and only weakly broadened), and the other island being small with at least one lower barrier (so here the charge states are farther apart and somewhat broadened). Because Coulomb islands in series act as an AND-gate (i.e. both should be conducting in order to get electron transport through the islands in series¹⁰), the total conductance is the convolution of the two individual island conductances. This explains the multiple peak structure observed by Field et al.¹¹ in conductance measurements on a narrow Si wire. In their device the random impurity configuration determines the pattern of the multiple Coulomb peaks. For our measurements such an explanation is very unlikely. From turnstile measurements we know that the oscillations with the larger period originate in the dot between the two gate barriers. The finestructure oscillations should then come from a second dot in series which is a few times larger than our intended dot, and is formed between a large impurity potential and one of the gate barriers. The channel conductance, however, is roughly 3 times the conductance quantum when no voltages are applied to the gates. This implies that there are no potential fluctuations in the wire which can block the transport strongly enough to give rise to charging. Although the impurity potentials may be influenced when we apply gate voltages, it is virtually impossible that a strong extra barrier is formed which could give rise to the sharp multiple peaks. An alternative origin for the finestructure could be an oscillating transmission through the rather wide barriers. The multiple peak structure is observed over a large range of barrier gate voltages. Even with an impurity state in the barrier, it is very unlikely that the barrier transmissions oscillate

with minima going to zero over a wide range of gate voltage. So far, we have been unable to find a physical origin within the standard Coulomb theory which is consistent with the experimental observations.

If the multiple peak structure does originate from localizing electrons in the dot, then our data shows a failure of the charging theory for quantum dots containing only of order 10 electrons; oscillations no longer represent a change of one electron. One way to explain the finestructure for the case of a single dot is by assuming that the electro chemical potential $\mu_d(N)$ for N electrons in the dot oscillates in a non-monotonic way on changing the confinement. An oscillating $\mu_d(N)$ crosses the electro chemical potentials of the reservoirs $\mu_{l,r}$ more than once. At each crossing electron transport is allowed. Between crossings transport is blocked, yielding a minimum within a Coulomb peak at the transition of N and $N - 1$ electrons in the dot.

A non-monotonic electro chemical potential contains parts where the compressibility is negative, i.e. a decreasing electro chemical potential when the system size is reduced. We have considered several possible correlations between a small number of electrons in a quantum dot looking for a negative compressibility. We found that independent electrons with an interaction described by a constant capacitance, the formation of a finite Wigner lattice, and an exact calculation of the energy spectrum of a few-electron parabolic dot¹² did not lead to a negative compressibility.

Another way which could, at least conceptually, explain the multiple peak structure is an oscillating tunnel rate with minima going to zero. If the few electrons in the dot form a strongly correlated electron state, as for instance, a finite Wigner lattice, or a *Wigner molecule*, tunneling through such a correlated state may be strongly suppressed due to an orthogonality catastrophe. If somehow, this tunnel suppression oscillates it could modify broadened Coulomb oscillations with finestructure having minima going to zero.

For the moment, however, we have to conclude that we can not explain the multiple peak structure, and that further measurements are needed on different geometries in order to obtain a better understanding of the behaviour of few electron quantum dots.

ACKNOWLEDGEMENT

We have benefited very much from the theoretical work of Juanjo Palacios on correlated electron dots. We wish to thank him for that, and Charlie Johnson, Nijs van der Vaart, Dick van der Marel, Hans Mooij, Leonid Glazman, and Dima Averin for valuable discussions. Financial support from

FOM is gratefully acknowledged.

REFERENCES

1. See for a review on metal systems: D.V. Averin and K.K. Likharev, in *Quantum Effects in Small Disordered Systems*, edited by B.Al'tshuler, P. Lee, and R. Webb (Elsevier, Amsterdam, 1990).
2. See for a recent review, including various semiconductor systems: *Single Charge Tunneling*, H. Grabert, J.M. Martinis, and M.H. Devoret, eds. (Plenum, New York, 1991).
3. See for a collection of recent work the special issue on Single Charge Tunneling in *Zeitschrift für Physik B-Condensed Matter* **85**, edited by H. Grabert (1991).
4. P.L. McEuen, E.B. Foxman, U. Meirav, M.A. Kastner, Y. Meir, N.S. Wingreen, and S.J. Wind, *Phys. Rev. Lett.* **66**, 1926 (1991).
5. L.P. Kouwenhoven, N.C. van der Vaart, A.T. Johnson, W.Kool, C.J.P.M. Harmans, J.G. Williamson, and A.A.M. Staring, *Z. Phys. B - Condensed Matter* **85**, 367 (1991);
See also chapter 7 in this thesis.
6. L.P. Kouwenhoven, A.T. Johnson, N.C. van der Vaart, C.J.P.M. Harmans, and C.T. Foxon, *Phys. Rev. Lett.* **67**, 1626 (1991);
See also chapter 8 in this thesis and in Ref. 3.
7. H. van Houten, B.J. van Wees, M.G.J. Heijman, and J.P. Andre, *Appl. Phys. Lett.* **49**, 1781 (1986).
8. A.T. Johnson, L.P. Kouwenhoven, W. de Jong, N.C. van der Vaart, C.J.P.M. Harmans, and C.T. Foxon, to be published.
See also chapter 9 in this thesis.
9. C.J.B. Ford, M. Field, P.J. Simpson, M. Pepper, D. Popovic, D. Kern, J.E.F. Frost, D.A. Ritchie, and G.A.C. Jones, to appear in *Proceedings of Quantum Effect Physics, Electronics and Applications*, Luxor, January 1992.
10. L.I. Glazman and I.M. Ruzin, to be published.
11. See in particular Fig. 13 in: S.B. Field, M.A. Kastner, U. Meirav, J.H.F. Scott-Thomas, D.A. Antonadis, H.I. Smith, and S.J. Wind, *Phys. Rev. B* **42**, 3523 (1990).
12. J.J. Palacios, private communication.

Summary

This thesis describes a number of experiments performed in the period 1988 to 1992 on submicron semiconductor structures. The submicron structures are defined in the two dimensional electron gas (2DEG) of a GaAs/AlGaAs hetero structure by means of metallic gates which are fabricated on top of the hetero structure. Applying negative voltages to the gates depletes the electron gas beneath them, leaving free electrons only in the ungated regions. A split-gate geometry with an opening and a length of a few 100 nm induces a channel in the 2DEG, which is short and narrow compared to the elastic mean free path in the 2DEG. The transport through such a constriction is therefore ballistic. The Fermi wave length of the electrons is about 50 nm and, therefore, also of order the constriction width, so the electron wave-nature affects the transport properties. The *quantum ballistic* transport regime in these submicron devices is the subject of the first part of this thesis.

The first part describes experiments on several sample geometries. As an introduction, the conductance of a short, narrow constriction, a *quantum point contact* (QPC), is discussed. The lateral confinement in a QPC causes the formation of 1D subbands. Each 1D subband contributes $2e^2/h$ to the conductance, yielding a quantized conductance equal to the number of populated 1D subbands times the conductance unit $2e^2/h$. The breakdown of the conductance quantization is studied in the non-linear transport properties of QPCs yielding a direct measurement of the energy separation between the 1D subbands.

On increasing the magnetic field, a gradual transition occurs from the quantized conductance at zero magnetic field to the quantum Hall effect at high magnetic fields of a few Tesla. QPCs have furthermore been used as special current and voltage probes to study the electron transport along the boundary of a 2DEG. It has been demonstrated that the integer quantized Hall conductance can be completely determined by the properties of the probes instead of the filling factor in the bulk 2DEG. This experiment has demonstrated that edge channels can be treated as independent 1D current channels over distances of several microns. We introduced *fractional edge channels* as a mechanism for transport in the many-body state of the fractional quantum Hall effect. It explains an experiment where a fractional quantum Hall effect is observed while the bulk 2DEG has an integer filling factor.

The properties of edge channels are demonstrated in a gate configuration where two QPCs are put in series and connected by a closed cavity. At zero magnetic field the individual QPC conductances add in an Ohmic way. However, when a high magnetic field is applied, the

electron transport occurs via edge channels. If scattering between edge channels is absent, electrons travel through the sample with conservation of edge channel quantum number, so-called *adiabatic* transport. The absence of scattering between edge channels is demonstrated by the observation of a series QPC conductance equal to the smallest of the two individual QPC conductances.

The 3D confinement in the cavity causes the energy states to split up into *0D-states*. The 0D-states show up in the conductance through the dot as oscillations when either the magnetic field is varied or the dot size is changed by means of a gate voltage. A conductance maximum corresponds to a tunneling resonance occurring when the Fermi energy of the leads coincides with a 0D-state in the dot. In a series of 15 coupled quantum dots, the 0D-states originating from the individual dots form a 1D *mini-band structure*. The finite number of unit cells in this 1D-*crystal* is reflected by the observation of 15 small conductance oscillations (reflecting the discrete energy band) enclosed by deeper peaks (reflecting the gaps in the band structure).

In the second part of this thesis we discuss *charging effects* in semiconductor quantum dots. When such a dot is only weakly coupled to the leads by tunnel barriers, the number of electrons in the dot is an integer. The addition of an extra electron charges the dot by the elementary charge e , resulting in an electro static energy increase of e^2/C , where C is the capacitance between the dot and ground. Charging experiments are performed in the linear and non-linear transport regime. The linear conductance oscillates when the number of electrons is varied by means of a gate voltage. Each period corresponds to a change of one electron in the dot. Current-voltage characteristics show the Coulomb staircase. A current step occurs when the bias voltage supplies sufficient energy to overcome the charging energy e^2/C . The interplay between 0D-states and charging results in Coulomb oscillations having maxima approaching the fundamental maximum value of e^2/h , a double-step staircase directly measuring the energy separation between successive 0D-states, and a measure of the 0D energy spectrum in a magnetic field.

Charging effects have been employed to realize a *quantum dot turnstile* using two out-of-phase RF signals to induce oscillating tunnel barriers. During each RF cycle an integer number of electrons pass the dot, resulting in *quantized current* plateaus at multiples of ef , where f is the RF frequency. In addition it is shown that when the two RF signals differ in amplitude, an integer number of electrons are *pumped* through the device each cycle resulting in current plateaus around zero bias voltage. It is proposed that an optical analog of the electron turnstile/pump could be realized by pumping single excitons in a vertical quantum dot with a pulsed laser.

Samenvatting

Dit proefschrift beschrijft een aantal experimenten die in de periode 1988-1992 zijn uitgevoerd aan submicron halfgeleider structuren. De submicron structuren zijn gedefinieerd in het twee dimensionale elektronengas (2DEG) van een GaAs/AlGaAs heterostruktuur door middel van metalen gates, die op de heterostruktuur zijn aangebracht. Door een negatieve spanning op de gates aan te brengen, wordt het elektronengas onder de gates gedepleerd. Een "split-gate" geometrie met een opening en een lengte van een paar honderd nm definieert een kanaal in het 2DEG, wat kort en smal is vergeleken met de vrije weglengte. Het transport door het kanaal is daardoor ballistisch. De Fermi golflengte van de elektronen bedraagt ongeveer 50 nm en is ook van dezelfde orde als de breedte van het kanaal. Hierdoor kan het golfkarakter van elektronen het transport gaan bepalen. Het resulterende *quantum ballistisch* transport door submicron structuren vormt het eerste gedeelte in dit proefschrift.

Dit gedeelte beschrijft experimenten aan een aantal sample geometrieën. Als een inleiding wordt de geleiding van een kort smal kanaal, een *quantum punt contact* (QPC), beschreven. De laterale opsluiting in een QPC resulteert in de vorming van 1D subbanden. Bij magneetveld nul draagt elke subband $2e^2/h$ bij aan de geleiding, zodat de totale geleiding is gequantiseerd in veelvoud van $2e^2/h$. Uit niet lineaire transport metingen aan QPCs kan het energieverschil tussen de 1D subbanden worden bepaald.

De gequantiseerde geleiding bij nul magneetveld blijkt geleidelijk over te gaan in het quantum Hall effect bij een hoog magneetveld. QPCs zijn verder gebruikt als speciale stroom- en spannings-contacten om het elektronen transport langs de rand van het 2DEG te bestuderen. Daarmee is aangetoond dat het quantum Hall effect volledig kan worden bepaald door de eigenschappen van de contacten in plaats van door de vulfactor in het 2DEG. Dit experiment laat zien dat randkanalen kunnen worden beschouwd als onafhankelijke 1D stroomkanalen over afstanden van een paar μm . In analogie hebben we het begrip *fraktionele randkanalen* geïntroduceerd als een transport mechanisme in de veel-deeltjes toestand van het fraktionele quantum Hall effect. Het verklaart onder andere een experiment waarin een fractioneel quantum Hall effect is waargenomen terwijl het bulk 2DEG een gehele vulfactor heeft.

De eigenschappen van randkanalen zijn bestudeerd in een configuratie waar twee QPCs in serie staan met daartussen een gesloten 2D holte. Zonder magneetveld en dus in afwezigheid van randkanalen, tellen de individuele QPC geleidingen op volgens de wet van Ohm. In een hoog magneetveld vindt het elektronen transport daarentegen plaats via randkanalen. Indien er geen

verstrooiing optreedt tussen de randkanalen, bewegen de elektronen door het sample met behoud van hun Landau-quantumgetal. Dit wordt *adiabatisch* transport genoemd. Adiabatisch transport is aangetoond door te laten zien dat de serie geleiding gelijk is aan de kleinste geleiding van een van de twee QPC.

Door de 3D opsluiting in de holte splitsen de energietoestanden op in *0D-toestanden*. De 0D-toestanden komen tot uiting als oscillaties in de geleiding wanneer het magneetveld of de grootte van de quantum holte wordt veranderd. Een geleidingsmaximum correspondeert met resonant tunnelen, wat optreedt als de Fermi energie van de aanvoerbanen, ofwel de reservoirs, samenvalt met een 0D-toestand in de holte. In een serie configuratie van 15 quantum holtes vormen de 0D-toestanden, afkomstig van de individuele holtes, een 1D *mini-bandenstructuur*. Het eindige aantal eenheidscellen in dit 1D-kristal geeft 15 kleine oscillaties in de geleiding van de holte (hetgeen de discrete energieband aantoont) tussen diepe pieken (die de energie gap aantonen).

In het tweede gedeelte van dit proefschrift beschrijven we *ladingseffecten* in halfgeleider quantum holtes. Indien een holte zwak is gekoppeld aan de reservoirs via tunnelbarrières, kan er alleen lading worden toegevoegd in stappen van de elementaire lading e . Dit geeft een elektrostatistische energie verhoging van e^2/C , waarin C de capaciteit is tussen de holte en aarde. Ladingsexperimenten zijn uitgevoerd in het lineaire en niet-lineaire respons regime. De lineaire geleiding oscilleert als het aantal elektronen wordt veranderd door middel van een gate spanning. Elke periode correspondeert met de verandering van één elektron in de holte. Stroom-spannings karakteristieken vertonen de Coulomb trap. Een stroomstap treedt telkens op als de spanning groter wordt dan de ladingsenergie e^2/C . De wisselwerking tussen 0D-toestanden en ladings-effecten resulteert in Coulomb oscillaties met geleidingsmaxima, die het fundamentele maximum van e^2/h benaderen; een dubbele-stap-trap hetgeen een directe maat is voor de opsplitsings-energie tussen opeenvolgende 0D-toestanden; en een meting van het 0D spectrum in een magneetveld.

Ladingseffecten zijn gebruikt om een *elektronen-draaihek* te realiseren door middel van RF geïnduceerde oscillerende tunnelbarrières. Er is aangetoond dat tijdens elke RF cyclus een geheel aantal elektronen de holte passeert. Dit geeft *gequantiseerde stroomplateaus* bij veelvouden van ef , met f de frequentie van het RF signaal. Tevens is laten zien dat wanneer de RF signalen verschillen in amplitude, een geheel aantal elektronen door het sample worden gepompt, resulterende in stroomplateaus rond nul spanning. Een optisch analogon van de elektronen draaihek/pomp moet realiseerbaar zijn door excitonen één voor één te pompen in een verticale quantum holte met gebruik van een gepulste laser.

Curriculum Vitae

Leo Kouwenhoven

December 10, 1963	Born at Pijnacker
1976 – 1982	V.W.O. at the Erasmus College, Zoetermeer
1982 – 1988	Applied Physics at the Delft University of Technology graduate research in the Solid State group of prof. dr. ir J.E. Mooij subjects: fabrication of nanostructures; transport properties of quantum point contacts.
1988 – 1992	PhD research at Delft University of Technology in the Solid State group of prof. dr. ir. J.E. Mooij.